THESIS FOR THE DEGREE OF DOCTOR OF PHILOSOPHY

RECONFIGURABLE MOTION CONTROL SYSTEMS FOR OVER-ACTUATED ROAD VEHICLES

LEO LAINE

Department of Applied Mechanics
CHALMERS UNIVERSITY OF TECHNOLOGY
Göteborg, Sweden 2007

Reconfigurable Motion Control Systems for Over-Actuated Road Vehicles

LEO LAINE
ISBN 978-91-7291-960-0

Doktorsavhandlingar vid Chalmers Tekniska Högskola
Ny serie nr 2641
ISSN 0346-718X

Department of Applied Mechanics
Chalmers University of Technology
SE–412 96 Göteborg
Sweden
Telephone: +46 (0)31–772 1000

Chalmers Reproservice
Göteborg, Sweden 2007

To Megan and Olivia

Reconfigurable Motion Control Systems for Over-Actuated Road Vehicles

LEO LAINE
Department of Applied Mechanics
Chalmers University of Technology

Abstract

Over-actuated systems, such as today's road vehicle configurations, have more motion actuators than controlled motions. For example, a passenger car has a combustion engine and four mechanical brakes, all of which can be used individually to correct any error in yaw rate when the vehicle becomes under- or oversteered. The over-actuation becomes even more obvious when the vehicle is configured with additional motion actuators such as electric motor(s). This is the case for Fuel Cell and Hybrid Electric Vehicles where blending between the use of different actuators is needed.

This thesis proposes how a motion control system for over-actuated road vehicles can be made reconfigurable within the context of both offline and online adaptivity. Offline, the proposed control system is easily reconfigured to handle a wide range of vehicle configurations, with different types and numbers of motion actuators, without changing the control law for the desired ground motion of the vehicle. Online, the motion control system adapts its use of the motion actuators to the current conditions of the available actuators and their ability to generate tyre forces on the ground. Another online feature is the smooth arbitration between desired actuator use to both minimize energy consumption and assure vehicle stability. This smooth arbitration is especially important for vehicle configurations which have an energy buffer.

The proposed motion control system uses control allocation which separates the control law for the ground motion from the distribution of the desired motion forces among the available actuators for the specific configuration. The optimization formulation of the control allocator considers the actuator limits in both position and rate of change. Through detailed modelling of different vehicle configurations and their actuators, drivetrains, and chassis, it was shown by simulation that the proposed motion control system is both offline and online reconfigurable. The results from different driving manoeuvres showed that the control allocator not only reconfigured the distribution when the actuators were saturated or limited by low road/tyre friction but also ensured that vehicle stability was upheld at all times. This was accomplished by prioritizing vehicle motion higher than energy management in the optimization formulation of the control allocator.

Keywords: road vehicle, hybrid electric vehicle, reconfigurable, motion control system, over-actuated, control allocation

List of publications

The work in this thesis is based upon the following papers. References will be made using the Roman numerals associated with each paper. The first seven papers are appended where Papers I-III provide the basic framework from which this thesis evolved and Papers IV-VII comprise the primary works of this thesis.

I. Leo Laine and Johan Andreasson, Generic Control Architecture Applied to a Hybrid Electric Sports Utility Vehicle, in *Proceedings of the Electric Vehicle Symposium, (EVS 20)*, Los Angeles, USA, November 2003.

II. Johan Andreasson and Leo Laine, Driving Dynamics for Hybrid Electric Vehicles Considering Handling and Control Architecture, *Journal of Vehicle System Dynamics*, Vol. 41, pp 497-506, 2004.

III. Leo Laine, Jonas Hellgren, Henrik Kinnunen, and Magnus Rönnberg, Reusable Control Architecture Implemented in a Scale Model of a Hybrid Electric Vehicle, in *Proceedings of the Electric Vehicle Symposium, (EVS 21)*, Monaco, April 2005.

IV. Leo Laine and Jonas Fredriksson, Brake Blending for Hybrid Electric Vehicles Using Control Allocation, Tech. Report R011/2007, Department of Signals and Systems, Chalmers University of Technology, Göteborg, Sweden, 2007. A shorter version is also submitted to *Int. Journal of Vehicle Systems Modelling and Testing, Special Issue on: Modelling and Testing of Alternative Vehicular Propulsion*.

V. Leo Laine and Jonas Fredriksson, Traction and braking of hybrid electric vehicles using control allocation, Tech. Report R012/2007, Department of Signals and Systems, Chalmers University of Technology, Göteborg, Sweden, 2007. A shorter version is also accepted (under revision) to *Int. Journal of Vehicle Design, Special Issue on: Advanced Traction/Braking Vehicle Control*.

VI. Leo Laine and Jonas Fredriksson, Coordination of Vehicle Motion and Energy Management Control Systems for Wheel Motor Driven Vehicles, accepted to *2007 IEEE Intelligent Vehicles Symposium (IV'07)*, Istanbul, Turkey, June 2007.

VII. Leo Laine and Johan Andreasson, Control Allocation Based Electronic Stability Control System for a Conventional Road Vehicle, submitted to *10^{th} International IEEE Conference on Intelligent Transportation Systems (ITSC'07)*, Seattle, WA,

October 2007.

The following papers are also discussed in the thesis but are not appended.

VIII. Leo Laine and Johan Andreasson, Modelling of Generic Hybrid Electric Vehicles, in *Proceedings of the* 3^{rd} *International Modelica Conference*, Linköping, Sweden, November 2003.

IX. Johan Andreasson, Leo Laine, and Jonas Fredriksson, Evaluation of a Generic Vehicle Control Architecture, in *Proceedings of the* 30^{th} *Congress of the International Federation of Automotive Engineering Societies, (FISITA'30)*, Barcelona, Spain, May 2004.

X. Leo Laine and Johan Andreasson, Reusable Functional Partitioning of Tractive Force Actuators Applied on a Parallel Hybrid Electric Vehicle, in *Proceedings of the* 7^{th} *International Symposium on Advanced Vehicle Control, (AVEC'04)*, Arnhem, Netherlands, August 2004.

XI. Jonas Hellgren, Leo Laine, Jonas Sjöberg, Magnus Rönnberg, Dennys Gomes, and Aizezi Abudings, Systematic Design and Development of Hybrid Electric Scale Model Car, Technical Report, Division of Mechatronics, Chalmers University of Technology, October 2004.

XII. Jonas Fredriksson, Johan Andreasson and Leo Laine, Wheel Force Distribution for Improved Handling in a Hybrid Electric Vehicle using Nonlinear Control, in *Proceedings of the* 43^{rd} *IEEE Conference on Decision and Control, (CDC'43)*, Paradise Island, Bahamas, December 2004.

XIII. Leo Laine, On Vehicle System Control Architecture for Fuel Cell- and Hybrid Electric Vehicles, Licentiate thesis, Department of Applied Mechanics, Chalmers University of Technology, Sweden, April 2005.

Contribution of Individual Authors in Appended Papers

The authors Leo Laine (LL), Jonas Fredriksson (JF), Johan Andreasson (JA), Jonas Hellgren (JH), Henrik Kinnunen (HK), and Magnus Rönnberg (MR) and their individual contributions in the appended papers are as follows:

- Paper I, LL and JA wrote the paper and performed the modelling together. JA developed the chassis library.
- Paper II, JA wrote the main part of the paper and performed most of the modelling. LL helped with editing the paper and provided suggestions on the modelling.
- Paper III, LL implemented the functional partitioning and signal interfaces in the control system and wrote the paper. JH performed the conceptual design of the power supply and drivetrain and helped with editing the paper. HK and MR implemented and calibrated sensors and actuators and made them perform as desired.
- Paper IV, LL modelled both the vehicle system and the proposed motion control system and wrote the paper. JF provided suggestions on the modelling and also helped with editing the paper. JF also made the simulations submitted in the paper.
- Paper V, LL modelled both the vehicle system and the proposed motion control system and completed both the writing and the simulations submitted in the paper. JF provided suggestions on the modelling and also helped with editing the paper.
- Paper VI, LL modelled both the vehicle system and the proposed motion control system and completed both the writing and the simulations submitted in the paper. JF helped with editing the paper.
- Paper VII, LL modelled the proposed motion control system, the motion actuators, drivetrain, and one of the chassis models. JA implemented the commercially available chassis model found in the Vehicle Dynamics Library inside the Matlab/Simulink environment that was derived for papers I-III. LL completed both the writing and the simulations submitted in the paper.

Acknowledgments

I would like to start by acknowledging my supervisor and examiner Prof. Em. Bengt Schmidtbauer who has given valuable advice and guidance and has also put things in a historical perspective thanks to his long professional background. I would also like to acknowledge Prof. Jonas Sjöberg for the guidance and supervision given during my licentiate degree. Special thanks to my co-supervisor Assistant Prof. Jonas Fredriksson who has gone in great depth with me when it comes to the control design and system modelling, it was inspiring. I am exceedingly grateful for the time that group leader of vehicle dynamics Associate Prof. Robert Thomson has put on tedious but necessary administration. One person who has kept this project going forward by his genuine enthusiasm and interest is undoubtedly the chairman of the steering group, Associate Prof. Bengt Jacobson, at Volvo Car Corporation. Thank you all in the steering group for keeping interest high during all five years. Thanks to Kanehira Maruo for being a highly inspiring room mate during your time at Chalmers. A special thanks also to recent PhD graduate Johan Andreasson who was highly involved in the first part of the project. It has been a great pleasure, Johan, to work with you and become as much friends as colleagues. Thanks also to PhD Jonas Hellgren. Jonas, it was challenging and fun to work on the 'real stuff' as in the scale model car. Thanks to Mattias Åsbogård and Lars Johannesson for all the fascinating discussions about HEVs and courses taken together. PhD Mathias Lidberg, thanks for taking me swimming laps and all the many constructive conversations we have had. Thanks also to Matthijs Klomp, your genuine interest in vehicle dynamics has resulted in long fruitful talks. Funny how hard but inspiring times bring people closer and one makes new friends. Thanks to all people not mentioned but who have still meant a lot in making my time more joyful during the working day.

I would also like to acknowledge my old chief Jan Christian Anker for encouraging me to start the graduate studies at Chalmers. I also would like to acknowledge Björn, Morgan, Joosef, and Ola for the pleasant times spent discussing the equation of state.

Now Megan, my wife to be, you are a piece of pure art. Not only do you keep our life sane and in order, and edit my papers, you also make arrangements for my

social events. For example, as a birthday gift she bought me and my childhood friend Kent Olofsson tickets to see Iron Maiden. That's love! Thank you Olivia, my daughter, who makes everything so much easier just by smiling and being goofy. Thanks also to my parents, Maire and Ossi, for being just the support one sometimes needs so badly. Thanks also to the Binghams for making Camano Island a safe haven. Thanks to all my friends, both old and new, and also to our new neighbours in Härryda, for making my spare time enjoyable.

Leo Laine, Göteborg, 2007

Table of contents

Chapter 1

Introduction

This chapter introduces the background, motivation, and objective for this thesis. It also states the limitations and main contributions.

1.1 Background

The automotive industry is undergoing a tremendous change in how road vehicles should be designed and configured in order to meet new legislation on emissions and the increasing desire for reduced fuel consumption. One way to achieve these goals is through the hybridization of the vehicle's power supply. This means that a buffer is assisting in the propulsion of the vehicle, storing the braking energy and reusing the stored energy during acceleration. There are now several different ways for the vehicle to accomplish the desired motion and the complexity of designing these cars increases significantly compared with conventional cars. To prepare for the changes within road vehicle design, the Swedish government and members of the automotive industry started a joint venture research cluster called Gröna Bilen/FCHEV. The goal of this venture was to contribute to vehicle development through academic research and to provide the industry with educated personnel within fuel cell and hybrid electric vehicle technology. Several parallel PhD projects were started within Gröna Bilen/FCHEV with different objectives on component, subsystem, and complete vehicle system levels. The component level projects considered buffer components, such as batteries and super capacitors, and different aspects of fuel cell and electric motor drive design and development. The subsystem level projects evaluated different concepts of hybrid electric vehicles. The complete system level projects studied energy management [29], vehicle dynamics [6], and main control, from which this thesis is a result. Cooperation with the two other complete system level projects has lead to direct research benefits in approaching how the complete system for any fuel cell or hybrid electric vehicle

should perform when energy management and vehicle dynamics are considered simultaneously.

1.2 Motivation

The road vehicle performs a basic function, it takes the driver, load, and sometimes passengers between different locations. However, the requirements of what functionality a modern road vehicle should include are increasing. It should not only provide transportation, it should also be comfortable, time and energy efficient, safe, assist the driver during driving, and even take over when the driver is unable to handle the situation. These new functionalities set requirements on the embedded control system of the vehicle. For the motion control system studied here, these requirements consist of four main items:

1. Integrate and coordinate the use of the available motion actuators to their full potential to achieve the desired ground motion.

2. Coordinate the available motion actuators energy efficiently and maintain vehicle stability.

3. Make the system's coordination and distribution adaptive for sudden changes in the environment or saturation and failure among the available actuators.

4. Make the system reusable for several vehicle configurations.

The first requirement can already been seen in the motion control systems of today's road vehicles where the integration and coordination of available motion actuators are used to assist the driver when the vehicle is becoming over- or understeered. This functionality has many names but for the purposes here it will be called Electronic Stability Control (ESC). ESC assists the driver by using the mechanical brakes individually to apply a correcting yaw torque to reduce or increase the turning radius of the vehicle depending on its over- or understeer tendency. Although the brakes are designed mainly to reduce the speed of the vehicle, they can also assist in turning the vehicle if they are properly coordinated. The lifesaving ability of ESC is said to be second only to seat belts in that it assists the driver in keeping the vehicle on the road and thereby prevents single crash tripped rollover accidents [4], [5]. The response to this additional functionality is impressive, about 29 percent of all light vehicles with model year 2006 sold in the USA were equipped with ESC systems, [4]. ESC is also proposed to become a minimum standard by the year 2011 on all light vehicles sold in the USA, [4], [5], [23]. This is an excellent example of the need to use the full potential of the available motion actuators.

The second requirement, energy efficient coordination, relates to vehicles equipped with an energy buffer such as Hybrid Electric Vehicles (HEVs). HEVs are becoming increasingly popular because they reduce fuel consumption without reducing performance or load capacity. HEVs reduce fuel consumption by regenerating brake energy, shutting off the engine at zero speed, and enabling the engine to work at more efficient operating points. Regenerative braking means that braking is not only performed by the mechanical brakes but also by the electric motor(s). To optimally use the available motion actuators, a high level of integration and coordination is needed to assure vehicle stability and energy efficiency. The use of the electric motor(s) must be smoothly blended with the rest of the available motion actuators not only during braking but also during traction.

The third requirement is the need for adaptivity to sudden changes in the environment. For a road vehicle, sudden changes in the tyre/road friction for one or several tyres is crucial information for making a correct redistribution of the usage between available actuators. Other important pieces of information are the actual limits in position and rates of change of the available actuators. This is not only to allow for fast coordination but also to know if one or several actuators are saturated and need to be assisted by others. The information should also include if the actuator has failed or is not working properly. Then the system should automatically re-distribute between the properly working actuators, generating a safe and redundant system.

The fourth requirement, reusability, is an industry motivated need for profit on each new vehicle configuration developed. One way to increase the profit is to reduce development costs. One cost that is increasing is the embedded vehicle control software. In the year 2000, development and calibration of control functions was estimated to be 4 percent of the total production cost of a car. It is estimated that in the year 2010 that figure will increase to 13 percent, [26]. One way automotive manufacturers and suppliers are trying to meet this increasing cost is to standardize functions and their interfaces within the software and electronics used in road vehicles, [9]. This gives a fundamental reason to develop reconfigurable motion control systems which allow them to be reused for several types of vehicle configurations. These systems should also have the potential to include technology such as steer-by-wire and more futuristic motion actuators such as the Autonomous Corner Modules (ACM) which can control the steering, rotation, and position individually at each wheel, [57].

Finally, these requirements motivate the development of a reconfigurable motion control system for road vehicles. The system should be adaptive during driving, online reconfigurable, by the automatic redistribution of available actuators based on maintaining vehicle stability in an energy efficient way. If the system is also applicable for several vehicle configurations, offline reconfigurable, then automotive manufacturers can reduce the development cost for each new vehicle

configuration.

1.3 Objective

The objective of this thesis was to identify how a reconfigurable motion control system can be designed to include a broad variety of over-actuated road vehicles. The aim was that the proposed motion control system should work as well for conventional road vehicles as for vehicles equipped with an energy buffer.

1.4 Method

The research problem was approached in two steps. Step one considered how a reusable functional control architecture for HEVs and FCVs can be designed when focusing on how the driver's intentions generate vehicle motion. The results were presented in the thesis for licentiate degree, Paper XIII. Step two considered the conceptual design of how a reconfigurable motion control system for over-actuated ground vehicles can be realised.

1.5 Limitations of Scope

The list below clarifies which areas have not been considered within this study. This does not mean that they can be neglected but rather that each is an important research topic by itself.

- The thesis does not consider how the computational architecture should be constructed, nor does it address how the proposed system could be realised and implemented in a fail-safe manner.
- The thesis does not include how observers or sensors should be designed to achieve accurate estimates of vehicle states and tyre/road friction.
- The thesis does not include how the human machine interface should be designed nor how the signals from driver interface should be interpreted. Therefore, the desired longitudinal, lateral, and yaw motion of the driver is mostly assumed to be known, as in Papers IV-VI, except for Paper VII where a reference model is used for the Driver Interpreter.
- The thesis does not include studies of heavy vehicle configurations. However, some parts of the main contributions will also be applicable for these cases.

1.6 Main Contributions

The main contributions from the research are stated below as a short list and are also presented in this thesis in more detail.

- It is shown by modelling and simulation how a reconfigurable motion control system for over-actuated road vehicles can be realised.
- It is shown how the limits in position and rate of change of the motion actuators, in combination with tyre force limits, can be used to achieve sufficient information for high level coordination between available actuators.
- It is shown that the proposed motion control system has a smooth arbitration between vehicle motion control and energy management which is achieved at all times with priority on vehicle stability.
- It is shown by simulation that the proposed motion control system also works as an Electronic Stability Control System according to a proposed test procedure from the National Highway Traffic Safety Administration.
- A simulation platform was developed in Matlab/Simulink which includes the proposed motion control system and the studied vehicle configurations. The studied vehicle configurations span from five up to ten motion actuators.
- A novel model is suggested for how a permanent magnet synchronous motor's torque limits depend both on rotational speed and on the temperature of the windings. This type of reference model should be demanded from suppliers of motion actuators.

1.7 Outline of the Thesis

The outline of the thesis is as follows. Chapter 2 states how the research project has evolved. Chapter 3 gives an overview of the proposed motion control system. In Chapter 4 simulation results are presented. In Chapter 5 concluding remarks and what the next steps could be are given. Finally, Chapter 6 summarizes the appended Papers I-VII.

Chapter 2

Evolution of the Proposed Control System

This chapter starts by giving an overview of vehicle control systems and their architectures. It then continues by illustrating how the proposed control system has evolved during the research.

2.1 Overview

To put vehicle control systems in perspective, this section gives a short overview on computerised controllers within automotive applications. It then introduces how the computerised controllers are partitioned.

2.1.1 Computerised Controllers

The combustion engine was the first automotive actuator to receive a computerised controller, generally called the Electronic Control Unit (ECU). By the early 1980s they were introduced into vehicles on a large scale. Soon after, a number of other application were installed with ECUs as controllers, eventually leading to a need for intercommunication between the ECUs. At the time, the amount of required wiring prevented the signals from being wired individually as separate cables. This problem was solved by a method called multiplexing which allows several channels to be carried within one cable. In the year 1983, Robert Bosch GmbH began an internal project to develop an in-vehicle network. The result of this project was the Controller Area Network (CAN) which was officially introduced in the year 1986. By 1992 the CAN network protocol was used in production cars [15] and is now the dominating standard for connecting ECUs.

The standard CAN protocol is event driven with prioritised signals sent on the network as messages. All messages with high priority are sent each cycle, whereas messages with low priority are cancelled if needed. This leads to a stochastic transmission of low priority messages. The next generation of computational networks are time-triggered protocols [38], such as the TTCAN [15], TTPC [37], and Flexray [55], created in order to accommodate future safety critical applications such as x-by-wire.

2.1.2 Partitioning

There are two different ways of approaching the structuring of control architectures, see e.g. [14] and [25]. The first, computational partitioning, concerns how the vehicle system control software is executed. Although it is not considered in this thesis, a brief overview is however provided. The second is functional partitioning, which shows how the software itself is partitioned. Explanations are also given as to the different types of functional partitioning and their various advantages.

Computational Partitioning

Computational partitioning considers how computing resources should be distributed across different computer nodes. One type is *centralised* partitioning, which concentrates all computer resources and the sensors and actuators on to one node. Another is *distributed* partitioning in which the sensors and actuators are attached to several nodes, and in turn are connected by a communication bus. *Distributed* partitioning can also be *topographically distributed*, in which the distribution is placed near the subsystem under control, or additionally it can be *functionally distributed*, in which the distribution is decided not by location but instead by functional responsibility.

Functional Partitioning

Whereas computational partitioning focuses initially on the placement and interconnection of nodes, functional partitioning has a completely different approach, concentrating primarily on how functions are prioritised and executed within the computational nodes. There are mainly three different types of functional partitioning, *centralised*, *peer-to-peer* and *hierarchical*.

In *centralised* functional partitioning, one top level function is used to control the whole system, see Figure 2.1. This central function contains all sensor information and can directly send requests to the specific actuators. The advantage to

centralised functional partitioning is that information from all sensors are simultaneously received. The main drawback is that the whole function is affected if the hardware configuration is changed.

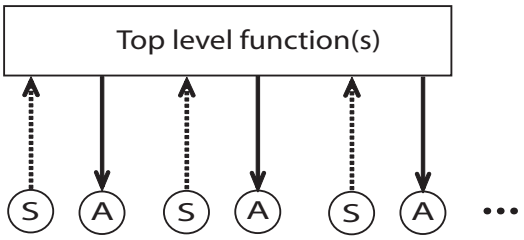

Figure 2.1: Centralised functional partitioning. Dashed and solid lines illustrate information and requests, respectively. Hardware is illustrated by A=Actuator and S=Sensor.

In *peer-to-peer* functional partitioning, no top level function is used to control the whole system, instead only local functions are used, see Figure 2.2. The coordination is achieved by sending states as information between the local functions. Every local function attempts to sub-optimise its own function. *Peer-to-peer* functional partitioning is the most modular when compared to *centralised* and *hierarchical*. The drawback with *peer-to-peer* functional partitioning is that conflicts between the local functions are hard to avoid.

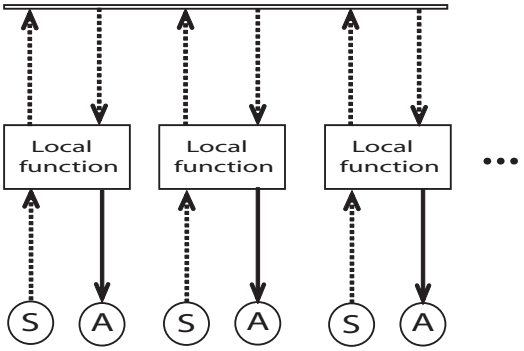

Figure 2.2: Peer-to-peer functional partitioning. Dashed and solid lines illustrate information and requests, respectively. Hardware is illustrated by A=Actuator and S=Sensor.

Hierarchical partitioning contains top level and local functions, giving both better modularity than *centralised*, and better coordination between local functions than *peer-to-peer*. *Hierarchical* functional partitioning provides the ability

to easily add, delete, and modify hardware [14]. It reduces the complexity of the system by having requests coming from the top level functions down to local functions, in this way creating a causal flow of requests. One drawback with the *hierarchical* approach is that enough information must be sent to top level functions to allow decisions on coordination to be performed. If the requests and information signals are made reusable for different hardware configurations only small changes would be needed in the top level functions.

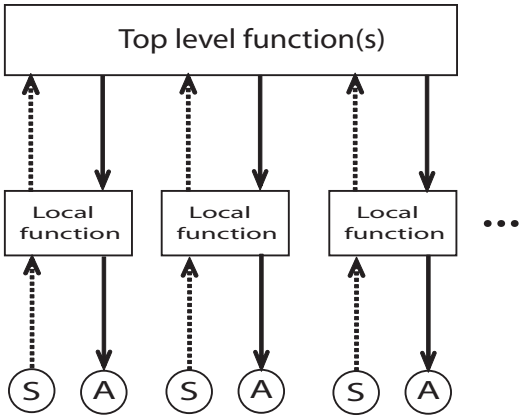

Figure 2.3: Hierarchical functional partitioning. Dashed and solid lines illustrate information and requests, respectively. Hardware is illustrated by A=Actuator and S=Sensor.

2.2 Fundamental Question about Control Architecture

The first part of this research tries to answer a fundamental question which serves as a basis or foundation. This question was motivated by the automotive manufacturers need for change in how road vehicles are constructed and built to meet new demands on reduced fuel consumption and emissions. There are several ways to reduce fuel consumption and emissions. The most obvious would be to build smaller size cars, however consumers have a certain set of standards for the performance and load capacity that a vehicle should have. Therefore, to meet these standards, technologies such as hybrid electric vehicles and fuel cell vehicles are a viable option. There is not one obvious solution that will replace the combustion engine as a propulsion system, it will likely be several simultaneous solutions depending on the price of both the alternative fuels and on the selected technology, see also [29]. This puts tremendous demands on the automotive manufacturers to

reduce development costs concerning the control architecture of each new vehicle configuration. An instant reduction of the development costs would be at hand if parts of an old control architecture could be reused when developing a new vehicle configuration. This leads to a formulation of the fundamental question:

How can a reusable control architecture be defined for HEVs and FCVs, focusing on how the driver's intentions generate vehicle motion?

The question was approached by a conceptual design phase followed by physical implementation to validate parts of the reusable control architecture. This is illustrated by using a V-diagram, see Fig. 2.4, see also Paper XIII for further details. The scope was limited by not studying how the computational architecture could be realised nor how it could be implemented in a fail safe manner.

2.2.1 Conceptual Design

The conceptual design of road vehicles has traditionally been seen as a set of subsystems that coexist in a peer-to-peer functional partitioning scheme, see Fig. 2.2 in Chapter 2.1.2. The development of functionality has focused on the subsystem and not on the integration of subsystems to achieve maximum available functionality for the vehicle. This has to do with the fact that the automotive suppliers were only responsible for delivering a specific subsystem which functioned as desired. Because of this, conflicts are hard to avoid when the separately developed subsystems are forced to be integrated into a complete functioning vehicle. Therefore, a complete vehicle control system of hierarchical functional partitioning, see Fig. 2.3 in Chapter 2.1.2, is highly desirable [17].

To address the fundamental question of how a reusable control architecture for HEVs and FCVs can be defined, the following system requirements are declared in Definition 2.2.1, see also Papers XIII and I.

Definition 2.2.1 *Generic/reusable control architecture, from Paper XIII*

1. *The control architecture should be hierarchical by functional decomposition.*

2. *Interfaces between top level and lower level functions should be made hardware independent.*

3. *The control architecture should be designed so as to accommodate any foreseeable future hardware developments for the system under consideration.*

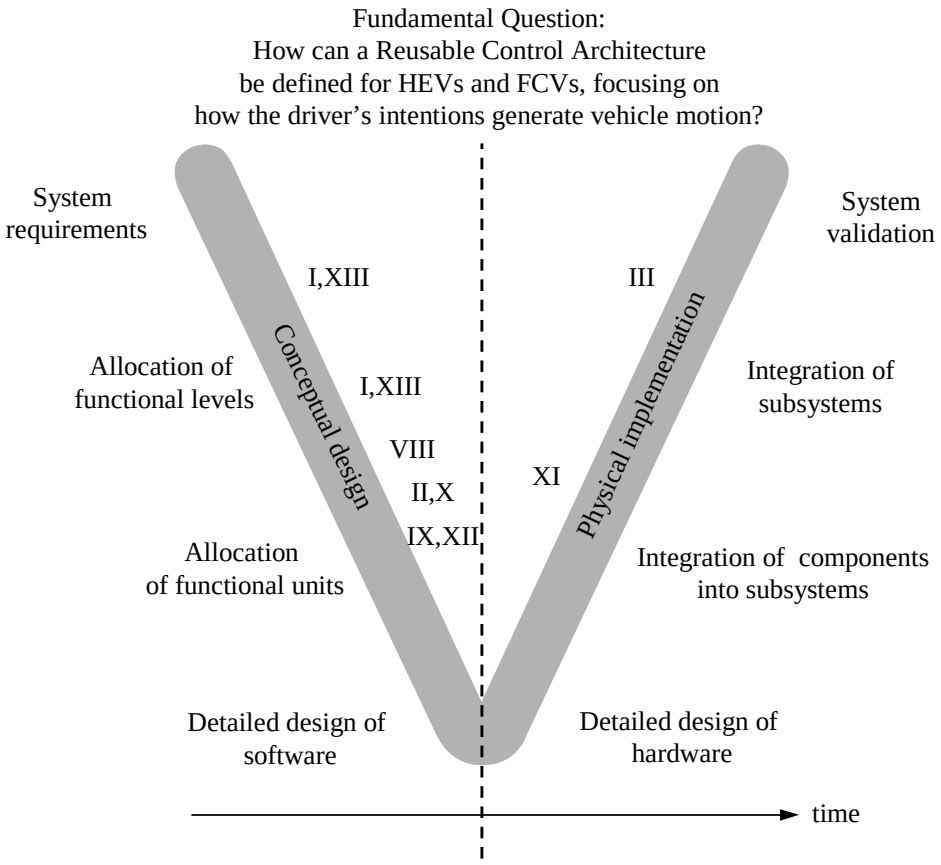

Figure 2.4: Illustration of how the fundamental question was approached by using a V-diagram. Roman numerals I-III and VIII-XIII refer to the papers that address the fundamental question.

The first item in Definition 2.2.1 states that the system should use hierarchical functional partitioning, see Chapter 2.1.2, in order to have good coordination and maintain modularity. The second item is to force the top level to be reusable for a wide range of vehicle configurations. The third item tries to assure that the architecture will not only handle hardware that is used today but also accommodate any predicted hardware developments.

When the system requirements are defined, the system is then decomposed into its main functions. Three main functions were identified within a road vehicle: driver interpreter, energy management, and vehicle motion control. These three main functions supervise the driver interface, power supply, and chassis, respectively. To formulate a control architecture which provides a high level of coordination between energy management and vehicle motion control, a hierar-

chical control architecture was found to be necessary. The hierarchical control architecture also provides that lower functions can be exchanged in a modular fashion if the interface signals between the functions are made generic. The derived architecture has three functional levels and the functions are placed into the levels depending on their coordinating authority over other functions. The following functions and levels were derived:

- Level 1 is the top level which includes functional units that coordinate lower level functions. These functions include the Driver Interpreter (DIp), which interprets the driver's input signals into the desired motion, Vehicle Motion Control (VMC), which tries to control the vehicle motion and distribute the tasks among the available motion actuators within Chassis, Energy Management (EM), which controls the Power Supply as energy efficiently as possible, and Strategic Control (SC), which works as an arbitrator between VMC and EM.

- Level 2 includes a vehicle's basic tasks. These include External Information (EI), which is all communication and information sent to and from the vehicle, Driver Interface (DIf), which is the human/man interface, Chassis (Ch), which includes all vehicle motion actuators, Power Supply (PS), which includes all energy carriers, and Auxiliary Systems (Aux), which includes all subsystems not used for generating the motion of the vehicle.

- Level 3 is the actuator and sensor level.

The functional units and their levels are shown in Fig. 2.5. Detailed information about the functions, levels, and their interfaces can be found in Papers I, XIII.

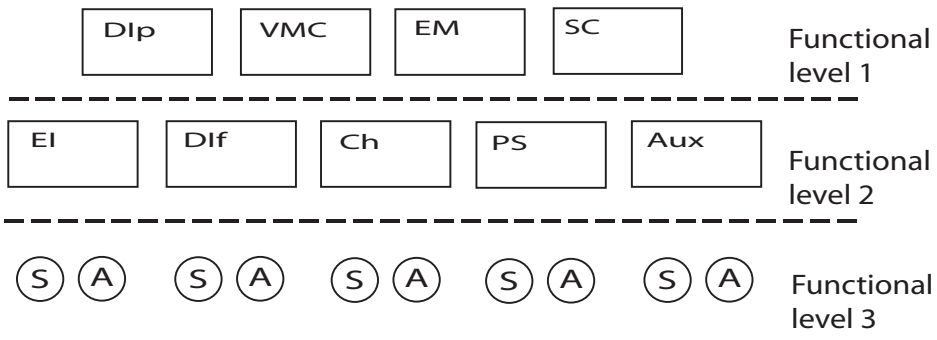

Figure 2.5: The suggested Functional Units within the generic Vehicle Control System, from Papers I,XIII.

The functions and their interfaces were checked for modularity for a wide variety of vehicle configurations by building virtual prototypes with the modelling language Modelica. Paper VIII was the basis for this modularity validation, see also Fig. 2.2.1. The Modelica language was found to be a powerful tool for this application. Thoughts on which interfaces should be used between the different functions were easily tested and validated for a wide variety of vehicle configurations.

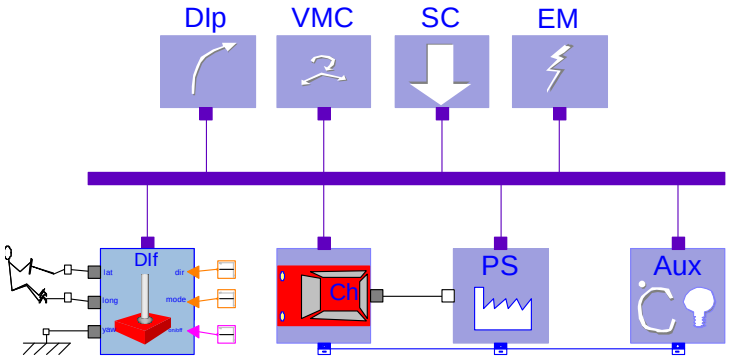

Figure 2.6: Main Model architecture in Modelica model `GenericVehicle`. The main functions within functional levels 1 and 2 are shown. The lines between the functional units describe the bus signal interface and the mechanical and electrical connectors between Ch, PS and Aux. Illustration from Paper VIII.

The next phase was to study how the authority functions such as DIp, VMC, EM, and SC could actually be realised in a reusable way. First attempt of how the desired global forces and moment of the vehicle could be distributed onto wheel forces was done in Paper II. A practical approach was proposed for how the forces could be distributed. In Papers IX and XII reusable DIp and VMC functionality was validated in Matlab/Simulink.

In short, Papers IX and XII describe how DIp generates the desired path and that the vehicle motion controller consists of a path controller and a force distributor, see Fig. 2.7. The path controller tries to keep the vehicle on the desired path by deriving the necessary global forces of the vehicle. These global forces were distributed out to the wheels by the force distributor. The force distributor used an optimization formulation that finds a minimum use of the forces when they are subject to both linear and nonlinear constraints and lower and upper limits of the wheel forces. The nonlinear constraints of the tyre force ellipse of each wheel were included. Different vehicle configurations were accommodated by introducing additional constraints on how the wheel forces could be distributed. For example an open differential constrains the longitudinal forces to be equal for the

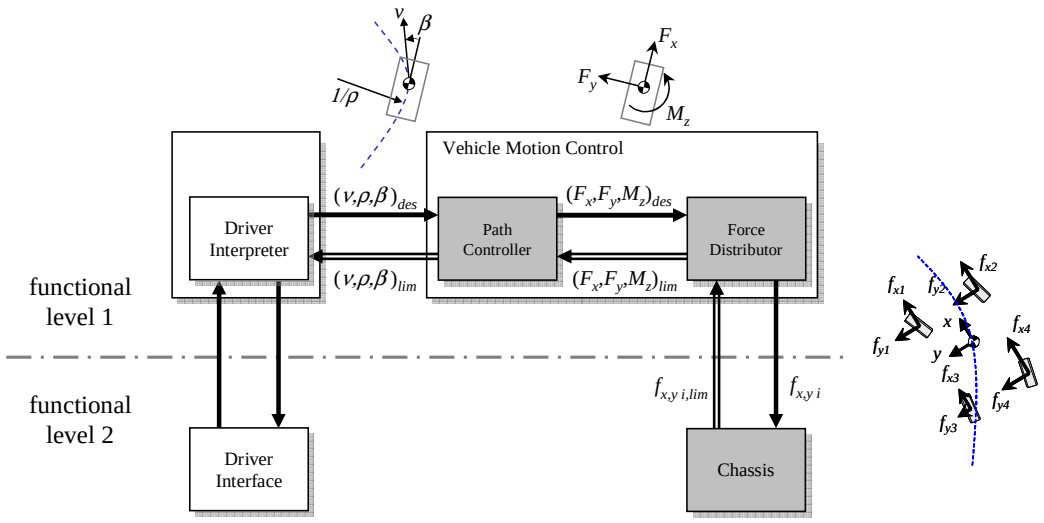

Figure 2.7: Illustration of the proposed and tested functionality within vehicle motion controller. VMC includes a path controller and force distributor. The gray shaded boxes show what parts Papers IX and XII focused upon.

connected wheel pair.

A suggestion for how the EM and SC functionality could be made reusable was shown in Paper X. In short the suggested EM function was defined as a transportation problem of energy in different networks depending on what buffers, converters, energy sources, and nodes were included in the specific PS. In the paper it was shown how the power management of a parallel hybrid electric vehicle with an automated manual gear box could be realized. The optimization formulation was a mixed integer formulation to include discrete steps of the gear box. The objective function was formulated to minimize the energy losses when using the power supply. The SC function was suggested to give authority to either VMC or EM requests depending on how critical their states were, see also Fig. 2.10 for an illustration of the critical state in VMC. The VMC state was proposed to overrule the EM state in cases of conflict.

2.2.2 Physical Implementation

The last phase in answering the fundamental question was performed by the physical implementation, as illustrated in Fig. 2.4, of a reusable vehicle control architecture within in a remote controlled Scale Model Car (SMC) of size 1:5, see Paper III. The SMC was equipped with a Digital Signal Processor (DSP) card which controlled all signal input/output. The vehicle was propelled with one elec-

tric motor connected to the rear wheels by an open differential. The motor was also used for regenerative braking for charging a buffer of super capacitors. A lead-acid battery was used for long term power demands. A DC/DC converter was used to handle the power flow between the battery, super capacitors, and motor. The vehicle was also equipped with wheel rotation and accelerometer sensors. In Fig. 2.8 the SMC hardware is shown.

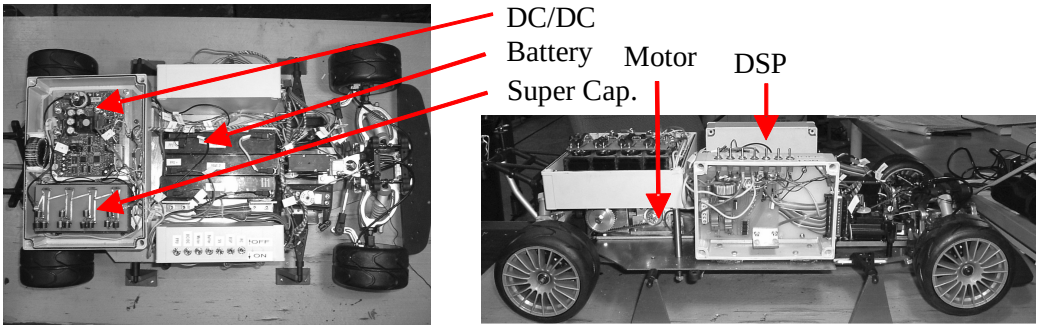

Figure 2.8: Top view (left) and Side view (right) of the SMC. It is rear wheel driven by one electric motor with a maximum power and torque of 230 W and 0.98 Nm, respectively. The motor is also used for regenerative braking. It is front wheel steered by servo and has a mass of 16 kg. Illustration from Paper III.

The SMC platform gave an understanding of how much effort it takes to make embedded control software to work with real hardware. The SMC worked and functioned according to the requirements that were set in the beginning of the SMC project. The conceptual design of the SMC is found in Paper XI. A reusable vehicle control architecture was implemented in the DSP as C-code, see Paper III. Fig. 2.9 illustrates how the vehicle control system's program loop was configured. It shows the order of how the functions were called upon and gives a description of what each function performed.

In Fig. 2.10 three acceleration tests were performed with the SMC on a ground surface with low friction. The test illustrates how an arbitration switch between energy management and vehicle motion control is used to decide which of the functions is critical and has priority. Both functions send a state variable of either 0 or 1 to operative decisions/strategic control for arbitration, where 1 stands for critical. Further details about the arbitration can be found in IX. The right plot in Fig. 2.10 shows that the VMC state was critical during the accelerations and that the angular velocity of the rear wheel oscillated around the front wheel value and thus avoided skidding, as shown in the left plot. This means that VMC decreased the desired velocity from the DIp during the accelerations and that the desired velocity from VMC was sent as a request by operative decisions due to VMC's

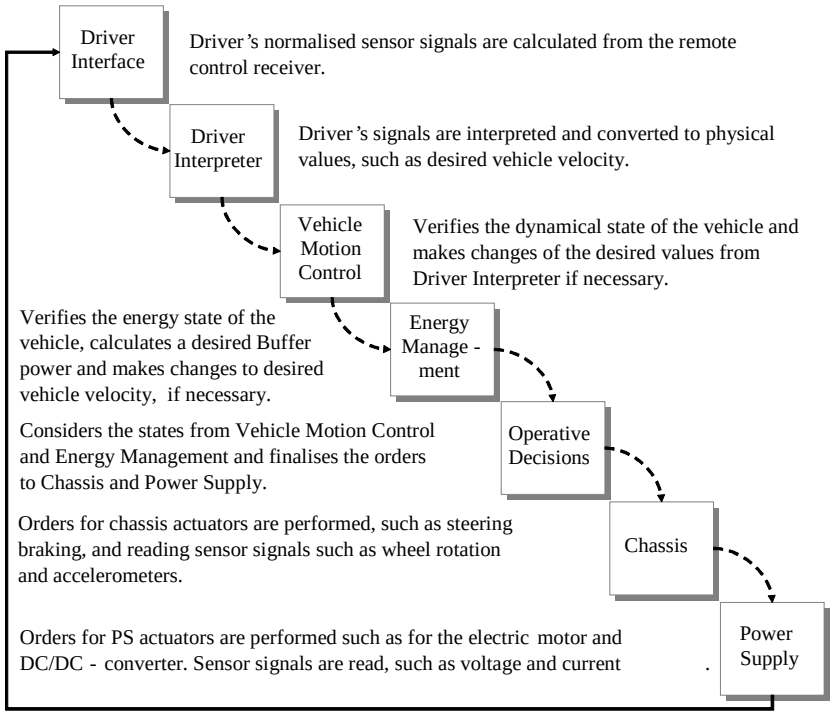

Figure 2.9: Program loop of the implemented vehicle control system within SMC, from Paper III.

critical state. Further details of the functionality implemented in the SMC can be found in Paper III.

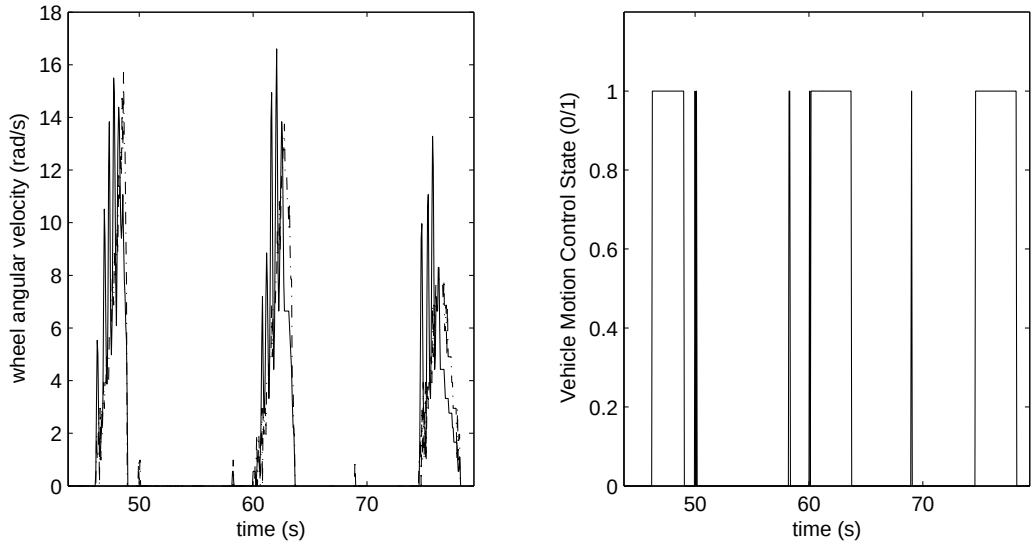

Figure 2.10: Anti-skid example, accelerations on surface with low friction, close to ice conditions. The left plot shows front (dashed) and rear (solid) wheel angular velocities. The right plot shows the VMC state, which is critical when VMC_state = 1.

2.3 Consequent Question about Over-Actuated Systems

The work presented in Section 2.2 exists as a foundation for the exploration of a consequent question. This exploration begins by viewing how longitudinal motion is controlled in a HEV where there is the possibility to use both the electric motor(s) and mechanical brakes to reduce the vehicle speed. In this situation there are more actuators than needed to control the motion, which is called over-actuation. During traction, depending on what type HEV is studied, there can be several motion actuators that need to be coordinated. A parallel HEV would have a combustion engine in combination with the available electric motor(s). A series HEV with more than one motor would also be over-actuated in traction. Now if one also studies today's conventional vehicles which are equipped with ESC systems, they use four mechanical brakes individually to generate correcting yaw torque to assist the driver if the vehicle becomes under- or oversteered. In this case there are four motion actuators to control one motion, yaw. According to a proposed safety standard from the National Highway Traffic Safety Administration, all light vehicles sold in the USA must be equipped with ESC by year 2011, [4]. This means that HEVs must also have the same ESC functionality. HEVs are even more over-actuated than conventional vehicles in applying correcting yaw torque on the vehicle which means that efficient coordination of motion actuators is especially crucial for HEVs. The following definition of an over-actuated road vehicle is proposed:

Definition 2.3.1 *Over-actuated road vehicle*
The road vehicle is equipped with more motion actuators than controlled motions and/or that more than one actuator influences at least one of the controlled motions.

The consequent question can now be described as:

How can a reconfigurable motion control system be designed for over-actuated road vehicles?

The requirements of the reconfigurable motion control system are motivated in Chapter 1.2. The question was approached by a conceptual design phase which is illustrated by using a V-diagram, see Fig. 2.11.

2.3.1 Conceptual Design

This section gives an overview of how the conceptual design was solved by the appended papers and how the papers link together. The first part of the concep-

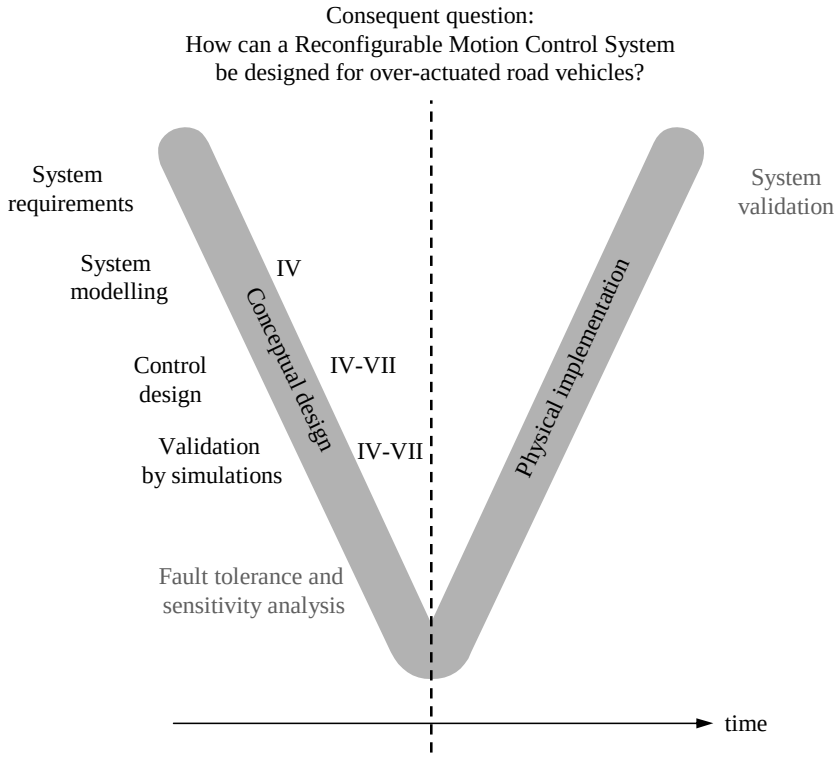

Figure 2.11: Illustration of how the consequent question was approached by using a V-diagram. Roman numerals refer to the Papers IV-VII which address the consequent question.

tual design phase was to model a selection of vehicle configurations, representing a wide variety, with a sufficient level of detail so that they could serve as a test platform for the proposed reconfigurable motion control system. Motion actuators were modelled to include first and second order dynamics. The drivetrain was modelled to include weak drive shafts and open differentials to make it more sensitive where the motion actuators were located. The drivetrain model also includes the inertia of wheels, flywheels, gearboxes, and power losses. The chassis was modelled as a two-track model to include load force distribution on each wheel due to pitch and roll effects. The tyres were modelled with a brush model which included a first order dynamic relaxation of the tyre slips. As illustrated in Fig. 2.11 the system modelling is found in Paper IV.

The second part of the process was the control design of the proposed motion control system. This was done in Papers IV-VII. All four papers include in principal the same control design. However the most basic design is found in Paper VII. Here the proposed motion control system is not controlling the front rack

steer actuator of the conventional vehicle, this is handled by the driver. The design in Paper IV is more sophisticated and includes all motion actuators for traction, braking, and steering for three different vehicle configurations. Paper V presents basically the same control design, however its a bit more advanced than in Paper IV and includes automated functionality for gear shifting. The most sophisticated control design is found in Paper VI which basically shows how vehicle motion control is prioritized over energy management at all times.

The third part of the process was validation by simulation. Different test procedures were used to validate the proposed motion control system. Paper IV focuses on test procedures where brake blending can be expected. Papers V-VI focuses on traction and braking. Some of the test procedures found in Papers IV-VI also include steering with small angles, less than 5 degrees. Paper VII includes the proposed NHTSA test procedure to validate ESC systems and includes high steering angles up to 17 degrees.

Fault tolerance and sensitivity analysis has not yet been performed, as is illustrated in Fig. 2.11 by gray shading. This would be the natural next step in implementing the proposed motion control system in production vehicles.

Chapter 3

The Proposed Reconfigurable Motion Control System

This chapter starts out by giving an overview of over-actuated systems and how control allocation has been used to solve the motion control problem in different applications. The system modelling of the studied road vehicle configurations is then discussed, followed by the control design of the proposed control system. The chapter then concludes with the main benefits and considerations.

3.1 Overview

The requirements of a modern road vehicle's motion control system is reaching a complexity which has mainly been seen only in flight and marine applications, see Chapter 1.2. It should be noted that the flight and aerospace industries have large budgets with which to design and construct their aircraft and therefore could include computerised controllers and develop advanced control functionality earlier on when computers were still expensive. In marine applications, especially when building large ships, the development cost of the control system is a small fraction of the total cost, making it possible to develop advance motion control systems. When the prices of computerised controllers became lower they also started to be popular in mass produced products such as road vehicles. With this in mind a literature survey is given on what has been done within flight, then marine, and finally within road vehicles to control over-actuated systems.

3.1.1 Flight Applications

Aircraft are designed with more motion actuators than motions to be controlled, so called over-actuation. The motion actuators in aircraft consist of control sur-

faces on the wings, tail, and even on the body. The control surfaces change their angle to achieve the desired motions in roll, pitch, and yaw, see Fig 3.1. The left figure shows the three main rotations of the airplane. The desired rotations can be achieved by several different settings of the control surfaces shown in the right figure. In this case there are up to 11 control surfaces that can be used for generating moments in the main rotation directions. Additionally, the engine thrusters are mainly used to control the longitudinal speed but are also used for generating the desired moments. This is the essence of situations where control allocation has been used for coordination within flight control.

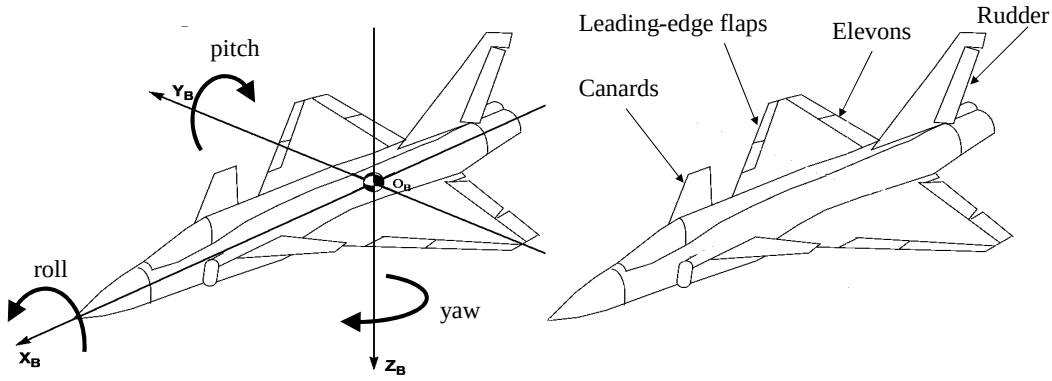

Figure 3.1: The left figure illustrates the desired moments, roll, pitch, and yaw, shown in the body-fixed reference frame. The right figure illustrates the available control surfaces which are used to generate the desired moments. The figures illustrate the ADMIRE model [1], original picture found in [10].

Over-actuation in aircraft was mainly done to improve performance and redundancy. One of the first attempts to address the over-actuation problem was done by using pseudo-controllers such as in [39]. They are also called pure mode controllers, for flight modes such as Dutch roll[1], roll and spiral modes. The pseudo-control variables are related by eigenvectors of the response modes to the motion actuators in a 'mixing' matrix which is used for allocation. The strength and weakness of the pseudo-controller is that pure modes can be achieved but not the maximum attainable moment in arbitrary directions. The first real attempt to separate the control law for the roll-, pitch-, and yaw-motion, v, and control allocation of the specific actuators, u, was done in [20], see also Fig. 3.2. The control allocation is seen as a constrained problem with maximum and minimum limits of the motion actuators. In [20] a direct allocation solution is given for the two attainable

[1]Dutch roll is an aircraft motion which combines out of phase tail wagging and rocking to side to side, a yaw roll combination, similar to the motion made by Dutch ice skaters.

moment set problem, in roll and yaw, that guarantees the maximum motion can be generated within the constraints of attainable moments. The direct allocation uses a geometric approach to solve the allocation problem. The limits of the actuators are projected through the control effectiveness matrix B to give the two dimensional geometry of the attainable moment set. In [21] direct allocation solutions for the three attainable moment set problem is given. In [22] the limits in rate of change of the motion actuators are addressed and how they can contribute to catastrophic pilot induced oscillations if they are not included in the constrained control allocation formulation.

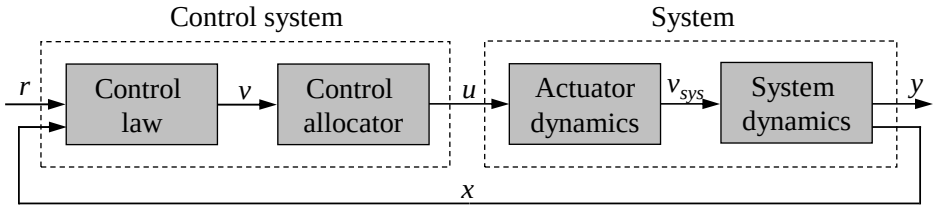

Figure 3.2: Illustration of how the control law for motion is separated for the control allocator within the control system. Illustrated originally in [31].

Reconfigurable aircraft that can handle actuator failure are highly desirable. In [18] this is accomplished through offline calculation using nonlinear constrained optimization of different 'mixer' solutions for different failure scenarios of the motion actuators. If failure is detected, the nominal entry control mixer is exchanged. Real time adaptive control allocation is suggested instead for handling the failure of motion actuators for a high performance aircraft by [19]. To be fully able to use control allocation online to achieve full manoeuvrability, efficiency, and handle failure/saturation effectively, which is not possible by using direct allocation methods or pseudo inverses, an optimization formulation for the control allocator has to be included. This has become feasible due to the increased computational capacity available in the control system. An evaluation of different optimization formulations is addressed in [12] where error minimization, control minimization, and mixed minimization formulation for the control allocator are discussed. The mixed minimization formulation is solved in [12] by rewriting it to a linear program formulation and solving it with the simplex method. Profound work on real-time implementation in aircraft using standard methods of constrained control allocation with optimization formulation was done in [31]. It uses active set method to solve optimized allocation problem, see also Appendix B. [31] also included a nicely packaged control allocation library for Matlab/Simulink, which has also been used, with minor modifications, in the proposed motion control system for over-actuated road vehicles presented in this the-

sis. In [46] a reconfigurable motion control system for the space manoeuvring vehicle X-40A is proposed. It uses inverse dynamics for designing the control law for roll, pitch, and yaw motion. The three desired motion accelerations were allocated on the six available motion actuators by using constrained control with a mixed optimization formulation to minimize the allocation error and the use of control signals. Most of the real-time control allocation discussed above is what one could call one-step predictors. They allocate the desired motions on the available motion actuators with consideration to the position and rate of change limits of actuators with what is attainable in one time step. However, when it is possible to include the dynamics of the motion actuators and predict several time steps ahead, a more sophisticated allocation can be performed, also called Model Predictive Control Allocation. This is used in [42] and [43] for a re-entry vehicle's guidance and control system. The sequential quadratic programming formulation is rewritten into a linear complementary problem, which can guarantee convergence to an optimal solution within a finite number of iterations if some conditions of the problem statement are fulfilled. This would open up for real time implementation of MPC-CA when the computing capacity is increased within a vehicle's control system.

3.1.2 Marine Applications

Marine vehicles, like aircraft, are also configured to be over-actuated in order to increase their manoeuvrability and performance. Typical motion actuators within marine applications are rudders and propeller or jet thrusters. Depending on whether the marine vehicle is operating on water or is a submersible, the desired motions of the vehicle can differ. However, similar to flight applications, marine vehicles are often equipped with more rudders and thrusters than needed to control the motion. One special issue when steering ships in water is that when the vehicle is travelling at low speed the rudders only generate steering force when thrust is used. This complicates the control allocation of the available motion actuators and cannot be solved with convex quadratic programming. This is addressed in [41] where an analytical solution to the non-convex rudder and propeller control allocation at low speed is proposed. Due to this non-convex control allocation problem, the allocation law is suggested to be pre-calculated offline by using multi-parametric nonlinear programming. This is done in [35] for marine surface vessels with rudders. However, the author also concludes by pointing out the weakness that the offline computed control allocation law does not easily admit online reconfiguration unless several cases are pre-computed. This means that all types of possible failures of the motion actuators have to be anticipated in advance. In [34], singularity avoidance is suggested by using a locally convex quadratic reformulation of the allocation problem. In [33], a control-Lyapunov

design approach is used to derive an optimizing nonlinear control allocation. This leads to asymptotic optimality and therefore the optimal solution is not needed to be found at each time step compared to a direct nonlinear programming approach. The singularities that occur for marine motion actuators clearly complicate the control allocation. A survey of different control allocation methods of ships and underwater vehicles is given in [24].

3.1.3 Road Vehicle Applications

The main degrees of freedom controlled in a road vehicle are the longitudinal, lateral, and yaw motions, see left the illustration in Fig 3.3. These motions are generated with different types of motion actuators. In the early days of road vehicle design, these motion actuators were solely controlled by the driver. Today, more and more of the actuator functionality is software controlled. This, in combination with newly added functionalities, such as individually controlled mechanical brakes, and the increased number of actuators, makes it possible to achieve these three basic road vehicle motions with several different inputs, see right illustration in Fig 3.3.

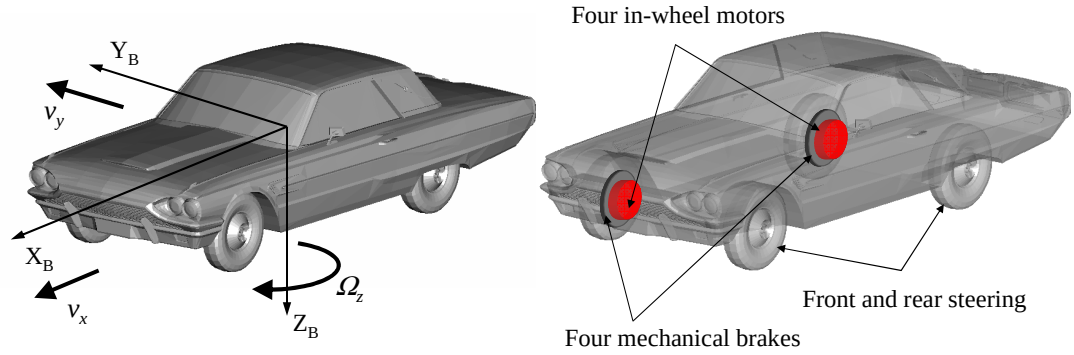

Figure 3.3: The left figure illustrates the Society of Automotive Engineers (SAE) coordinate system [51]. The symbols v_x, v_y, and ω_z correspond to vehicle's longitudinal, lateral, yaw velocities. These are the main ground motion velocities controlled for a road vehicle. The right figure illustrates a specific vehicle configuration with following motion actuators: four in-wheel motors, four mechanical brakes, and front- and rear steering. This makes a total of 10 motion actuators to generate the three ground motions. The 3D model of a 1964 Ford Thunderbird, is originally found in [2].

Contrary to flight and marine applications, road vehicles have not traditionally been viewed as over-actuated systems. Instead, different subsystems and their functionalities have coexisted to give the desired performance. These function-

alities are, for example Anti-lock Braking Systems (ABS), Electronic Stability Control (ESC), and Traction Control Systems (TCS). They have specific purposes without really viewing the complete vehicle performance. This is elegantly illustrated in [27] by using the 'ball in a bowl' analogy. The ball represents the vehicle states and how they are kept in the stable region of operation, represented by the walls of the bowl, by the system controller. In the left illustration of Fig. 3.4 it is shown how today's coexistent functionalities do not provide smooth walls on the bowl due to the fact that they only become active when the vehicle is almost unstable. Additionally, the traditional functionalities are not coordinated sufficiently to give smooth walls as illustrated in the right Fig. 3.4.

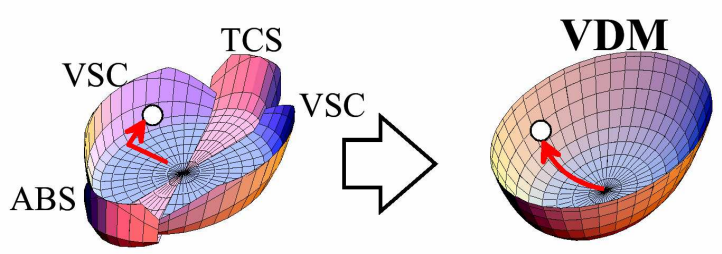

Figure 3.4: Illustration of traditional coexistent functionalities such as ABS, VSC, and TCS and their ability to keep the vehicle in the stable region (left) and how a highly integrated and coordinated control system such as Vehicle Dynamics Management (VDM) can keep the vehicle in the stable region (right). VSC means Vehicle Stability Control and has the same functionality as ESC, Electronic Stability Control. Illustration from [27].

The concept of the smooth bowl is called Vehicle Dynamics Management (VDM) in [27]. The following elements are used to achieve the VDM: hierarchical functional partitioning, feedforward force and moment control for the vehicle dynamics, and a nonlinear optimum distribution method which coordinates the operations of each motion actuator. The distribution of the global chassis forces and moment are allocated onto longitudinal and lateral wheel forces by using a optimization function which minimizes the error in global forces and minimizes the slip ratio of each wheel. In [44] and [36] different types of wheel force distributors are designed for handling a road vehicle with independently steered, driven, and braked wheels.

A quadratic programming based control allocation method is used for coordinating the available motion actuators for an over-actuated road vehicle in [50] and [49]. The allocation method is similar to what has been used within flight and marine applications. In [50] it is shown that different vehicle configurations with mechanical braking and steering were successfully allocated to achieve the desired side slip and yaw rate of the vehicle. For the side slip and yaw rate a Linear

Quadratic Regulator control law was used. However, the limits on the motion actuators included only tyre force and steering angle limits. Additionally, no detailed consideration to actual actuator limits in position or rate of change for mechanical brakes or steering was performed. In [56] yaw stabilization of road-vehicles is suggested by using control allocation. The allocation scheme is calculated offline by using multi parametric nonlinear programming similar to [35]. However, offline solutions will have difficulties to include all types of motion actuator failures that can occur to be safe and redundant.

A traction force distributor for an in-wheel motored electric vehicle is presented in [28]. Sequential quadratic programming based control allocation is used as a traction force distributor. The optimization in the control allocation is based upon error in the desired and actual slip in the wheel motors. The desired slip is based on friction estimation. In [7], inverse dynamics are used to calculate the global forces and moment of the vehicle and control allocation is used to distribute the task on to the available actuators. A least squares optimization formulation on tyre grip potential is used for the control allocator. The objective is to keep each wheel's tyre grip potential low and preferably equal.

In [52], untripped rollover prevention is proposed by using mechanical brakes. A linear control law is used for reducing the lateral acceleration. If it is higher than a certain threshold in lateral acceleration, then the control law applies the total braking force. The total braking force is then distributed onto the mechanical brakes by using weighted least squares control allocation [31]. This will prevent untripped rollover crashes but with the compromise that the vehicle must depart from the desired path to some extent. This compromise can be questioned when considering that the vast majority of all real life rollover crashes occur when a vehicle runs off the road and strikes a tripping mechanism such as soft soil, a ditch, a curb or a guardrail [4]. This is an ongoing research topic at the NHTSA and will certainly be discussed further within the active safety community.

To summarize, even though road vehicle applications were late when compared with flight applications to investigate if control allocation could be used to solve over-actuated motion control problems, previous research indicates that this is a powerful way to integrate and coordinate available actuators. However, there are also major differences in the time constants in the dynamical response of the vehicle, how the motion forces are generated, and how the forces are limited when road vehicle applications are compared with flight and marine applications. This makes it challenging to use control allocation within road vehicle applications.

3.2 System Modelling

The purpose of any system modelling is to try to build a model that represents how the physical system would behave for a certain input. The objective of the modelling in this thesis is to explore the following question: Can real-time control allocation methods, like weighted least squares [31], be used in road vehicle applications? To find an answer, the necessary dynamics and system specific time constants need to be modelled. The modelling consists mainly of three parts, motion actuators, drivetrain, and chassis, as illustrated in Fig. 3.5. These are combined together to study different vehicle configurations with different numbers and types of motion actuators.

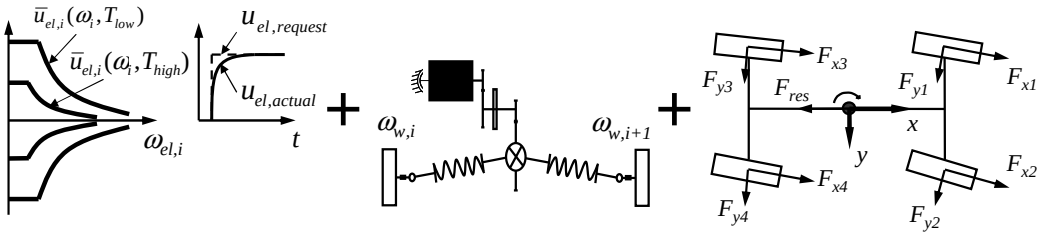

1. Actuator 2. Drive train 3. Chassis and tyre

Figure 3.5: The system modelling consists mainly of three parts: 1. Actuator modelling. Observe how limits $\overline{u}_{\text{el},i}$ are not only constrained by rotational speed $\omega_{\text{el},i}$ but also by temperature T_i. 2. Drivetrain modelling of differentials, drive shafts, gear ratios, and inertias. 3. Chassis and tyre modelling to predict vehicle's ground motion.

One important aspect of the modelling is the motion actuator's dynamics and their limits in position and rate of change. This information is crucial to achieve safe control allocation [22]. First and second order models were used to model the dynamics of the available motion actuators such as the mechanical brakes (mb), electric motors (el), internal combustion engine (ice), and steering. The disc brakes and electric motors also included a lumped mass temperature model which reduced the available actuator limits, see Paper IV. The limits in position can be described by

$$\begin{aligned} \underline{u}_{\text{el},i}(\omega_i, T_i) \leq u_{\text{el},i} \leq \overline{u}_{\text{el},i}(\omega_i, T_i) \\ \underline{u}_{\text{ice}}(\omega) \leq u_{\text{ice},i} \leq \overline{u}_{\text{ice}}(\omega) \\ \underline{u}_{\text{mb},i}(T_i) \leq u_{\text{mb},i} \leq \overline{u}_{\text{mb},i}(T_i) \end{aligned} \tag{3.1}$$

where ω_i and T_i are the angular velocity and temperature of the actuator, respectively. The limits in rate of change $[\underline{\rho}, \overline{\rho}]$ for the motion actuators modelled as a

first order system are simply a function of the time constant of the system. For a second order model the rate limits can be determined using an equivalent time constant definition as described in [40].

The modelled drivetrain configurations include the most important time constants. The inertia of the wheels, gearboxes, electric motors and their losses were included. Additionally, drive shafts were modelled as weak whenever found in configurations. Open differentials were also included in most of the configurations. Effects like inertia, power losses, weak drive shafts, and open differentials are quite important because these effects make a difference wherever a motion actuator is mounted in the topology of the drivetrain is a motion actuator mounted and assisting the motion. For example, an electric motor mounted between the combustion engine and gear box introduces more delays and losses when assisting in traction and braking than with a wheel mounted electric motor.

The chassis model developed for this study is a so-called two track model which has five degrees of freedom: longitudinal, lateral, yaw, roll, and pitch motions. The aim of the model is to be capable of predicting the chassis dynamics on flat surfaces. The SAE standard coordinate system [51] provided the main guidance for defining the axis orientations. A brush tyre model [47] was used together with dynamic relaxation to describe the tyre dynamics. The chassis parameters correspond to those of a medium sized sedan car. Details about the modelling and used parameters can be found in Paper IV.

The vehicle configurations were selected to represent a wide variety of drivetrains, from a conventional vehicle to a parallel HEV with electric four wheel drive and a series HEV propelled by in-wheel motors, see Fig 3.6. The models are implemented as first level s-functions in the Matlab/Simulink environment. A summary of the four vehicle configurations is presented below:

1. *Conventional vehicle 1 (CV1).* The combustion engine has 133 kW at 6000 rpm as the maximum output power and a maximum torque of 230 Nm. It is connected to the front wheels via an open differential (1 input). This model has individual mechanical braking (4-inputs) which gives a total of 5 inputs to control the braking and traction. Used in Paper VII.

2. *Conventional vehicle 2 (CV2).* Same as CV1 but front and rear rack steering are also included in the control allocation, resulting in 2 additional inputs. This gives a total of 7 inputs to control the traction and braking. Used in Papers IV-V.

3. *Parallel HEV with electric four wheel drive (HEV E4WD).* Every wheel has individual mechanical braking (4-inputs). The rear axle has an electric motor of 50 kW connected by an open differential (1-input). The front wheels are connected to an open differential which connects to an Integrated Starter

Generator (ISG) of 11 kW located between the gear box and combustion engine, same as CV (2-inputs). Front and rear rack steering is also included (2-input). This model is seen as a 9-input configuration. Used in Papers IV-V.

4. *Series HEV with wheel motors (HEV WM)*. Every wheel has individual mechanical braking (4-inputs) and is also equipped with wheel motors of 40 kW (4-inputs). An extra energy source such as a fuel cell is needed to allow a continuous output power of 30 kW. The continuous power is sufficient to overcome the resistance forces at a constant speed of 130 km/h. The total output power is 30 kW plus 135 kW when the battery buffer mass of 90 kg is selected. It also includes front and rear rack steering (2-inputs). This model is seen as an 10-input configuration. Used in Papers IV-VI.

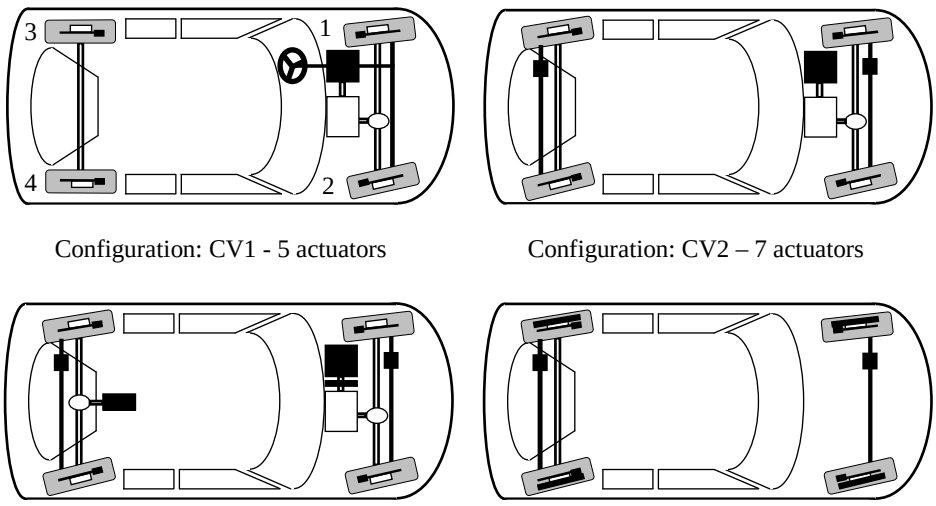

Configuration: CV1 - 5 actuators

Configuration: CV2 – 7 actuators

Configuration: HEV E4WD – 9 actuators

Configuration: HEV WM – 10 actuators

Figure 3.6: Illustration of the four modelled vehicle configurations. The black boxes indicate motion actuators. The numbering 1 to 4 on configuration CV1 indicate the order of the wheels which is also used for the numbering of the actuators.

3.3 Control Design

The design of the proposed reconfigurable motion control system is illustrated in Fig. 3.7. It is useful to begin with a comparison with Fig. 3.2 which is a basic layout of a control system where control allocation is included. The gray shaded boxes in the illustrations are comparable. This shows that the motion control system consists mainly of a path controller and a control allocator, compare also with Fig. 2.7. Desired inputs includes the driver interpreter, energy management, and steering. The control system and the functionality of its smaller functions will be explained in greater detail ahead.

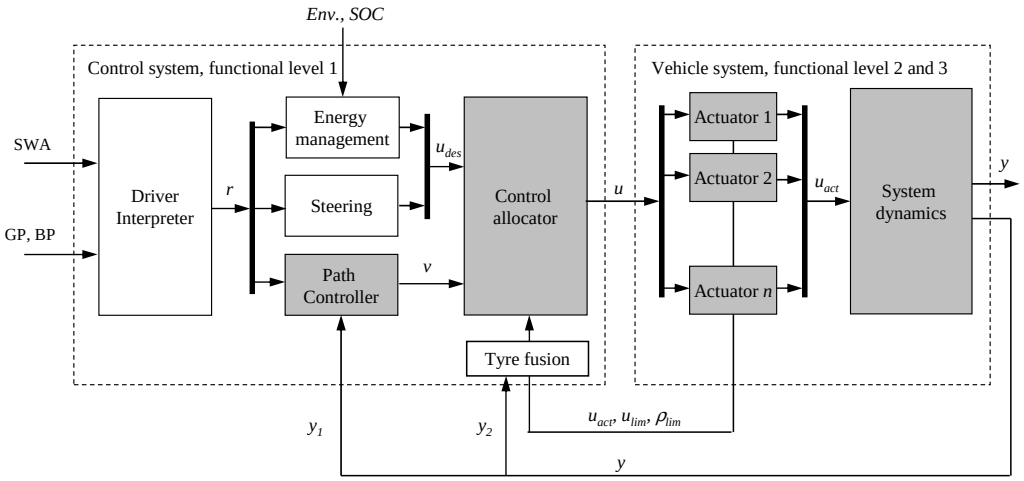

Figure 3.7: Illustration of how the proposed reconfigurable motion control system would be designed for a future HEV which also includes steer by wire. The gray shaded boxes illustrate the similarities with the more basic illustration Fig. 3.2. Used abbreviations include Brake Pedal (BP), Gas Pedal (GP), Steering Wheel Angle (SWA), Environment (Env.), State of Charge (SOC). Illustration from Paper VI.

The separation of the path controller from the control allocator is the key issue and will be explained first. Independent of the specific applications studied, a class of nonlinear systems can be described in the affine form

$$\dot{x} = f(x) + g(x)\,u \tag{3.2}$$

$$y = h(x)\,. \tag{3.3}$$

Control allocation can be applied if the control input can be perturbed without

affecting the system dynamics. The system can therefore be rewritten as

$$\dot{x} = f(x) + v \tag{3.4}$$
$$y = h(x) \tag{3.5}$$

where $v = g(x)u$, v is also called the virtual control input. The control design can be divided into two steps. The first step is to design a control law that controls the virtual control input $v \in R^k$. The second step is to design a control allocator that maps the virtual control input to true control input, $v(t) \mapsto u(t)$, where $u \in R^m$ and $k < m$. This separation of $f(x)$ and $g(x)u = v$ is shown in Papers IV-V for road vehicle configurations where steering is included in the control allocation. In Paper VII the separation is shown for a configuration where the driver is solely controlling the steering.

3.3.1 Desired Input

The desired input functionality in the proposed motion control system can be seen as feedforward-like controllers. The desired input part consists of the driver interpreter, energy management, and optionally steering if it is included in the control allocation.

Driver Interpreter

The driver interpreter uses the driver input and a reference model of the road vehicle to derive the desired path $r = \left[\begin{array}{ccc} v_x & v_y & \omega_z \end{array} \right]^T$. By using friction estimation, limits in maximum yaw rate, for example, can be calculated here. A novel proposal of how a driver interpreter could be realised for a vehicle configuration where the driver controls the steering is presented in Paper VII. The driver interpreter used a bicycle model to calculate the desired yaw rate ω_z. This yaw rate was limited by the maximum yaw rate allowed by the tyre/road friction. When front and rear wheel steering are included in the motion control system it raises the question how the desired path of the vehicle should be defined. A vehicle configured with independent front and rear rack steering can move sideways without any yaw rate $\omega_z = 0$ or be turning without any lateral velocity $v_y = 0$ meaning that the side slip of the vehicle is kept at zero. This is a quite complicated matter and has therefore been left out from the scope of this study. Therefore, when steering is included in the control system the reference signal r is said to be known. This is the case in Papers IV-VI.

Energy Management

The objective of the energy management function is to minimize fuel consumption and assure power availability at any time. A standard energy management function considers only the actual State Of Charge (SOC) and vehicle speed and acceleration to calculate if the buffer should be charged or not. A finite state machine energy management function was implemented in Paper VI. By calculating how much buffer power is desired one also determines the desired use of the electric motors during braking and acceleration. The desired use of electric motors, combustion engine, and mechanical brakes is the first part of the u_{des} vector illustrated in Fig. 3.7, see Paper VI for further details. More information about energy management can be found in [29].

More complex energy management functions would also include information about the driving route, topography, and traffic information. This information is used in a predictive control sense [32]. Such energy management algorithms also fit well into the proposed motion control system.

Steering

A steering function is suggested to be included in vehicles with steer-by-wire. The steering function calculates the desired steering angle(s), which are the second and last part of the u_{des} vector illustrated in Fig. 3.7. In Paper VI a bicycle model was used to identify the steering angles needed for the front and rear wheels to achieve the desired lateral and yaw motions.

3.3.2 Feedback Path Controller

The purpose of the feedback path controller is to keep the vehicle on the desired path. The error in the path $e = r - y_1$ is used to calculate the desired global longitudinal and lateral forces and yaw moment $v = \left[\begin{array}{ccc} F_x & F_y & M_z \end{array} \right]^T$ of the vehicle, see also Fig. 3.7. Different control laws could be used to achieve this. In Papers IV-VII standard PI controllers with anti-wind up strategy were found to work sufficiently [54]. More advanced path controllers have used an inverse dynamics of the system to calculate v [7]. In a flight application a PID controller was complemented with an inverse dynamics controller [46] to control the desired roll, pitch, and yaw accelerations.

3.3.3 Control Allocation

Control allocation is an option for coordination when one has more input signals $u \in R^m$ than virtual signals controlled $v \in R^k, k < m$. The basic theory of

control allocation is given in Appendix B. The idea is to map the virtual control input onto u, $v \mapsto u$. If $g(x)u$ in Eq. 3.3 can be linearised then it can be rewritten as $g(x)u \approx Bu$. Then the mapping can be described by a control effectiveness matrix B with size $k \times m$ and rank k

$$Bu\,(t) = v\,(t)\,. \tag{3.6}$$

Now the key issue is how to select the control input set u from all possible combinations. Here a constrained optimization formulation is used to achieve the allocation. The limits in position $\overline{u}$ and rate $\overline{\rho}$ constrain the feasible solution of u. In addition a two-step optimization problem, sequential least squares (sls), is used to for the mapping

$$u = \arg \underbrace{\min}_{u \in \Omega} \|W_u(u - u_{des})\|_p \tag{3.7}$$

$$\Omega = \arg \underbrace{\min}_{\underline{u} \leq u \leq \overline{u}} \|W_v(Bu - v)\|_p \tag{3.8}$$

where W_u and W_v are weighting matrices and u_{des} is the desired control input [31]. The two step optimization problem is well suited for FCVs and HEVs. Eq. 3.8 constrains the possible set $u \in \Omega$ to be only u's that will be in nullspace of $N(Bu - v)$ or minimize the error of the desired forces, $Bu - v$, needed for fulfilling the desired motion of the vehicle. This can be seen as the vehicle motion controller. Eq. 3.7 minimizes the error of the desired control input, $u_{des} - u$. The desired control input, u_{des}, coming from the energy management and steering controller, specifies how the motion actuators should be used when optimizing the use of onboard energy. This can be seen as a smooth arbitration between energy management and vehicle motion control. Numerically Eqs. 3.7- 3.8 can also be solved in one step, using weighted least squares (wls),

$$u = \arg \underbrace{\min}_{\underline{u} \leq u \leq \overline{u}} \|W_u(u - u_{des})\|_p + \gamma \|W_v(Bu - v)\|_p. \tag{3.9}$$

where $p = 2$. Setting the weighting parameter γ to a high value gives priority to minimize the error in motion $Bu - v$. The wls formulation was used in Papers IV-VII. A small comparison of using wls and sls was done in Paper VI.

Motion Actuator Limits

The control allocator receives the limits from the motion related actuators, $[\underline{u}(t), \overline{u}(t)]$ and their limits in rate of change $[\underline{\rho}, \overline{\rho}]$, as illustrated in Fig. 3.7. This specific way of designing the control system allows the control law to be independent of the available actuators, which makes the controller reusable for different hardware

configurations, and also allows the control allocator to handle both limits and even actuator failure. The rate limits can be rewritten as position constraints using an approximation of the time derivative. The position constraints can now be written as

$$\overline{u}(t) = \min\left(\overline{u}(t), u(t - t_T) + t_T\overline{\rho}\right) \tag{3.10}$$

$$\underline{u}(t) = \max\left(\underline{u}(t), u(t - t_T) + t_T\underline{\rho}\right) \tag{3.11}$$

where t_T is the sampling time.

Tyre Fusion

For road vehicles there are additional limits that need to be considered, such as how much longitudinal and lateral force can be applied on each wheel. In the proposed system the actuator limits are limited once more by the 'tyre fusion' function, see Fig. 3.7. Tyre fusion would need estimates of each tyre's actual friction and the vehicle's velocities and accelerations to calculate each wheel's normal force distribution. This is illustrated by the feedback y_2 in Fig. 3.7. The force limits of each tyre are a function of friction and normal force. When the tyre force limits are calculated they are used to verify if actuator limits need to be reduced. When several motion actuators are connected to one wheel the following priority order of the traction and braking actuators is proposed:

1. Electric motor
2. Combustion engine
3. Mechanical brakes

The idea is to always let the electric propulsion receive the maximum of available tyre force limits. When the limits of the electric motor are less than the maximum wheel forces the difference is given to the next actuator on the list. This is illustrated in Fig. 3.8 where an electric motor is connected to two wheels by an open differential and each wheel also has individual mechanical brakes. The longitudinal tyre force limits are received by estimating the actual lateral force used on each tyre. More details about tyre fusion functionality for the studied vehicle configurations can be found in Paper V.

3.4 Main Benefits and Considerations

The main benefits of the proposed system is that it is offline and online reconfigurable. Another main benefit is the optimization formulation used within the

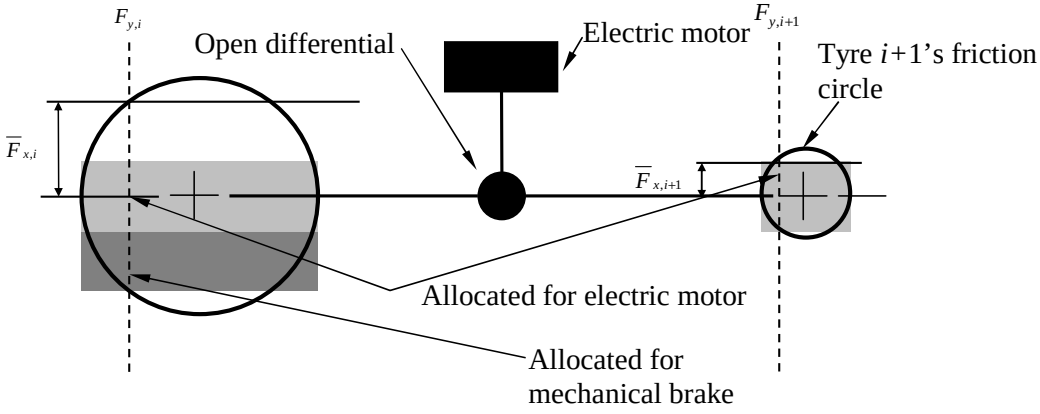

Figure 3.8: Illustration of how tyre fusion considers the case of an electric motor is connected to two wheels by an open differential with individual mechanical brakes. This is comparable to vehicle configuration HEV E4WD's rear axle. Dashed lines illustrate actual lateral force F_y. From Paper V.

control allocator which allows the vehicle motion control to be prioritized higher than energy management at all times, see Eq. 3.9. This means that, when needed, the true control input u can smoothly divert from the desired input signals u_{des} calculated by energy management and steering, see also Fig. 3.7. The main considerations are the need for correct information from the motion actuators about their actual limits in position and rate of change and the estimation of tyre force limits. Other considerations are the sensitivities of slow or highly nonlinear actuators.

3.4.1 Main Benefits

This section starts out by giving a summary of the statements motivating the use of the control allocation scheme within the proposed motion control system

a) It is fast and gives both a feasible solution at each time step and an optimum solution in a finite number of time steps. This is achieved by using the active set method for solving the control allocation problem.

b) The optimization formulation includes both the minimization of the control error $u - u_{des}$ and the allocation error $Bu - v$, which has been shown to be a viable option for hybrid electric vehicles, see Paper VI.

c) Even though when the tyre force and actuator limits combined are nonlinear constraints, these can be linearised at each time step, allowing the selected control allocation scheme to be used, see also Paper V.

d) Even though $g(x)u$ is approximated by $B(x)u$, it has shown to be sufficient for a wide range of vehicle configurations, see Papers IV-VII.

e) The selected allocation scheme, developed by [31], using least squares, norm 2, in the objective function, has been found to be very robust and uses more actuators simultaneously when compared with using norm 1 in the objective function. Using norm 2 makes the allocation less sensitive for actuator failure because it already uses several actuators [48].

Offline Reconfigurable

The proposed motion control system is easily reconfigured for different vehicle configurations. The control law for the path controller can be the same for different vehicle configurations. In Papers IV-V it was shown that the same control law could be used for vehicle configurations CV2, HEV E4WD, and HEV WM without even changing the control parameters of the PI controller. The separation of the control law and control allocation gives this specific benefit. The control allocator is easily reconfigured for different vehicle models. The only parts that need to be changed in the control system are the control effectiveness matrix B, weighting matrices W_u for the desired signals, see Eq. 3.9, the limits in position and rate of change for the added motion actuators, and finally the 'tyre fusion' function for the specific configuration.

If the inertia of the system is neglected when applying the input to the actuators the approximation $g(x)u \approx Bu$ can be used. The control effectiveness matrix basically describes how effective each actuator is in generating the virtual control input v

$$\underbrace{\begin{bmatrix} F_x \\ F_y \\ M_z \end{bmatrix}}_{v} = \underbrace{\begin{bmatrix} b_{11} & \dots & b_{1i} & \dots & b_{1m} \\ b_{21} & \dots & b_{1i} & \dots & b_{2m} \\ b_{31} & \dots & b_{1i} & \dots & b_{3m} \end{bmatrix}}_{B_{\text{vehicle configuration}}} \underbrace{\begin{bmatrix} u_1 \\ \vdots \\ u_i \\ \vdots \\ u_m \end{bmatrix}}_{u} \tag{3.12}$$

where the elements $b_{j,i}$ are the influence of the i$^{\text{th}}$ actuator on the j$^{\text{th}}$ global force or moment. $m > 3$ is the number of motion actuators available in the studied configuration. In Papers IV-V B-matrices for vehicle configuration CV2, HEV E4WD, and HEV WM are derived and in Paper VII the B-matrix for CV1 is derived.

The diagonal weighting matrix W_u is a design parameter which need to be considered. It is important to attempt to penalize the use of actuators in a way that

makes brake/traction load distribution on the front and rear axles appealing from a vehicle stability point of view. When braking, for example, the use of the front brakes should be penalized lower in W_u than the rear brakes. Another aspect is that the order in which the actuators are blended is directly controlled in W_u. In Papers IV-VI the electric motors are penalized less than the mechanical brakes. Then the electric motors are more likely to be used and the mechanical brakes are blended in when needed. In Paper VI $W_u(v)$ was designed to be scaled linearly depending on the desired longitudinal force of the vehicle $v_1 = F_x$.

Online Reconfigurable

The limits in position and rate of change of each motion actuator and its ability to achieve specific tyre forces give the ultimate constraints for the control allocator. Updated information about the actual limits needs to be sent back to the control allocator as illustrated in Fig. 3.7. This allows the control allocator to automatically re-distribute between available motion actuators if they become saturated or even fail. How limits in position and rate of change can be calculated by actuator reference models is shown in Paper IV.

Another important online reconfiguration feature is the smooth arbitration between energy management and vehicle motion control at all times. This is provided by the optimization formulation within the control allocator, see Chapter 3.3.3. This is crucial for hybrid electric vehicles to allow for correct blending of the electric motors and to preserve vehicle stability at all times. In Paper VI this smooth arbitration is exemplified for vehicle configuration HEV WM.

3.4.2 Considerations

Information

One consideration when using control allocation is the fact that correct information about what abilities each motion actuator has at each new allocation time step is needed. This information exchange from lower control functions is not clearly standardized between suppliers of motion actuators and auto manufacturers, see Fig. 3.9 for an illustration.

Actuator information is crucial for any type of successful coordination within a hierarchical control system. For example, a supplier that provides electric motors should also include a local controller that sends actual input achieved and updated limits and rates of torque. For an electric motor, states such as the rotational speed and temperature would reduce the limits. This is also important from a responsibility point of view. The electric motor will not be used above its capacity according to limits provided from the supplier developed local controller. A

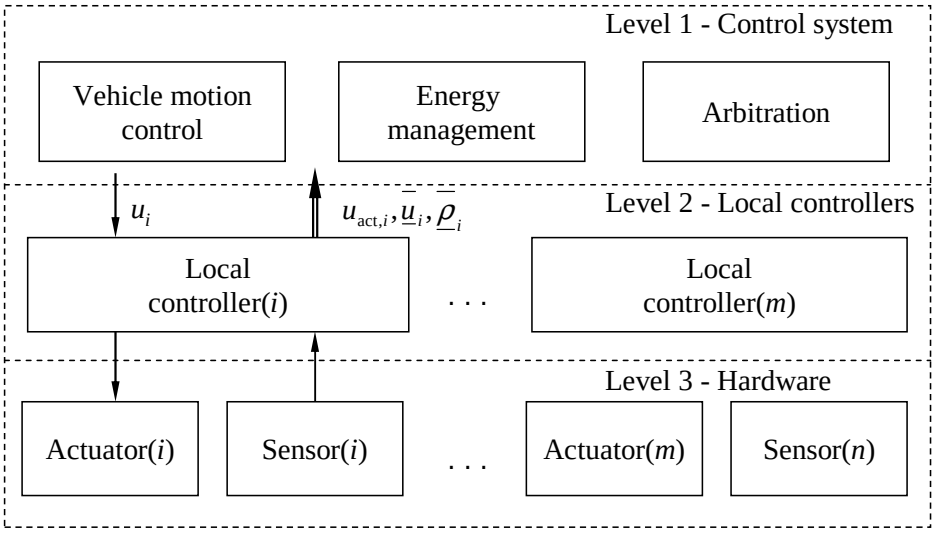

Figure 3.9: Illustration of functional levels within a vehicle system controller and the information about limits in position and rate of change from each motion actuator.

novel suggestion on how these limits are made rotational speed and temperature dependent for a permanent magnet synchronous motor is provided in Paper IV.

Updated and sufficient estimations for each wheel's tyre/road friction and reliable estimates of the normal force distribution between the available wheels are needed. Friction estimation is a highly prioritized research topic. However, if the friction estimation is not updated fast enough the author suggests that the wheel's longitudinal slip is used in addition to the friction estimation within tyre fusion to control the limits of the mounted motion actuators for the considered wheels.

Information about actuator failure should also be properly addressed. This can be done by using a observer model that calculates what the motion actuator should have performed for a certain input. If the observer model's output differs significantly from the actual output from the motion actuator the author suggests that the limits are set equal to zero if the actuator is not responding. If the actuator is stuck in a certain position, jamming brakes, for example, the limits of the actuator should be reduced to be equal to the jam torque. This informs the control allocator which can then account for and counteract the jamming brake.

Highly Nonlinear Dynamics

Highly nonlinear dynamics is one of the most sensitive issues of control allocation. The mapping from virtual control input to actuator input is simplified by using the linearization of $g(x)u \approx Bu$. However, there are times when the $g(x)$ term is

highly nonlinear, for example when gear shifting is performed. When the clutch is open some motion actuators will not have any effectiveness to accomplish the desired global forces and moment v. This can be accomplished by letting the $B(x)$-matrix become vehicle state x dependent. This was done in Paper VI which illustrated how gear shifting can be accounted for within the control allocator. Another example, found in Papers IV-VI, is that the steering is assumed to have linear cornering stiffness within B. This could be modified by using a nonlinear cornering stiffness inside the vehicle state dependent $B(x)$-matrix.

Slow Actuators

The use of slow actuators should be avoided. A good example is the introduction of steer-by-wire in production road vehicles. It is important that the steering actuators are made fast enough so that catastrophic driver induced oscillations, similar to what have been seen in flight applications can be avoided, [22]. If really slow steering actuators are used, the driver will not get the response he is expecting. If the driver then starts to turn the steering wheel back and forth and the system is responding too late, the result is driver induced oscillations. It is also important to give correct feedback to the driver by resistance in the steering wheel which matches the time constant of the steering actuators. Effects on how steering gain, steering response, and steering torque should be applied to give 'good' driver's feeling are studied in [16] and [30].

3.5 Suggested Approach for Implementation

The proposed motion control system has shown that it can be used for a wide variety of vehicle configurations and can handle both conventional and hybrid electric vehicles, see Papers IV-VI. It has also been shown in Paper VII that the control system passes the proposed test procedure for ESC. It could be a natural first step for implementation to use part of the proposed motion control system as an ESC system in a conventional road vehicle. The conventional vehicle is assumed to have five motion actuators, combustion engine and individually controlled mechanical brakes, to achieve the correcting yaw torque. Then when over-actuation increases with increased number of available motion actuators, the full version of the proposed motion control system could be implemented, see also Fig. 3.10 for illustration.

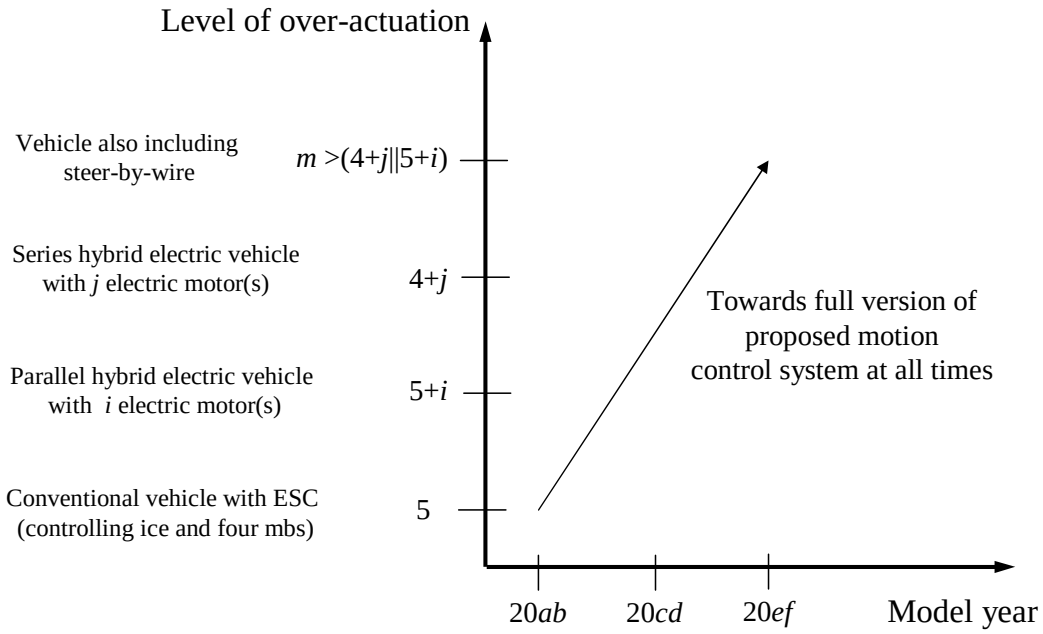

Figure 3.10: Illustration of how the proposed motion control system could be implemented.

Chapter 4

Simulations and Results

This chapter shows through simulations that the system requirements defined in Motivation Chapter 1.2 are fulfilled by the proposed motion control system described in Control Design Chapter 3.3.

A simulation platform was built in Matlab/Simulink to validate the proposed reconfigurable motion control system. The overall aim was to show that even though a linearised control effectiveness matrix $Bu \approx g(x)u$ was used, it achieved the desired performance on a nonlinear system modelled as $\dot{x} = f(x) + g(x)u$. This is one of the key issues when using control allocation, especially for road vehicles where nonlinearities are found in the motion actuators themselves. The nonlinearities in the drivetrain, chassis, and tyres, independently or in combination, influence the final effectiveness of each actuator u_i.

The simulations and the results presented in this chapter are presented from the point of view of the system requirements, see Chapter 1.2. The outline of the Chapter is as follows:

- Section 4.1 addresses system requirement one; the integration and coordination of the available motion actuators to their full potential to achieve the desired ground motion.
- Section 4.2 addresses system requirement two; energy efficient coordination with priority on vehicle stability.
- Section 4.3 addresses system requirement three; online adaptivity for sudden changes in the environment or saturation and failure among the available actuators.
- Section 4.4 addresses system requirement four; the proposed control system is reusable for several vehicle configurations.

- Section 4.5 discusses robustness for vehicle parameter changes.
- Finally, Section 4.6 contains concluding remarks about the presented simulations and results.

4.1 Integration and Coordination of the Available Motion Actuators

Two test procedures are used to illustrate how the proposed motion control system functions on this requirement. The first test procedure is the proposed standard test by the NHTSA [4] for Electronic Stability Control systems, sine-with-dwell. It is shown that the NHTSA ESC test is passed by the proposed control allocation based controller. The second test procedure is circle driving with low constant acceleration on low friction. This illustrates how the motion control system uses available motion actuators for three different vehicle configurations when the vehicle velocity is reaching the physical limit that can be used to keep the circle constant.

4.1.1 Sine-with-Dwell

This section gives a short review of the results found in Paper VII. The aim with the simulations is to show that the proposed motion control system functions also as an Electronic Stability Control System for a conventional vehicle. The steering angle is given as input for the test procedure and is therefore only applicable on vehicle configuration CV1, see Chapter 3.2. Because of this, the proposed motion control system is reduced to not include steering in the control allocation as illustrated in Fig. 4.1.

The configuration is front wheel steered by the driver. The modelling of the motion actuators, chassis, tyre, and drivetrain are shown in Paper IV. Verification simulations were also made with a commercially available Vehicle Dynamics Library(VDL) [3] to assure that the proposed motion control system functions on a system not developed by the author.

Assumptions

The control system is assumed to control the combustion engine and the mechanical brakes at each wheel, giving a total of five motion actuators. The tyre/road friction is assumed to be equal to 1. This is assumed to be known by the driver interpreter, which uses a linear bicycle model to calculate the reference yaw rate. The reference yaw rate was limited by the attainable maximum yaw rate at tyre/road

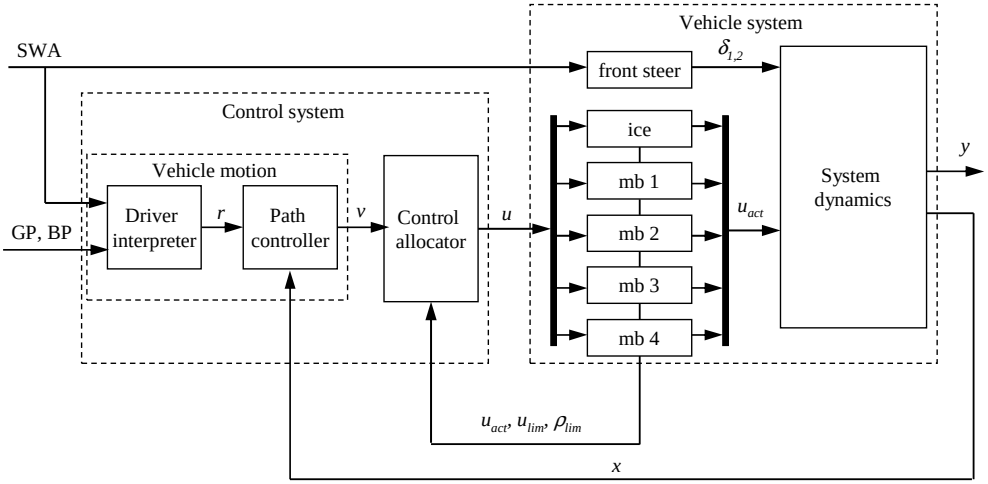

Figure 4.1: Illustration of how control allocation is suggested to be used within the control system for a conventional road vehicle. Observe how the Steering Wheel Angle (SWA) is passed directly through to system dynamics. Used abbreviations include Brake Pedal (BP), Gas Pedal (GP), internal combustion engine (ice), and mechanical brakes (mb). Illustration from Paper VII.

friction 1. The steering input, sine-with-dwell is assumed to be given directly to the motion actuators within the modelled system, see Fig. 4.2. The control effectiveness matrix $B \in R^{3\times5}$ is assumed to be linear. This means that no inertia effects or nonlinearities are accounted for in the control system for the mapping of the virtual control input into the true control input of the motion actuators $v \mapsto u$. However, the system modelled and controlled includes nonlinearities which are found in actuators, chassis, tyres, and drivetrains. Weighting matrices W_u and W_v in the control allocation scheme are kept constant, and the desired control input u_{des} for the motion control actuator is given as a zero vector, see also Chapter 3.3.3.

Overall Results

The vehicles equipped with the proposed motion control system pass the NHTSA standard test procedure for ESC. In Fig. 4.2 the resulting yaw rates for different SWA amplitudes are shown for the chassis modelled according to Paper IV. The ESC system is on and the max amplitude of the Steering Wheel Angle (SWA) is varied between 100 and 270 degrees. The black dots indicate the two stability criteria that need to be fulfilled. The results show that yaw rates are well below the these black dots.

The results are also confirmed with a commercially available chassis and tyre

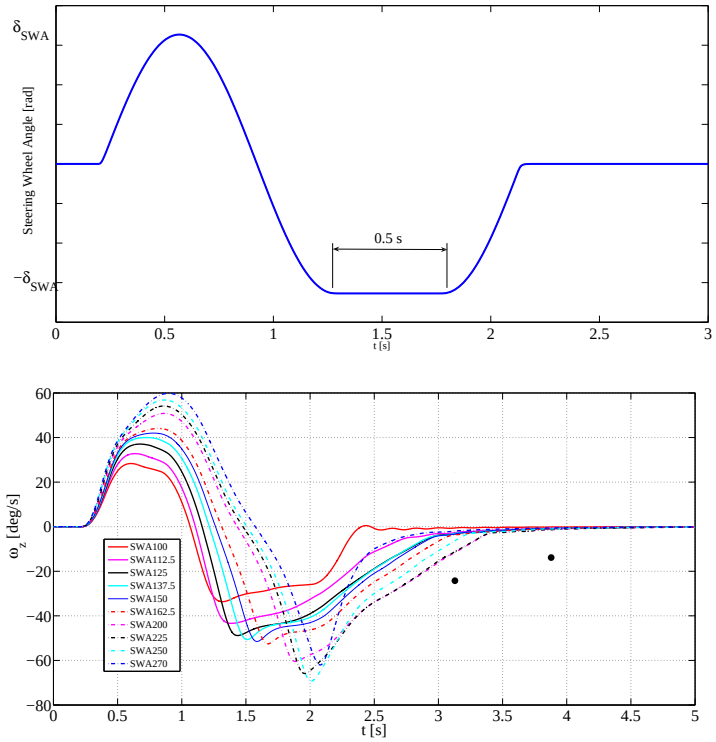

Figure 4.2: SWA input as function of time (upper plot) and yaw rate results (lower plot) for Chassis modelled according to Paper IV when ESC is active. SWA max amplitude was varied between 100-270 degrees. Results from Paper VII.

model [3]. No changes in the control system's parameters were made when the chassis was switched. The only modification was to change the signs of the lateral velocity and yaw rate when the VDL model was used. This is due to the fact that the VDL chassis is modelled with ISO coordinates whereas the chassis in Paper IV uses SAE coordinates.

Detailed Results

The simulation results show not only that the mechanical brakes are mainly applied on one side of the vehicle at a time, but also that the combustion engine is used which gives positive torque on one of the front wheels when the other is locked by the mechanical brakes, see Fig. 8 in Paper VII. The use of the combustion engine was also switched off by sending a maximum torque limit of zero to the control allocator. The new vehicle configuration still passes the test procedure. The VDL chassis is actually easier to control and the probable reason for this is

that the elasticity modelled in the steering makes the vehicle a bit more understeered. This is shown in that the vehicle handled a SWA of 137.5 degrees when ESC was switched off in comparison to the chassis modelled, according to Paper IV, which only handled a SWA of 75 degrees.

4.1.2 Circle Driving with Constant Longitudinal Acceleration

In this test procedure the aim is to see how the proposed motion control system's control allocator manages three different vehicle configurations, CV2, HEV E4WD, and HEV WM, see Chapter 3.2 for configuration details, when the path controller is kept unchanged. The selected test procedure is circle driving with constant acceleration of 0.05g with a driving radius of 200 m and the tyre/road friction set to 0.3. The aim is to study how close each configuration can come to the limiting velocity and how the control allocator uses the available motion actuators. The limiting v_{lim} velocity can be calculated as

$$\begin{aligned} F_{fric} = F_{centripetal} \Leftrightarrow \mu \cdot m \cdot g = \frac{m \cdot v_{init}^2}{R} \\ v_{lim} = \sqrt{\mu \cdot g \cdot R} = 24.26 \text{ m/s.} \end{aligned} \tag{4.1}$$

The control system not only controls the tractive and braking motion actuators, but also the front and rear steering actuators. The simulations presented here are found in Paper V.

Assumptions

The control system is assumed to know the actual friction and to be able to properly estimate each tyre's force limits. This information is used within the tyre fusion function to combine the limits of the motion actuators with the tyre forces. The weighting matrices W_u and W_v are kept constant in addition to the control effectiveness matrix $B(x)$. The desired control input for the motion actuators u_{des} was set equal to a zero vector.

Overall Results

The most interesting result is that even though different vehicle configurations are used, the proposed motion control system handles each configuration quite well. Fig. 4.1.2 shows the reference and simulated longitudinal, lateral, and yaw velocities for the three configurations CV2, HEV E4WD, and HEV WM. It can be noted that all three configurations reach about 90 percent of the maximum speed before they start to diverge from the reference yaw velocity. Another interesting observation is that configuration CV2, with only a combustion engine connected to the front wheels, starts to use the mechanical brakes when the vehicle is almost reaching the critical velocity, which can be seen by the oscillations occurring at about 18 seconds in lateral velocity and yaw rate.

Detailed Results

In Fig. 4.4 the use of the actuators and their combined limits are shown for CV2. Observe how actuator 1, the combustion engine, increases the tractive torque when the mechanical brakes, actuators 3 and 5, are beginning to be used as yaw stabilizing actuators at time 15 s. This is basically what today's ESC systems do, however here it is automatically performed by the control allocator. The actuators and their combined limits for configuration HEV E4WD and HEV WM during the test procedure are shown in Fig. 4.5 and Fig. 4.6 respectively. In configuration HEV E4WD the electric motors, actuators 2 and 3, are mainly used for traction, but the combustion engine, actuator 1, is also used. The mechanical brakes are not used at all as yaw stabilizing actuators in comparison to configuration CV2. Similar behaviour could be observed for HEV WM. More details about the results can be found in Paper V.

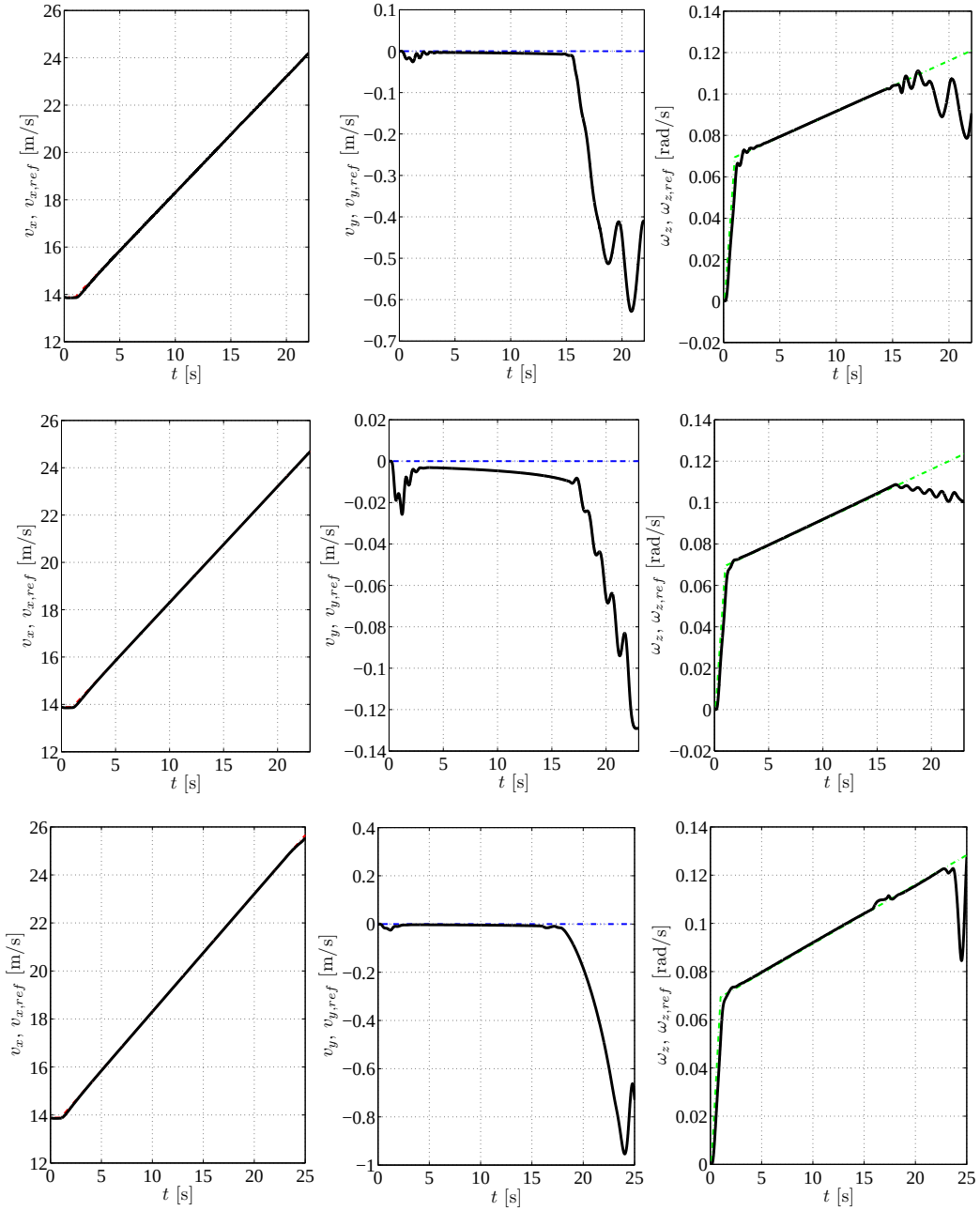

Figure 4.3: Longitudinal v_x, lateral v_y, and yaw ω_z velocities for configuration CV2 (top), HEV E4WD (middle), and HEV WM (bottom) respectively during test procedure constant circle.

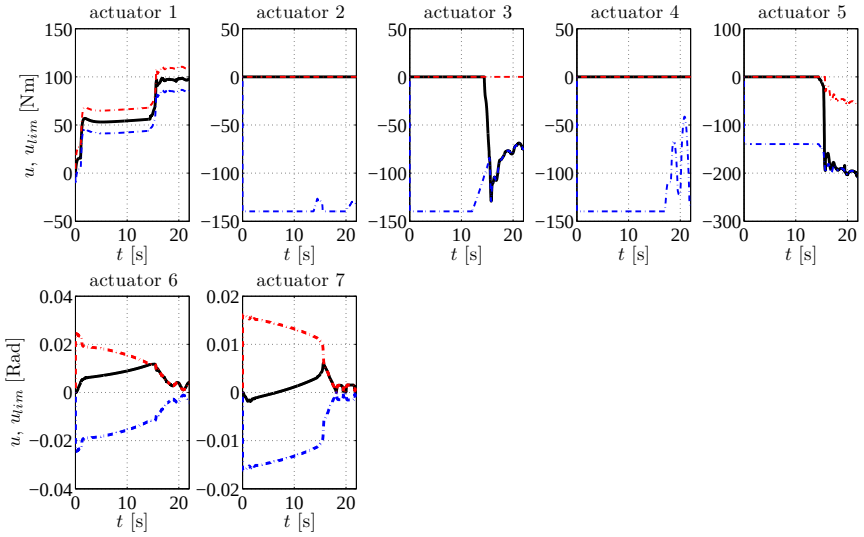

Figure 4.4: Input set u and its limits for configuration CV2 during test procedure constant circle. The black solid line represents actual u, while the dashed red and blue lines represent upper and lower combined limit respectively. Actuator numbering 1: combustion engine, 2-5: mechanical brakes, 6-7: front and rear steer.

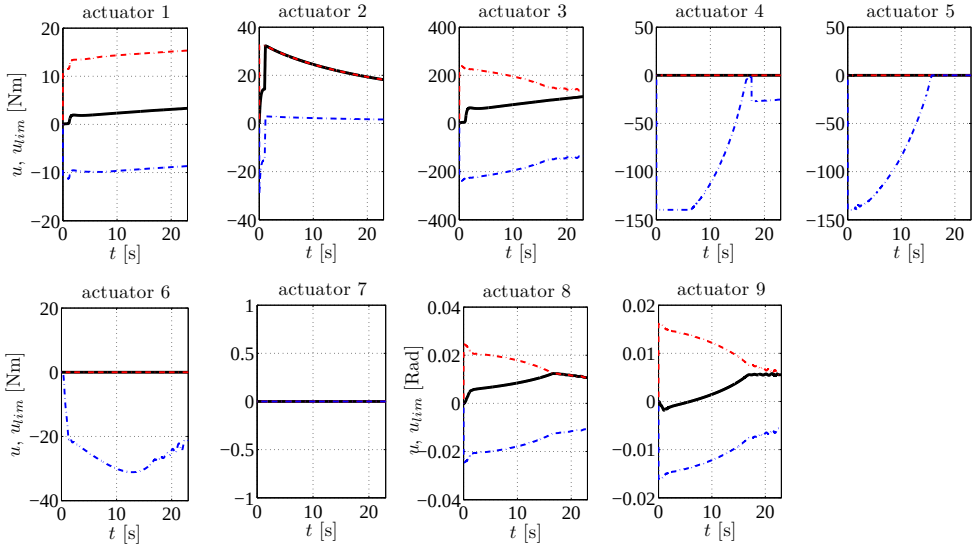

Figure 4.5: Input set u and its limits for configuration HEV E4WD during test procedure constant circle. The black solid lines represent actual u, while the dashed red and blue lines represent upper and lower combined limit respectively. Actuator numbering 1: combustion engine, 2: integrated starter generator, 3: rear axle motor, 4-7: mechanical brakes, 8-9: front and rear steer.

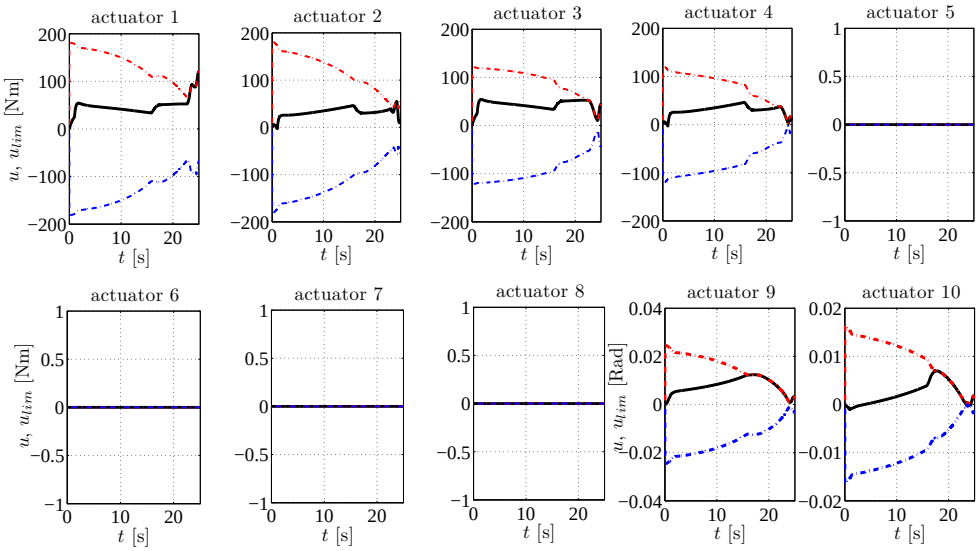

Figure 4.6: Input set u and its limits for configuration HEV WM during test procedure constant circle. The black solid lines represents actual u, while the dashed red and blue lines represent upper and lower combined limits, respectively. Actuator numbering 1-4: wheel motors, 5-8: mechanical brakes, 9-10: front and rear steer.

4.2 Energy Efficient Coordination of the Available Motion Actuators with Priority on Vehicle Stability

Constrained control allocation with mixed optimization formulation is used for solving the over-actuated HEV problem to allow smooth arbitration between desired inputs from energy management and vehicle motion control. This will be illustrated for vehicle configuration HEV WM, see Chapter 3.2 for configuration details. Two test procedures are used for illustration. The first is straight braking with different deceleration demands. The second is cruising at a fixed velocity and slowly increasing yaw rate up to the friction limited yaw rate. The aim is to show how true control input is smoothly diverted from the desired control input from energy management and steering law for front and rear wheels when needed. Details about Energy Management its finite state machine and used rules, and the steering law can be found in Paper VI. In these simulations the complete complexity of the proposed motion control system as illustrated in Fig. 3.7, is used.

4.2.1 Straight Braking

The purpose with this test procedure is to change the deceleration during straight braking on asphalt with a friction of 1.0. The initial velocity was set to 100 km/h. The first part begins with soft braking of -0.1g until 80 km/h is reached then applies hard braking of -0.8g until 40 km/h is reached. The final part of the braking is performed with -0.1g again until standstill. This is done to trigger re-generative braking in the first part, then blended braking in the second part and then again re-generative braking for the final part. This was done for the vehicle configuration HEV WM. This test procedure is also presented in Paper VI.

Assumptions

The control system is assumed to know the actual friction and to be able to properly estimate each tyre's force limits. This information is used within the tyre fusion function to combine the limits of the motion actuators with the tyre forces. The weighting matrix $W_u(v)$ is linearly weighted against the desired global longitudinal force. This will influence whether the front or rear motors are penalized. The weighting matrix W_v is kept constant in addition the control effectiveness matrix B. The desired control input for the motion actuators u_{des} is decided by the energy management and steering law. Further details can be found in Paper VI. The wheel motor and disc brakes have an initial temperature of 30 ^{o}C. The

initial SOC of buffer was assumed to be 0.6. The SOC window was set to be 0.4 to 0.99.

Overall Results

The overall deceleration is performed well by HEV WM. The reference velocities and actual velocities for the straight braking test procedure are shown in Fig. 4.7. The fast response is evident as the braking acceleration is increased from 0.1g to 0.8g. When the braking acceleration is reduced again to 0.1g, at about 7 s, the actual longitudinal velocity slightly overshoots.

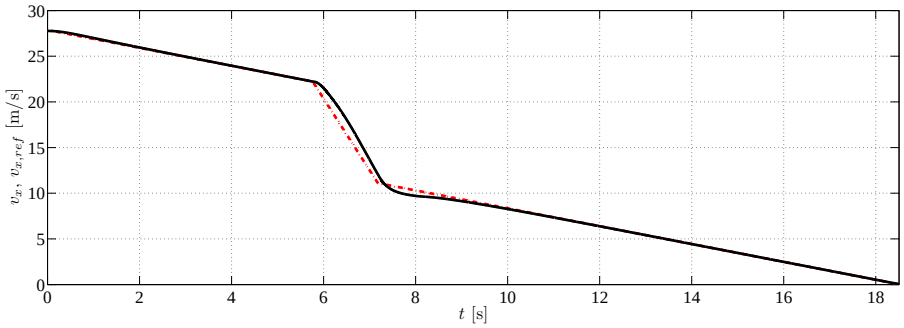

Figure 4.7: Reference and actual longitudinal v_x velocities during test procedure straight braking.

Detailed Results

The desired and actual input signals for wheel motors and disc brakes are shown in Figs. 4.8 and 4.9, respectively. The interesting part is to see how smoothly the actual input signals u are diverted from the desired input u_{des} when needed. This is thanks to the smooth arbitration provided by the control allocation optimization formulation, see Eq. 3.9.

The steering input signals were neglected because no steering was needed in this test procedure. The overshoot in velocity is due to the fact that the rate limits of the mechanical disc brakes take some time to release the brake pressure. This is however attempted to be compensated for by the wheel motors giving a positive torque at about 8s. Further details about the test procedure can be found in Paper VI.

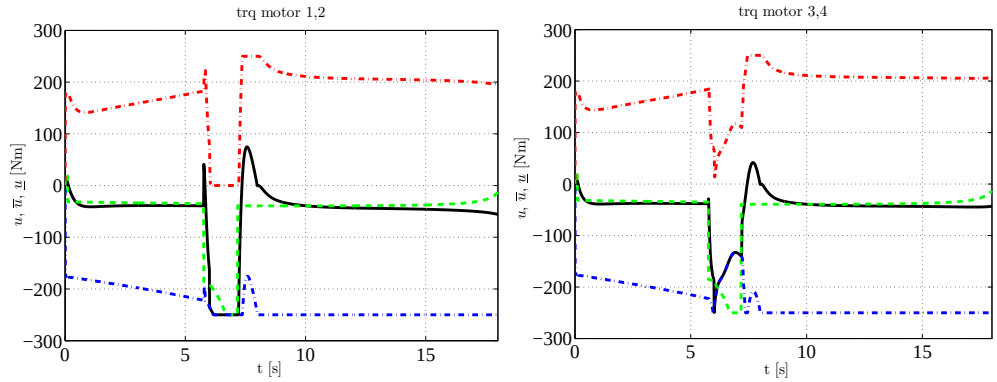

Figure 4.8: Input set u for the wheel motors and their limits u_{des} during test procedure straight braking. The black solid lines correspond to actual u, the dashed green lines correspond to desired u_{des}, and the dotted/dashed red and blue lines are the upper and lower combined limits, respectively.

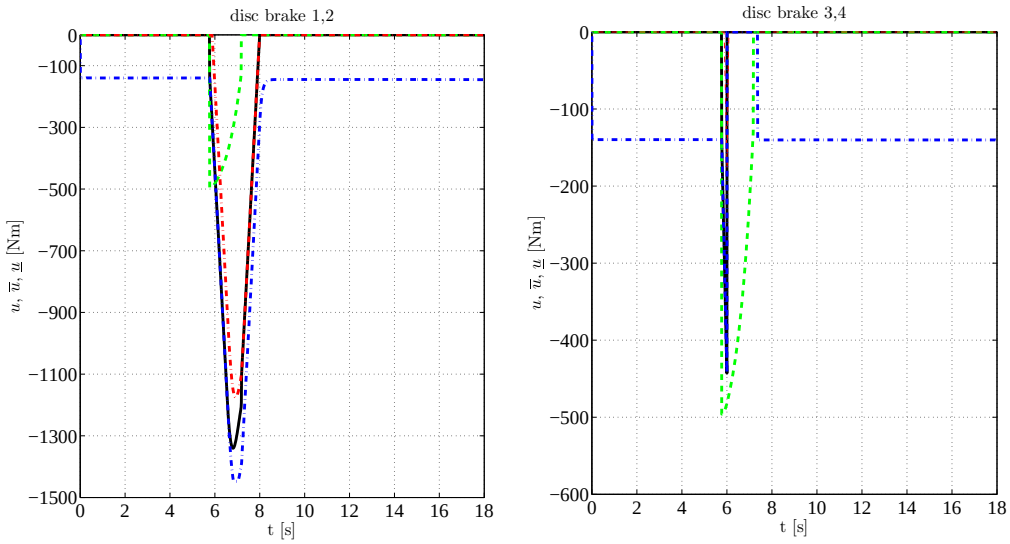

Figure 4.9: Input set u for the disc brakes and their limits u_{des} during test procedure straight braking. The black solid lines correspond to actual u, the dashed green lines correspond to desired u_{des}, and the dotted/dashed red and blue lines are the upper and lower combined limits, respectively.

4.2.2 Constant Velocity with Slow Increase in Yaw Rate

This test procedure aims to show how energy management's desired motor inputs are diverted when other actuators are reaching their limits and in order to maintain vehicle stability. The HEV WM configuration is again studied here with the full functionality as explained in Paper VI. The test procedure starts out with straight driving at a constant cruising speed of 100 km/h and then the yaw rate is slowly increased to the friction limited yaw rate. The minimum turning radius that can be taken at 100 km/h with tyre/road friction 1 is about 78.65 m which gives a limiting yaw rate of about 0.35 rad/s. In the simulations the yaw rate is ramped up to the limiting value over a period of 30 s. This is an additional simulation which is not found in any of the appended papers.

Assumptions

The same assumption exist as in the straight braking case, see Chapter 4.2.1.

Overall Results

Usually when energy management functions are designed and developed they neglect the yaw rate. This is natural in most cases, here is an example when it can become a problem. Here the vehicle is forced to try to reach the physical limit for yaw rate for the selected cruising velocity and road/tyre friction. The vehicle almost reaches the physical yaw rate limit for the studied cruising velocity of 100 km/h. In Fig. 4.10 the reference and actual velocities are shown. A jump in the yaw rate can be observed at 18 s. The final steady state maximum yaw rate that can be achieved with the current model is about 6 percent lower than the physical maximum yaw rate limit calculated by hand.

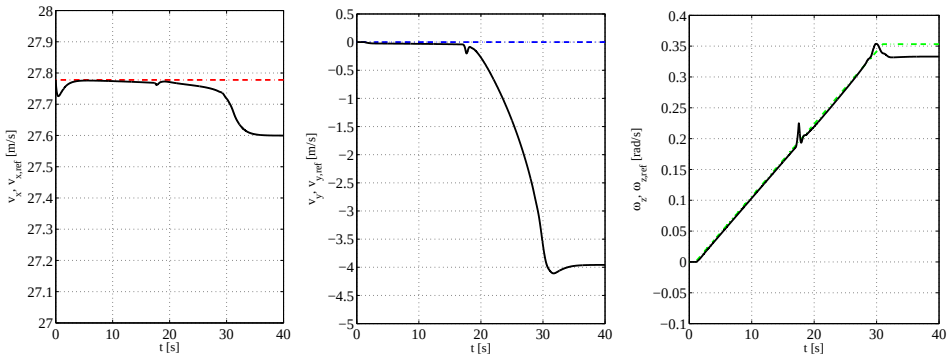

Figure 4.10: Reference and actual longitudinal v_x, lateral v_y, and yaw ω_z velocities during test procedure constant velocity with slow increase of yaw rate.

Detailed Results

In Fig. 4.11 the actual and desired actuator inputs are plotted. The mechanical brakes are not plotted because they are not used. Upon closer study how the allocator handles this case it is apparent that the desired input from energy management for the four electric motors is followed quite nicely until about 18 s. Similar results are shown when the actual steering is compared with the desired steering input of the front and rear wheels. The desired input is for the steering is calculated with the inverse of a linear bicycle model which has not been given any cut-off values for the steering, see also Paper VI. At time 18 s the front steering hits the limit estimated by the tyre fusion function, see Paper V for details. The minimum of the maximum lateral force of each wheel on the front and rear axles is used and multiplied by two. This force is then used to calculate the maximum allowed steering angle. This method is quite conservative and explains why the limit for front steering is already reached at 18 s. Soon after, rear steering also hits the limit. This is now compensated for by the wheel motors and all six active motion actuators divert after 18 s from the desired inputs of energy management and steering law.

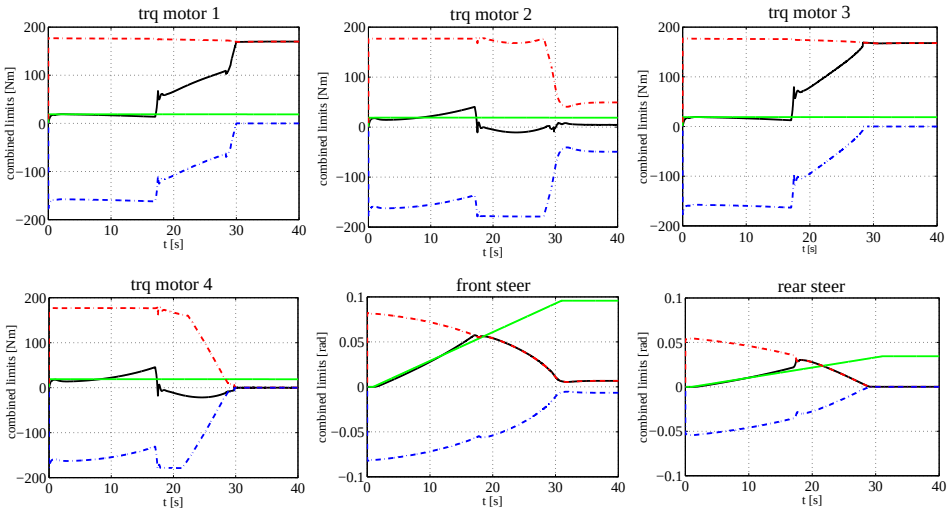

Figure 4.11: Input set u for the wheel motors and front and rear steer with their limits during test procedure constant velocity with slow increase of yaw rate. The black solid lines correspond to actual u, the dashed green lines correspond to desired u_{des}, and the dotted/dashed red and blue lines are the upper and lower combined limits, respectively.

4.3 Online Adaptivity for Sudden Changes in the Environment or Among the Available Actuators

Already in Sections 4.1 and 4.2 the proposed motion control system has been shown to be adaptive. In this section this will be illustrated further by studying two alternative test procedures. The first includes sudden changes in friction during straight braking, here called braking with step friction. The second includes repeated hard braking and acceleration, which illustrates a long term adaptivity when the electric motors saturate due to heating. Both test procedures are studied using vehicle configuration HEV WM, see Chapter 3.2 for configuration details. These test procedures are not found in any of the appended papers. The full complexity of the proposed motion control system as illustrated in Fig. 3.7 is used, see also Paper VI.

4.3.1 Braking Step Friction

Braking with a deceleration of 0.7g is performed when the vehicle is coasting at 100 km/h. At 1 s the tyre/road friction is suddenly reduced from 1.0 to 0.3 for 2 s after which the friction returns to 1.0. The aim with the test procedure is to see how the proposed motion control system adapts its limits and manages the situation during low friction.

Assumptions

The same assumptions exist as in the straight braking case, see Chapter 4.2.1.

Overall Results

In Fig. 4.12 the reference and actual longitudinal velocities are shown. During the low friction time window of 1 to 3s it is noticeable that the deceleration steepness is reduced. After the low friction window deceleration increases again. The last part of the braking is soft until the velocity becomes close to zero. This behaviour is tuned by the PI-controllers within the path controller.

Detailed Results

During the braking situation it is visible that the wheel motors in Fig. 4.13 have a reduced minimum limit during 1 to 3 s. This limit reduction is obeyed in the simulations. The mechanical brakes assist before the step friction but during the step friction all four brakes are limited to zero in minimum torque. This is due to the proposed tyre fusion function which always prioritizes electric braking before

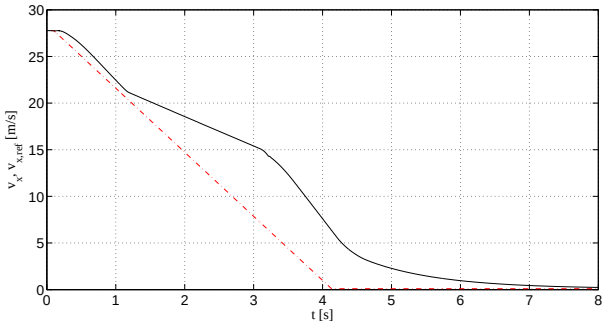

Figure 4.12: Reference and actual longitudinal v_x velocities during test procedure braking with step friction.

mechanical. In short, the function checks the tyre force limits are and if the electric motor limits are smaller, as in this case before and after step friction window, then full limits are given to the electric motors. The residual is then given to the mechanical brakes. If the tyre force limits are smaller or equal to the limits of the electric motor then only the electric motor will receive limits not equal to zero. More details about tyre fusion function can be found in Chapter 3.3.3, see also Paper V. The front wheels lock for a moment when the friction is suddenly reduced at about 1 s, which gives a longitudinal wheel slip of -1. This is because it takes some time for the mechanical brakes to release due to the limits in rate of change. However, by using a tolerance of about 10 percent for the longitudinal force limit and the release of the mechanical brakes, the locking of the wheels disappears during the low friction window. The slip level reaches a steady state of -0.04 during the residual part of the low friction window. The rear wheel stays unlocked during the whole braking procedure.

After 3 s the control allocator adjusts to the new limits on the mechanical brakes and starts again to use the front mechanical brakes to maximize the deceleration efficiency, see Fig. 4.13. Brake blending with a priority on electric braking is important for HEVs and especially for those having a high percentage of their tractive force coming from electrical propulsion. This should also be applied in cases where the tyre/friction is at a permanent low level and during repeated hard braking situations. For configuration HEV WM the electric propulsion percentage is 100.

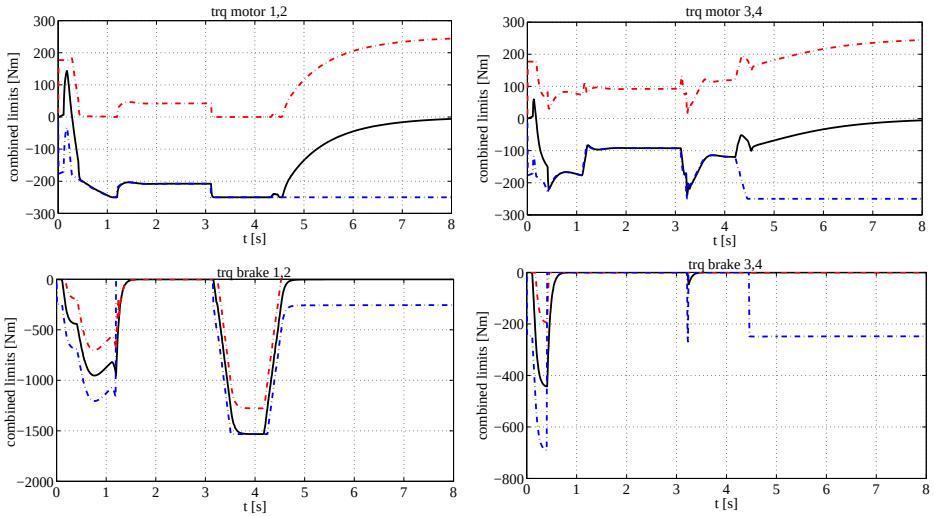

Figure 4.13: Input set u and its limits for configuration HEV WM during braking with step friction. The black solid lines represent actual u, while the dashed red and blue lines represent upper and lower combined limits, respectively.

4.3.2 Repeated Hard Braking and Acceleration Test

This test procedure is inspired by the brake test developed by Auto Motor und Sport (AMS) [8]. They use this test on premium cars to investigate the braking performance. These types of test procedures are not standard for HEVs but based on how they are marketed, usually as premium cars, it can be expected that similar tests will soon become standard for premium HEVs as well. The studied configuration is again HEV WM, see Chapter 3.2 and Paper VI for details. The selected test procedure is a combination of two parts of the real AMS test. The first part of the test begins with the vehicle at 80 percent of its maximum velocity. For the HEV WM the following performance data is derived by simulations: it takes 7 s to accelerate from 0 to 100 km/h and 38 s to reach maximum velocity of 232 km/h. This means that the initial velocity was 185.5 km/h from which hard braking with 1.0g to zero was desired. After standstill in 4 s, ten repetitions with hard acceleration are performed to 103 km/h which is kept for 2 s and is followed by hard braking to zero with a 2 s standstill before the next acceleration. This is given as a reference velocity for the proposed motion control system.

The aim with the test procedure is to show that the proposed motion control system always prioritizes the use of the electric motors for regenerative braking. This is important in HEVs with a high percentage of their traction coming from electric propulsion. If only mechanical braking is used during hard braking, then the buffer will not be recharged for the next acceleration. This will eventually

lead to reduced acceleration performance due to low SOC in buffer. By encouraging the use of the electric motors for regenerative braking, the problem with degraded acceleration performance at the end of the test procedure can potentially be avoided, increasing the marketability of premium HEVs.

Assumptions

The same assumptions exist as in the straight braking case, see Chapter 4.2.1.

Overall Results

The overall result is that the HEV WM fails to follow the reference velocity after about 80 s during the acceleration phases. However, this is not how the real AMS test would be conducted. There the desired velocity of 103 km/h would have been reached between every braking even though it would take a longer time in every acceleration. When using a predefined reference velocity it illustrates how the performance in acceleration is reduced. This is due to the air cooled electric motors heating up. To prevent the electric motors from overheating, the limits in maximum torque are slowly reduced. The braking is conducted without any degradation. The last part of the braking is somewhat soft which is due to the selected settings of the path controller's PI parameters.

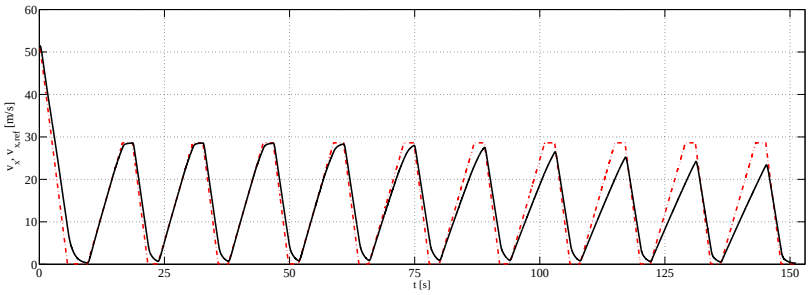

Figure 4.14: Reference and actual longitudinal v_x velocities during test procedure repeated braking and acceleration, inspired by the AMS-test.

Detailed Results

The electric motors and mechanical brakes on the front wheels are blended during every braking phase. In Fig. 4.15 the electric motor's actual torques and combined limits are shown. It can be seen how the maximum and minimum torque limits reduce with time. This is due to the thermal model for the electric motors. The

electric motor is assumed to have only air cooling. A lumped mass model calculates an estimated temperature for the electric motors as shown in the lower plots in Fig. 4.15. The initial temperature is 30 ^{o}C which rises slowly to about 180 ^{o}C. The model is tuned so that when the temperature increases above 100 ^{o}C it starts to linearly reduce the maximum torque and power of the motor to only be able to produce continuous torque and power at 200 ^{o}C. This illustrates how long term adaptivity is included in the proposed motion control system by having detailed models of what the motion actuator's limits actually are, see Paper IV for further modelling details.

The SOC of the buffer starts at 0.8 and cyclically charges and provides power during the braking and acceleration, respectively. The end SOC is about 0.48, the fuel cell is only used during accelerations to assist the buffer. The used energy management rules do not permit any charging of the buffer by the fuel cell during the test procedure conditions. Paper VI describes the used energy management algorithm.

The front mechanical brakes, based on their thermal model, indicates that the temperature goes up to about 750 ^{o}C already during the first braking from 80 percent of maximum vehicle velocity, as shown in Fig. 4.16. To model brake fading in the brake model, the friction between the braking pads and disc is assumed to be temperature dependent. This reduces the minimum limits of the brakes already during the first seconds of using the mechanical brakes, see right plot in Fig. 4.16. The test procedure is somewhat demanding when combining the two braking phases of 80 percent of maximum velocity with the 10 repetitions of braking from 103 km/h. This can be seen in the temperatures estimated by the thermal model for the front brakes: they come close to 1000 ^{o}C yet still continue to produce good braking except for the reduction in limits in the initial braking. In reality, additional degradation of the mechanical brakes could be expected. This is due to that the friction materials are used above their operating temperatures. Another possible scenario is that the brake fluid could reach its boiling point which would also reduce the performance of the brakes. Neither of these effects are included in the temperature model of the mechanical brakes, see Paper IV for modelling details. The rear mechanical brakes are used much less. The main reason for this is the weight shift which gives the front wheels larger longitudinal force limits whereas the rear wheels have to cope with smaller force limits. Thus electrical braking limits are accommodated first and then secondly mechanical brakes. The final temperature of the rear brakes is about 130 ^{o}C.

The results show that if models similar to the ones suggested here for the electric motor and mechanical brakes are used to calculate actual limits, it will not only save the health of the motion actuators but will also give vital information for the control allocator about how the actual limits change during different states such as rotational speed and temperature.

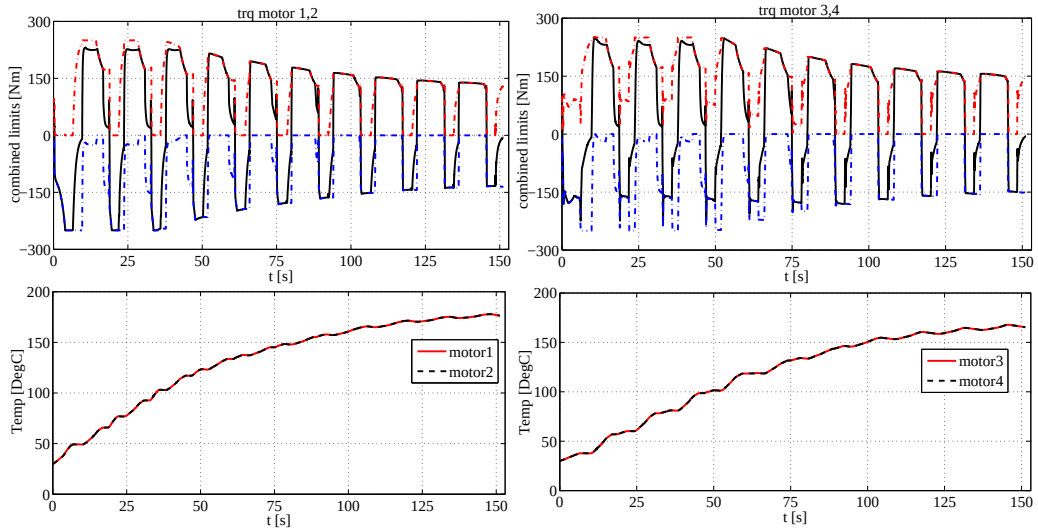

Figure 4.15: The two top plots show the input set u and its limits for configuration HEV WM and its motors during the repeated braking and acceleration test. The black solid lines represent actual u, while the dashed red and blue lines represent upper and lower combined limits, respectively. The two lower plots show the temperature of the motors.

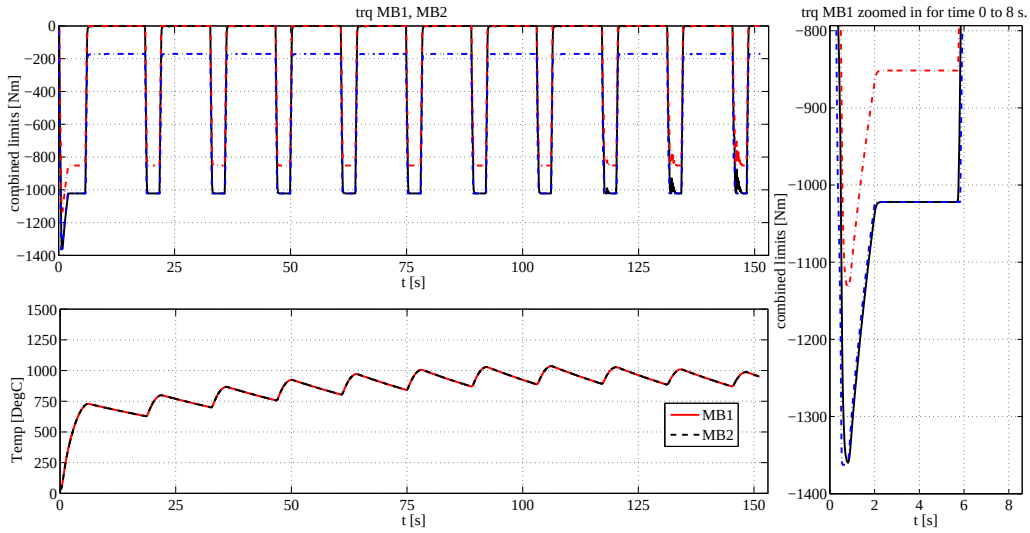

Figure 4.16: The top plot shows the input set u and its limits for configuration HEV WM and its front brakes during the repeated braking and acceleration test. The black solid lines represent actual u, while the dashed red and blue lines represent upper and lower combined limit, respectively. The lower plot shows the temperature of the front mechanical brakes.

4.4 Offline Reconfigurable for Several Vehicle Configurations

Offline reconfigurability is an appealing feature for vehicle control systems, especially commercial automotive systems. To cut development costs, as much of the embedded software as possible has to be reusable when different vehicle configurations are developed. The aim here is to show that the proposed motion control system is offline reconfigurable for a wide variety of vehicle configurations.

4.4.1 Different test procedures

In Papers IV and V different test procedures are conducted with three vehicle configurations, CV2, HEV E4WD, and HEV WM, see Chapter 3.2 for configuration details. The test procedures in Papers IV and V focused on brake blending cases and on traction and braking, respectively. In Paper VII a reduced version of the proposed motion control system is used for vehicle configuration CV1 to study its Electronic Stability Control capabilities.

Assumptions

In Papers IV, V, and VII the following assumptions are made for the control system. The control effectiveness matrices $B_{CV1} \in R^{3\times5}$, $B_{CV2} \in R^{3\times7}$, $B_{HEV\ E4WD} \in R^{3\times9}$, and $B_{HEV\ WM} \in R^{3\times10}$ are assumed to be linear. This means that no inertia effects or nonlinearities are accounted for in the control system for the mapping of the virtual control into the true control input of the motion actuators $v \mapsto u$. However, the modelled and controlled system includes many of the major nonlinearities. Weighting matrices W_u for each configuration and W_v in the control allocation scheme are kept constant, and the desired control input u_{des} for the motion control actuator is given as a zero vector, see also Papers IV and V for details. The only parts changed in the control system are the control effectiveness matrix B, the weighting matrix W_u, the new motion actuator limits, and a modified tyre fusion function for each configuration. The path controller's PI -parameters are kept identical when different vehicle configurations are simulated in Papers IV and V.

Overall Results

The overall results show that the proposed motion control system can easily be adjusted for the different vehicle configurations. The path controller's parameters do not need to be tuned for different vehicle configurations.

Detailed Results

The parts of the control system that need the most attention when switching between the different vehicle configurations are the tyre fusion functions and the setting of the weighting matrix W_u for each configuration. However, the separation of the control law and control allocation opens up for a structural way to handle a wide variety of vehicle configurations.

4.5 Robustness for Vehicle Parameter Changes

All of the previously presented simulations results have been performed with the prerequisite that the controller has knowledge of several important vehicle parameters such as the centre of gravity, vehicle mass, and tyre/road friction, for example. An important aspect when designing or proposing a controller is its robustness to parameter variations. This however has not been an issue in this work, but various simulations have been performed in order to address this problem and to see how the controller handles some interesting cases. Again it is the HEV WM configuration that is studied with the full functionality as explained in Paper VI. Four different types of parameter changes are tested. The first type is related to vehicle mass, the second type is related to the location of the centre of gravity, the third is related to the inertia in the yaw direction and the fourth is related to the tyre/road friction.

For the four different cases, the test procedure is to drive in a circle with a constant of radius 200 m on ice with friction 0.3. The initial velocity is set to 10 m/s. The vehicle is accelerated with 0.1g until 90 percent of the limiting velocity is reached. Then the velocity is kept constant for 5 s. The final part is braking with -0.1g until reaching 10 m/s. During the whole procedure the aim is to keep the driving circle radius constant.

The proposed control system handles the tested cases very well. Simulations indicate that the controller is robust and can handle natural parameter variations like change of mass and centre of gravity, but further analysis is necessary to make a more general statement. The test cases are summarized in Table 4.5. Plots are omitted for brevity. The evaluation criteria is the mean square error between the actual and reference trajectories. The results can be compared to the nominal case, when all parameters are known for the controller. For the first three test scenarios no major deviation can be noticed, but for the last test scenario it can be noticed that the mean square error in longitudinal velocity for a change in wheel radius is a magnitude larger and this is due to an initial wheel speed error.

When the known friction for the controller is assumed to be 1.0, the error actually reduces in lateral velocity in comparison to the nominal case. The tyre

Table 4.1: Robustness test for vehicle parameter changes. Mean square error (mse) for longitudinal, lateral, and yaw velocities.

Changed parameter	Value (Nominal)	mse_v_x	mse_v_y	mse_ω_z
Nominal case	-	29.16	237.95	0.91
Mass, m	1875 kg (1675)	36.00	235.39	0.90
	2175 kg (1675)	47.61	214.75	0.93
Centre of gravity,	0.963 m (1.07)	31.36	292.57	0.93
distance to front axle, L_f	1.177 m (1.07)	29.24	196.51	0.88
Yaw inertia, I_z	2355 kgm^2 (2617)	29.46	242.23	0.89
	2879 kgm^2 (2617)	29.43	240.59	0.92
Tyre/road friction	$R_w = 0.27$ m (0.3)	226.95	178.72	0.59
	$\mu_{ctrl} = 1$ (0.3)	33.33	10.07	0.87

fusion function is conservative when calculating the allowed steering angle limits, thus by using 1.0 in friction, steering can be used without reaching the combined limits which in this specific test procedure leads to a smoother vehicle motion.

4.6 Conclusions about the Simulations and Results

The results from any simulations should be viewed critically. Simplifications in models and neglecting to model important aspects can make the results hard to interpret or even misleading. Usually these shortcomings are discovered, at the latest, when real hardware is used in the loop. However, simulations are a very strong tool to use in the conceptual design phase to validate different concepts and have here been used solely due to the cost and time involved in implementing the proposed motion control system in real hardware. With this in mind, the following conclusions about the simulations are drawn.

The simulations indicate that the system requirements defined in Motivation Section 1.2 are fulfilled by the proposed motion control system found in Control Design Section 3.3. One of the most interesting overall results is that the constrained control allocator with mixed optimization is really a viable option for solving the over-actuated HEV problem, allowing for a smooth arbitration between the vehicle motion controller and energy management. The proposed tyre fusion function together with motion actuator limits in position and rate of change provide sufficient information between the highest control level and the system level to make proper allocation decisions.

Chapter 5

Concluding Remarks

This chapter concludes the findings of this thesis and also proposes what the potential next steps could be.

5.1 Conclusions

This thesis shows that a motion control system for over-actuated road vehicles such as Hybrid Electric Vehicles can be made both offline and online reconfigurable. Detailed conclusions are stated below as a list.

- A reconfigurable motion control system for over-actuated road vehicles was proposed and validated by simulations. The simulations showed that even though a linearised control effectiveness matrix was used for the control allocation it achieved allocation on a road vehicle system modelled with realistic nonlinearities and dynamics. The control system integrates and coordinates the available motion actuators in an energy efficient way with priority on vehicle stability. The control system uses control allocation with a constrained optimization formulation to separate the control law of motion from allocation on the available motion actuators. It was shown that the proposed system suits as well for conventional as hybrid electric vehicles.

- The control system is hierarchical in its functional partitioning and it was shown how energy management, vehicle motion, and arbitration functionality can be performed in the highest functional level by using constrained control allocation with an optimization formulation. It was also shown that actual limits in position and rate of change from available motion actuators, combined with tyre force limits, are needed as interface signals between the high level functions and the low level functions to allow for reliable coordination.

- The control system was offline reconfigurable. It was shown that it is easily reconfigured for different vehicle configurations with different types and numbers of motion actuators.

- The control system was online reconfigurable. It was shown that it can blend and handle saturation of motion actuators such as mechanical brakes, electric motors, combustion engine, steering, and tyre force limits. The control allocation makes the system redundant; if an actuator fails it automatically redistributes the task among the available functioning actuators. This feature will be important when more safety critical functions such as steer-by-wire are included. Another important online feature is the smooth arbitration between energy management and vehicle motion with priority on vehicle motion at all times.

- It was shown by simulation that the control system also functions as an Electronic Stability Control (ESC) system according to the proposed test procedure for ESC from the National Highway Traffic Safety Administration in the USA.

- It is possible to implement the used control allocation as a real-time optimization formulation because it uses an active set method which guarantees to find the optimal solution within a finite number of iterations and always finds a feasible suboptimal solution for each iteration [31].

5.2 What are the Next Steps?

During this research the following topics emerged as important areas for future research and development linked to the work presented in this thesis.

- Study how observers can be designed to achieve reliable information for the control allocator.

- Make a sensitivity analysis and fault tolerance study of the proposed motion control system.

- Discuss how interface signals could be standardized between suppliers of motion actuators and automotive manufacturers to allow for reliable coordination in the vehicle control system.

- Compare the difference in results when the constrained control allocation with mixed optimization is solved with different methods and is stopped before the optimal solution is reached. In particular, compare the active set

method with the Primal-Dual Interior Point method [48]. The Primal-Dual IP method not only seems to have smoother premature results [48], but can also handle significantly larger over-actuation problems without needing to increase the number of iterations to find the optimal solution and without having the cpu time increase exponentially with the over-actuation number, as is the case for active set. The active set method is faster though if the over-actuation is lower than 15 actuators [48] but always converges to optimal solution in finite number of iterations independent of the level of over-actuation.

- Study how a dynamical control allocation scheme which penalizes the rate of the specific actuators can be used to allow slow and fast actuators to take the slow and fast dynamic responses of the vehicle, respectively. See Chapter 9 in [31].

- Study steer-by-wire, focusing on the design, to ensure the avoidance of driver induced oscillations. Test procedures for the validation of steer-by-wire systems, e.g. the sine-with-dwell procedure for ESC systems, need to be modified to include steer-by-wire. Define the desired path of a vehicle equipped with front and rear steering capabilities.

- Study if Model Predictive Control (MPC) with control allocation could be used to predict several steps ahead to ease allocation of motion actuators with highly different dynamics and effectivenesses to achieve the desired global forces and moments of the vehicle.

- Study how the system could be implemented as an ESC system in a conventional vehicle. Then in later stages, when more motion actuators are introduced by hybrid electric or fuel cell vehicle technology, a full version of the proposed motion control system could be implemented.

- Study how roll and pitch prevention can be included by adding the roll and pitch moments to the virtual control signals within the control allocator and only use the active suspension to distribute correcting normal forces to minimize the roll and pitch angles.

Chapter 6

Summary of Appended Papers

This chapter gives a short summary of each appended paper.

6.1 Paper I

This paper discusses how the control architecture of fuel cell and hybrid electric vehicles can be be generic. It proposes a hierarchical functional partitioning of the control system. The hierarchical system is proposed to contain three functional levels. The highest level includes functions such as driver interpreter, energy management, vehicle motion control, and strategic control. The second level contains the driver interface, chassis, power supply, and auxiliary systems. The third level is the actuator sensor level. The paper also discusses where different functions are located.

6.2 Paper II

This paper is the first paper in this thesis to discuss how the desired global forces F_x, F_y and moment M_z of the vehicle can be allocated onto a specific wheel's longitudinal and lateral forces. A practical approach is used to allocate the global yaw moment by splitting the task into longitudinal and lateral forces by a weighting function $k(F_x, F_y)$ such that $M_z = k\Delta F_x + (1-k)\Delta F_y$. The idea is to not allocate wheel forces near saturation, which was accounted for with $k(F_x, F_y)$. Simulations showed that this practical approach gave fairly good results.

6.3 Paper III

This paper shows how a reusable control architecture was designed and implemented in a remote controlled scale model car. The same functions found in Paper VI were implemented and tested with specific functionality to drive and steer the fuel cell emulated vehicle with an energy buffer of super capacitors. Test driving showed that both energy management and vehicle motion control worked as desired.

6.4 Paper IV

This paper includes the main system modelling of chassis, drivetrains, and motion actuators for the three studied vehicle configurations, CV2, HEV E4WD, and HEV WM. The configurations have seven, nine, and ten motion actuators respectively to control longitudinal, lateral, and yaw motion. The motion control system uses control allocation with a constrained optimization formulation to separate the control law of motion from the allocation of the available motion actuators. This makes the control system reusable for a wide variety vehicle configurations. It is shown by simulation how control allocation can be used within the control system to generate the brake blending of different motion actuators. It also identifies the importance of weighting and prioritizing the blending of the available motion actuators during braking by using the weighting matrix W_u within the optimization formulation used in the control allocator.

6.5 Paper V

This paper focuses on the traction, braking, and steering of the same three vehicle configurations modelled in Paper IV. It is shown how nonlinearities such as gear shifting can be included in the control allocation scheme by making the control effectiveness matrix $B(x)$ vehicle state dependent. It also explains in more detail how the actuator limits in position and rate of change are combined with the tyre force limits and sent back to the control allocator. It is shown by simulation how the motion actuators are automatically re-distributed when needed due to saturation or the reaching of tyre force limits. It also identifies the importance of differently weighting and prioritize the blending of the available motion actuators during traction and braking by using the weighting matrix W_u within the optimization formulation used in the control allocator.

6.6 Paper VI

This paper is the most futuristic, studying the vehicle configuration HEV WM and how energy management and vehicle motion control are coordinated in the proposed motion control system. A finite state machine together with a set of rules are used as an energy management function to derive the desired input of the motion actuators. A bicycle model is used to calculate the desired front and rear steering angles. It is shown by simulation how smoothly the actual input signals u for the motion actuators are diverted from the desired input signals u_{des}. This is accomplished by the optimization formulation used within the control allocator. A proposal is also given on how the weighting matrix $W_u(v)$ can be made longitudinal force dependent and how linear interpolation can be used for the weighting and blending of the available motion actuators.

6.7 Paper VII

This paper studies how the proposed motion control system can function as an ESC system for vehicle configuration CV1. This vehicle configuration is the closest configuration to today's mass produced road vehicles of all the studied configurations. The steering is solely managed by the driver. Five control inputs are used to control the longitudinal force and yaw moment. It was shown by simulation that the motion control system, based upon control allocation, passes the proposed test procedure by NHTSA for ESC systems. It is also concluded that the proposed test procedure cannot be applied to vehicle configurations that have steer-by-wire facilities because the steering wheel angle is used as the input for the test procedure sine-with -dwell. In a software based steering control the input can be manipulated. Therefore a desired yaw rate is suggested instead as the input for the test procedure to also include vehicle configurations which are equipped with steer-by-wire.

Appendix A

Nomenclature and Glossary

The Nomenclature found here is only for the thesis part, not the appended papers.

Symbol	Definition
Greek letters	
β	vehicle's slip angle
γ	weighting parameter in CA optimization
μ	road/tyre friction
ω_z	vehicle's yaw rate
ρ	rate of change, curvature of road
$\underline{\rho}$	true control input's minimum limit in rate of change
$\overline{\rho}$	true control input's maximum limit in rate of change
Latin letters	
B	control effectiveness matrix
$F_{i,j}$	j[th] wheel's forces in i=x,y direction
I_z	vehicle's yaw inertia
L_f	length from front axle to centre of gravity
m	vehicle's mass
$r = \begin{bmatrix} v_x & v_y & \omega_z \end{bmatrix}^T$	vehicle's reference velocity
r_{fg}	final gear ratio
R_w	wheel radius
t_T	sampling time of the CA function
T	temperature of mechanical brakes or electric motors
u	true control input, vehicle's motion actuator input
u_{el}	input for electrical motor
u_{mb}	input for mechanical brake
u_{des}	desired control input from energy management and steering
$\underline{u}$	true control input's minimum limit
$\overline{u}$	true control input's maximum limit
$v = \begin{bmatrix} F_x & F_y & M_z \end{bmatrix}^T$	virtual control input, global forces and moment
v_x	vehicle's longitudinal velocity
v_y	vehicle's lateral velocity
W_u	weighting matrix for true control input in CA optimization
W_v	weighting matrix for virtual input in CA optimization
x	vehicle system states, vehicle's longitudinal direction
y	vehicle system output, vehicle's lateral direction
z	vehicle's vertical direction

Glossary

Actuator (A) Device responsible for activating or putting into action.

Arbitration Process of evaluating and prioritizing request signals, where the number of incoming requests is greater than outgoing requests. The opposite of Coordination.

Architecture Organisation of system hardware and software.

Auxiliary Systems (Aux) Vehicle functionality not required for generating vehicle motion.

Brake Pedal (BP) Driver's brake pedal for controlling the level of braking.

Buffer (bf) Energy carrier which stores a limited amount of energy and can contribute both positive and negative power to the system.

Chassis (Ch) Part of the vehicle responsible for the generation of ground motion including converters located after differentials and excluding Power Supply.

Connector (c) Physical interface between Functional Units, such as mechanical and electrical.

Control Allocation A function used for the coordination of actuators within an over-actuated system.

Converter (Conv) Hardware which converts energy into a different form, for example, a combustion engine converting chemical energy into mechanical or an electric motor converting electrical energy into mechanical.

Coordination Process of splitting request signals by evaluation, where the number incoming requests is less than outgoing requests. The opposite of arbitration.

Drivetrain The transmission, shafts, and the differential.

Driver Interface (DIf) Device which receives driver input and provides sensor information in order to change certain sensor values and drive the vehicle.

Driver Interpreter (DIp) Function that interprets the driver's intentions and sets a desired driving path.

Electronic Stability Control (ESC) A function which assist the driver when vehicle is becoming over- or understeered.

Energy Carrier (EC) Apparatus which carries energy in the vehicle. Examples of primary ECs are the gasoline tank and hydrogen tank. Secondary ECs can be batteries or super capacitors.

Energy Management (EM) Function that controls the power coordination between the available energy carriers within Power Supply.

Fuel Cell Vehicle (FCV) Vehicle containing a converter where chemical hydrogen energy is converted to electrical which is then used mainly to propel the vehicle.

Function (Fn) Action or activity that must be accomplished to achieve a desired outcome.

Functional Decomposition Process of identifying fundamental functions within a system and decomposing the system into Functional Units.

Functional Unit (FU) Entity of software and/or hardware capable of accomplishing a specific function.

Gas Pedal (GP) Driver's gas pedal for controlling the level of acceleration.

Interface Shared boundary between two Functional Units, such as signals and/or connectors.

Information signal Estimates of performed requests or request limits.

Generic Hardware independent.

Hybrid Electric Vehicle (HEV) Vehicle containing two or more energy carriers used for propulsion, where at least one is electrical.

Limits (lim) Upper and lower boundaries of request signals.

Limits in position Upper and lower boundaries of request signals relating both to the steering angle input in the steering system and the torque for the mechanical brakes and electric motors.

Over-actuated system A system with more actuators than controlled motions. The system has more than one actuator to influence at least one of the motions.

Oversteered When less steering angle is needed compared with a neutral steered vehicle for the desired motion.

Power Supply (PS) Part of the vehicle responsible for the main energy carriers and also converters such as a fuel cell.

Request Signal used for controlling a function.

Reconfigurable Control System Offline: A control system that is easily adapted to different types and number of actuators. Online: A control system that automatically adapts to new conditions and re-coordinates in between the actuators to meet the desired demand.

Regenerative braking Using the electric motors to control the braking of the vehicle. The electric energy from the electric motors are stored in a buffer.

Sensor (S) Device that responds to a signal or stimulus.

State of Charge (SOC) Level of energy within a buffer.

Steering Wheel Angle (SWA) The turning angle of the steering wheel. When divided by the steer gear ratio wheel angle is achieved.

Strategic Control (SC) Function that makes final arbitrations on request signals.

Understeered When more steering angle is needed compared with a neutral steered vehicle for the desired motion.

Underdetermined When the number of unknowns exceeds the number of system equations. Same as over-actuated system.

Vehicle Motion Control (VMC) Function that controls the vehicle's ground motion and coordinates the Wheel Units.

Wheel Motor (WM) An electric motor for individual wheels that controls their rotational speed or torque.

Wheel Unit (WU) Wheel with controlled actuators.

Appendix B

Control Allocation

B.1 Introduction

Consider the system described as

$$\dot{x} = f(x) + g(x)u \tag{B.1}$$

$$\underline{u} \leq u \leq \overline{u} \tag{B.2}$$

where $g(x)u = v$, v is also called the virtual control input. A control law regulates the virtual control input v. The demand $v \in R^k$ is mapped onto the true control input of the actuators $v \mapsto u$, where $u \in R^m$ and $k < m$. The allocation problem lies in that there are several input sets of u that can give the control demand v. Additionally, the true control input u, is constrained which limits the feasible solutions. The outline of the appendix is as follows: Section B.2 gives a simple brake blending example to illustrate control allocation. This example will be revisited throughout this appendix. Section B.3 describes solutions by using a pseudoinverse and direct allocation. Section B.4 discusses the mixed optimization based control allocation and how it can be solved by using the active set method.

B.2 Brake Blending Example

To illustrate the practicality and usefulness of control allocation, consider the following system for a simple case of brake blending of a vehicle

$$\dot{x} = u_1 + u_2 \tag{B.3}$$

$$-0.3g \leq u_1 \leq 0.3g \tag{B.4}$$

$$-1g \leq u_2 \leq 0 \tag{B.5}$$

where x is the vehicle velocity, u_1 is the input for the electric motor, u_2 is the mechanical brakes, and g is the gravity constant. Because the model in Eq. B.3 is simple, $f(x) = 0$ and $g(x) = B$ when compared with Eqs. B.1-B.2, the desired braking acceleration $\dot{x}$ is directly related to the virtual control input $v = \dot{x}$

$$v = Bu \tag{B.6}$$

$$B = \begin{bmatrix} 1 & 1 \end{bmatrix}. \tag{B.7}$$

To achieve a desired braking of $v = -0.7g$ there are several possible solutions. Mechanical brakes could solely be used, $u_1 = 0$ and $u_2 = -0.7g$. Brake blending could be used, $u_1 = -0.3$ and $u_2 = -0.4g$. Even full traction of the electric motors and full mechanical braking could be used, $u_1 = 0.3$ and $u_2 = -1.0g$. The latter is of course not an energy efficient solution. There is a subset of linear combinations of feasible u_1 and u_2 that fulfil the actuator constraints and the desired virtual control input of $v = -0.7g$, as illustrated in Fig. B.1.

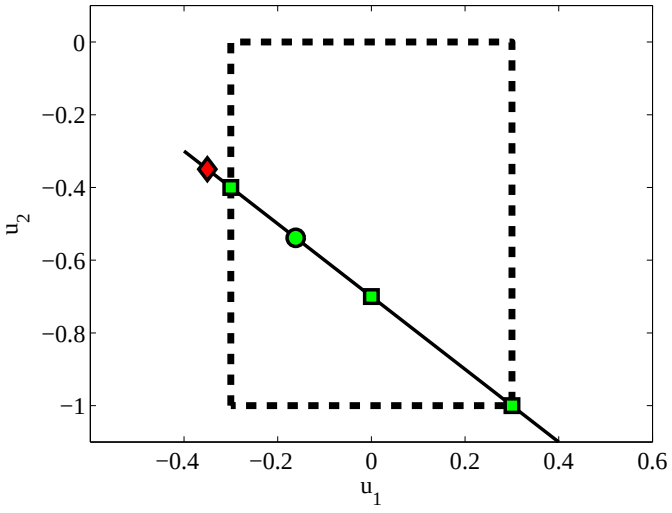

Figure B.1: Illustration of how the subset of $u \in \Omega$, the large dashed square, constrains the solution of $v = -0.7g$, the black line. The part of the black line inside the dashed square denotes all possible solutions. The green square markers indicate specific solutions mentioned in text. The circular and diamond markers are pseudoinverse solutions. The red diamond marker, calculated with a standard Moore-Penrose pseudoinverse, is not a feasible solution. The green circle marker, calculated with a weighted pseudoinverse, is a feasible solution.

If the control effectiveness matrix B in Eq. B.6 had been square and full rank

the inverse B^{-1} would have existed and it would have been possible to directly compute the solution $u = B^{-1}v$. In this case, however, the inverse of B does not exist. This simple example illustrates an over-actuated system where the number of true control inputs $u \in R^m$ exceeds the number of virtual control inputs $v \in R^k$, where in the above example $m = 2 > k = 1$. To solve the coordination of the available actuators control allocation can be used.

B.3 Pseudoinverse and Direct Allocation

Pseudoinverse

As mentioned earlier, the inverse of the matrix B does not exist within example B.3. One way to solve the underdetermined system of the equation is to calculate the pseudoinverse, also called the generalized inverse [13]. The pseudoinverse is the solution of the minimum l_2 norm of u

$$\underbrace{\min}_{u} ||u||_2 \quad \text{subject to } v = Bu \tag{B.8}$$

where $B \in R^{k \times m}$ and $k < m$. The pseudoinverse $B^\dagger$ then basically gives the minimum length vector $u = B^\dagger v$. In [13] it is shown how $B^\dagger$ can be derived by using a classical approach to solve constrained optimization problems. Here, constrained refers to $v = Bu$. By introducing the scalar function, Eq. B.8 becomes unconstrained

$$L(u, \lambda) = 0.5u^T u + \lambda^T (v - Bu) \tag{B.9}$$

where $\lambda \in R^{k \times 1}$ is the Lagrangian multiplier vector. An extremum is found when the gradients are $\partial_u L(u, \lambda) = 0$ and $\partial_\lambda L(u, \lambda) = 0$. Taking the gradients of Eq. B.9 gives

$$\partial_u L(u, \lambda) = u^T - \lambda B = 0 \Leftrightarrow u^T = \lambda B \Leftrightarrow u = B^T \lambda \tag{B.10}$$

$$\partial_\lambda L(u, \lambda) = v - Bu = 0 \Leftrightarrow v = Bu. \tag{B.11}$$

Inserting u from Eq. B.10 into Eq. B.11 gives

$$v = BB^T \lambda. \tag{B.12}$$

Solving λ gives

$$\lambda = (BB^T)^{-1} v. \tag{B.13}$$

Inserting the solution for Eq. B.13 into Eq. B.10 gives finally

$$u = B^T (BB^T)^{-1} v \equiv B^\dagger v. \tag{B.14}$$

To assure that this is still a minimum, the second derivative can be studied to verify that $\partial_u^2 L(u,\lambda) = 1$ and $\partial_\lambda^2 L(u,\lambda) = 0$ are non-negative.

Using Eq. B.14 on the example Eq. B.3 for achieving the desired virtual control input of $v = -0.7g$ gives $B^\dagger = \begin{bmatrix} \frac{1}{2} & \frac{1}{2} \end{bmatrix}^T$ with the solution $u_1 = u_2 = -0.35g$, see also Fig. B.1. The achieved solution in u_1 is not feasible due to the minimum limit of the electric motor $\underline{u}_1 = -0.3g$. One way to still use the pseudoinverse and more likely achieve a feasible solution is to introduce a weighting matrix W_u in a minimum 2-norm

$$\underbrace{\min}_{u} ||W_u u||_2 \quad \text{subject to } v = Bu \tag{B.15}$$

where W_u is a diagonal matrix of size $m \times m$. In [53] it is proposed that the weighting of the true control input can be penalized by its limits $\overline{u}$ to assure feasible solutions, accordingly $W_u = \text{diag}\begin{bmatrix} 1/\overline{u}_1 & \dots & 1/\overline{u}_m \end{bmatrix}$. In a similar way as described before, the weighted pseudoinverse can be derived by including W_u in Eq. B.9

$$L(u,\lambda) = 0.5 u^T W_u u + \lambda^T (v - Bu). \tag{B.16}$$

Now the derivative of $\partial_u L(u,\lambda) = 0$ to find the extremum becomes

$$\partial_u L(u,\lambda) = u^T W_u - \lambda B = 0 \Leftrightarrow u^T = \lambda B W_u^{-1} \Leftrightarrow u = W_u^{-1} B^T \lambda. \tag{B.17}$$

Inserting u from Eq. B.17 into Eq. B.11 gives

$$v = B W_u^{-1} B^T \lambda. \tag{B.18}$$

Solving λ gives

$$\lambda = (B W_u^{-1} B^T)^{-1} v. \tag{B.19}$$

Inserting the solution Eq. B.19 into Eq. B.10 gives finally

$$u = W_u^{-1} B^T (B W_u^{-1} B^T)^{-1} v \equiv B_{W_u}^\dagger v. \tag{B.20}$$

To assure that this is still a minimum, the second derivative $\partial_u^2 L(u,\lambda) = W_u$ and $\partial_\lambda^2 L(u,\lambda) = 0$ can be examined which says that if W_u is a positive definite matrix then the solution is a minimum.

Example Revisited

In revisiting example Eq. B.3 by using the weighted pseudoinverse the weighting matrix $W_u = \text{diag}\begin{bmatrix} 1/0.3 & 1/1 \end{bmatrix}$ is selected. This will penalize the use of electric motors more due to the smaller limit band when compared with the mechanical brakes. This gives a weighted pseudoinverse of $B_{W_u}^\dagger = \begin{bmatrix} 0.231 & 0.769 \end{bmatrix}^T$.

The solution of $v = -0.7g$ then becomes $u_1 = -0.162g$ and $u_2 = -0.538g$, which is a feasible solution, see Fig. B.1. Even if the deceleration is increased to maximum braking $v = -1g$, a feasible solution is given by the weighted pseudoinverse, $u_1 = -0.231g$ and $u_2 = -0.769g$. However, the full potential of the electric motor is never used during the braking. For example, if only regenerative braking is wanted during $-0.3g \leq v < 0$, the weighting matrix W_u has to be changed depending on the desired v. Most methods solving control allocation can be defined as pseudoinverse methods [31]. However, pseudoinverse solutions have their disadvantage in that the limits of the true control input $\underline{u}$ are not accounted for directly, and therefore adjustments have to be made on the achieved solution.

Direct Allocation

Another method of achieving control allocation is by using the direct allocation method [20], [21], and [13]. This method uses the geometry of the Attainable Moment Subset. The $k-$dimensional geometry of AMS is achieved by using the limits of the control input $\underline{u}$ and mapping them through the control effectiveness matrix B. A geometric search is used to find a feasible input u for v with the maximum magnitude a. This is described by [12] and [31] as

$$\begin{aligned} &\underbrace{\max}_{a,u}\, a \\ &\text{subject to } av = Bu \\ &\qquad\qquad \underline{u} \leq u \leq \overline{u} \end{aligned} \tag{B.21}$$

and if $a > 1$ then $u = \frac{1}{a}u$ else $u = u$.

B.4 Optimization Based Control Allocation

In [31] it is shown how constrained mixed optimization based control allocation can be solved by using the active set method. For further reading on the active set method, see also [45], [11], and [48]. This section will only give a short overview of this concept. The section is outlined as follows: In subsection B.4.1 the constrained mixed optimization formulation of the used CA is revisited. Subsection B.4.2 discusses why the l_2 norm is preferred in the objective function. Finally, in Subsection B.4.3 the active set method is shown.

B.4.1 Mixed Optimization Formulation

A two-step optimization problem, sequential least squares (sls), see Eqs. B.22-B.23, is one of the optimization formulations used for selecting the allocated input of the feasible u, the subset within the constraints of the specific actuators.

$$u = \arg \underbrace{\min}_{u \in \Omega} \|W_u(u - u_{des})\|_2 \tag{B.22}$$

$$\Omega = \arg \underbrace{\min}_{\underline{u} \leq u \leq \overline{u}} \|W_v(Bu - v)\|_2 \tag{B.23}$$

where W_u is the weighting matrix for penalizing the use of specific actuators and W_v is the weighting matrix for penalizing the specific virtual control input, in this case the global forces and moment of the vehicle. u_{des} is the desired control input. The two step optimization formulation in Eqs. B.22-B.23 can be rewritten as an one step optimization by approximation. This is done by using a scalar weighting parameter γ for the allocation error B.23, accordingly

$$u = \arg \underbrace{\min}_{\underline{u} \leq u \leq \overline{u}} \|W_u(u - u_{des})\|_2 + \gamma \|W_v(Bu - v)\|_2. \tag{B.24}$$

Eq. B.24 is a mixed optimization formulation. It not only tries it to minimize the allocation error $(Bu - v)$ but also the error in the desired input $(u_{des} - u)$ is minimized whenever feasible. The formulation in Eq. B.24 is referred to as weighted least squares (wls).

B.4.2 Why the l_2 Norm?

In Subsection B.4.1 the norm l_2 was used for the optimization formulation. This subsection illustrates some of the differences in using the l_1 and l_2 norms in the optimization formulation. Consider the simplified control allocation formulation

$$\begin{aligned} &\underbrace{\min}_{u} ||u||_p \\ &\text{subject to } v = Bu \\ &\underline{u} \leq u \leq \overline{u} \end{aligned} \tag{B.25}$$

where p is the norm of the objective function. The matrix and vectors have the following sizes $B \in R^{k \times m}$ and $k < m$, $v \in R^{k \times 1}$, and $u \in R^{m \times 1}$. If the norm is set to $p = 1$, the problem can be solved by linear programming methods, such as the simplex method. These methods are both fast and robust. This appears to be a natural choice instead of using the l_2 norm with $p = 2$.

Example Revisited

In revisiting the brake blending example stated in Eq. B.3, contours can be drawn for when the objective function in Eq. B.25 is using the l_1 and l_2 norms, respectively, see Fig B.2.

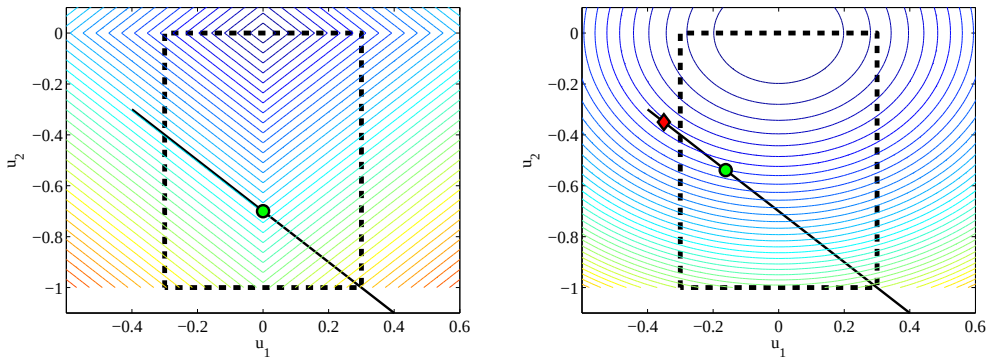

Figure B.2: The left plot shows the contours when the objective function, $||u||_p$, uses the l_1 norm. The right plot shows the contours when the l_2 norm is selected. The large dashed square corresponds to the boundary of the subset of $u \in \Omega$. The black line corresponds to the solution $v = -0.7g$. The part of the black line inside the dashed square denotes all possible solutions. The circular green marker in the left plot is the solution when using linear programming to solve the problem. The circular and diamond markers in the right plot are the pseudoinverse solutions discussed in Section B.3.

In the left plot in Fig. B.2 the contours are drawn for the l_1 norm, which forms square contour shapes. The linear programming solution[1] to the problem for $v = -0.7g$ is $u_1 = 0$ and $u_2 = -0.7g$, see the left plot in Fig. B.2. The linear programming solution does not use the u_1 electric motor at all, only the mechanical brakes u_2. In the right plot in Fig. B.2 the contour shapes are circular for when the l_2 norm is used in the objective function. The pseudoinverse solutions for when using the l_2 norm are also plotted. The l_2 norm solutions use both $u_1 \neq 0$ and $u_2 \neq 0$ to achieve the desired $v = -0.7g$. This illustrates the main benefit of using the l_2 norm. Instead of only using a few of the available actuators as l_1, it tends to use several. This makes the l_2 norm less sensitive for actuator failure as more actuators are automatically used and when needed, they then easily compensate for the loss of the failed actuator [48].

[1]The `linprog` function within the Matlab optimization toolbox was used.

B.4.3 Active Set Method

The word active set refers to that when the input u is calculated, the u's are divided into saturated controls, named the active set, and unsaturated controls, named the free set. The wls optimization formulation in Eq. B.24 is rewritten as a least squares problem of the form

$$\underbrace{\min}_{u} \|Au - b)\|_2 \tag{B.26}$$

$$Bu = v \tag{B.27}$$

$$Cu \geq U \tag{B.28}$$

$$C = \begin{pmatrix} I \\ -I \end{pmatrix} \tag{B.29}$$

$$U = \begin{pmatrix} \underline{u} \\ \overline{u} \end{pmatrix} \tag{B.30}$$

where the actuator constraints $\underline{u} \leq u \leq \overline{u}$ are rewritten as an inequality by using Eqs. B.29-B.30. The rewriting of the wls Eq. B.24 becomes

$$\begin{aligned} &\|W_u(u - u_{des})\|_2 + \gamma\|W_v(Bu - v)\|_2 \\ &= \| \begin{pmatrix} \gamma^{1/2}W_vB \\ W_u \end{pmatrix} u - \begin{pmatrix} \gamma^{1/2}W_vv \\ W_uu_d \end{pmatrix} \|_2. \\ &= \|Au - b\|_2. \end{aligned} \tag{B.31}$$

Initiation of the Active Set Method

If it is the first time the active set function is called upon for solving Eqs. B.26-B.30, all u's belong to the free set, unsaturated controls, and an initial guess is set to $u_0 = (\overline{u} + \underline{u})/2$. The next time, the initial guess is equal to the previous calculated solution $u_0 = u_{prev}$ which was calculated in maximum iterations i. An initial residual d is then computed from the initial guess of u

$$d = b - \alpha Au \tag{B.32}$$

where α a scaling parameter $0 \leq \alpha \leq 1$. For the initial residual α is set to 1.

Iteration within the Active Set Method

The iteration starts out by eliminating any controls that are saturated, i.e. the active set. Then an improved solution for the free set is calculated with the pseudoinverse

$$p_{free} = A_{free}^{\dagger} d \tag{B.33}$$

$$u_{free} = u_{free} + p_{free} \tag{B.34}$$

where p_{free} is the perturbation vector, u_{free} is the free set, and A_{free} are the corresponding columns of A for the free set. The new u_{free} is then checked for feasibility, $\underline{u}_{free} \leq u_{free} \leq \overline{u}_{free}$.

- If the solution is infeasible, then the most infeasible $u_{free,infe}$ is used for calculating a step length α to achieve a feasible solution. The step length is decided by studying the $u_{free,infe}$ normalized distance to its limits $\underline{u}_{free,infe}$ or $\overline{u}_{free,infe}$. Then a feasible solution is updated by calculating a new residual, see Eq. B.32, and a feasible update of $u_{free} = u_{free} + \alpha p$ is made.

- If the solution is feasible, a step length of $\alpha = 1$ is used for calculating the residual d and update of u_{free}. This is then checked to see if the solution is optimal by calculating the Lagrange multipliers for the active set

$$\lambda_{active\ set} = A_{active\ set}^{T} d. \tag{B.35}$$

  If all $\lambda_{active\ set} >= 0$ then the optimum solution is found and the iteration is terminated. Otherwise, the one among the active set (saturated control) with the most negative λ is removed from the active set and becomes a free set control and a new iteration starts.

This iteration continues until all Lagrange multipliers are $\lambda >= 0$ or the number of maximum iterations are reached. The convergence is fast when a good initial guess is chosen. This is the case when the virtual control input $v(t)$ changes slowly over time, making the previous u_{prev} a good initial guess for the next mapping of $v \mapsto u$. The active set method will reach an optimum solution in a finite number of iterations.

Example Revisited

The simple braking problem stated in Eq. B.3 is now revisited. To begin with, the design parameters of the wls optimization formulation need to be set, see Eq. B.24. The weighting matrix of the control input is selected to be $W_u = \text{diag}\begin{bmatrix} 0.1 & 1 \end{bmatrix}$ which means that the electric motors are penalized ten times less, thus encouraging the use of the electric motors. The desired input is selected to be

$u_{des} = \begin{bmatrix} 0 & 0 \end{bmatrix}^T$ which means that the optimum is when the actuators are used as little as possible. The weighting parameter is set to $\gamma = 1e4$, which means that the error $W_v(Bu - v)$ is prioritized more than the desired input $W_u(u - u_{des})$. Sufficient accuracy is found when γ is selected to be high enough. The weighting matrix for the virtual control input is set to $W_v = 1$. Now A and b, see Eq. B.31, become

$$A = \begin{pmatrix} \gamma^{1/2} W_v B \\ W_u \end{pmatrix} = \begin{pmatrix} 100 & 100 \\ 0.1 & 0 \\ 0 & 1 \end{pmatrix} \tag{B.36}$$

$$b = \begin{pmatrix} \gamma^{1/2} W_v v \\ W_u u_d \end{pmatrix} = \begin{pmatrix} -70 \\ 0 \\ 0 \end{pmatrix}. \tag{B.37}$$

Initiation
The initial guess, $u_1 = 0$ and $u_2 = -0.5$ gives the initial residual $d = \begin{bmatrix} -20 & 0 & 0.5 \end{bmatrix}^T$, see Eq. B.32.

First Iteration
The iteration process is then started and during this first iteration, all actuators are in the free set, none are saturated, $A_{free} = A$. A new updated solution is calculated with Eqs. B.33-B.34, which gives the perturbation vector $p_{free} = \begin{bmatrix} -0.693 & 0.493 \end{bmatrix}^T$ and the updated solution $u = \begin{bmatrix} -0.693 & -0.007 \end{bmatrix}^T$. Is the solution feasible? No, u_1 is below its lower limit $u_1 < \underline{u}_1$. Fig. B.3 illustrates how the updated solution by the weighted pseudoinverse is outside the feasible solution for the studied problem. u_1 is now placed in the active set, due to the fact that it is saturated and u_2 is still left in the free set. The next step is to modify the step length by checking which distance to its constraints is smallest, in this case $\lambda = (\underline{u_1} - u)/p_1 = 0.433$. Now the solution is updated by $u_{free} = u_{free} + \alpha p$ which gives $u = \begin{bmatrix} -0.300 & -0.287 \end{bmatrix}^T$, see Fig. B.3. The residual $d = \begin{bmatrix} -11.343 & 0.030 & 0.287 \end{bmatrix}^T$ is also updated by Eq. B.32.

Second Iteration
The second iteration starts with u_1 in the active set and $A_{free} = \begin{bmatrix} 100 & 0 & 1 \end{bmatrix}^T$ which corresponds to the column for u_2 in the free set. A new perturbation vector, now scalar, is calculated with Eqs. B.33-B.34 which gives $p_{free} = -0.1134$. The solution is updated $u = \begin{bmatrix} -0.3 & -0.4 \end{bmatrix}^T$. Is it a feasible solution? Yes, both are within the boundaries. The residual is updated $d = d - A_{free} p_{free} = \begin{bmatrix} 0.004 & 0.03 & 0.4 \end{bmatrix}^T$. Is it an optimum solution? Yes, the Lagrange multipliers are checked by $\lambda = A^T d$ which gives $\lambda_1 = 0.397$ and $\lambda_2 = 0$, the optimum is found. The iteration is terminated.

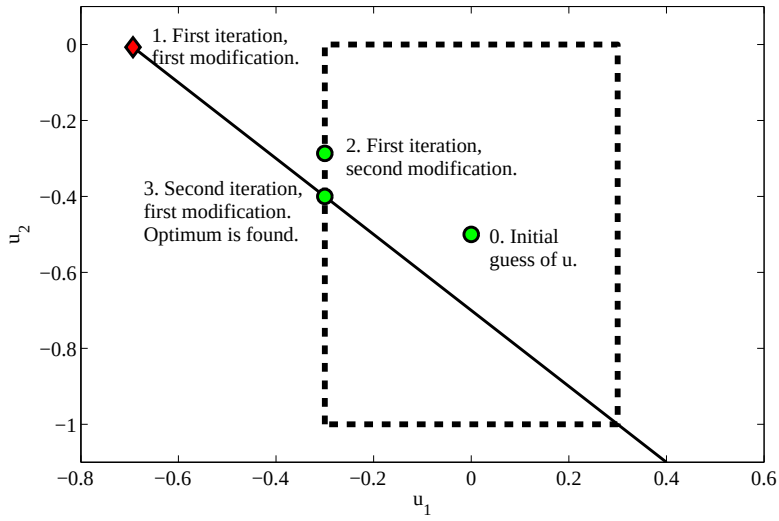

Figure B.3: Illustration of how the active set method iterates to find the optimal solution. The subset of $u \in \Omega$, the large dashed square, constrains the solution of $v = -0.7g$, the black line. The part of the black line inside the dashed square denotes all possible solutions.

Concluding Remark

In comparison to earlier solutions where only a weighted pseudoinverse was used, which did not consider the actuator constraints, a weighting matrix W_u penalized the usage of the electric motors more due to its smaller constraints $\pm 0.3g$. This leads to the undesirable result that the usage of the electric motor is small, compared with the mechanical brakes, during low deceleration demands. The active set method for wls instead allows for maximizing the use of the electric motors and the rest is then blended with the mechanical brakes to achieve the desired brake acceleration of -0.7g.

Bibliography

[1] "ADMIRE (The Aerodata Model in Research Environment)", http:/www.foi.se/admire.

[2] "DXF file of a 1964 Ford Thunderbird", http://www.demo.com.hk/dxf.htm.

[3] "The VehicleDynamics Library version 1.1 - Users Guide", http:/www.modelon.se.

[4] *Federal Motor Vehicle Safety Standards; Electronic Stability Control Systems*. US Department of Transportation, National Highway Traffic Safety Administration, Docket No. NHTSA-2006-25801, RIN:2127-AJ77, 2006.

[5] *Proposed FMVSS No. 126 Electronic Stability Control Systems, Preliminary Regulatory Impact Analysis*. US Department of Transportation, National Highway Traffic Safety Administration, Aug. 2006.

[6] ANDREASSON, J., *On Generic Road Vehicle Motion Modelling and Control*. PhD thesis, Division of Vehicle Dynamics, KTH, Sweden, 2006.

[7] ANDREASSON, J. and BÜNTE, T., "Global chassis control based on inverse vehicle dynamics models", *J. of Vehicle System Dynamics, vol.44*, 2006.

[8] AUTO MOTOR UND SPORT, "http://www.auto-motor-und-sport.de/", 2006.

[9] AUTOMOTIVE OPEN SYSTEM ARCHITECTURE(AUTOSAR), "http://www.autosar.org/", 2006.

[10] BACKSTRÖM, H., *Report on the usage of the Generic Aerodata Model*. Saab Aircraft AB, May 1997.

[11] BJÖRCK, ., *Numerical methods for least squares problems*. SIAM, 1996.

[12] BODSON, M., "Evaluation of optimization methods for control allocation", *Journal of Guidance, Control, and Dynamics, vol. 25, no. 4, pp. 703−711*, July 2002.

[13] BORDIGNON, K. A., *Constrained Control Allocation for Systems with Redundant Control Effectors*. PhD thesis, Dep. of Aerospace Engineering, Virginia Polytech Institute and State University, USA, 1996.

[14] BURBA, J., "Consideration of control system architecture in Electric and Hybrid Electric Vehicles", *Proceedings of the 18th International Electric Vehicle Symposium*, 2003.

[15] CAN IN AUTOMATION (CIA) INTERNATIONAL USERS AND MANUFACTURERS GROUP, "http://www.can-cia.de", 2004.

[16] CHAI, Y., SAITOU, Y., SAKAKIBARA, Y., KANO, Y., and ABE, M., "A study of effect of steering gain and steering torque on driver's feeling for sbw vehicle", in *The Fédération Internationale des Sociétés d'Ingénieurs des Techniques de l'Automobile (FISITA)*, (Barcelona, Spain), May 2004.

[17] COELINGH, E., CHAUMETTE, P., and ANDERSSON, M., "Open-interface definitions for automotive systems, application to a brake by wire system", *SAE 2002-01-0267*, 2002.

[18] COTTING, M. and BURKEN, J., "Reconfigurable control design for the full x-33 flight envelope", *National Aeronautics and Space Administration (NASA), NASA/TM-2001-210396*, 2001.

[19] DAVIDSON, J., LALLMAN, F., and BUNDICK, W., "Real-time adaptive control allocation applied to a high performance aircraft", in *Proc. of 5^{th} SIAM Conference on Control and Its Application*, 2001.

[20] DURHAM, W., "Constrained control allocation", *Journal of Guidance, Control, and Dynamics, vol. 16, no. 4, pp. 717−725*, July 1993.

[21] DURHAM, W., "Constrained control allocation: Three-moment problem", *Journal of Guidance, Control, and Dynamics, vol. 17, no. 2, pp. 330−336*, March 1994.

[22] DURHAM, W. and BORDIGNON, K., "Multiple control effector rate limiting", *Journal of Guidance, Control, and Dynamics, vol. 19, no. 1, pp. 30−37*, January 1996.

[23] FORKENBROCK, G., ELSASSER, D. H., O'HARRA, B. C., and JONES, R. E., *Development of Electronic Stability Control (ESC) Performance Criteria*. US Department of Transportation, National Highway Traffic Safety Administration, report no.DOT HS 809 974, Sept. 2006.

[24] FOSSEN, T. I. and JOHANSEN, T., "A survey of control allocation methods for ships and underwater vehicles", in *14^{th} Mediterranean IEEE Conference on Control and Automation*, 2006.

[25] GÄFVERT, M., *Topics in Modeling, Control, and Implementation in Automotive Systems*. PhD thesis, Dep. of Automatic Control, Lund Institute of Technology, Sweden, 2003.

[26] HARDUNG, B., KÖLZOW, T., and KRÜGER, A., "Reuse of software in distributed embedded automotive systems", *Fourth ACM International Conference on Embedded Software (EMSOFT 2004), PISA, Italy*, 2004.

[27] HATTORI, Y., KOIBUCHI, K., and YOKOYAMA, T., "Force and moment control with nonlinear optimum distribution for vehicle dynamics", in *Proceedings of the 6th International Symposium on Advanced Vehicle Control*, (Hiroshima, Japan), September 9-13 2002.

[28] HE, P., HORI, Y., KAMACHI, M., WALTERS, K., and YOSHIDA, H., "Future motion control to be realized by in-wheel motored electric vehicle", in *Industrial Electronics Society, 2005. IECON 2005. 32^{nd} Annual Conference of IEEE*, November 2005.

[29] HELLGREN, J., *A Methodology for the Design of Cost Effective Hybrid and Fuel Cell Powertrains*. PhD thesis, Dep. of Machine and Vehicle Systems, Chalmers University of Technology, Sweden, 2004.

[30] HISAOKA, Y., YAMAMOTO, M., and FUJINAMI, H., "A study on desirable steering responses and steering torque for driver's feeling", in *Int. Symposium on Advanced Vehicle Control, AVEC'96*, (Aachen University of Technology, Germany), June 1996.

[31] HÄRKEGÅRD, O., *Backstepping and Control Allocation with Applications to Flight Control*. PhD thesis, Department of Electrical Engineering, Linköping University, SE–581 83 Linköping, Sweden, May 2003.

[32] JOHANNESSON, L., *On Energy Management Strategies for Hybrid Electric Vehicles*. Licentiate thesis, Department of Signals and Systems, Chalmers University of Technology, Sweden, 2006.

[33] JOHANSEN, T., "Optimizing nonlinear control allocation", in *Proceedings of 43rd IEEE Conference on Decision and Control*, (Bahamas), December 2004.

[34] JOHANSEN, T., FOSSEN, T., and BERGE, S. P., "Constrained nonlinear control allocation with singularity avoidance using sequential quadratic programming", *IEEE Transactions on Control Systems Technology, vol. 12, no. 1*, 2004.

[35] JOHANSEN, T., FUGLSETH, T., TØNDEL, P., and FOSSEN, T. I., "Optimal constrained control allocation in marine surface vessels with rudders", in *IFAC Conf. Manoeuvring and Control of Marine Craft*, (Girona), 2003.

[36] JONASSON, M., *Aspects of Autonomous Corner Modules as Enabler for New Vehicle Chassis Solutions*. Licentiate thesis, Div. of Vehicle Dynamics, KTH, Sweden, 2006.

[37] KOPETZ, H. and BAUER, G., "The timetriggered architecture", *Proceedings of the IEEE, vol 91:1*, 2003.

[38] KOPETZ, H. and GRUNSTEIDL, G., "TTP a timetriggered protocol for fault-tolerant realtime systems", *In The Twenty Third International Symposium on Fault Tolerant Computing. IEEE*, 1993.

[39] LALLMAN, F., "Relative control effectiveness technique with application to airplane control coordination", *National Aeronautics and Space Administration (NASA), Technical paper nr 2416*, 1985.

[40] LENNARTSON, B., *Reglerteknikens grunder*. Studentlitteratur, 2001.

[41] LINDEGAARD, K.-P. and FOSSEN, T., "Fuel-efficient rudder and propeller control allocation for marine craft: Experiments with a model ship", *IEEE Transactions on Control Systems Technology, vol. 11, no. 6, pp. 850−862*, November 2003.

[42] LUO, Y., SERRANI, A., YURKOVICH, S., DOMAN, D., and OPPENHEIMER, M., "Model predictive dynamic control allocation with actuator dynamics", in *Proc. of American Control Conf.*, (Boston, MA), July 2004.

[43] LUO, Y., SERRANI, A., YURKOVICH, S., DOMAN, D., and OPPENHEIMER, M., "Dynamic control allocation with asymptotic tracking of time-varying control input commands", in *Proc. of American Control Conf.*, (Portland, OR), June 2005.

[44] MOKHIAMAR, O. and ABE, M., "Simultaneous optimal distribution of lateral and longitudinal tire forces for the model following control", *J. of Dynamic Systems, Measurement, and Control, Vol. 126, pp. 753−763*, 2004.

[45] NOCENDAL, J. and WRIGHT, S. J., *Numerical Optimization 2^{nd} Ed.* Springer Science-Business Media, LLC, 2006.

[46] OPPENHEIMER, M. and DOMAN, D., "Reconfigurable control design for the x-40a with in-flight simulation results", in *Proceedings of AIAA Guidance, Navigation, and Control Conference*, (Rhode Island), August 2004.

[47] PACEJKA, H. B., *Tyre And Vehicle Dynamics 2^{nd} edition*. Butterworth-Heinemann, 2002.

[48] PETERSEN, J. and BODSON, M., "Constrained quadratic programming techniques for control allocation", *IEEE Transactions on Control Systems Technology, vol. 14, no. 1, pp. 91−98*, January 2006.

[49] PLUMLEE, J., *Multi-Input Ground Vehicle Control Using Quadratic Programming Based Control Allocation*. Master thesis report, Auburn University, Alabama, 2004.

[50] PLUMLEE, J., BEVLY, D., and HODEL, A., "Control of a ground vehicle using quadratic programming based control allocation techniques", in *Proc. of American Control Conf.*, (Boston, MA), July 2004.

[51] SAE, "Surface vehicle recommended practice, vehicle dynamics terminology", *SAE 1976-07, J670e*, 1976.

[52] SCHOFIELD, B., HÄGGLUND, T., and RANTZER, A., "Vehicle dynamics control and controller allocation for roll over prevention", in *Proc. of the International IEEE Conference on Control Applications*, (Munich, Germany), October 2006.

[53] SNELL, S., ENNS, D. F., and GARRARD, W. L., "Nonlinear inversion flight control for a supermaneuverable aircraft", *Journal of Guidance, Control, and Dynamics, vol. 15, no. 4, pp. 976−984*, July 1992.

[54] ÅSTRÖM, K. and HÄGGLUND, T., *PID Controllers: Theory, Design, and Tuning*. Instrument Society of America, 1995.

[55] THE FLEXRAY CONSORTIUM , "http://www.flexray.com", 2004.

[56] TØNDEL, P. and JOHANSEN, T. A., "Control allocation for yaw stabilization in automotive vehicles using multiparametric nonlinear programming", in *Proc. of American Control Conf.*, (Portland, OR), June 2005.

[57] ZETTERSTRÖM, S., "Electromechanical steering, suspension, drive and brake modules", *VTC 2002, Vancouver, Canada*, 2002.

Paper I

Generic Control Architecture applied to a Hybrid Electric Sports Utility Vehicle

in

Proceedings of the Electric Vehicle Symposium, (EVS 20), Los Angeles, USA, November 2003.

Generic Control Architecture applied to a Hybrid Electric Sports Utility Vehicle

Leo Laine, M. Sc.
Div. of Machine and Vehicle Systems, Chalmers University of Technology
SE-412 96 GÖTEBORG, Sweden
Phone: +46 31 772 58 52, Fax: +46 31 772 13 80
laine@mvs.chalmers.se

Johan Andreasson, M. Sc.
Div. of Vehicle Dynamics, Royal Institute of Technology (KTH)
SE-10044 STOCKHOLM, Sweden
Phone: +46 8 790 77 14, Fax: +46 8 790 93 04
johan@fkt.kth.se

Abstract

For future vehicles it is a necessity to have tight integration between different actuators/sensors. Here, functional decomposition is utilized on a Hybrid Electric Vehicle to construct a generic hierarchical control architecture.

Specific functions are identified and allocated in different functional levels. Three functional levels are suggested; main control level, subsystem level, and actuator/sensor level.

The main control contains a *driver interpreter*, *energy management, vehicle motion control* and a *strategic control*. These main functions are made hardware independent and independent of hybrid configuration. The subsystem level contains the following: *driver interface*, *chassis*, *power supply*, and *auxiliary systems*.

The suggested control architecture is validated in an object oriented modelling language. Two different power supplies (serial) and (parallel) were implemented for a Hybrid Electric Sport Utility Vehicle and changed without affecting the contents of the Main Control level of the architecture.

Keywords: control system, communication, hybrid strategy, HEV.

1 Introduction

In order to handle the complexity of several actuators/sensors interacting in future Hybrid Electric Vehicles (HEV) one has to aim for suitable control architecture. The control architecture should not only perform well but also be reusable for different hardware configurations.

One way to achieve this goal is to construct both hardware and software in a modular fashion. These modules would have their own controller. The interface signals between the modules should be general and non specific for the actual hardware to allow easy switch of configurations. A set of modules are then grouped together to form a HEV.

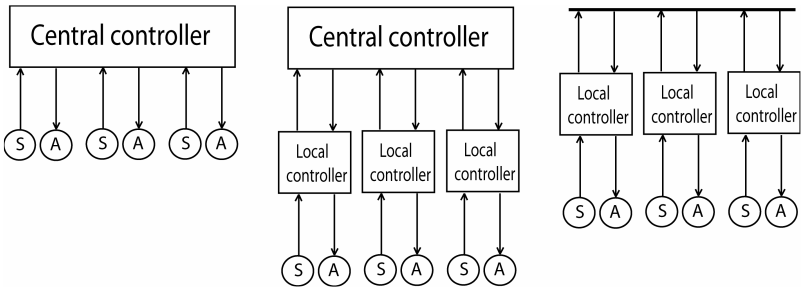

Figure 1: Illustration of a centralized (left), hierarchical (middle), and peer (right) control architecture. S=sensor, A=actuator.

In Figure 1 three main types of architectures for partitioning are shown i.e. centralized, hierarchical, and peer architecture. The centralized architecture collects data from all sensors and computes data to all actuators. The benefit is that all signals are available simultaneously. The drawback is the lack of modularity that makes it hard to add new functionality. The hierarchical structure consists of a top level control block and several low level control blocks. This allows good modularity and also a central controller is available to coordinate the interaction between the actuators/sensors. The Peer architecture is the most modular one, but without a coordinator between the different actuators/sensors conflicts will be hard to avoid.

The architecture should be generic and work for several types of HEV configurations such as parallel, serial, and split etc. It must also fulfil the requirements on interfaces between automotive supplier and manufacturer so that brand specific qualities can be kept in-house. For both these demands, the hierarchical control architecture is suitable.

The paper discusses future automotive aspects, a terminology is given and different types of control architectures are discussed, and a definition of the generic control architecture is given. The method functional decomposition is utilised and applied on a Hybrid Electric Sport Utility Vehicle and modelled in an object oriented modelling language, Modelica [1].

2 Future automotive aspects, short review

The control architectures commonly used in today's vehicles do not handle the complexity efficiently when subsystems are integrated. The automotive subsystem suppliers develop more or less independent subsystems [2]. This leads to increasing complexity when a new subsystem is introduced, as illustrated in Figure 2 (left). The vision is to have an integrated Complete Vehicle Control (CVC) where all the functions of the subsystems are emerged (right). This is even more important when new technologies based on hybrid propulsion are to be implemented.

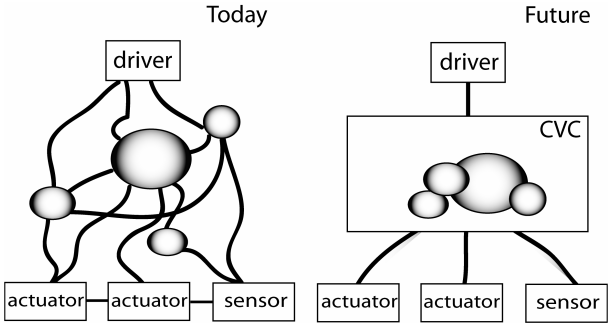

Figure 2: Illustration of how today's commonly used control architectures (left). For each new sensor, actuator or function, the complexity increases drastically. For future vehicles using a functional architecture (right), the complexity increases minimally [2].

When more onboard electric power is available by the hybrid electric propulsion the potential to replace mechanical and hydraulical actuators by electrical ones increases. This will introduce the by-wire technique in large scale in automotive vehicles. This technique will allow easier algorithmic partitioning and tighter integration of actuators to achieve better performance of the vehicle. Already some applications are implemented such as electronic throttle control and power windows. Safety critical subsystems such as steer- and, brake-by-wire must be redundant and fault tolerant before they can be implemented without mechanical backup [3]. Safety related fault tolerant x-by-wire systems for vehicles were investigated in [4]. The suggested fault tolerant architecture was demonstrated in prototype for steer-by-wire without mechanical backup. In this paper, a driver interface and a driver interpreter is introduced to handle x-by-wire control of the vehicle.

When HEVs are introduced, different configurations will be utilised and reusable control system architectures will be needed to make vehicle development feasible. In [5], a reusable architecture for hybrid powertrains is suggested. The system architecture must include a hierarchical structure that handles various engine, motors, transmission, and buffer configurations. The powertrain supervisory controller uses a torque based strategy and suites fine for parallel HEVs. In this work we try to go a step further and look at the vehicles energy sources as a Power Supply function and use force and power based strategy to control the Power Supply. This allows serial, parallel and split HEV configurations.

An open architecture for networking the control systems of an automobile called CARTRONIC was developed by Bosch GmbH [6]. It is an ordering concept for all vehicle control. The communication is divided into orders, responses, inquiries and requests. A hierarchical flow of orders is used where the vehicle coordinator places the orders and detects conflicts. Here, a similar function is performed by Strategic Control.

In this paper, all components in a wheel are seen as one function for applying force to the ground. The wheel unit function allows tight integration of the different actuators for applying longitudinal, lateral, and vertical forces within a wheel. This Wheel Unit can contain actuators such as braking, traction, suspension, and steering. The wheel as the centre of motion is also acknowledged as second x-by-wire generation in [3]. An example of how future wheel units can be designed is shown in [7]. A more detailed description of how the desired global forces are distributed to the wheel units is shown in [8].

3 Terminology

To be able to define a generic control architecture for HEVs some of the used terms are explained in this Section.

- *Complexity:* The number of actuators/sensors that have to interact defines the level of complexity.
- *Centralized control architecture:* A single controller which computes control signals for all actuators of the vehicle and has complete knowledge of the entire system.
- *Peer to Peer control architecture:* All subsystems have their own control block has knowledge of some (or all) remote states in addition to all local states. There is no supervisory control block with global knowledge of the system.
- *Function:* When something is performed, e.g. applying driving force to the wheels. This should not be confused with the specific actuators. Different actuators or sensors can sometimes perform the same task.
- *Functional decomposition*: By identifying the different functions a vehicle have one can declare the dependency between the functions and decide the hierarchy within the functions.
- *Functional level*: Depending on the function it is placed in different levels. The lowest functional level is the control of a specific actuator e.g. an electric machine for applying

driving torque, next level is the subsystem control, and the highest is the main control which controls and integrates all subsystems.

- *Generic interface signals*: The interface signals between different functions should be made hardware independent.
- *Generic control architecture*: A reusable control architecture that is not hardware dependent or configuration dependent.
- *Hierarchical control architecture:* All subsystems have their own controller (with local state knowledge) and there also exist a supervisory controller with knowledge of the entire vehicle.
- *Power supply:* Onboard energy sources in the vehicle.
- *Reusable:* The same software/hardware can be utilised in different configurations. Only small modifications should be needed. Examples of hardware configurations are parallel, serial, and split for HEV.
- *Subsystem:* A part of the whole system with clearly specified purpose, e.g. mechanical brake actuators/sensors with its control. Note that several subsystems may corporate to perform the same function, e.g. the mechanical brake subsystem together with the wheel motors can generate brake torque.

4 The suggested generic control architecture

There are different reasons for choosing a certain type of architecture. The centralized control architecture can always outperform the hierarchical and the Peer architecture. The hierarchical architecture also introduces additional conditions by using generic control signals. But if one considers the design and engineering benefits then the hierarchical architecture is a suitable partitioning scheme for HEV. In [9] hierarchical partitioning is recommended. Different partitioning schemes are also discussed in [10] and [11].

4.1 Definition of a generic control architecture for HEVs

By using the terminology stated in Section 3 one can now define the generic control architecture:

The control architecture type should be hierarchical by functional decomposition. Generic interface signals should be used between the functions. By minimum effort the architecture should be reusable and allow new subsystems to be implemented.

Evaluation of the control architecture should be made by measuring the handled complexity, performance, reusability, and the sensitivity of communication- and computational delays.

4.2 Functional decomposition

In [12] a method for functional decomposition is given considering vehicle control systems. The highest functional level is denoted here as main control. Based upon [12] the following guidance is given:

1. The function needs to be at a level high enough to allow it to coordinate lower level functions that it has authority over.
2. The information, i.e. system status, can be observed by many and is allowed to flow in all directions; up, down, and across in the hierarchy.
3. The orders to actuators are only allowed to flow down to lower level functions. This upholds a causality of the orders within the hierarchical architecture.
4. If a particular function effects the vehicle's brand characteristics (can be observed by a customer) it is qualified to the highest level (main control) only if it does not jeopardise the reusability of the main control for different HEV configurations.
5. Durability is also a consideration for choosing the level at which partition a function. Local control of any potentially damaging functions is recommended.
6. The interfaces within the control system should be generic, i.e. not hardware dependent.

Item 4 allows manufacturer to retain ownership of the brand specific functions while suppliers can provide controls for various subsystem functions. This also allows the manufacturer to change the vehicle characteristics from optimizing the drivability to fuel economy. Item 5 also matches well with the supplier and manufacturer relationships. Item 6 allows hardware to be changed without redesigning the functional architecture.

4.3 Main architecture

The Main Control consist of three major parts; Driver Interpreter (DIp) interprets the driver's demands, Vehicle Motion Control (VMC) controls the vehicle according to these demands and Energy Management (EM) assures that this is done in a energy efficient way. Additionally there is the Strategic Control (SC) which summarizes the input from them both and makes the overall decisions considering reliability and safety. The functional decomposition with three hierarchical levels is shown in Figure 3. The highest of these levels is the Main Control. The communication is handled with a network.

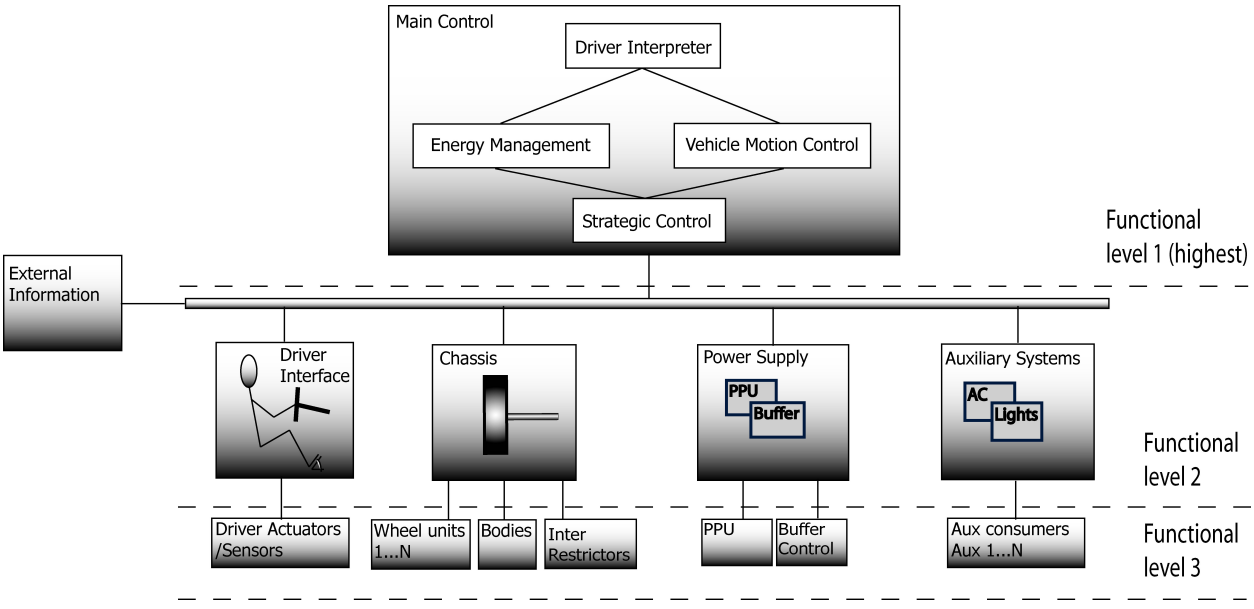

Figure 3: Schematic sketch of the functional architecture. It contains three levels.

In Figure 4 the signal flow from the Driver Interpreter to Chassis and Power Supply is shown in more detail while auxiliary systems and Driver Interface are excluded for simplicity. This illustrates how driver's intentions generate vehicle motion and the needed energy.

4.3.1 Driver Interpreter

Driver Interpreter handles the communication with the Driver Interface. The incoming signals are translated into a desired path and according to the limitations given by Energy Management and Vehicle Motion Control, feedback signals are sent to the Driver Interface.

4.3.2 Vehicle Motion Control

Vehicle Motion Control calculates the global forces Fx, Fy, and Mz that are required to generate the desired accelerations received from Driver Interpreter. Then it determines how the forces should be distributed between the Wheel Units (WU). More detailed description of the VMC and WU functions are found in [8]. The idea is to already from the beginning determine the force distribution between the wheel units and by this achieve overall performance with smooth behaviour that considers the maximum force surface (fx_i, fy_i, fz_i) for each Wheel Unit to generate desired forces within the stable region. Similar

approach is also used in [13]. A conventional vehicle have different safety systems such as ABS, VSC (Vehicle Stability Control, TCS (Traction Control System), these functions are usually only used in critical situations, and thus don't have a smooth behaviour.

4.3.3 Energy Management

EM calculates the desired power needed from Power Supply considering the total tractive force and needed auxiliary power. EM calculates a State of Charge (SOC) target where it considers vehicle speed. A coefficient of desired electric regenerative braking is also calculated and sent to both Chassis and Power Supply. It considers if the SOC is higher or lower than SOC target. Logic for maximum auxiliary power use is also located in EM. The overall traction force is estimated by Energy Management and is sent to Strategic Control that finally sends the order to Power Supply.

4.3.4 Strategic Control

The SC is the part in Main Control that finally places the orders from EM and VMC. It considers if EM or VMC signals that the vehicle status is critical and then Strategic Control gives priority to primary functions as suggested from either part.

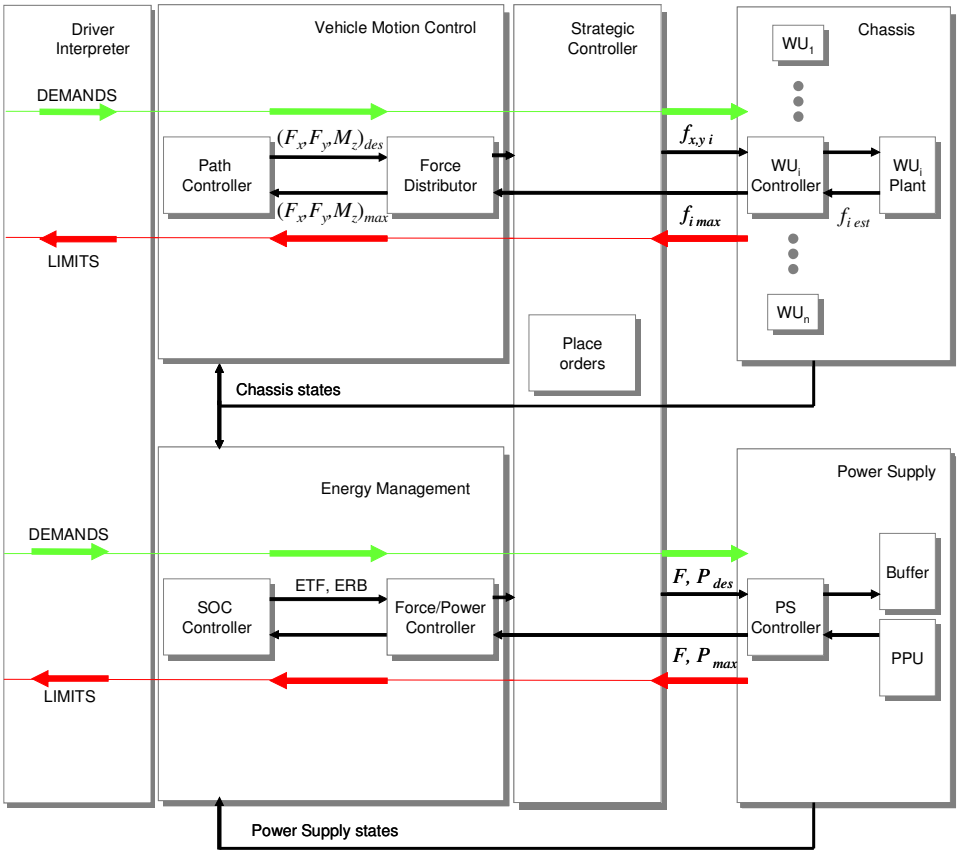

Figure 4: Signal flow between Driver Interpreter, Chassis and Power Supply. All demands have to be authorized by the Strategic controller.

Generic interfaces are utilised for the orders and the information e.g. vehicle states. By using generic interfaces, hardware can be changed without re-designing the Functional level 1. Some of the allocated functions in functional level 1 are summarized in Table 1. Table 2 shows a subset of functions for level 2. The signal interfaces between functional level 1 and 2 are made generic. There are specific subsystems within the different classes in functional level 2.

Table 1: Some of the allocated functions in Functional level 1 –Main Control.

Driver Interpreter	Definitions
Driver intentions	Determines the desired global accelerations by interpreting the information given by sensors in Driver Interface and the feedback from the Vehicle Motion Control, Driver Interpreter.
External information	If it is activated, it uses available external information, e.g. distance to vehicles ahead, traffic flow and road conditions to automate the driver's intentions. This includes functions as cruise control (keeping a desired speed)
Driver feedback	By limit feedback input from Vehicle Motion Control and Energy Management the level of feedback is determined and sent to Driver Interface. This could be force feedback on steering wheel and pedals.
Vehicle Motion Control	Definitions
Global forces	Determines the desired global vehicle forces from Driver Interpreter.
Wheel Unit forces	Determines the longitudinal, lateral, and vertical wheel forces for each wheel unit for vehicle dynamic optimal driving for current vehicle state and the desired global forces.
Limit feedback	Interprets and feeds back limitations on achievable accelerations to the Driver Interpreter.
Energy Management	Definitions
State of charge (SOC) target	By considering vehicle state (vehicle speed), driver's intentions, and environmental data (e.g. known topology, traffic information) a suitable SOC target for the buffer is determined.
Buffer	SOC regulation according to SOC target.
Traction force/power	Determines a traction force for energy optimal driving.
Split Traction force	If a parallel or split HEV configuration is the current system then the suggested level (0...1) should be generated by the electric motors.
Split Braking force	Defines the level (0...1) that should be used to regenerate energy.
Auxiliary load	Determines the maximum power allowed for the auxiliary system.
Strategic Control	Definitions
Arbitration of demands from EM and VMC	Summarizes the demands from Energy Management and Vehicle Motion Control and decides which is most critical.
Vehicle mode	Here, different vehicle characteristics are accounted for by driver's choice. The different modes could be sport, normal, or economical driving.
Authorisation of orders	Sends final orders to functional level 2.
Shut down logic	When bad state of health is sent from some actuator/sensor it is allowed to shut down by Strategic Control.

Table 2: Some of the allocated functions in Functional level 2 –Driver Interface, Chassis, Power Supply, Auxiliary systems.

Driver interface	Definitions
steering, accelerator, brake, mode	Determine the level and rate of change of the pedals and steering wheel or joystick. Sends the information to Driver Interpreter along with mode settings as e.g. sport/normal/economy.
Forward / Reverse	Determines the direction of the vehicle
Chassis	Definitions
Wheel unit control	The forces are distributed by the VMC is generated at each WU. Typically, the desired forces are translated into steering angle and tractive/braking torque.
Actuator coordination	Several actuators may perform the same function, this requires

	coordination. Typically this could be to split the requested tractive/braking force between current available actuators according to guidance given by Strategic Control.
Inter-restrictor coordination	When introducing inter-restrictors, one actuator may affect several wheel units, typically a rack steering which constrains the steering angle of two wheels.
Power Supply	Definitions
PPU	Control of the Primary Power Unit. For an ICE and transmission this would include elementary engine functions such as spark, air, fuel etc. plus shift scheduling for the transmission.
SOC/SOH level	Determines the SOC/SOH level of the buffer and send this information to Energy Management.
DC-DC	Determine the charging or discharging mode for DC to DC voltage converter.
Auxiliary Systems	Definitions
Climate control	Regulate the cabin temperature.
Lights	Regulate lights.

4.4 Power supply

The conventional powertrain concept with a combustion engine, transmission, and driveline is not a valid description for a HEV. The HEV concept includes handling of a major electricity source in combination with a conventional or parts of a conventional powertrain. A more suitable name of this function is Power Supply. The Power Supply includes both the Primary Power Unit (PPU) and a buffer and can be anything from an internal combustion engine to a fuel cell. The buffer can be an electric buffer such as a battery, super capacitor or a mechanical one e.g. flywheel. Figures 5 and 6 show how the power supply is defined for a serial, parallel, and split HEV configuration. The examples include inter-restrictors between Wheel Units. The restrictors illustrates that the driving torque applied to two wheels is restricted by e.g. a differential or an electric machine connected by a differential. Restrictors are explained in Section 4.5.3.

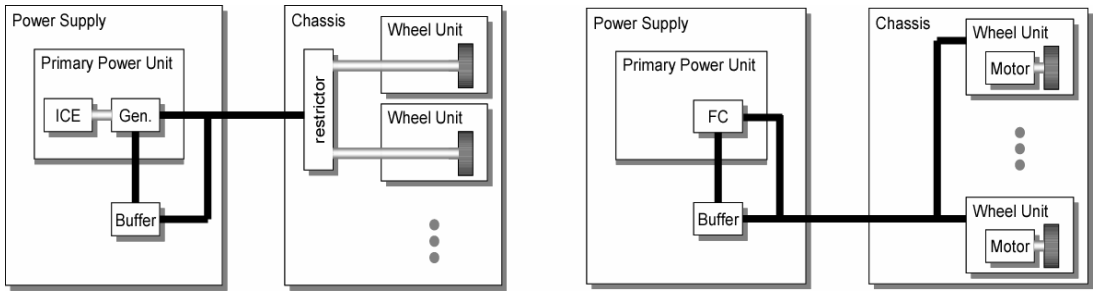

Figure 5: Illustration of power supply for serial with internal combustion engine (left) and serial with fuel cell (right) HEV configuration. ICE=Internal Combustion Engine, Gen=Generator, FC=Fuel Cell, Black line=electrical power, and Grey line=mechanical power.

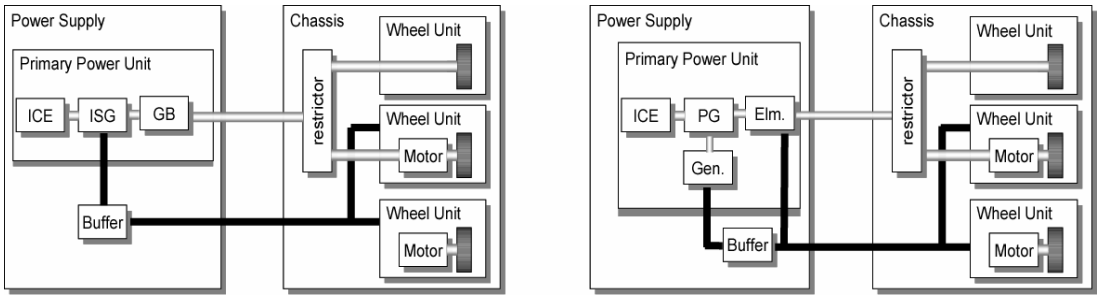

Figure 6: Illustration of power supply for parallel (left) and split (right) HEV configuration. ISG=Integrated Starter/Generator, GB=GearBox, PG=Planetary Gear, Elm=Electric machine.

4.5 Chassis

The chassis is thought of as a body onto which a number of wheel units are mounted, see Figure 7. Each wheel is then considered as an autonomous unit and by default decoupled from the other wheels. Depending on the linkage carrying the wheel as well as the available actuators, there are different possibilities to generate ground contact forces. A very simple case is a wheel with only brakes and no steering possibility and passive suspension, while other wheel units may have drive, steering, camber control and active damping.

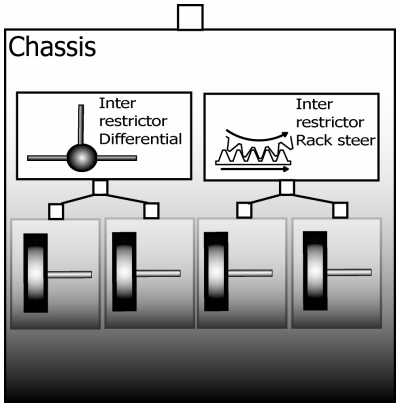

Figure 7: Schematic sketch of a chassis containing 4 wheel units and the inter-restrictor differential and rack steering.

There are various kinds of restrictions for each wheel's motion. An obvious case is the steering of a traditional car which couples the steering angle of the front wheels. To handle this in a clean and efficient way, the chassis is thought of as consisting of three types of components at any amount each; bodies, wheel units and restrictors.

4.5.1 Body

The body's main task is to frame the vehicle which essentially means to carry the wheel units as well as passenger and goods. In addition to this, the body also carries properties such as mass, inertia, and a geometric reference frame as well as sensors to measure its states. The main idea with the function body is that more than one body can be used when defining articulated busses, semi trailer combinations or week chassis. The body includes the specific wheel units that are attached to the specific body inter restrictors define the connections between the bodies.

4.5.2 Wheel Unit

The distributed forces from the Strategic control is realised at each WU that also sends information about maximum achievable force. To generate the tractive force, fx_i, the wheel unit checks how much rotational torque is available directly by Power Supply on the actual wheel unit and then coordinates the available actuators to meet the desired order. Typically the wheel unit could be realized as in [7]. More details about vehicle motion control and wheel unit are presented in [8].

4.5.3 Restrictors

Today’s conventional chassis have constraints and limit the controllability of each wheel unit. To handle this in a systematic way restrictors are introduced. A restrictor can either restrict the wheel's motion relative to the body, i.e. within the wheel unit or relative to another wheel unit; these are referred to as intra-acting and inter-acting, respectively. Furthermore, these could be either 'active', meaning that they could be controlled, or 'passive' units like e.g. a standard strut. Some examples are presented in Table 3.

Table 3: Example of different type of utilised restrictors. Note that parts of a traditional powertrain that are used to distribute tractive force are as restrictors within the chassis.

	Inter-restrictor	Intra-restrictor
Active	Limited slip differential Rack steering	Wheel motor Mechanical brake unit
Passive	Differential Anti-roll	Suspension linkage Strut

5 Modelling of Hybrid Electric Sport Utility Vehicle

An object oriented modelling language is used to test how the control architecture works [1]. Two models of a Hybrid Electrics Sports Utility Vehicle are modelled. The first configuration uses a combustion engine with Integrated Starter Generator (ISG), automated manual transmission, battery buffer and electric motors at the rear wheels. This concept allows a more economical utilisation of the four wheel drive and a similar concept study was made in [14]. The second example is a future version with serial HEV configuration with a fuel cell, buffer, and autonomous Wheel Units. In Figure 8 (left) the total vehicle model is shown and in the right screen shot shows how different Power Supplies can be used due to the modularity in the architecture.

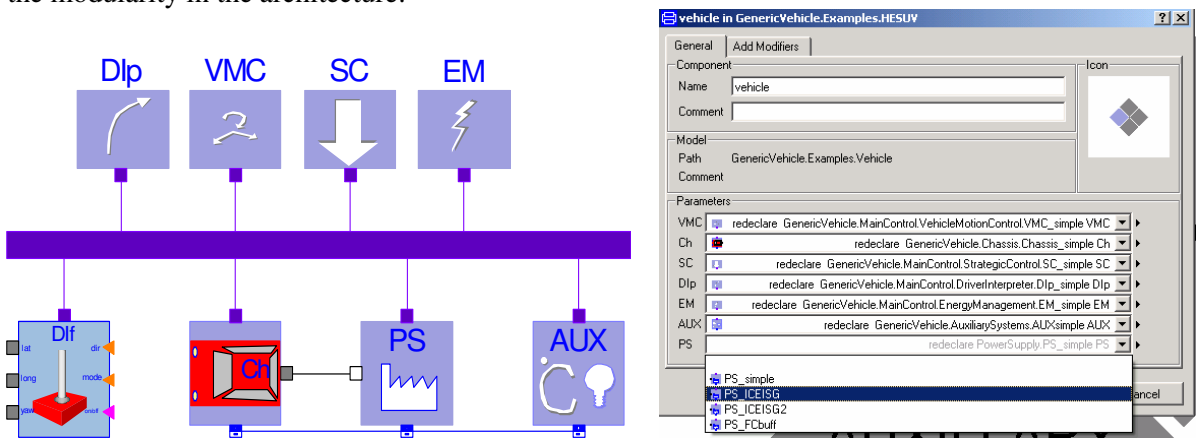

Figure 8: Total vehicle model (left). Due to the generic architecture, the configuration can be changed by selecting options from drop down boxes and no remodelling is necessary (right).

In Figure 9 the two chassis configurations are shown. The first configuration has rotational power (dotted, black) is distributed to the front wheels via the differential. In the front there is also a rack steering to constrain the wheels' steering angle and both front and rear, there are anti roll linkages. The dashed, purple line shows the bus connection and the solid, blue lines are mechanical connections. In the second configuration only electric power is used and no inter-restrictors are used since all wheel units are independent. Roll control is managed by active components in the suspensions.

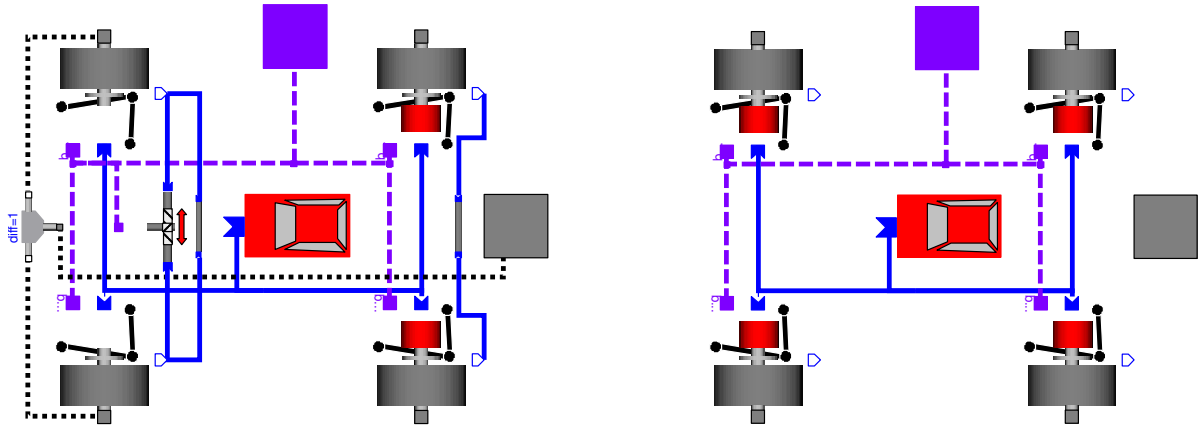

Figure 9: Chassis models corresponding to the first configuration (left) and the second configuration (right).

The two different Power Supply configurations that were implemented could be changed without affecting the rest in the generic control architecture. The chassis configuration could be changed, but further work on handling the inter-restrictors in an efficient will be made.

6 Conclusions and future work

Here a methodology and a definition for generic control architecture for HEVs are given. Hierarchical partitioning and functional decomposition is utilised to place the functions in different functional levels. The highest functional level includes the functions *Driver Interpreter, Energy Management*, *Vehicle Motion Control,* and *Strategic Control.* The second functional level includes the sub functions *Driver Interface, Chassis, Power Supply, External Information* and *Auxiliary Systems.* The generic control architecture has been implemented in object oriented modelling language and is proven to work.

In this paper, the Wheel Units are seen as a function to apply forces to the ground and by default are decoupled. But today's cars have constraints between the wheels. This is suggested to be handled by defining inter-restrictors. These will be further studied in future work along with other vehicle configurations.

7 References

[1] www.modelica.org, The Modelica Association, (2002)

[2] Erik Coelingh, Pascal Chaumette, and Mats Andersson. *Open-Interface Definitions for Automotive Systems, Application to a Brake by Wire System,* SAE 2002-01-0267.

[3] Nico A. Kelling and Patrick Leteinturier, *X-by-Wire: Opportunities, Challenges and Trends,* SAE 2003-01-0113

[4] *X-By-Wire, Safety Related Fault Tolerant Systems in Vehicles,* Project No. BE 95/1329, Contract No: BRPR-CT95-0032, X-By-Wire Consortium, 1998.

[5] Michael Larsen, Steve De La Salle and Dave Reuter, *A Reusable Control System Architecture for Hybrid Powertrains*, SAE 2002-01-2808.

[6] Torsten Bertram, Rainer Bitzer, Rainer Mayer and Asmus Volkart, *CARTRONIC - An Open Architecture for Networking the Control Systems of an Automobile*, SAE-980200.

[7] Sigvard Zetterström, *Electromechanical Steering, Suspension, Drive and Brake Modules,* VTC 2002, Vancouver, Canada, September 24 - 28, 2002.

[8] Johan Andreasson and Leo Laine, *Driving Dynamics for Hybrid Electric Vehicles Considering Handling and Control Architecture,* To be presented at IAVSD'03, 18th Int. Symp. Dynamics of Vehicles on Roads and Tracks, Japan, 24-29 Augusti 2003.

[9] Joseph C. Burba, *Consideration of Control System Architecture in Electric and Hybrid Electric Vehicles,* Electric Vehicle Symposium 18, Berlin, 2001

[10] Magnus Gäfvert, *Topics in Modeling, Control, and Implementation in Automotive Systems,* Dep. of Automatic Control, Lund Institute of Technology, Sweden, 2003.

[11] John Yook, Dawn Tilbury, Kalyani Chervela, and Nandit Soparkar. *Decentralized, Modular Real-Time Control for Machining Application.* url: citeseer.nj.nec.com/246337.html, 1997.

[12] Anthony M. Phillips. *Functional Decomposition in a Vehicle Control Systems* American Control Conference, Anchorage 2002.

[13] Yoshikazu Hattori, Ken Koibuchiyy, and Tatsuaki Yokoyama, *Force and Moment Control with Nonlinear Optimum Distribution for Vehicle Dynamics*, AVEC'02, Japan, 2002.

[14] Mikael Arnelind and Gustav Widén, *Design and Control of an E4WD system for a soft hybrid electric vehicle*, Chalmers University of Technology, Sweden, June 2003.

8 Authors

Leo Laine, Chalmers University of Technology, Sweden. Received his M.Sc. in Structural Mechanics in 1996 from Chalmers. Worked at Swedish Defence Research Establishment as research engineer until 1998. Then as a numerical consultant at ANKER – ZEMER Engineering AS. In 2002 he started his Ph.D. studies at Chalmers, Dep. of Machine and Vehicle Systems, Div. of Mechatronics. The name of the project is HEV Main Control.

Johan Andreasson, Royal Institute of Technology (KTH), Sweden. Received his M.Sc. in Mechatronics in 2001 from KTH. In 2002 he started his Ph.D. studies at KTH, Div. of Vehicle Dynamics. The name of the project is HEV Driving Dynamics.

Paper II

Driving Dynamics for Hybrid Electric Vehicles Considering Handling and Control Architecture

in

Journal of Vehicle System Dynamics, Vol. 41, pp 497-506, 2004.

DRIVING DYNAMICS FOR HYBRID ELECTRIC VEHICLES CONSIDERING HANDLING AND CONTROL ARCHITECTURE

Johan Andreasson* and Leo Laine†

SUMMARY

The use of hybrid techniques together with the increasing demands on vehicle performance require an improved vehicle architecture to be feasible in the long run. In this paper, a generic control architecture is suggested and especially the information flow between driver's intentions to vehicle motion is discussed.

The idea is that the driver's intentions are transformed to a global force equivalent. Then, a practical approach is utilised to solve the control allocation problem of distributing the global forces to local wheel unit forces. A strategy to find wheel angles and wheel spin from desired wheel forces has been suggested and implemented.

1 INTRODUCTION

Although the research on Hybrid Electric Vehicles (HEV) is driven by environmental reasons, it is relevant to study the new technology from a driving dynamics point-of-view to be able to design competitive vehicles in the future. Except for the environmental advantages, two other aspects can be identified; the potential of improved handling as well as a need for a more structured control architecture.

Additional electric propulsion improves controllability of the vehicle behaviour compared to a conventional power-train for several reasons [1]. The torque applied to the wheels axes can be faster and more precise than with an Internal Combustion Engine (ICE) and hydraulic brakes. For an Anti lock Braking System (ABS), a more precise brake torque makes it possible to reduce vibrations and quicker response can be used to improve performance. Also, it is reasonable to have more than one electric motor for propulsion and thus it is possible to achieve active wheel torque distribution without advanced differentials. Even bidirectional torque distribution is possible with electric machines

*Div. of Vehicle Dynamics, KTH, SE-100 44 Stockholm, Sweden, e-mail: johan@fkt.kth.se, phone: +46 8 790 77 14, fax: +46 8 790 93 04

†Div. of Mechatronics, Chalmers University of Technology, SE-412 96, Gothenburg, Sweden, e-mail: laine@mvs.chalmers.se, phone: +46 31 772 58 52, fax: +46 31 772 13 80

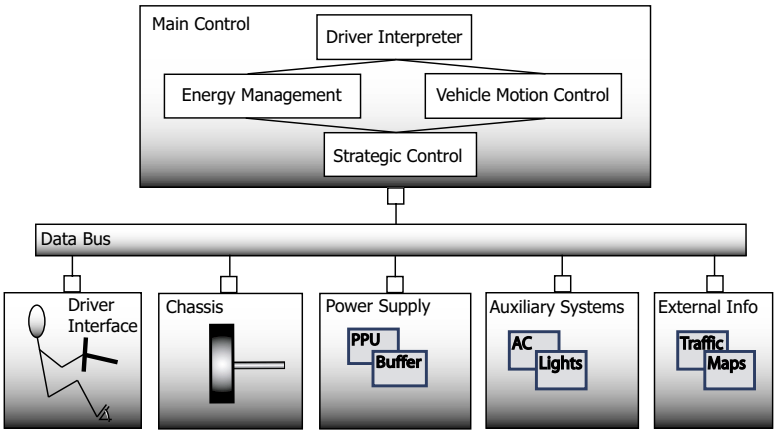

Figure 1: Schematic sketch of the functional architecture for a vehicle.

which adds possibilities to enhance the functionality of today's Vehicle Stability Controllers (VSC).

The other aspect relates to the fact that different subsystems are needed to be integrated in today's vehicles for better drivability and handling [2]. This increases the complexity of the vehicle system. Also, there are a variety of HEV configurations and most of them add more components to the vehicle. To handle this in an efficient way a hierarchical control architecture is suggested with generic interface signals. This opens up for reusability for different hardware configurations in a modular fashion [3].

2 GENERIC CONTROL ARCHITECTURE

Functional decomposition was used to identify functions within a HEV and place them in an hierarchical structure. The purpose was to make a generic control architecture[1] for HEVs [4]. Generic interface control signals was utilised between the identified functions to make it easy to change configuration [5]. Different components may perform similar tasks, e.g. electric wheel motors can perform as braking discs and in this work, all components within a wheel unit is seen as a function for applying force to the ground. This to allow tight integration of the different actuators for applying longitudinal, lateral, and vertical forces within the wheel unit.

The suggested functional architecture is shown in Figure 1. It is based on generic assumptions such that a vehicle must have a driver interface, an interaction with the ground (Chassis), power source(s) (Power Supply) and possibly also external information functions and auxiliary systems that are not involved in the vehicle motion. The system needs to communicate with the driver (Driver

[1]Generic Control architecture: A reusable control architecture that is not hardware dependent or configuration dependent.

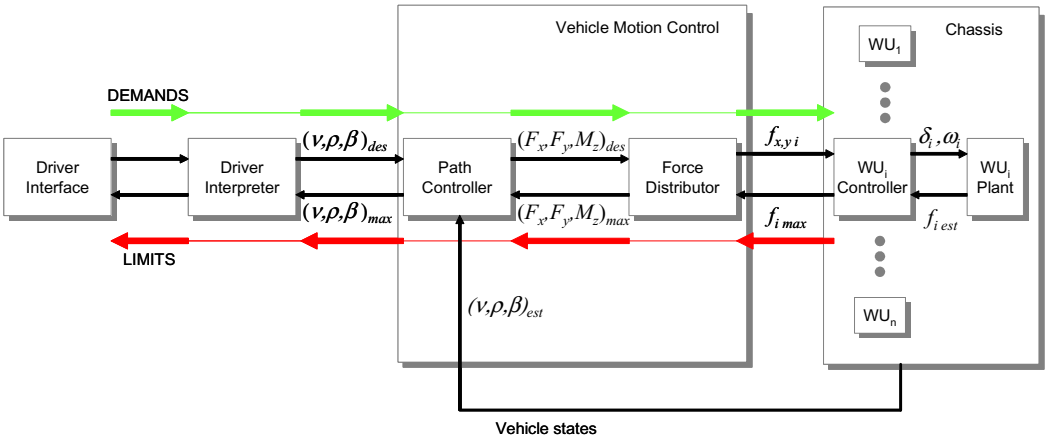

Figure 2: Signal flow between driver interface and chassis wheel units (WU). Note that only one WU is shown.

Interpreter), to control the vehicle's motion (Vehicle Motion Control), and to manage the energy flow (Energy Management). The chassis is considered as number of bodies, each with number of wheel units that can generate forces. A more thorough description is found in [3].

In [6], a structured and hierarchical way to handle the integration of different wheel controls is shown. However, all systems are based on a traditional car in the sense that there is a division into power train, chassis, brakes etc. that makes them less suitable for HEVs in general. Here, a Vehicle Motion Control that considers the desired motion and distributes forces to the wheel units is presented.

3 STRUCTURE FOR DRIVER'S INTENTIONS TO VEHICLE MOTION

Figure 2 shows the signal flow between Driver Interface and Chassis in more detail. Four isolated functions are used to transform the Driver Interface signals into vehicle motion and respond with suitable feedback; driver interpretation, path control, force distribution and wheel unit control. Each function has to set demands to the next one and send limits to the previous in order to guarantee that it can fulfill its own demands.

3.1 Driver interpretation

The task is to interpret the signals from the driver interface to a suitable path that is achievable according to the limitation set up by the path control. Also feedback signals are calculated and sent to the driver. The communication signals exchanged with the driver interface are all in percentage of their maximum values, respectively. Thus, the driver interface hardware can be exchanged from

steering wheel and pedals and to e.g. a joystick. This step is left out of the further discussion within this work and instead a predefined path is given.

3.2 Path control

The task of the path controller is to follow the path set up by the driver interpreter by giving force and torque demands to the force distribution. The path is described by the velocity v, the vehicle's slip angle β and the curvature ρ. These values are chosen to give the opportunity to keep the path well defined even at low speeds and standing still. Both the current and desired path are treated as public information within the vehicle since they are considered to be generic signals. Together with the force distribution, this is the Vehicle Motion Controller. Within this work a P-controller is used but the structure opens up for more advanced solutions as well.

3.3 Force distribution

The distribution of forces depends on the controllability and the number of wheel units. This can be considered as a linear control allocation problem

$$\mathbf{B}u(t) = v(t) \tag{1}$$

where $v(t)$ is the desired global forces F_x, F_y, M_z, $u(t)$ is the desired wheel unit forces $f_{x,i}$,$f_{y,i}$ and $\mathbf{B}$ is a 3×8 transformation matrix. This is similar to control allocation problems for flight control, see e.g. [7] for a good overview.

However, while aircrafts normally have to deal with componentwise rudder deflection limitations, vehicles equipped with tyres instead have nonlinear, coupled constraints due to tyre friction ellipses. In [8], circular constraints are replaced by polygons, allowing standard solvers to be used. Possibly, the problem can also be rewritten into a second order cone program [9] that can be solved by e.g. interior point method.

For ground vehicles, a nonlinear optimisation algorithm is suggested for the case where individual torque control can be applied [6], but a combination of individual steering and drive is not found by the authors. Within this paper, finding an optimal solution is not the main focus and thus a practical approach was chosen for the control allocation problem, that is carried out in a few steps.

Consider Figure 3, first the division of yaw torque M_z between lateral and longitudinal forces are done with a weighting function $k(F_x, F_y)$ such that $M_z = k\Delta F_x + (1-k)\Delta F_y$. The weighting function k is here realised by summation of two second order polynomials, shown in Figure 4.

$$\begin{aligned} k &= \frac{1}{2}(a_x + b_x|F_x| + c_x F_x^2 + a_y + b_y|F_y| + c_y F_y^2) \\ a_x &= 0.5,\ b_x = (1+\sqrt{2})/F_{xmax},\ c_x = -0.5b_x^2 \\ a_y &= 0.5,\ b_y = -(1+\sqrt{2})/F_{ymax},\ c_y = 0.5b_y^2 \end{aligned} \tag{2}$$

The idea is to avoid using forces that are near saturation so k should be small for high F_x. Also very low F_x should generate small k since it otherwise requires

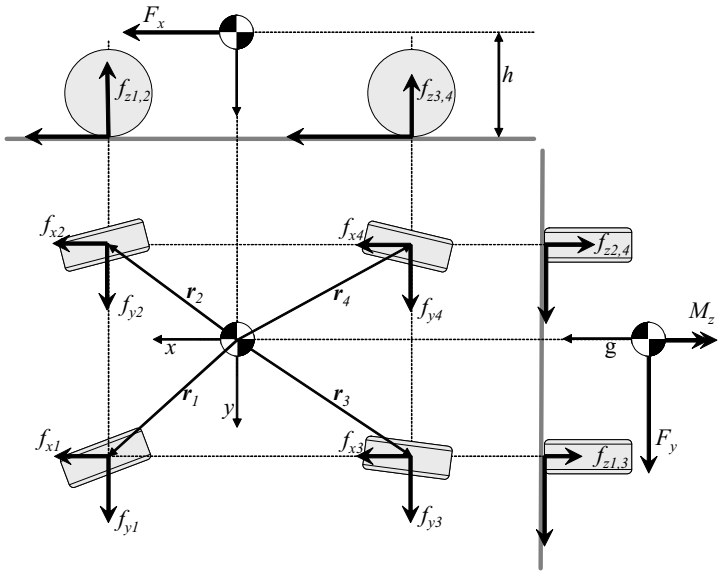

Figure 3: Vehicle model used for force distribution.

reversed forces left-right or front-rear. For mid range F_x, k is instead maximised, see Figure 4, left. For F_y, $(1-k)$ is instead considered, making k antisymmetric around $F_x/F_{xmax} = F_y/F_{ymax}$. The polynomials are used to give a smooth behaviour but of course, any other appropriate mapping could be chosen for this purpose.

Then, left and right longitudinal forces as well as the front and rear lateral forces are calculated according to:

$$\begin{aligned}
&\frac{(r_1+r_3)}{2} \times (f_{x1}+f_{x3}) + \frac{(r_2{+}_4)}{2} \times (f_{x2}+f_{x4}) = \Delta F_x \\
&(f_{x2}+f_{x4}) + (f_{x1}+f_{x3}) = F_x \\
&\frac{(r_1+r_2)}{2} \times (f_{y1}+f_{y2}) + \frac{(r_3+r_4)}{2} \times (f_{y3}+f_{y4}) = \Delta F_y \\
&(f_{y1}+f_{y2}) + (f_{y3}+f_{y4}) = F_y
\end{aligned} \tag{3}$$

The last step is to decide the internal distribution to each wheel and it is done to distribute the force reserve at each wheel evenly. The maximum contact force for each wheel unit are assumed to be a function of ground conditions and the normal force. Thus, the distribution of the longitudinal forces between front and rear are defined by the lateral force reserve at the front and rear respectively. The lateral forces are distributed correspondingly between left and right.

3.4 Wheel Unit control

At each wheel unit, the desired forces have to be transformed into proper steering angles δ_i and wheel spin velocities ω_i. This is not done in the vehicle motion

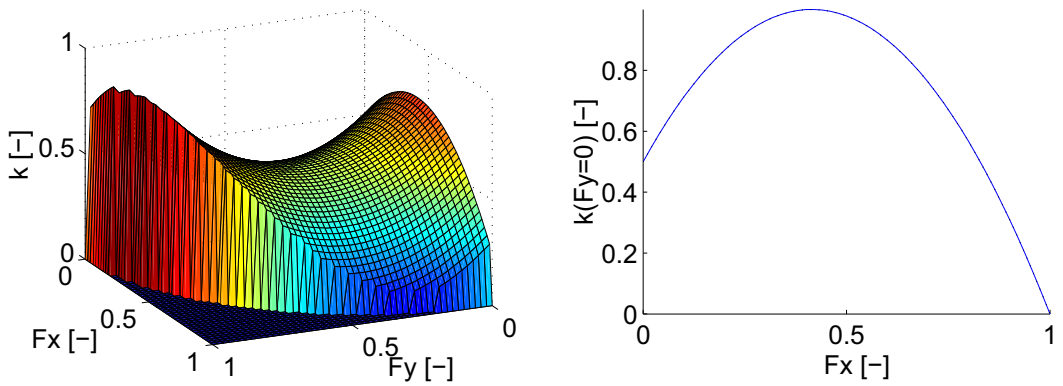

Figure 4: Normalised weighting surface $k(F_x, F_y)$, left, and $k(F_x, F_y = 0)$, right.

control since it requires that the vehicle has knowledge about each tyre's properties and thus $(\delta, \omega)_i$ cannot be generic.

Assuming that the tyre properties can be found by the wheel unit itself, there are two main problems to overcome when calculating $(\delta, \omega)_i$ from $(f_x, f_y)_i$. These are the nonlinearities of the tyre and the nonlinear transformation from chassis frame to wheel frame $\mathbf{T}(\delta_i)$.

The tyre nonlinearities are handled by approximating the tyre characteristics with a polynomial

$$f(s) = bs + cs^2 + ds^3 \tag{4}$$

where s is the magnitude of the slip and f the force respectively. The coefficients can be calculated from the Magic Formula [10] parameters according to

$$\begin{aligned} b &= BCD \\ c &= -1/2(BCD + 3D(BCs_{max} - 2)/s_{max})/s_{max} \\ d &= D(BCs_{max} - 2)/{s_{max}}^3 \end{aligned} \tag{5}$$

In Figure 5, a comparison is shown between a variety of tyre properties generated by the Magic Formula and the corresponding polynomials.

The advantage with this representation is that $f(s)$ is easily invertible using Cardanus' formula. Since $f(s) \leq D$ for all relevant s there are always three real solutions to s of which the following is the proper one:

$$\begin{aligned} s &= -\frac{1}{12d}{Q_1}^{1/3} + \frac{-c^2 + 3db}{3d{Q_1}^{1/3}} - \frac{1c}{3d} + \frac{1}{2}\sqrt{-3}\left(\frac{1}{12d}{Q_1}^{1/3} + \frac{-c^2 + 3db}{3d{Q_1}^{1/3}}\right) \\ Q_1 &= 36bcd + 108f(s)d^2 - 8c^3 + 12\sqrt{3}Q_2 d \\ Q_2 &= \sqrt{-c^2b^2 + 4db^3 + 18bcdf(s) + 27f(s)^2d^2 - f(s)c^3} \end{aligned} \tag{6}$$

Once the slip magnitude s is found, the components are calculated as $(s_x, s_y) = \frac{s}{f}(f_x, f_y)$. However, due to the steering angle the following nonlinear relation

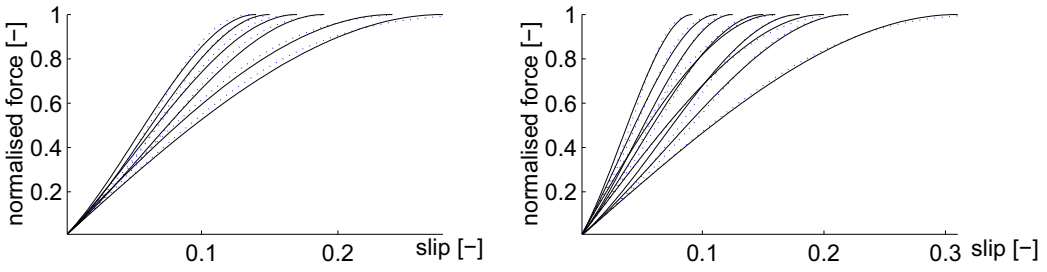

Figure 5: Comparison of generated polynomial (solid) with corresponding Magic Formula characteristics (dotted), these are generated with B between 3 and 6, C between 1.4 and 1.8 while D and E are kept constant at 1 and -20, respectively.

between the slips expressed in chassis frame $\overline{s}_i = (s_x, s_y)_i^T$ and wheel frame $\overline{s}_{iW} = (\kappa, \alpha)_i^T$

$$\overline{s}_i = T(\delta_i)\overline{s}_{iW} = \begin{pmatrix} \cos\delta_i & -\sin\delta_i \\ \sin\delta_i & \cos\delta_i \end{pmatrix} \overline{s}_{iW} \tag{7}$$

Since $\alpha_i = \beta_i - \delta_i$, it is difficult to find δ_i from equation 7. Instead $\mathbf{T}(\delta_i)$ is linearised around $\delta_i = \beta_i$ which corresponds to zero tyre side slip, giving

$$T(\delta_i)|_{\delta_i=\beta_i} = \begin{pmatrix} \cos\beta_i & -\sin\beta_i \\ \sin\beta_i & \cos\beta_i \end{pmatrix} + \begin{pmatrix} \sin\beta_i & \cos\beta_i \\ -\cos\beta_i & \sin\beta_i \end{pmatrix} \alpha_i \tag{8}$$

This is relevant as long as the maximum side force is generated at small angles. To improve accuracy for larger slip angles, δ_i from previous time step can be used.

Equation 8 is now used to solve equation 7 giving a system of polynomial equations with the solution

$$\begin{aligned} \alpha_i &= \frac{1}{6}\left(108Q_4 + 12Q_3\right)^{1/3} - 2\frac{(-1+Q_5)}{Q_5\left(-108Q_4 + 12Q_3\right)^{1/3}} \\ \kappa_i &= Q_5 - \alpha_i^2 \\ Q_3 &= \sqrt{-12Q_5^3 + 36Q_5^2 - 36Q_5 + 12 + 81Q_4^2} \\ Q_4 &= -\sin\beta_i s_{xi} + \cos\beta_i s_{yi} \\ Q_5 &= -\cos\beta_i s_{xi} - \sin\beta_i s_{yi} \end{aligned} \tag{9}$$

Finally, the desired steering angle and wheel speed are calculated as

$$\begin{aligned} \omega_i &= \frac{v_{xiW}}{R_e}(1+\kappa_i) \\ \delta_i &= \beta_i - \alpha_i \end{aligned} \tag{10}$$

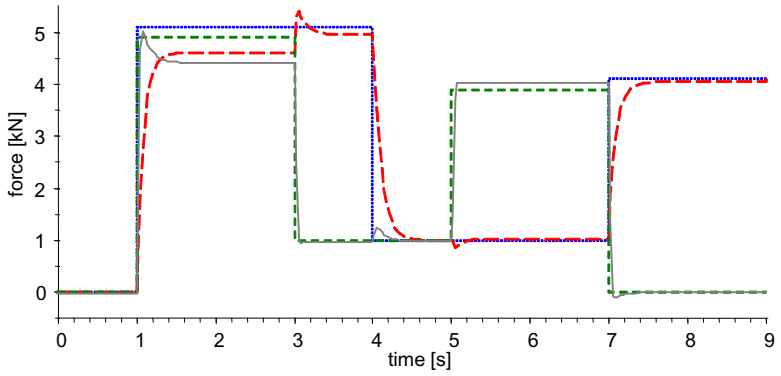

Figure 6: Desired and achieved forces for one wheel unit mounted on a test rig with predefined motion. Desired f_x (dotted), desired f_y (dashed), actual f_x (long-dashed) and actual f_y (solid).

4 SAMPLE SIMULATIONS

As a test bench for the control architecture for driving dynamics, a vehicle model in Modelica [11] is built according to Figure 1. Driver Interface, Driver Interpreter, Energy Management and Auxiliary Systems are made simple to facilitate evaluation of the results. The path control and the force distribution described above are implemented in the Vehicle Motion Control. The wheel units are realised with the controller suggested above together with a mechanical linkage suggested for autonomous corner modules presented in [12], steering actuators and wheel motors are modelled as first order filters with rate limits. To illustrate the ability of the implemented structure, two example simulations are shown, more information about the model can be found in [13].

In the first simulation, one WU is forced along a pre-defined path and is commanded to generate forces in series of steps(f_x, f_y). An available tyre model [14] with dynamics was used and the tyre characteristics was estimated separately. The simulation result is shown in Figure 6. During time=1-3s, the WU is commanded to generate more force than possible and the actual force is thus downscaled. Due to the linearisation in equation 8, actual f_y is sligthly too high for large slips as seen when time=5-7s.

The second simulation is of a full vehicle model following a lane change path, Figure 7. At this stage, only a simple P-controller is used to follow an intended path. In figure 8 a screen shot from the animated result is shown.

5 CONCLUSIONS AND FUTURE WORK

- A generic control architecture for driver's intentions to vehicle motion as described in Figures 1 and 2 has been implemented.

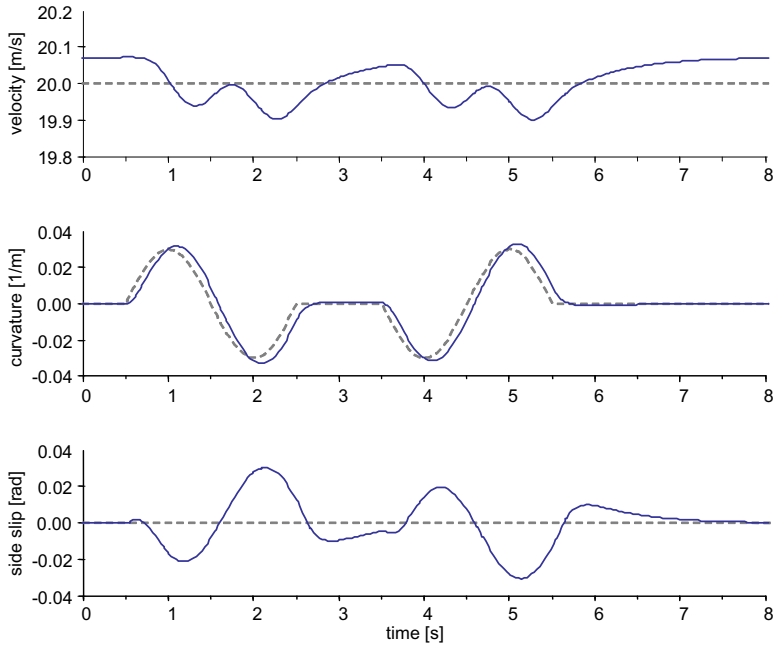

Figure 7: Desired (dashed) and achieved (solid) path for a vehicle with four wheel units.

- Forces are used as control signals between Vehicle Motion Control and Chassis which have been proven to be generic.
- A practical approach is utilised to solve the control allocation problem of distributing global forces to local wheel unit forces.
- A strategy to find wheel angles and wheel spin from desired wheel forces has been suggested and implemented.

The work is intended to continue with the following aspects in mind: 1) As suggested in section 3.3, the control allocation is not optimised. It will be further examined whether available control allocation theory can be used to improve performance of the force distributor. Especially when taking into account the dynamic limitations of tyres and actuators 2) The tyre characteristics has to be estimated continuously onboard the vehicle. Possibly, the friction circle assumption and the polynomial approximation must be refined to handle all types of tyre characteristics. 3) Today's cars have constraints between the wheels such as rack steering, differentials etc. These restrict the wheels' motion and thereby the force generation. This must be handled by the force distribution in a proper way. 4) Currently, the sensor information used is always accurate. It has to be examined how inaccuracies affects the performance.

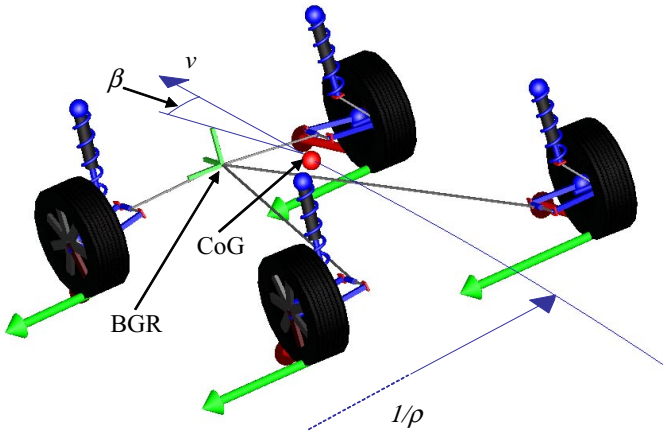

Figure 8: The animated vehicle with wheel unit linkages according to [12]. Vectors at the wheels indicate the generated tyre forces. Side slip angle (β), velocity (v), path curvature (ρ), Body Geometric Reference (BGR) and Centre of Gravity (CoG) are also indicated.

REFERENCES

1. S. Sakai and Y. Hori. Advanced vehicle motion control of electric vehicle based on the fast motor torque response. *Proceedings of the 5th International Symposium on Advanced Vehicle Control, Ann Arbor, Michigan, August 22-24*, 2000.
2. M. Yamamoto. Active control strategy for improved handling and stability. *SAE transactions, paper 911902*, pages 1638–1648, 1991.
3. L. Laine and J. Andreasson. Generic control architecture applied to a hybrid electric sports utility vehicle. *To be presented at the 20th International Electric Vehicle Symposium, Long Beach, CA, november 15-19*, 2003.
4. A. Phillips. Functional decomposition in a vehicle control system. *Proceedings of the American Control Conference, Anchorage, AK May 8-10*, 2002.
5. E. Coelingh and et al. Open-interface definitions for automotive systems. *SAE transactions, paper 2002-01-0267*, 2002.
6. Y. Hattori and et al. Force and moment control with nonlinear optimum distribution for vehcile dynamics. *Proceedings of the 6th International Symposium on Advanced Vehicle Control, Hiroshima, Japan, September 9-13*, 2002.
7. M. Bodson. Evaluation of optimization methods for control allocation. *AIAA Guidance, Navigation, and Control Conference and Exhibit, Montreal, Canada, August*, 2001.
8. L. Lindfors. Thrust allocation method for the dynamic positioning system. *10th International Ship Control Systems Symposium (SCSS'93), Ottawa, Canada*, 1993.
9. M. Akerblad and A. Hansson. Efficient solution of second order cone program for model predictive control. *IFAC 2002*, July 2002.
10. E. Bakker, H.B. Pacejka, and L. Lidner. A new tire model with application in vehicle dynamics studies. *SAE transactions, paper 890087*, pages 83–93, 1989.
11. Modelica Association. http://www.modelica.org.
12. S. Zetterstrom. Electromechanical steering, suspension, drive and brake modules. *VTC 2002-Fall, Vancouver, Canada, September 24-28*, 2002.
13. J. Andreasson and L.Laine. Implementation of a generic hybrid electric vehicle library in Modelica. *To be submitted*, 2004.
14. J. Andreasson and J. Jarlmark. Modularised tyre modelling in Modelica. *Proceedings of Modelica'2002 Conference*, 2002.

Paper III

Reusable Control Architecture Implemented in a Scale Model of a Hybrid Electric Vehicle

in

Proceedings of the Electric Vehicle Symposium, (EVS 21), Monaco, April 2005.

In *Proceedings of Electric Vehicle Symposium (EVS) 21*, Monaco, Apr 2005

Reusable Control Architecture Implemented in a Scale Model of a Hybrid Electric Vehicle

Leo Laine*, Jonas Hellgren*, Henrik Kinnunen, and Magnus Rönnberg

Abstract

A reusable control architecture for Vehicle System Control has been implemented in a scale model 1:5, of a series Hybrid Electric Vehicle with a Power Supply containing a fuel cell emulator as a primary power unit and supercapacitors as a buffer. The aim is to verify the effectiveness of the reusable control architecture with real hardware by using a scale model car. This type of architecture allows for easy exchange of hardware configurations without having to change the functional structure of the Vehicle System Controller. The structure for the Hybrid Electric Vehicle system is obtained through functional decomposition, which orders the system functions into different functional levels. Three functional levels have been defined. The highest level contains functions that are common for all foreseen Hybrid Electric Vehicles: Driver Interpreter, Vehicle Motion Control, Energy Management, and Operative Decision Control. The second level contains the necessary subsystems for a vehicle: Driver Interface, Chassis, Power Supply, and Auxiliary Systems. The third level is the actuator/sensor level. Using hardware independent signals between the functions allows for hardware configurations to be changed in modular fashion without affecting the higher functional levels. The Scale Model Car was tested and the logged data verified against simulation models both for ordinary drive cycle results and anti-skid behaviour with decent agreement.

Keywords: Vehicle System Control, Hybrid Electric Vehicle, Reusable Control Architecture, Scale model

1 Introduction

Already today vehicles are becoming increasingly dependent on computers and their software controllers. Therefore, it is important that the control architecture be reusable, enabling different vehicle configurations to be designed with minimum effort. In order to handle the complexity of several actuators and sensors interacting in future Hybrid Electric Vehicles (HEVs) and to allow for easy exchange of hardware configuration, it is necessary to have control architecture with suitable functional partitioning [1], [2]. The architecture should not only be reusable but should also work with several types of hybrid powertrain configurations. It must also fulfil interface requirements between automotive suppliers and manufacturers so that brand specific qualities can be kept in-house, [3], [4]. Brand specific qualities of vehicles are more and more dependent on the algorithms within the software, making it important for manufacturers to protect 'their' algorithms.

The objective of this study is to implement a reusable control architecture in a Remote Controlled (RC) Scale Model Car (SMC) of a series HEV, see Figure 1. The length of the car is 0.9 meters. The implemented reusable control architecture is based on hierarchical partitioning. This hierarchical structure then contains three functional levels. Functional level 1 consists of a main central controller. Functional level 2 includes several low level control blocks. Functional level 3 is the sensor and actuator level, as

* This work is supported by the Swedish national research programme Gröna Bilen/FCHEV. Gröna Bilen is financed by Swedish automotive industry and the Swedish research foundation Vinnova.

shown in Figure 1. The hierarchical partitioning allows for good modularity and coordination between the different low level control blocks.

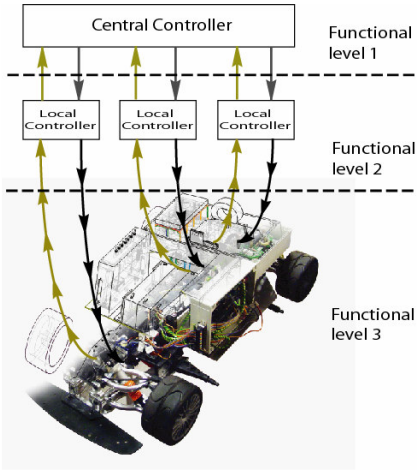

Figure 1: Hierarchical control architecture implemented in the Scale Model Car. Functional level 1 includes the central controller; Functional level 2 includes the local controllers; Functional level 3 is the actual hardware.

Computer based vehicle modelling and simulation are useful tools for examining different vehicle control architectures. However, since it is necessary to simplify modelled hardware in simulations, it is therefore crucial to verify and test ideas with real hardware. A generic hierarchical control architecture was developed, modelled, and tested on different simulated hardware configurations [5]-[8]. The main features of this generic control architecture were implemented and tested on the SMC.

There are two major aspects to consider when using scale model HEVs. Firstly, building a full scale HEV would be very expensive and time consuming. A more cost effective alternative is to use scale models to study vehicle behaviour and controller development [9]-[14]. Secondly, it is important to be able to predict what the vehicle dynamics of the scale model would correspond to in a full scale version. This can be done with dimensional analysis, such as the PI Buckingham Theorem, [15]. This method has been used to study controllers for vehicle lateral dynamics, [16] and [17]. With this dimensional analysis the SMC can easily be configured as different types of vehicles such as cars, buses, and trucks by changing weight distributions and power output. The dimensional analysis on the current SMC configuration indicated that the lateral and longitudinal dynamics of the SMC correspond to a Hybrid Electric Sports car in full scale.

The outline of the article is as follows. Section 2 describes how the reusable control architecture is structured and gives an overview of implemented control strategies and algorithms. Section 3 shows the actual hardware used in the SMC. Section 4 illustrates how the control architecture and algorithms are implemented in the control unit. Section 5 compares the SMC prototype against simulation models. Section 6 describes the conclusions.

2 Methodology used to design a reusable control architecture

A hierarchical control architecture was chosen for various reasons. One of these reasons is that it has been shown to provide better modularity compared to that of a centralised architecture [1]. Additionally, the coordination between local controllers is also improved compared to that of a peer architecture. Different partitioning schemes are also discussed in [2].

Generic interface signals were used between the local and top level controllers because they allow for hardware to be exchanged without affecting the top level controller. Generic control signals are exemplified here with a simple example, considering that we have different hardware to drive and steer a vehicle, see Figure 2. In Case 1 we have a steering wheel, brake and gas pedal. In Case 2 we have a joystick with longitudinal and lateral motion. Case 1 has three sensor signals, $[\alpha_1, \alpha_2, \alpha_3]$, sent from functional level 3 to level 2, while Case 2 has only two, $[\beta_1, \beta_2]$. Generic[1] control signals are used if and only if the signals S_1 and S_2 between Functional level 2 and 1, are equal $S_1=S_2$. This allows Functional level 1 to be reused despite changes of hardware configurations.

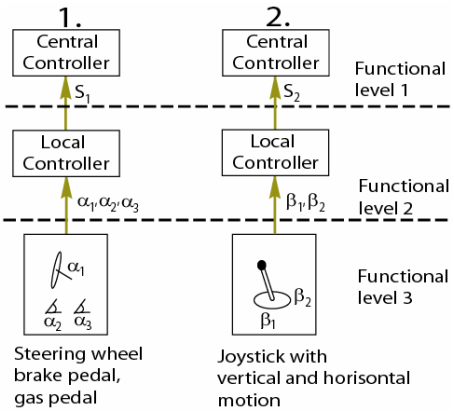

Figure 2: Two Simple examples of using generic interface signals with different hardware. Case 1: Steering wheel, brake and gas pedal. Case 2: Joystick with longitudinal and lateral motion.

The vehicle system can be seen as a set of functions. Functions within hierarchical control architectures are consigned into different levels through functional decomposition, see Definition 2.1 In this article, reusable control architecture and functional decomposition are defined as follows:

Definition 2.1 Functional decomposition
The following statements characterise an architecture with functional decomposition:

(1) Functions are placed into different levels due to their coordinating authority over other functions.
(2) Information on the system status can be observed by all functions and is allowed to flow in all directions, up, down, and across in the hierarchy.
(3) Commands are only allowed to flow down to lower level functions. This upholds a causality of orders within the hierarchical architecture.
(4) Vehicle brand characteristics should only be contained within the top level functions.
(5) Low level functions should have control over hardware health and durability.

Item 4 in Definition 2.1 allows manufacturers to retain ownership of brand specific functions while suppliers can provide controls for various subsystem functions. Through this, manufacturers can change vehicle characteristics such as optimizing drivability and fuel economy. Item 5 in Definition 2.1 makes the supplier responsible for the durability of its hardware.

Definition 2.2 Reusable control architecture for HEVs

(1) The control architecture should be hierarchical by functional decomposition.
(2) Interfaces between top level and lower level functions should be made hardware independent.

[1]Generic here means hardware independent.

(3) The control architecture should be designed so as to accommodate any foreseeable future hardware developments.

Item 2 in Definition 2.2 allows hardware to be exchanged without redesigning the functional architecture. For example, Item 3 in Definition 2.2 could include future versions of HEVs with Wheel Units, which can independently apply traction, steering, and suspension forces.

2.1 Functional levels

The control architecture's overall function is to collect and analyse information about the vehicle's internal and external conditions and to initiate appropriate responses.

The control architecture is divided into three functional levels. Level 1: The highest functional level is the main switching unit within the vehicle's architecture. It is where signals flow to and originate from. It relays messages, and compares and analyses information. Using generic interface signals allows Level 1 to become hardware independent. Level 2: The second level contains the basic functional tasks of any ground vehicle. These functional tasks can include, for example, generating ground motion, interaction with the driver, power supply and auxiliary systems. Level 3: The third level is the sensor and actuator level. These are controlled and coordinated by different basic functional tasks in level 2.

2.2 Functional level 1

Functional level 1, Main Control, consists of four major parts. Driver Interpreter interprets the driver's demands. Vehicle Motion Control controls the vehicle according to these demands. Energy Management assures that this is done in an energy efficient way. Additionally, Operative Decisions summarizes the input from Energy Management and Vehicle Motion Control and makes the overall decisions considering reliability and safety. Functional level 1 and its subsystem dependencies within the hierarchical architecture are illustrated in Figure 3.

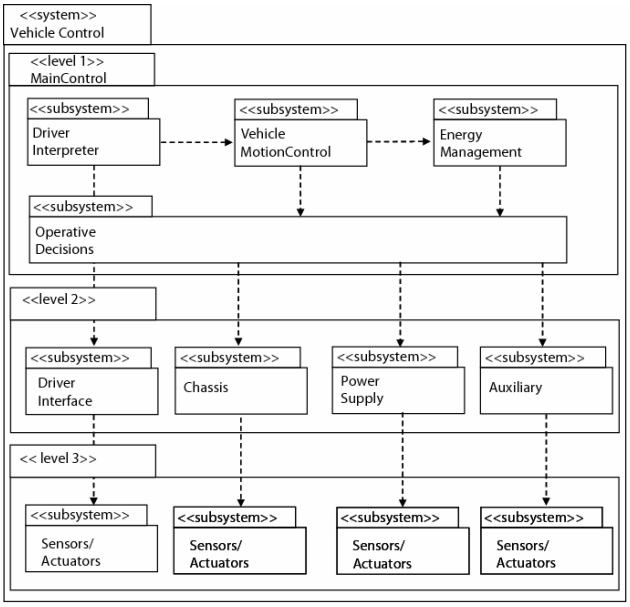

Figure 3: System architecture and subsystem dependencies according to Unified Modelling Language (UML). The architecture is made up of three functional levels. Level 1 is responsible for system coordination. Level 2 contains the basic functional tasks of a ground vehicle. Level 3 is the actual vehicle hardware.

2.2.1 Driver Interpreter (DIp)

The driver's instructions are translated into desired motion within Driver Interpreter (DIp). This is done by reading and analysing the sensor signals received from Driver Interface on level 2.

2.2.2 Vehicle Motion Control (VMC)

Vehicle Motion Control (VMC) handles the safety aspects of the vehicle's dynamics. It assures that the vehicle is avoiding a critical dynamic state. For example, typical sub functions could include traction control, anti-lock braking or vehicle stability. It uses the desired motions received from DIp and the Chassis sensor readings to consider what motions are possible without reaching the critical dynamic limits of the vehicle.

The vehicle's dynamic state must be within a certain allowed set of states, otherwise it is determined to be critical (state=1). For example, a simple slip controller is used here with the following expression

$$state_{VMC} = \begin{cases} 0, \text{ if } (\lambda_{rear}) \in \mathbf{S}_1 \\ 1, \text{ else} \end{cases} \quad \text{(eq.1)}$$

where $\mathbf{S}_1$ is the allowed set of slip values for the rear wheel. When the state is equal to 1, VMC suggests that the desired longitudinal velocity from DIp is reduced with the following expression

$$\text{VMC.x}_{vel} = \text{DIP.x}_{vel}(1-|\lambda_{rear}|) \quad \text{(eq.2)}$$

The desired signals and state are then sent to Operative Decisions, see further in Section 2.2.4.

A more advanced VMC is planned to be implemented in a SMC according to [7].

2.2.3 Energy Management (EM)

Energy Management (EM) controls the vehicle's energy sources for efficiency with regards to fuel consumption and wear. It decides how the energy flow is distributed between the Primary Power Unit (PPU) and the Buffer considering the current power demand for generating ground motion and auxiliary systems.

EM determines if the Power Supply is in a critical state and passes the information along to Operative Decision. If the EM state is considered critical the desired speed of the vehicle is evaluated by the following expression

$$state_{EM} = \begin{cases} 0, \text{ if } (SOC_i) \in \mathbf{S}_2 \\ 1, \text{ else} \end{cases} \quad \text{(eq.3)}$$

where $\mathbf{S}_{2,i}=\{SOC_i: 0<SOC_{i,min}<SOC_i<SOC_{i,max}\}$ and is the i^{th} buffer within Power Supply.

EM calculates a State of Charge (SOC) reference value for current vehicle states such as vehicle velocity. The SOC reference is a numerical value representing the current desired SOC for the buffer. One example of a simple Power Management algorithm using a SOC reference within EM is as follows

$$SOC_{ref} = 0.5 + C_0(0.5 - (\frac{x_{vel}}{6})^2) \quad \text{(eq.4)}$$

where the C_0 and C_1 are constants.

By using SOC reference values and sensor readings of the current SOC, EM distributes the requested power to both the PPU and the buffer. In the test run, presented in Sec 5, the buffer power is controlled as follows

$$P_{buff} = \begin{cases} -k_1(SOC_{ref} - SOC), & \text{if } (x_{acc}) \le a_1 \\ k_2 P_{em} & \text{if } (x_{acc}) > a_2 \\ k_3 P_{em} & \text{else} \end{cases} \quad \text{(eq.5)}$$

where a_1, a_2, k_1, k_2, and k_3 are constants.

A more sophisticated rule based algorithm for calculating the buffer power demand will be implemented according to [18] in a future version of the SMC.

2.2.4 Operative Decision (OD)

Operative Decisions (OD) considers the vehicle state values given by VMC and EM. If the vehicle status is critical, OD then gives priority to either VMC or EM. As an example, if VMC is in a critical state=1, OD will allow mechanical braking. If instead EM has critical state=1, OD approves the use of maximum regenerative braking and charging. In Table 1 an example is given as to how the OD state controller could be configured.

VMC State	EM State		Priority VMC/EM	Comment
0	0	➔	EM	Prioritise efficiency if no Critical state
1	0	➔	VMC	Prioritise vehicle stability if VMC critical
1	1	➔	VMC	Prioritise vehicle stability if both critical
0	1	➔	EM	Prioritise efficiency if EM critical

Table 1: Operative Decisions gives priority to either VMC or EM depending on the vehicle's states. When both states are critical focus is on vehicle stability. While under normal driving conditions minimizing fuel consumption and wear is prioritised.

The desired actions from VMC and EM are finalised into orders by OD. These orders are then sent to level 2.

2.3 Functional level 2

Functional level 2 contains the basic tasks of any ground vehicle. Driver Interface reads the sensor signals from the driver. Chassis generates the ground motion. Auxiliary Systems includes all subsystems which are not necessary for generating ground motion. Finally, Power Supply generates the needed mechanical and electrical energy for Chassis and Auxiliary Systems.

2.3.1 Driver Interface (DIf)

Driver Interface (DIf) reads the sensor signals from the driver. These are normalised to be values between [-1,1]. All software functions associated with reading hardware used by the driver are located in DIf.

2.3.2 Chassis (Ch)

The local controllers of actuators and sensors that directly affect Chassis (Ch) dynamics are placed within Ch. Brake servos and wheel motors are examples of Ch actuators. Accelerometers and wheel rotation sensors are examples of Ch sensors. Ch is mainly controlled by VMC.

2.3.3 Power Supply (PS)

Power Supply (PS) contains all energy sources and local controllers of energy converters, buffers, and sensors which are needed to produce the vehicle's power demand. The energy can be stored in different forms such as electrical, fluid, and mechanical. A topology 'cut' is used to determine whether tractive force

actuators such as electric motors are placed within PS or Ch. For example, if an electric motor is mounted before a differential its function is placed within PS. PS is mainly controlled by EM.

2.3.4 Auxiliary Systems (Aux)

All subsystems not directly related to generating vehicle motion are contained within Auxiliary Systems (Aux). Aux is supervised by EM. In the SMC there are currently no subsystems included in Aux.

3 Scale Model Car (SMC) Configuration

The Scale Model Car (SMC) is a standard model car of size 1:5. The Ch includes suspension, wheels, and body from a manufacturer named 'FG Modellsport'. Pictures of the present configuration of the Hybrid SMC are shown in Figure 4. A Schematic drawing of the Ch and PS is shown in Figure 5. The car is rear wheel driven by an electric motor. Details about the design and development process of the Hybrid Electric SMC are found in [19].

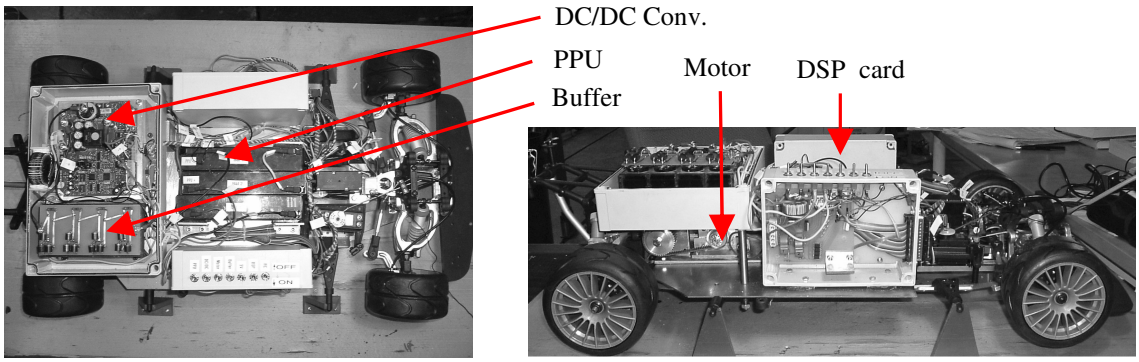

Figure 4: Top view (left) and Side view (right) of SMC.

In Table 2 a summary of vehicle dynamic parameters are listed. Further details can be found in [20].

Vehicle mass, m	16 kg
c.o.g. to front axle, L_f	0.3499 m
c.o.g. to rear axle, L_r	0.1813 m
Wheel radius, R_ω	0.06 m
Track width, T_ω	0.12 m
Cornering stiffness front, $C_{\alpha f}$	96 N/rad
Cornering stiffness rear, $C_{\alpha r}$	187 N/rad
Yaw inertia, I_z	0.6 kgm^2
Air drag Coeff., C_d	0.28
Frontal Area, A	0.0804 m^2
Roll resistance, f_{roll} (concrete)	0.04

Table 2: Vehicle dynamics data of the hybrid SMC [20].

3.1 Chassis Configuration

Chassis contains two main actuators. The first actuator is the steering servo, A_{st}, which is connected to the rack steer. The second actuator is the mechanical brakes, A_{br}, which are located on the front wheels and servo controlled. A schematic sketch of the Ch configuration is shown in Figure 4. The Figure shows also how the actuators between Ch and PS are divided by the mechanical connector 'Mc'.

There are three main sensors within Ch. The first is the rotational sensor circuit, $S_{ws,}$ mounted on the front right wheel WU_2, see Figure 5. Details about the wheel rotation sensor can be found in [21]. The other two

sensors are accelerometers which are mounted on the car giving the longitudinal, $S_{ax,}$ and lateral acceleration, S_{ay}.

One of the basic functions of `Ch` is to estimate the actual vehicle speed. The following simple but efficient algorithm is used

$$x_{vel} = \begin{cases} x_{vel,nobrake} = \omega_{w,front} R_w, & \text{if no mechanical brake} \\ x_{vel,brake} = x_{vel,nobrake} + \sum_{i=k_{nobrake}}^{k} x_{acc} dt, & \text{else} \end{cases} \qquad \text{(eq.6)}$$

If mechanical brakes are not used, the vehicle velocity is calculated as rotational speed multiplied by wheel radius. If mechanical brakes are applied, the front wheels may slip and thus the last velocity value with no braking, $x_{vel,\ nobrake}$, at step $k_{nobrake}$, is used and the accelerometer reading is numerically integrated and used to estimate the actual vehicle velocity [22]. Another basic function of `Ch` is to estimate front and rear slip.

3.2 Power Supply Configuration

The current `PS` configuration contains many components. It includes a battery for a PPU, used as a fuel cell emulator. Super Capacitors are used as a buffer and a DC/DC converter directs the electrical power flow. An electric motor is used to convert the electrical power to mechanical power in order to propel the vehicle. Four implemented external voltage, S_u, and current sensors, S_i, allow for supervision of the actual power flow to the buffer and electric motor. These will explained in further detail and a schematic diagram of the electrical connections of `PS` is also shown in Figure 5.

The fuel cell PPU was emulated by two lead acid batteries in series, each with a nominal voltage of 12 volt and 2.3 Ah. The buffer is made of 3 super capacitors, Maxwell 2.5 V 350 F, that are connected in series. The energy flow in and out from the buffer is handled by the full bridge DC/DC converter through a requested buffer voltage, $U_{buff,\ req}$. A local controller was implemented in `PS` to control the requested buffer voltage by the input signal desired buffer power. It has a continuous current of 70 A, an input voltage of 24 V, and an output voltage of 0-24 V. The electric motor is a brushless synchronous DC-motor. Power electronics are included so that the rotation speed, $\omega_{em,req}$, is easily controlled. The machine can operate in four quadrants, in other words, it can be used as a generator. It has an operating voltage of 24 V, a maximum output power of 230 W and a maximum torque of 0.98 Nm. The driveline has a total gear ratio of 4.174.

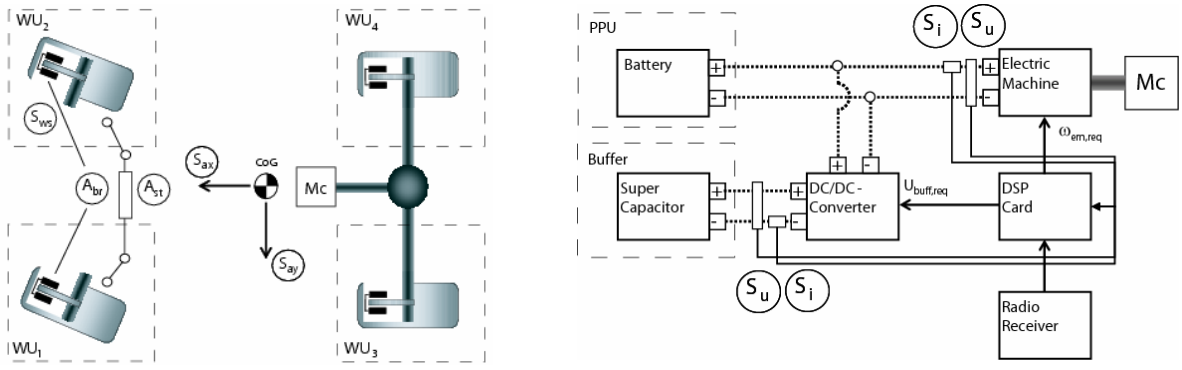

Figure 5: Chassis configuration (left) and Power Supply configuration (right), A: Actuator, S: Sensor, WU: Wheel Unit, and Mc: Mechanical connector.

4 Implemented Vehicle System Control Code and Structure

The control architecture with its algorithms was implemented in the SMC. A technician downloads the Vehicle System Control (VSC) code to the Digital Signal Processor (DSP) card.[2] The downloaded VSC code, programmed in C, must interact with different input and output signals. A Driver gives input such as desired longitudinal and lateral motion, braking, or power switch. The SMC is controlled by a RC system.[3] Due to the fact that is a hybrid electric vehicle, the VSC Code decides between the mechanical or regenerative braking. Sensor signals are interpreted and used to estimate the vehicle internal states. Examples of such sensor signals are WU rotational speed, motor speed, accelerometers, and current and voltage sensors. These input signals are processed by the VSC and final output request signals are sent to the actuators such as electric motor, DC/DC voltage, steering servo, and mechanical brake servo.

The functions within VSC, as discussed in Section 2, are defined as C-functions. The functions are called within a main loop in a certain order as shown in Figure 6.

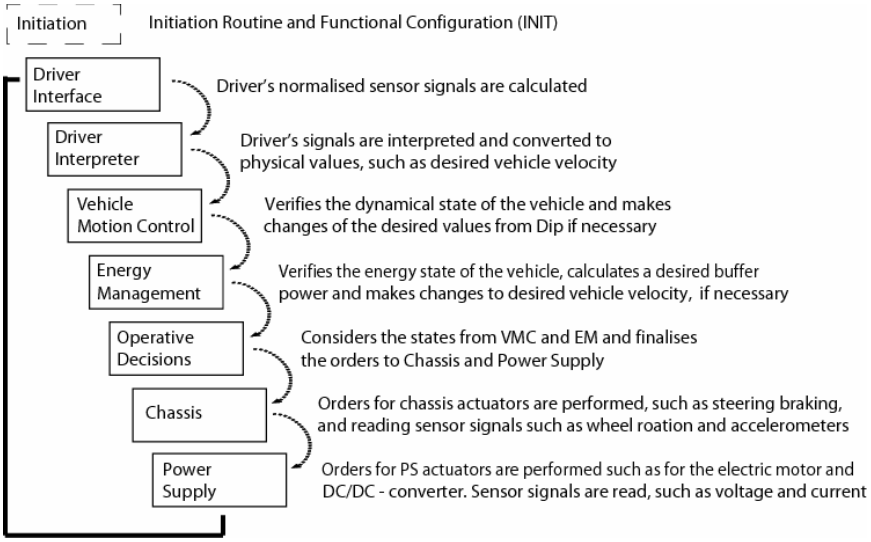

Figure 6: Program loop used in the Vehicle System Control.

The signal interfaces between the functions are structure based and are made as reusable as possible for different hardware configurations.

5 Test run of SMC

The SMC was tested on how it performs with the implemented functions within VSC. See Section 2.2 for further details about the used algorithms within `VMC`, `EM`, and `OD`.

5.1 Traction Control testing

A simple traction controller is located within `VMC` function, see Section 2.2.2. A max acceleration test was performed on a surface with low friction, close to ice conditions. The implemented traction controller within `VMC` improves the acceleration performance, see Figure 7. The time to reach the longitudinal

[2] The DSP used is a TMS320LF2407A processor from Texas Instruments which is mounted on an evaluation module from Spectrum Digital.
[3] Hitec Laser 4 FM transmitter, and a Hitec HFS-04MG receiver.

velocity of 1.5 m/s or 25 rad/s in the front wheels was 2.65 s without the controller, and 2.2 s with the controller activated. Further details can be found in [23].

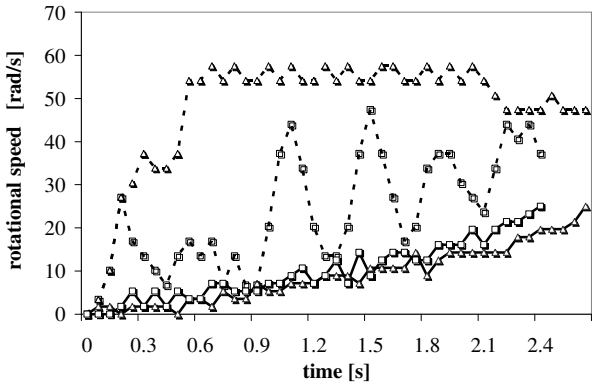

Figure 7: Front (continuous line) and rear (dashed line) wheels, with VMC function activated (squares) and without (triangles).

5.2 Drive cycle testing

The SMC was evaluated during a drive cycle test, driven indoor on concrete. This tested the simple energy management algorithm that is located within EM function, see Section 2.2.3. The drive cycle is shown in left Figure 8.

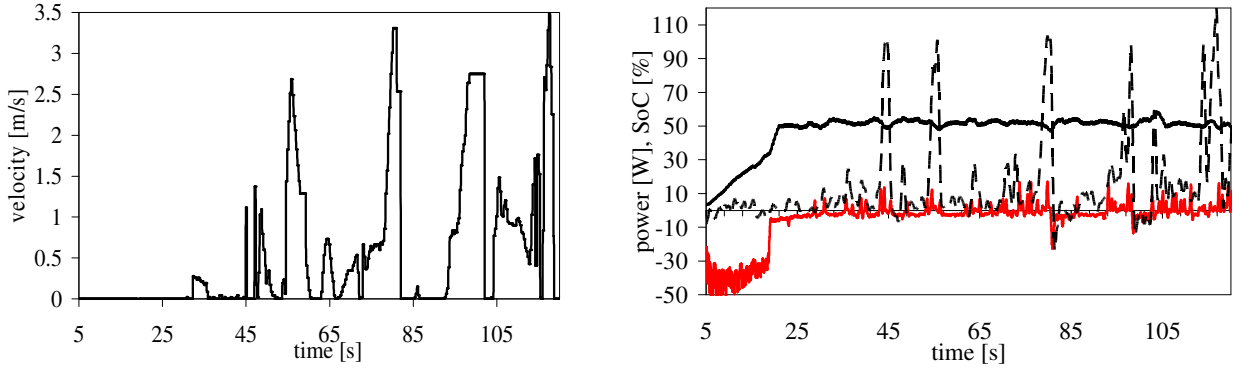

Figure 8: Drive cycle velocity as function of time (left). Actual motor power (black dashed), buffer power (red solid), and State of Charge (black solid) as function of time (right).

The right Figure 8 shows how the buffer is charged during the first 25 s, to reach the SoC target level of 50 percent. Motor power demand is high during accelerations and the buffer assists during accelerations. The level of buffer assist during acceleration can be changed by increasing the constant k_2, see eq. 5. Here in this drive cycle test, k_2=0.1, was used. During deceleration one can see that the buffer power is negative and is charged by the regenerative braking by the electric motor.

6 Conclusions

The overall conclusion is that scale model cars are an appealing option for universities and the automotive industry to use for teaching and research about vehicle systems. They are relatively inexpensive compared to full scale vehicles, safe to drive, and do not require large storage spaces.

The control architecture allowed easy exchange of hardware and the top level functionality was not affected during changes in the lower lever functions, for example when different sensors were changed within chassis and power supply.

The simple traction control implemented in `VMC` and the state controller within `OD` worked overall as desired. However, due to the fact that different speed rotational sensors, with different accuracy, were used for front and rear wheels introduced for the implemented traction controller compared to the simulated results.

Logging data from the test run shows that `PS` of the SMC works as intended. The test run also verifies that the computer model of the SMC is accurate.

References

[1] Joseph C. Burba, *Consideration of Control System Architecture in Electric and Hybrid Electric Vehicles*, Electric Vehicle Symposium 18, Berlin, 2001.

[2] Magnus Gäfvert, *Topics in Modeling, Control, and Implementation in Automotive Systems*, Dep. of Automatic Control, Lund Institute of Technology, Sweden, 2003.

[3] Erik Coelingh, Pascal Chaumette, and Mats Andersson. *Open-Interface Definitions for Automotive Systems*, Application to a Brake by Wire System, SAE 2002-01-0267.

[4] Anthony M. Phillips, *Functional Decomposition in a Vehicle Control Systems*, American Control Conference, Anchorage, 2002.

[5] Leo Laine and Johan Andreasson, *Modelling of Generic Hybrid Electric Vehicles*, in Proceedings of the 3rd International Modelica Conference, Linköping, Sweden, November 2003.

[6] Leo Laine and Johan Andreasson, *Generic Control Architecture applied to a Hybrid Electric Sports Utility Vehicle*, in Proceedings of the Electric Vehicle Symposium, (EVS 20), Los Angeles, 2003.

[7] Johan Andreasson, Leo Laine, and Jonas Fredriksson, *Evaluation of a Generic Vehicle Control Architecture*, in Proceedings of the 30th Congress of the International Federation of Automotive Engineering Societies, (FISITA'30), Barcelona, 2004.

[8] Leo Laine and Johan Andreasson, *Reusable Functional Partitioning of Tractive Force Actuators Applied on a Parallel Hybrid Electric Vehicle,* in Proceedings of the 7th International Symposium on Advanced Vehicle Control, (AVEC'04), Arnhem, Netherlands, August 2004.

[9] P. Hoblet, R.T.Jr. O'Brien, Piepmeier J.A., *Scale-Model Vehicle Analysis for the design of a Steering Controller*, Proceedings of the 35th Southeastern Symposium on System Theory, 2003.

[10] M. Shinoa, M. Nagaib, *Independent wheel torque control of small-scale electric vehicle for handling and stability improvement*, JSAE Review 24, 2003.

[11] R. S. Woodley, L. Acar, *Neural Network Based Control for a Backward Maneuvering Trailer Truck*, Proc. Of the 37th IEEE Conference on Decision and Control, Florida, USA, 1998.

[12] J. Pereira, J. B. Bowles, *A Comparison of PID and Fuzzy Control of a Model Car*, Electrical and Computer Engineering, University of South Carolina, Columbia, USA, 1993.

[13] K. Nishimori, S. Hirikawa, K. Fujimura, H. Tokutaka, S. Kishida, H. Hiraga, N. Ishihara, *Automatic Tuning Method of Membership Functions in Simulations of Driving Control of a Model Car*, Proc. Of International Joint Conference on Neural Networks, 1993.

[14] S.-J., Chang, C.-W. Cheng, T.-H. S. Li, *Design and Implementation of Fuzzy Garage-Parking Control for a PC-based Model Car*, National Cheng Kung University, Taiwan, 1996.

[15] E. Buckingham, On Physical similar systems: Illustrations of the use of dimensional equations, Physical Rev, vol. 4, pp. 345-276, 1914.

[16] S. Brennan, A. Alleyne, The Illinois Rodway Simulator: A Mechatronic Testbed for vehicle Dynamics and Control, IEEE/ASME Transactions on Mechatronics, vol. 5, no. 4, 2000.

[17] S. Brennan, A. Alleyne, Using a Scale Testbed: Controller Design and Evaluation, IEEE Control Systems Magazine, vol. 21, June 2001.

[18] Jonas Hellgren, *Conceptual Powertrain Design and Energy Management of Hybrid Electric Vehicles using Evolutionary Algorithms and Sugeno Fuzzy Logic*, Submitted to IEEE Transaction on Vehicular Technology, 2004.

[19] Jonas Hellgren, Leo Laine, Jonas Sjöberg, Magnus Rönnberg, Dennys Gomes, and Aizezi Abudings, *Systematic Design and Development of a Hybrid Electric Scale Model Car*, Technical Report, Dept. of Machine and Vehicle Systems, Chalmers University of Technology, Sweden, 2004.

[20] D. E. B. Gomes, *Design and Development of a Hybrid Electric Scale Model Car*, Master thesis report, Dep. of Machine Vehicle Systems, Chalmers University of Technology, Sweden, 2004.

[21] Magnus Rönnberg, *Implementation of a Control System for a Scaled Series Hybrid Electric Vehicle*, Master thesis report, Dep. of Machine Vehicle Systems, Chalmers University of Technology, Sweden, 2004.

[22] Chui Ki Song, Michael Uchanski, and J Karl Hedrick, *Vehicle Speed Estimation Using Accelerometer and Wheel Speed Measurements*, SAE 2002-01-2229, 2002.

[23] Patrick Labenda, Development, Implementation and Testing of a Traction Control Algorithm for Hybrid Electric Scale Model Car, Dep. of Signals and Systems, Chalmers University of Technology, Sweden, 2005.

Author

Leo Laine, PhD student, Chalmers University of Technology, Dep. of Applied Mechanics, Div. of Vehicle Dynamics, SE-412 96 Göteborg, Sweden, ph:+46 31 772 58 52, e-mail: leo.laine@me.chalmers.se. Received his M.Sc. .in structural mechanics in 1996 from Chalmers. Worked at the Swedish Defence Research Establishment as research engineer until 1998. The then worked as a consultant at ANKER – ZEMER Engineering AS. In 2002 he started his Ph.D. studies at Chalmers, Dep. of Machine and Vehicle Systems, Div. of Mechatronics. The name of the project is HEV Main Control.

Jonas Hellgren, PhD, Consat Engineering AB, Ögärdesvägen 19A, 433 30 Partille, Sweden ph: +46 31 340 00 00, e-mail:jonas.hellgren@consat.se. Was born in 1974. He received the Master's degree in mechanical engineering in 1999, from Linköping University, Sweden. In 2004 he finalized his Ph.D. studies at the Department of Machine and Vehicle Systems, Chalmers University of Technology, Göteborg, Sweden. His Ph.D. thesis named "A Methodology for the Design of Cost Effective Hybrid and Fuel Cell Powertrains" deals with conceptual design of HEVs.

Henrik Kinnunen, MSc Student at the department of electrical engineering at Chalmers University Of Technology. Specialized in computer programming and microcomputers. e-mail: ei99kihe@etek.chalmers.se

Magnus Rönnberg, MSc, www.ourego.com, Magnus received his MSc in 2004 at the department of electrical engineering at Chalmers University Of Technology. e-mail: magnus@ourego.com

Paper IV

Brake blending for hybrid electric vehicles using control allocation,

in

Tech. Report R011/2007, Department of Signals and Systems, Chalmers University of Technology, Göteborg, Sweden, 2007. A shorter version is also submitted to *Int. Journal of Vehicle Systems Modelling and Testing, Special Issue on: Modelling and Testing of Alternative Vehicular Propulsion*.

Brake Blending for Hybrid Electric Vehicles using Control Allocation

Leo Laine* and Jonas Fredriksson

Department of Applied Mechanics* and Department of Signals and Systems,
Chalmers University of Technology SE-412 96 Göteborg, Sweden
E-mail: leo.laine@chalmers.se and jonas.fredriksson@chalmers.se
* corresponding author

Abstract

Coordinating the actuators that generate vehicle ground motion will become the next challenge in the development of hybrid electric vehicles. The actuators should not only be coordinated in an energy efficient manner, they also must not jeopardize vehicle stability. In this paper three different ground vehicle configurations, with different numbers of motion actuators, are modelled and analyzed with consideration to the main time constants in the vehicle and motion actuators when generating the desired motion. The purpose is to study how to accomplish brake blending. Here, a reusable control system is suggested which can handle a broad variety of configurations. This is possible when the control law for generating the desired ground motion and the coordination the motion actuators are separated within the control system. A reusable control law is designed for generating the desired ground motion and an optimization based method called control allocation, which also handles actuator limits, is used for coordinating the motion actuators. Simulations confirm that control allocation is a powerful option for brake blending for all three vehicle configurations.

Keywords: Hybrid Electric Vehicles; Brake Blending; Modelling; Control Allocation.

1 Introduction

New technology in vehicle design has lead to more motion actuators and more subsystems to be controlled and coordinated to achieve the desired vehicle motion. Today's vehicle systems usually make an arbitration when the actual vehicle motion differs from the driver's desired motion. Then stability programs, such as the Electronic Stability Control system (ESC), [1] and [2], take over control, coordinating the mechanical brakes and a reducing of the engine torque

to achieve a correcting yaw motion. Another example of necessary coordination due to new technology is the braking functionality within hybrid electric vehicles (HEV) which requires which requires the disc brakes and the electric motors to be blended. In a premium HEV with a high degree of hybridization, i.e. a significant part of the traction force is generated by electric motors, one would with classical arbitration, only use mechanical brakes during hard braking. The car magazine Auto Motor und Sport, [3], has developed the AMS braking test for analyzing the performance of premium cars which in the future would likely include premium HEVs. The AMS-test is basically a repetition of several hard accelerations directly followed by hard braking. Premium HEVs designed with classical arbitration in HEVs exhibit different vehicle performances in the beginning and the end of the test due to the fact that the buffer is never re-charged and therefore cannot assist in accelerating hard again. Who wants to buy a premium HEV that performs like a small sized vehicle just because one is repeatedly doing hard braking? This paper concerns how the coordination between the different motion related actuators for a ground vehicle can be made to achieve the desired vehicle motion.

Overactuated systems are systems with more actuators than controlled degrees of freedom. They are commonly found in application areas such as flight and marine vessels, but are also found in automotive systems. One promising way to manage the coordination of overactuated systems is to use control allocation. Control allocation deals with the problem of distributing the control demand among the available set of actuators. The control allocation problem is posed as a constrained optimization problem which provides automatic redistribution of the control effort when one actuator saturates in position or in rate. Control allocation has been used successfully within flight applications, see [4]. It has also been used within marine vessels, see [5] and [6]. Ground vehicles can also be seen as overactuated systems, and control allocation has previously been used for yaw stabilization, see [7], [8] and [9]. In these articles the mechanical brakes and steering were in focus without direct consideration to the actuator limits.

In this paper a reusable control law is set up for the longitudinal, lateral, and yaw-motions of a ground vehicle. Since many researchers are involved in the area of energy management for HEVs, this paper is instead focusing on the vehicle motion controller. The problem studied here is how to blend between re-generative and conventional mechanical braking for a hybrid electric vehicle during different situations such as soft and hard braking on different types of surfaces with fully or partly low tyre/road friction. The goal is to avoid allocation problems in HEVs like the one seen in the AMS-test. The idea with the controller is that it should, in a safe way, follow a desired trajectory, interpreted from the driver's current steering actions. The presented vehicle motion controller is designed based on feedback linearization of a nonlinear vehicle model, followed by control allocation, which is used to distribute the task of generating the desired motion. It is also shown how the system controller can be reused for different vehicle configurations when control allocation is used for coordination of the actuators to generate the vehicle motion. The vehicle system is also modelled and analyzed with consideration oto the main time constants found in a vehicle when generating the desired motion and includin the internal states within the motion related actuators that will affect its limits and rate of change

of limits.

The outline of the paper is as follows: The background is presented in Section 2. Section 3 describes the modelled systems. Section 4 describes the used control law and how the control allocator is set up. In Section 5 some simulations of different braking situations are presented to show how the proposed control system is working. Section 6 concludes the findings.

2 Background

Standardized interface signals, [10], and reusable controllers, [11], are highly desirable for reducing future vehicle development costs. This is of special importance for hybrid vehicles, where a number of configurations can be considered. To handle this efficiently a hierarchical control architecture is preferable. In [12], a vehicle control system architecture for fuel cell- and hybrid electric vehicles is proposed. The control system architecture is generic in the sense that the information flow structure allows for the adding and removing of components, which is essential. The control architecture is derived from functional decomposition and is configured in a modular fashion, see Fig. 1.

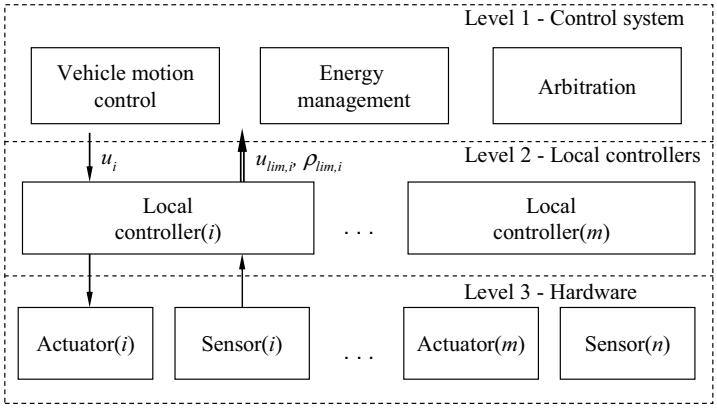

Figure 1: Illustration of functional levels within a vehicle system controller.

Functional level 1 includes the overall functionality and decision making needed to generate vehicle motion such as the vehicle motion controller and energy management. One can say that vehicle motion controller is a short-time horizon controller tries to keep the desired vehicle course. Energy management is a more long-time horizon controller for how the on-board energy sources should be used consideration to the vehicle states and the environment. Functional level 2 includes the local controllers for different functions. This can be for example a local controller for an electric motor. Here in this paper it is shown how the interface signals between level 1 and level 2 should be formed in order to design a vehicle controller considering both vehicle motion control and energy management. In Fig. 1 this is illustrated in that the local controller i is sending the limits u_{lim} and the rate of change limits ρ_{lim} to functional level 1. Functional level 3 is what could be called an advanced actuator/sensor level (hardware

level). The general idea is that the highest level remains unchanged no matter how the vehicle is configured or changed.

As mentioned earlier control allocation is an option for coordination when one has more input signals going into the system than the number of output states. An optimization objective is used to select the input set vector for the available actuators. Control allocation also handles the redistribution of the control signals, when one or more actuators saturates. Using control allocation allows for the vehicle to be reconfigurable, meaning that the same controller(s) can be used for different hardware configurations, i.e. it is well suited for the proposed vehicle system architecture.

For the vehicle motion controller, which is of in the focus of this paper, the control system architecture can be rewritten as illustrated as is shown in Fig. 2. The control system is comparable to functional level 1 in Fig. 1 and the system is comparable to functional level 2 and 3. In [13] and [14] it was shown that the control system can be divided into two parts, one controller and one force distributor where the input vector is selected as the longitudinal and lateral wheel forces. The control law only tells what net effort of global forces needs to be produced to meet the driver's desired motion but does not say how they are to be distributed over the specific wheels and their wheel forces. This is solved by the force distributor, which is realized using control allocation. If the mapping is successful then the system generates the net effort. In [13] it was also shown how constraints were applied on the wheel force distribution to account for the available motion actuators and their ability to generate the desired wheel forces.

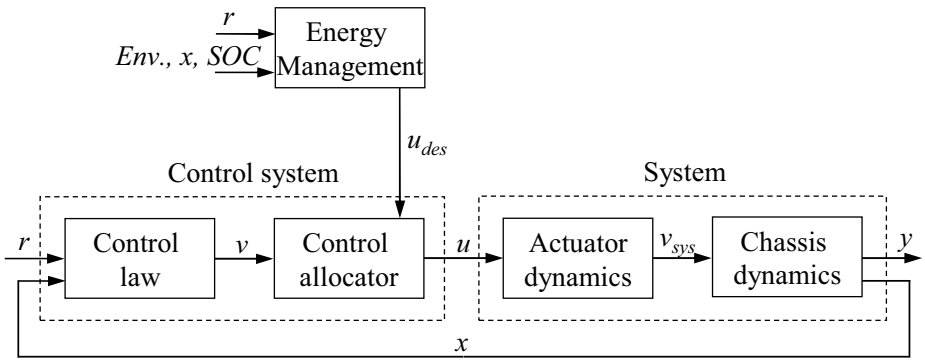

Figure 2: Control system structure when control allocation is used.

In this paper however, a different approach is made on the control allocation. Instead of using wheel forces as input, the available motion actuators are directly used. For example the electric motor torque and steering angle for rack steer are used as inputs. Another difference when compared with earlier work is that the global optimization problem for the control allocator does not only include the drivers desired path but also directly accounts for energy management's desired input u_{des}, see also Fig. 2. This automatically allows for smooth arbitration between the vehicle motion controller and energy management. Another benefit when allocation is performed directly on the available actuators is that the control effectiveness matrix, which maps the global forces onto the available motion actuators, is the only parameter that needs to be changed in the control

system when a new vehicle configuration is designed. Furthermore, more computationally efficient algorithms for solving the control allocation problem are proposed in comparison to the ones used in [14]. In the next section the vehicle system model will be described.

3 Vehicle System Modelling

The vehicle system modelling is divided into two different parts, the chassis dynamics and the actuator dynamics, see Fig. 2. The actuator dynamics are in turn divided into two separate parts, the driveline and the motion actuators, i.e. the combustion engine, the electric motor, etc. The focus is to include both the necessary dynamics of the system and the most important system specific time constants. The different delays in response in the motion actuators, driveline and tires are necessary to model in order to show if control allocation can in fact be used for automotive systems.

3.1 Chassis Modelling

The chassis model is a so called two track model and has five degrees of freedom: longitudinal-, lateral-, yaw-, roll-, and pitch motion. The model aims at bing capable of at predicting the chassis dynamics on flat surface. The SAE standard [15] provided the main guidance for defining the axis orientations. The variables used in this paper will be defined in the text or in the figures.

The governing equations for the 5-DOF chassis model are set by Newton's laws of motion. A top view of the vehicle model is shown in Fig. 3.

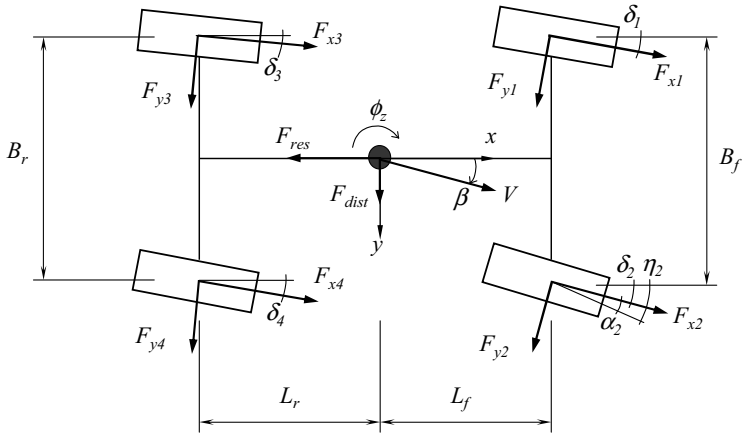

Figure 3: Chassis model, x-y view, from top.

The sum of forces in longitudinal (x) and lateral (y) direction are described as

$$ma_x = \sum_{i=1}^{4} F_{x,i}\cos(\delta_i) - \sum_{i=1}^{4} F_{y,i}\sin(\delta_i) - F_{res} - F_{dist_x} \tag{3.1}$$

$$ma_y = \sum_{i=1}^{4} F_{y,i}\cos(\delta_i) + \sum_{i=1}^{4} F_{x,i}\sin(\delta_i) - F_{dist_y} \tag{3.2}$$

where the accelerations are approximated as $a_x \approx \ddot{x} - \dot{y}\dot{\phi}_z$ and $a_y \approx \ddot{y} + \dot{x}\dot{\phi}_z$, and F_{res} denotes the resistance force and $F_{dist_{x,y}}$ are the wind disturbance forces in x and y direction respectively. The resistance force and the wind disturbance forces are assumed to be acting in the centre of gravity of the vehicle. The resistance force, F_{res}, is composed from aerodynamical drag and rolling resistance as

$$F_{res} = F_{drag} + F_{roll} \tag{3.3}$$

where

$$F_{drag} = 0.5 C_d A_f \dot{x}^2 sign(\dot{x}) \tag{3.4}$$

$$F_{roll} = fmg\left(1 - \frac{1}{e^{0.5|\dot{x}|}}\right) sign(\dot{x}). \tag{3.5}$$

The sum of moments around the centre of gravity in the yaw direction (about z-axis) gives

$$\begin{aligned} I_{zz}\ddot{\phi}_z = {} & L_f\left(\sum_{i=1}^{2} F_{y,i}\cos(\delta_i) + \sum_{i=1}^{2} F_{x,i}\sin(\delta_i)\right) \\ & - L_r\left(\sum_{i=3}^{4} F_{y,i}\cos(\delta_i) + \sum_{i=3}^{4} F_{x,i}\sin(\delta_i)\right) \\ & + \frac{b_f}{2}\left(\sum_{i=1}^{2} (-1)^{1+i} F_{x,i}\cos(\delta_i) + \sum_{i=1}^{2} (-1)^{i} F_{y,i}\sin(\delta_i)\right) \\ & + \frac{b_r}{2}\left(\sum_{i=3}^{4} (-1)^{1+i} F_{x,i}\cos(\delta_i) + \sum_{i=3}^{4} (-1)^{i} F_{y,i}\sin(\delta_i)\right). \end{aligned} \tag{3.6}$$

Figure 4 shows the roll angle ϕ_x. The sum of moments around the roll centre gives

$$I_{xx}\ddot{\phi}_x = -e_r(ma_y + g\phi_x) + K_{\phi x}\phi_x + D_{\phi x}\dot{\phi}_x \tag{3.7}$$

where $K_{\phi x} = K_{\phi x,f} + K_{\phi x,r}$ and $D_{\phi x} = D_{\phi x,f} + D_{\phi x,r}$ are the roll stiffness and roll damping respectively, and $e_r = e_{r,r} + (e_{r,f} - e_{r,r})\, L_r/L$ is the roll eccentricity at centre of gravity.

Figure 5 shows the pitch angle ϕ_y. The sum of moments around the pitch centre gives

$$I_{yy}\ddot{\phi}_y = e_p m(a_x + g\phi_y)) - K_{\phi y}\phi_y - D_{\phi y}\dot{\phi}_y \tag{3.8}$$

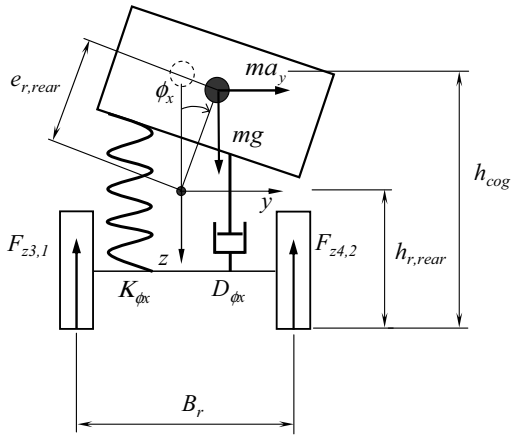

Figure 4: Chassis model, y-z view, from rear.

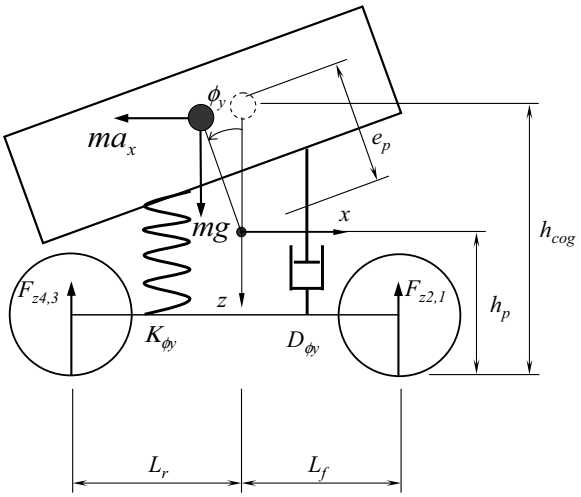

Figure 5: Chassis model, x-z view, from side.

where $K_{\phi y}$ and $D_{\phi y}$ are the pitch stiffness and pitch damping respectively.

The model also includes the normal forces, which are the sum of static load, pitch weight transfer and roll weight transfer. The normal force distribution is

described by

$$F_{z1} = \frac{mgL_r}{2L} - \frac{ma_x e_p + K_{\phi y}\phi_y + D_{\phi y}\dot{\phi}_y}{2L} + \frac{ma_y e_{r,f} + K_{\phi x,f}\phi_x + D_{\phi x,f}\dot{\phi}_x}{2b_f} \tag{3.9}$$

$$F_{z2} = \frac{mgL_r}{2L} - \frac{ma_x e_p + K_{\phi y}\phi_y + D_{\phi y}\dot{\phi}_y}{2L} - \frac{ma_y e_{r,f} + K_{\phi x,f}\phi_x + D_{\phi x,f}\dot{\phi}_x}{2b_f} \tag{3.10}$$

$$F_{z3} = \frac{mgL_f}{2L} + \frac{ma_x e_p + K_{\phi y}\phi_y + D_{\phi y}\dot{\phi}_y}{2L} + \frac{ma_y e_{r,r} + K_{\phi x,r}\phi_x + D_{\phi x,r}\dot{\phi}_x}{2b_r} \tag{3.11}$$

$$F_{z4} = \frac{mgL_f}{2L} + \frac{ma_x e_p + K_{\phi y}\phi_y + D_{\phi y}\dot{\phi}_y}{2L} - \frac{ma_y e_{r,r} + K_{\phi x,r}\phi_x + D_{\phi x,r}\dot{\phi}_x}{2b_r} \tag{3.12}$$

where $e_{r,f}$, $e_{r,r}$, and e_p are the front roll, rear roll and pitch eccentricity respectively.

3.2 Tyre Modelling

To calculate the tyre forces one has to predict the wheel slip. First the longitudinal $v_{x,i}$ and lateral $v_{y,i}$ wheel speeds are calculated for the wheels, where the index i represents the i-th wheel. The wheel speeds are determined by the following expressions

$$v_{w,i} = Q_{z,i} T_{z,i} v_c \tag{3.13}$$

$$v_{w,i} = \begin{bmatrix} v_{x,i} & v_{y,i} \end{bmatrix}^T \tag{3.14}$$

$$Q_{z,i} = \begin{bmatrix} \cos(\delta_i) & \sin(\delta_i) \\ -\sin(\delta_i) & \cos(\delta_i) \end{bmatrix} \tag{3.15}$$

$$T_{z,i} = \begin{bmatrix} 1 & 0 & a_i \\ 0 & 1 & b_i \end{bmatrix} \tag{3.16}$$

$$v_c = \begin{bmatrix} \dot{x} & \dot{y} & \dot{\phi}_z \end{bmatrix}^T \tag{3.17}$$

where $Q_{z,i}$ is the orthonormal rotation matrix and $T_{z,i}$ is the transformation matrix of vehicle velocity v_c to wheel velocity $v_{w,i}$. For wheel $i = 1$: $a_1 = \frac{b_f}{2}$ $b_1 = L_f$; $i = 2$: $a_2 = -\frac{b_f}{2}$ $b_2 = L_f$; $i = 3$: $a_3 = \frac{b_r}{2}$ $b_3 = -L_r$ and $i = 4$: $a_4 = -\frac{b_r}{2}$ $b_4 = -L_r$. The longitudinal slip ratio κ_i is calculated for the individual wheel as

$$\kappa_i = \begin{cases} \frac{R_{w,i}\dot{\phi}_{w,i} - v_{x,i}}{R_{w,i}\left|\dot{\phi}_{w,i}\right|}, & \text{if } \left|R\dot{\phi}_{w,i}\right| \geq |v_{x,i}| \\ \frac{R_{w,i}\dot{\phi}_{w,i} - v_{x,i}}{|v_{x,i}|}, & \text{else} \end{cases} \tag{3.18}$$

and lateral slip ratio α_i as

$$\alpha_i = \delta_i - \arctan\left(\frac{v_{y,i}}{v_{x,i}}\right) \tag{3.19}$$

where $R_{w,i}$ is the wheel's radius.

The build up of tyre slip is modelled as a first order system which is a system specific time constant and is accounted for by

$$\begin{aligned} t_{x,i}\dot{\kappa}_{i,dyn} &= \kappa_i - \kappa_{i,dyn} \\ t_{y,i}\dot{\alpha}_{i,dyn} &= \alpha_i - \alpha_{i,dyn} \end{aligned} \tag{3.20}$$

where $t_{x,i} = \frac{L_{x,i}}{v_{x,i}}$ and $t_{y,i} = \frac{L_{y,i}}{v_{y,i}}$ are the dynamic relaxation time constants. To avoid singularities, a minimum velocity is used and was set to 5 km/h. The brush tyre model, see [16], is used to determine the tyre forces. An isotropic behavior is assumed in the bristles with friction $\mu_{x,i} = \mu_{y,i} = \mu_i$ and stiffness $cp_{x,i} = cp_{y,i} = cp_i$. The combined slip can now be calculated with the use of practical slip relationships according to

$$\begin{aligned} \sigma_{x,i} &= \frac{\kappa_{i,dyn}}{1 + \kappa_{i,dyn}} \\ \sigma_{y,i} &= \frac{tan\left(\alpha_{i,dyn}\right)}{1 + \kappa_{i,dyn}} \\ \sigma_i &= \sqrt{\sigma_{x,i}^2 + \sigma_{y,i}^2}. \end{aligned} \tag{3.21}$$

The total force of the tyre is the calculated by the following expression

$$\begin{aligned} \theta_i &= \frac{2cp_i \cdot a_i^2}{3\mu F_{z_i}} \\ a_i &= a_0\sqrt{\frac{F_{z,i}}{F_{z0}}} \\ \lambda_i &= 1 - \theta_i\sigma_i \\ F_i &= \begin{cases} \mu_i F_{z,i}\left(1 - \lambda_i^3\right), \text{ if } \sigma_i \leq \frac{1}{\theta_i} \\ \mu_i F_{z,i}, \text{ else} \end{cases} \end{aligned} \tag{3.22}$$

The tyre force components $F_{x,i}$ and $F_{y,i}$ are given by

$$\begin{bmatrix} F_{x,i} \\ F_{y,i} \end{bmatrix} = F_i \begin{bmatrix} \frac{\sigma_{x,i}}{\sigma} \\ \frac{\sigma_{y,i}}{\sigma} \end{bmatrix}. \tag{3.23}$$

The aligning torque is given by

$$M_{z,i} = \begin{cases} -\mu_i F_{z,i}\lambda_i^3 a_i\left(1 - \lambda_i\right) sign\left(\alpha_{i,dyn}\right), \text{ if } \sigma_i \leq \frac{1}{\theta_i} \\ 0, \text{ else.} \end{cases} \tag{3.24}$$

The longitudinal force limit $F_{x,i,lim}$ is given by

$$F_{x,i,lim} = \sqrt{\left(\mu F_{z,i}\right)^2 - F_{y,i}^2} \tag{3.25}$$

The used chassis parameters are shown in Appendix A.

3.3 Driveline Modelling

The driveline is modelled with the main time constants found for generating motion. Three different driveline configurations are considered, they are:

i. CV - A conventional vehicle.

ii. HEV E4WD - A parallel HEV with electric four wheel drive.

iii. HEV WM - A series HEV with four wheel motors.

The driveline is a bit different for all three studied configurations. In Fig. 6, the drive line is shown for configuration 2. Configuration 1 is without the permanent magnet synchronous motors ISG and E4WD in front and rear respectively.

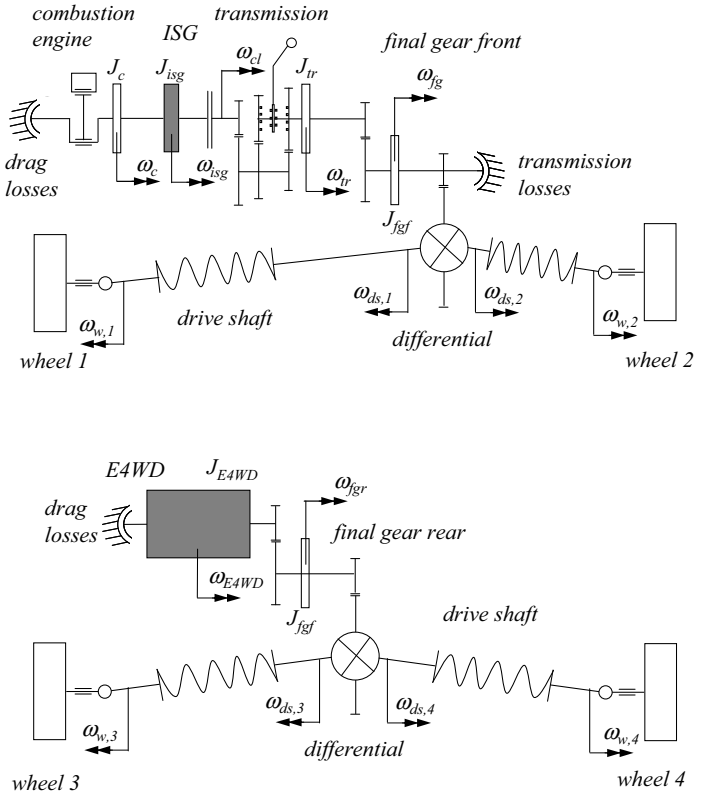

Figure 6: Driveline sketch for configuration 2 - HEV E4WD.

The driveline model for the first and second configuration includes weak driveshafts and open differentials. The weak driveshafts are an additional system specific time constant when generating the desired motion. The third configuration includes only the inertia in wheels.

The driveline model for the second configuration will be presented in this paper. By removing the ISG and the E4WD from the model presented, the first configuration can easily be determined. The third configuration only includes wheel motors and wheels in the driveline configuration. The driveline equations

for configuration 2 are as follows

$$(J_c + J_{isg})\dot{\omega}_{isg} = T_c + T_{m,isg} - (d_c + d_{isg})\omega_{isg} - T_{cl,1} \tag{3.26}$$
$$\omega_{cl,1} = \omega_{isg} \tag{3.27}$$

where T_c and $T_{m,isg}$ are the torque from the combustion engine and the ISG, respectively. The clutch is modelled as stiff when engaged

$$\omega_{cl,1} = \omega_{cl,2} \text{ if engaged, else } \omega_{cl,1} \neq \omega_{cl} \tag{3.28}$$
$$T_{cl,1} = T_{cl,2} \text{ if engaged, else } T_{cl,1} = T_{cl,2} = 0 \tag{3.29}$$

where $T_{cl,1}$ and $T_{cl,2}$ are the clutch torques on the engine and transmission side respectively. The manual five speed gearbox will have the following impact on the torque and angular speed

$$J_{tr}\dot{\omega}_{tr} = T_{tr} - d_{tr}\omega_{tr} - T_{fgf} \tag{3.30}$$
$$T_{tr} = r_i T_{cl,2} \tag{3.31}$$
$$\omega_{tr} = \frac{1}{r_i}\omega_{cl,2} \tag{3.32}$$

where T_{tr} is the transmission torque, and T_{fgf} is the final gear torque. Now the final gear increases the torque delivered to the differential T_{diff}

$$J_{fgf}\dot{\omega}_{fgf} = T_{fgf} - T_{diff} \tag{3.33}$$
$$T_{fgf} = r_{fgf}T_{tr} \tag{3.34}$$
$$\omega_{fgf} = \frac{1}{r_{fgf}}\omega_{tr}. \tag{3.35}$$

The differential is modelled as an open differential with the following equations

$$T_{diff} = T_{ds,i} + T_{ds,j} \tag{3.36}$$
$$T_{ds,i} = T_{ds,j} \tag{3.37}$$
$$\omega_{diff} = r_{diff}(\omega_{ds,i} + \omega_{ds,j}) \tag{3.38}$$

where $T_{ds,i}$ and $T_{ds,j}$ are the drive shaft torques on each side of the differential, and $i = 1, j = 2$. The four drive shafts, $i = 1, 2, 3, 4$, are seen as weak with rotational stiffness $k_{ds,i}$ and damping $d_{ds,i}$ which finally gives the driving torque T_{di} at the wheels

$$T_{d,i} = k_{ds,i}(\phi_{ds,i} - \phi_{w,i}) + d_{ds,i}(\omega_{ds,i} - \omega_{w,i}) \tag{3.39}$$
$$\dot{\phi}_{ds,i} = \omega_{ds,i} \tag{3.40}$$
$$\dot{\phi}_{w,i} = \omega_{w,i} \ , \ i = 1, 2. \tag{3.41}$$

For the rear wheels the equations are as follows

$$J_{e4wd}\dot{\omega}_{e4wd} = T_{m,e4wd} - T_{fgr} - d_{e4wd}\omega_{e4wd} \tag{3.42}$$
$$J_{fgr}\dot{\omega}_{fgr} = T_{fgr} - T_{diff} \tag{3.43}$$
$$T_{fgr} = r_{fgr}T_{m,e4wd} \tag{3.44}$$
$$\omega_{fgr} = \frac{1}{r_{fgr}}\omega_{m,e4wd} \tag{3.45}$$

where $T_{m,e4wd}$ is the actual torque from the rear permanent magnet synchronous motor. Same type of open differential according to Eqs. 3.37-3.38 is used for the rear with numbering $i = 3, j = 4$. Same drive shafts as in the front are also found in the rear, i.e. Eqs. 3.39-3.41 with $i = 3, 4$.

Fig. 7 shows the wheel rotation angle ϕ_w. The sum of moments around wheel rotation centre gives

$$I_{w,i}\ddot{\phi}_{w,i} = T_{d,i} - T_{b,i} - F_{x,i}R_i \tag{3.46}$$

where $T_{d,i}$ and $T_{b,i}$ are the actual driving and actual braking torque respectively.

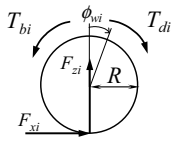

Figure 7: Wheel model for i:th wheel, x-z view, from side.

Used parameters for the driveline model can be found in Appendix A. Configuration 1, the conventional driveline has similar equations as above but excluding permanent magnet synchronous motors. Configurations 3 with wheel motors has only the following simple driveline model

$$J_{wm}\dot{\omega}_{wm} = r_{wm}T_{m,wm} - T_{di} - d_{wm}\omega_{wm} \tag{3.47}$$

$$\omega_{wi} = \frac{1}{r_{wm}}\omega_{m,wm} \tag{3.48}$$

where $T_{m,wm}$ is the actual torque from the wheel motor and T_{di} is the driving torque on wheel i, see Eq. 3.46.

3.4 Motion Actuators Modelling

The modelling of motion related actuators focuses on the internal states that limit the desired output. For example an electric motor is limited by the angular speed of the drive shaft and the temperature of the windings. Here a novel suggestion is implemented for how the limits for the motion related actuators should be defined in order to fit into the proposed vehicle system control architecture:

$$\underline{u} \leq u \leq \overline{u} \tag{3.49}$$

$$\underline{\rho} \leq \dot{u} \leq \overline{\rho} \tag{3.50}$$

where also the rate $\dot{u}$ is also limited.

Here a short overview of the tractive and braking actuator models can be found. The models are either first or second order models for the torque build up. The control input for the traction and braking actuators are assumed to be the desired torque. The electric motor and mechanical disc brake models include a

lumped mass temperature model for estimating the temperature. The models presented are an internal combustion engine model, a permanent magnet synchronous motor model, a electro hydraulic disc brake model, a steering actuator model and finally a battery model.

Internal combustion engine

The combustion engine is a complex energy converter to model in detail. If one wants to include the fuel and air intakes, volumes, temperatures, pressures, and the mechanics of the pistons and crank shaft it would lead to a far too detailed model for this study. Here a non-linear second order model is used for the mean torque, see [17] for further details.

$$\ddot{T}_c = -c_1(T_c - \bar{T}_c(\phi_{des}, \omega_c))\omega_c{}^2 - c_2\omega_c\dot{T}_c \tag{3.51}$$

where T_c is the mean torque, $\bar{T}_c(\phi_{des}, \omega_c)$ is the stationary torque as shown in Fig. 8, ω_c is the rotational speed of the engine and an input parameter and c_1 and c_2 are engine specific constants. According to [17] it takes approximately two crank shaft turns to reach the stationary torque for a four cylinder four stroke engine. This is ensured by selecting $c_1 = 0.1$ and $c_2 = 0.882$.

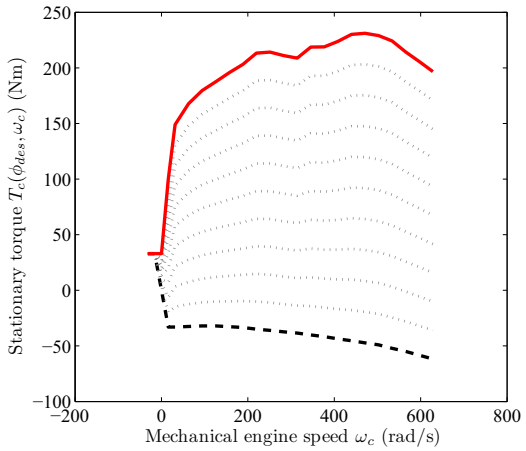

Figure 8: Stationary torque limits used for the combustion engine model with a maximum power of 123 kW at 6000 rpm. Maximum torque limit at throttle 100 % (solid red line), minimum torque limit at throttle 0 % (dashed black line), and throttle in increments of 10 % (dashed grey lines) are illustrated.

The limits depend, of course, on the engine modelled. The maximum and minimum torque limits are dependent on engine speed, as seen in Fig. 8. The rate limits can be determined using an equivalent time constant definition for second order systems as described in [18].

$$-\left(\frac{c_2}{2} + \sqrt{\frac{c_2^2}{4} - c_1}\right)\omega_c \leq \dot{T}_c \leq \left(\frac{c_2}{2} + \sqrt{\frac{c_2^2}{4} - c_1}\right)\omega_c \tag{3.52}$$

Permanent magnet synchronous motor

The model consists of a first order system for simulating the mechanical torque from the motor. A thermal lumped mass model similar to the disc brakes is also included for the motor. A novel suggestion is made for how the maximum torque and power limits are scaled by actual motor temperature down to continuous torque and power. The model is made scalable and is used for the integrated starter generator (ISG), rear electric four wheel drive motor (E4WD) and wheel motor.

The mechanical torque generated from the permanent magnet synchronous motor (PMSM) model is simplified to a first order model accordingly

$$t_m \dot{T}_m = T_{m,des} - T_m \tag{3.53}$$

where t_m is the time constant. The electric motor torque T_m is limited by the torque and power limits

$$T_m = \min\left(|T_{m,des}|, |k_1 \cdot T_{m,max}|, |k_2 \cdot \frac{P_{m,max}}{\omega_m}|\right) \tag{3.54}$$

where $k_1(\vartheta_m)$ and $k_2(\vartheta_m)$ are temperature dependent constants and $T_{m,max}$ and $P_{m,max}$ are the maximum peak torque and peak power, respectively, that the electric machine can deliver. The temperature dependent constants are assumed to reduce the torque by the following linear interpolation equations

$$k_1(\vartheta_m) = 1 - \left(1 - \frac{T_{mc,max}}{T_{m,max}}\right) \frac{\vartheta_m - \vartheta_{m,l}}{\vartheta_{m,h} - \vartheta_{m,l}} \tag{3.55}$$

$$k_2(\vartheta_m) = 1 - \left(1 - \frac{P_{mc,max}}{P_{m,max}}\right) \frac{\vartheta_m - \vartheta_{m,l}}{\vartheta_{m,h} - \vartheta_{m,l}} \tag{3.56}$$

where $T_{mc,max}$ and $P_{mc,max}$ are the maximum continuous torque and power that the electric machine can deliver respectively, and $\vartheta_{m,h}$ is the high threshold temperature when only continuous torque and power can be delivered. $\vartheta_{m,l}$ is the low threshold temperature when T_m has begun to reduce.

The temperature of the PMSM is calculated using the following lumped mass model

$$C_m \dot{\vartheta}_m = Q_{m,source} - Q_{m,cond} - Q_{m,conv} - Q_{m,rad} \tag{3.57}$$

$$C_m = m_m c p_m \tag{3.58}$$

$$Q_{m,source} = |T_m \omega_m (\frac{1}{\eta} - 1)| \tag{3.59}$$

$$Q_{m,cond} = l k_{cond} (\vartheta_m - \vartheta_{amb}) \tag{3.60}$$

$$Q_{m,conv} = h_v A_{m,conv} \alpha_{conv} (\vartheta_m - \vartheta_{amb}) \tag{3.61}$$

$$Q_{m,rad} = e A_{m,rad} \sigma (\vartheta_m^4 - \vartheta_{amb}^4) \tag{3.62}$$

where the C_m is the heat capacity, $Q_{m,source}$ is the heat generated by the power losses when operating the electric machine, $Q_{m,cond}$ is the heat conduction into the frame, $Q_{m,conv}$ is the heat convection out from the windings, and finally $Q_{m,rad}$ is the heat radiation out from the windings.

The heat is calculated by the following relationships $Q_{m,source} = P_{m,in} - P_{m,out}$ and $\eta(\omega_m, T_{m,act}) = P_{m,out}/P_{m,in}$. The efficiency $\eta(\omega_m, T_{m,act})$ is given by an efficiency map as shown in Fig. 9.

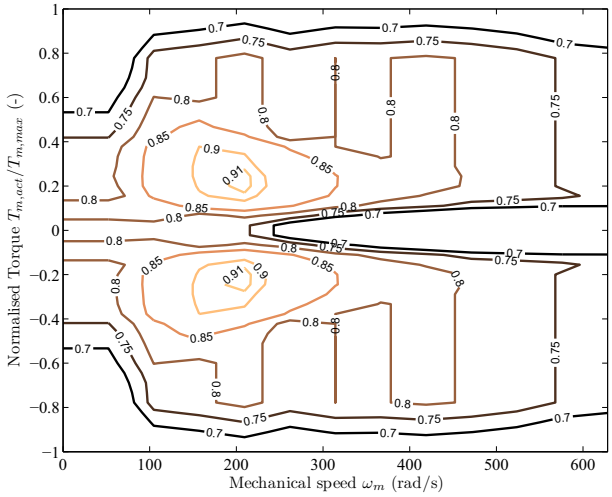

Figure 9: Efficiency map used for PMSM model.

The model is calibrated so that when the motor is running with continuous power it will reach the lower threshold temperature $\vartheta_{m,l}$ asymptotically when time goes to infinity. When the motor is running with maximum power the temperature reaches the higher threshold temperature within 2 minutes. This has been seen in experiments for an air cooled motor. The threshold temperatures were set to $\vartheta_{m,l} = 100\ ^oC$ as the lower threshold and $\vartheta_{m,h} = 200\ ^oC$ as the higher threshold, $200\ ^oC$ is also when the windings for the PMSM are starting to melt. Fig. 10 illustrates how the maximum torque is limited for different constant temperatures.

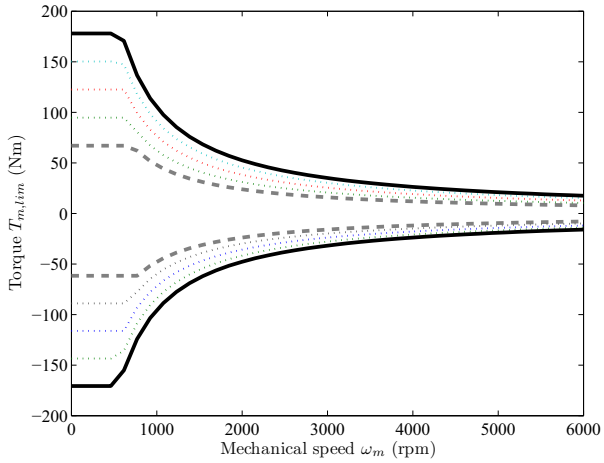

Figure 10: Torque limits $T_{m,lim}$ for ISG as a function of mechanical speed for different constant temperatures, threshold temperature $\vartheta_{m,l}$ (black solid line) and $\vartheta_{m,h}$ (grey dashed line).

The used parameters for the PMSM model are given in Appendix 3.

Electro-hydraulic disc brakes

In the wheel, Eq. 3.46, $T_{b,i}$ is the mechanical brake torque delivered from the disc brake model. A first order model is used to describe how the electro-hydraulic inlet valve generates the braking pressure

$$t_{b,i}\dot{p_{b,i}} = p_{b,i,des} - p_{b,i}. \tag{3.63}$$

where $p_{b,i}$ is the actual pressure for the i-th wheel, $p_{b,i,des}$ is the desired pressure and $t_{b,i}$ is the time constant. The same behavior is assumed for the outlet valve, i.e. the release of braking pressure. The braking torque $T_{b,i}$ is given by multiplying the normal force, $N_{b,i}$ with the temperature dependent friction between the braking pads and disc, $\mu_{b,i}(\vartheta_{b,i})$. The normal force, $N_{b,i}$, is governed by actual hydraulic pressure acting on the piston area $A_{b,i}$ as

$$N_{b,i} = p_{b,i}A_{b,i}. \tag{3.64}$$

The maximum normal force $N_{b,i,max}$ is generated by the asymptotic pressure $p_{asym,i}$ of the hydraulic system $N_{b,i,max} = p_{asym,i}A_{b,i}$. When combining these together the limits for the disc brakes becomes

$$0 \leq T_{b,i} \leq r_{b,i}\mu_i(\vartheta_{b,i})N_{b,i,max} \tag{3.65}$$

$$-\frac{r_{b,i}\mu_i(\vartheta_{b,i})N_{b,i,max}}{t_{b,i}} \leq \dot{T}_{b,i} \leq \frac{r_{b,i}\mu_i(\vartheta_{b,i})N_{b,i,max}}{t_{b,i}} \tag{3.66}$$

where $r_{b,i}$ is the disc brake radius.

When the disc is heated up the friction between the braking pads and disc is reduced. This starts at temperatures of around 200 ^{o}C as illustrated in Fig. 11. This is called brake fading. The friction, $\mu_i(\vartheta_{b,i})$, varies strongly with the selection of materials and the design used for the braking pads and disc.

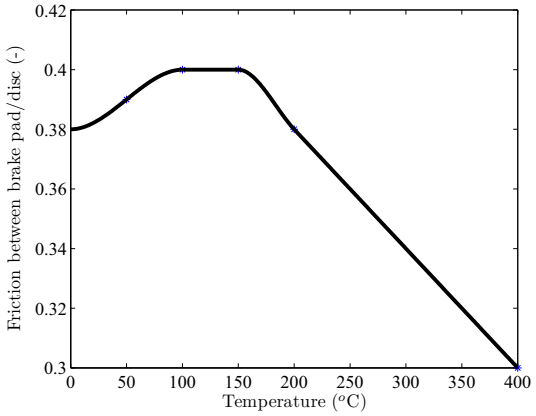

Figure 11: How friction can vary between braking pad and disc as a function of temperature.

A simple lumped state model is used to calculate the i-th disc temperature $\vartheta_{b,i}$.

The model is presented and discussed in [19], see also [20].

$$C_{b,i}\dot{\vartheta}_{b,i} = Q_{b,source,i} - Q_{b,cond,i} - Q_{b,conv,i} - Q_{b,rad,i} \tag{3.67}$$
$$C_{b,i} = m_{d,i}cp_{d,i} \tag{3.68}$$
$$Q_{b,source,i} = T_{b,i}\omega_w \tag{3.69}$$
$$Q_{b,cond,i} = lk_{b,cond,i}(\vartheta_{b,i} - \vartheta_{hub}) \tag{3.70}$$
$$Q_{b,conv,i} = A_{b,conv,i}\alpha_{conv}(\vartheta_{b,i} - \vartheta_{amb}) \tag{3.71}$$
$$Q_{b,rad,i} = eA_{b,rad,i}\sigma(\vartheta_{b,i}^4 - \vartheta_{amb}^4) \tag{3.72}$$

where the $C_{b,i}$ is the heat capacity of the disc, $Q_{b,source,i}$ is the braking power, $Q_{b,cond,i}$ is the heat conduction into the wheel hub and rim, $Q_{b,conv,i}$ is the heat convection out from the disc, and finally $Q_{b,rad,i}$ is the heat radiation from the disc. Used parameters for the brake model are given in Appendix A.

Front and rear steering

The front and rear steering is seen as a first order system with a time constant of 0.1. The steering limit was set to ±20 degrees.

$$0.1\dot{\delta}_i = \delta_{i,des} - \delta_i \tag{3.73}$$

Buffer

For vehicle configuration 2 and 3 a simple buffer model is used to predict the current State-of-Charge (SoC). It is based on the following equations

$$\dot{SoC} = \frac{P_{el}}{E_{buf,max}} \tag{3.74}$$

where SoC is the state of charge, $E_{buf,max}$ is the maximum buffer energy, and P_{el} is the electrical power taken from or delivered to the buffer from the permanent magnet synchronous motors.

$$P_{el} = \begin{cases} \min\left(P_{el}, m_{buf}\chi_{buf,dis}\right), \text{if } P_{el} \leq 0 \\ \max\left(P_{el}, m_{buf}\chi_{buf,char}\right), \text{else} \end{cases} \tag{3.75}$$

where m_{buf} is the mass of the buffer, $\chi_{den,dis}$ is the power density when discharging, and $\chi_{den,char}$ is the power density when charging. The working range was set to $0.4 \leq SoC \leq 0.8$. Used parameters for the buffer model are given in Appendix A.

3.5 Vehicle Modelling

As mentioned in the beginning of the section, three different powertrain configurations were considered, a conventional vehicle (CV), a parallel HEV with electric four wheel drive (HEV E4WD), and a series HEV with wheel motors (HEV WM). The chassis model is the same for all three vehicles. By combining

together the components modelled, the three vehicles can be configured. These three vehicle models represent and simulate the system as shown in Fig. 2. A summary of the vehicles is presented below:

i. CV. Usually conventional vehicles have a pre-determined mechanical brake distribution between the front and rear axle, however when a dynamical limit of e.g. yaw is exceeded then individual braking is allowed. This model has individual mechanical braking (4-input) braking with combustion engine connected to the front wheels via differential (1 input) giving a total of 5 inputs.

ii. HEV E4WD. Every wheel has individual mechanical braking (4-inputs). The rear axle has an electric motor connected by an differential (1-input). The powertrain includes an Integrated Starter Generator (ISG) located between the gear box and combustion engine (2-inputs) which are connected to the front wheels by an open differential. This model is seen as a 7-input configuration.

iii. HEV WM. Every wheel has individual mechanical braking (4-inputs) and is also equipped with wheel motors (4-inputs). This model is seen as a 8-input configuration. An extra energy source, such as a fuel cell is needed to allow for a continuous output power of 30 kW. The continuous power is sufficient enough to overcome the resistance forces at constant speed of 130 km/h. The total output power is 30 kW plus 135 kW when a buffer mass of 90 kg is selected.

If front and/or rear steering is included the total input on each configuration increases by two inputs.

4 Control Design

The objective of the control design is to regulate the longitudinal-, lateral-, and yaw-motions for a ground vehicle. Looking at the vehicle system it can easily be seen that the system is overactuated, there are only three control objectives but 7, 9 or 10 input signals depending on the vehicle configuration. In linear control theory there exists a wide range of methods which can handle this kind of problem, like LQ- and $\mathcal{H}_\infty$-control. Unfortunately, most of these methods cannot handle actuator saturations and/or constraints efficiently. As mentioned earlier control allocation is an option for coordination when one has more input signals to the system than the number of output states. Control allocation is attractive since it can handle actuator constraints, reconfiguration is unnecessary if the effectiveness of the actuators change over time and the actuator utilization can be treated independently, [4]. Control allocation can be applied to a class of linear and nonlinear systems. If it can be applied, the control design can be divided into two steps. The first step is to design a control law determining the net control effort. The second step is mapping the net control demand onto the individual actuators.

Independently of the specific applications studied, a class of nonlinear systems can be described in the affine form

$$\dot{x} = f(x) + g(x)\,u \tag{4.1}$$
$$y = h(x) \tag{4.2}$$

If the studied nonlinear system can be written in this affine form and certain conditions are fulfilled control allocation can be applied. Control allocation can be applied if the control input can be perturbed without affecting the system dynamics. The system can therefore be rewritten as

$$\dot{x} = f(x) + v \tag{4.3}$$
$$y = h(x) \tag{4.4}$$

where $v = g(x)u$, v is also called the virtual control input. A control law regulates the net effort v. The control allocator maps then the net effort of the virtual control input onto the true control input, $v(t) \mapsto u(t)$. Unfortunately, the mapping of the net effort to the true control signal is complicated since the $g(x)$-matrix is not invertible. Using a pseudo-inverse to find a solution could be one way of solving this. However, this could lead to an unrealistic solutions since the true control signals are limited by several different constraints. Instead a constrained optimization problem is proposed and solved.

The nonlinear vehicle system can be formulated in the affine form by selecting the following state variables $x = \begin{bmatrix} v_x & v_y & \dot{\phi}_z \end{bmatrix}^T$. The roll and pitch motion are seen as secondary effects for generating the desired motion on a flat surface and are thus neglected.

The lateral slip, α_i, can be separated into two parts, one due to the steering angle and one due to vehicle states as

$$\alpha_1 = \delta_1 - \frac{x_2 + L_f x_3}{x_1 + \frac{b_f}{2} x_3} \tag{4.5}$$
$$\alpha_2 = \delta_2 - \frac{x_2 + L_f x_3}{x_1 - \frac{b_f}{2} x_3} \tag{4.6}$$
$$\alpha_3 = \delta_3 - \frac{x_2 - L_r x_3}{x_1 + \frac{b_r}{2} x_3} \tag{4.7}$$
$$\alpha_4 = \delta_4 - \frac{x_2 - L_r x_3}{x_1 - \frac{b_r}{2} x_3}. \tag{4.8}$$

If small angles are assumed the lateral force, $F_{y,i}$, can be calculated as

$$F_{y,i} = C_{\alpha,i}\alpha_i \tag{4.9}$$

where $C_{\alpha,i}$ is the cornering stiffness for tyre i. This separation means that the lateral tyre force can be written as a sum of lateral forces due to the steering angle, $F_{y,i}(\delta)$, and vehicle states, $F_{y,i}(x)$.

$$F_{y,i} = F_{y,i}(\delta) + F_{y,i}(x) \tag{4.10}$$

By using Eqs. 4.9-4.10 in combination with Eqs. 4.5-4.8 where the track width front and rear is assumed to be equal $b_t = b_f = b_r$ and all four wheels are assumed to be equal, i.e. the cornering stiffness is equal for all four wheels, $C_\alpha = C_{\alpha,i}$, and the radius is also equal, $R_w = R_{w,i}$, the chassis Eq. 3.1-3.6 can be rewritten as

$$f(x) = \begin{bmatrix} mx_2x_3 - D_1x_1 - D_2m\text{sgn}(x_1)x_1^2 \\ -mx_1x_3 - C_\alpha \frac{8x_1(2x_2+(L_f-L_r)x_3)}{4x_1^2-b_t^2x_3^2} \\ -L_fC_\alpha \frac{8x_1(2x_2+L_fx_3)}{4x_1^2-b_tx_3^2} + L_rC_\alpha \frac{8x_1(2x_2-L_rx_3)}{4x_1^2-b_tx_3^2} \end{bmatrix} \tag{4.11}$$

$$g(x)\,u = \begin{bmatrix} \sum_{i=1}^{4} F_{x,i} \\ C_\alpha \sum_{i=1}^{4} \delta_i \\ L_fC_\alpha \sum_{i=1}^{2} \delta_i - L_rC_\alpha \sum_{i=3}^{4} \delta_i + \frac{b_t}{2} \sum_{i=3}^{4} (-1)^{1+i} F_{x,i} \end{bmatrix} \tag{4.12}$$

$$h(x) = \begin{bmatrix} x_1 & x_2 & x_3 \end{bmatrix}^T \tag{4.13}$$

where D_1 and D_2 are constants related to aerodynamic and wheel rolling resistance. The system can now be written as:

$$M\dot{x} = f(x) + g(x)u \tag{4.14}$$

$$y = h(x) \tag{4.15}$$

where M is the mass matrix

$$M = \begin{bmatrix} m & 0 & 0 \\ 0 & m & 0 \\ 0 & 0 & I_z \end{bmatrix}.$$

Since the mass matrix is invertible, the system can be written in the affine form. Furthermore, the vehicle system model presented is general and independent of the three configurations. Moreover, $g(x)u$ can be written as a constant matrix times the control signal, Bu. The B matrix is often called the *control effectiveness matrix*. Since it is linear, control allocation can be applied if the rank of the B-matrix is less than the number of control signals. This is the case for the vehicle system presented here. This allows us to separate the control law for keeping the desired path of the vehicle from the control allocation of the specific motion actuators. The virtual control input is set equal to the global vehicle forces, $v = \begin{bmatrix} F_x & F_y & M_z \end{bmatrix}^T$.

Control Effectiveness Matrix B

As mentioned earlier the virtual control signals are the global forces. Looking at the model (Eqs. 4.11-4.15) the control signals are the longitudinal wheel forces $F_{x,i}$ and the wheel steering angles δ_i. The wheel forces are controlled by the motion actuators via the driveline. For the three configurations the following control input signals exist

$$u_{c_1} = \begin{bmatrix} \tau_{ice} & \tau_{mb_1} & \tau_{mb_2} & \tau_{mb_3} & \tau_{mb_4} & \delta_f & \delta_r \end{bmatrix}^T \tag{4.16}$$

$$u_{c_2} = \begin{bmatrix} \tau_{ice} & \tau_{isg} & \tau_{ram} & \tau_{mb_1} & \tau_{mb_2} & \tau_{mb_3} & \tau_{mb_4} & \delta_f & \delta_r \end{bmatrix}^T \tag{4.17}$$

$$u_{c_3} = \begin{bmatrix} \tau_{wm_1} & \tau_{wm_2} & \tau_{wm_3} & \tau_{wm_4} & \tau_{mb_1} & \tau_{mb_2} & \tau_{mb_3} & \tau_{mb_4} & \delta_f & \delta_r \end{bmatrix}^T \tag{4.18}$$

where τ_i is the torque from the traction and braking actuators and $\delta_f = \delta_1 = \delta_2$ and $\delta_r = \delta_3 = \delta_4$ are the front and rear rack steering angles were the Ackermann angle is neglected. Steering was included in the control allocation to allow for an objective comparison of the three different vehicle configurations. Today's cars usually have conventional steering which the driver solely manages by a mechanical link from the steering wheel to the wheels. This would delete the last two elements in control input vector u_c and the corresponding columns in the control effectiveness matrix B.

Unfortunately, if the motion related actuators and driveline are added to the system model, the mapping from v to u cannot be performed via a constant control effectiveness matrix. However, if no inertia effects in the driveline nor wheels i.e. $J\dot{\omega} = 0$, no weak drive shafts, no losses, and no time delays or nonlinearities in developing tyre forces i.e. $F_{x,i} = \frac{\tau_{w,i}}{R_w}$ are assumed, constant control effectiveness matrices can be formulated. The assumptions are realistic for the control design phase. The control effectiveness matrices for the three cases become:

$$B_1 = \begin{bmatrix} \frac{r_i r_{fgf}}{R_w} & \frac{1}{R_w} & \frac{1}{R_w} & \frac{1}{R_w} & \frac{1}{R_w} & 0 & 0 \\ 0 & 0 & 0 & 0 & 0 & 2C_\alpha & 2C_\alpha \\ 0 & \frac{b_t}{2R_w} & \frac{-b_t}{2R_w} & \frac{b_t}{2R_w} & \frac{-b_t}{2R_w} & 2L_f C_\alpha & -2L_r C_\alpha \end{bmatrix} \tag{4.19}$$

$$B_2 = \begin{bmatrix} \frac{r_i r_{fgf}}{R_w} & \frac{r_i r_{fgf}}{R_w} & \frac{r_{fgr}}{R_w} & \frac{1}{R_w} & \frac{1}{R_w} & \frac{1}{R_w} & \frac{1}{R_w} & 0 & 0 \\ 0 & 0 & 0 & 0 & 0 & 0 & 0 & 2C_\alpha & 2C_\alpha \\ 0 & 0 & 0 & \frac{b_t}{2R_w} & \frac{-b_t}{2R_w} & \frac{b_t}{2R_w} & \frac{-b_t}{2R_w} & 2L_f C_\alpha & -2L_r C_\alpha \end{bmatrix} \tag{4.20}$$

$$B_3 = \begin{bmatrix} \frac{r_{fg}}{R_w} & \frac{r_{fg}}{R_w} & \frac{r_{fg}}{R_w} & \frac{r_{fg}}{R_w} & \frac{1}{R_w} & \frac{1}{R_w} & \frac{1}{R_w} & \frac{1}{R_w} & 0 & 0 \\ 0 & 0 & 0 & 0 & 0 & 0 & 0 & 0 & 2C_\alpha & 2C_\alpha \\ \frac{r_{fg} b_t}{2R_w} & \frac{-r_{fg} b_t}{2R_w} & \frac{r_{fg} b_t}{2R_w} & \frac{-r_{fg} b_t}{2R_w} & \frac{b_t}{2R_w} & \frac{-b_t}{2R_w} & \frac{b_t}{2R_w} & \frac{-b_t}{2R_w} & 2L_f C_\alpha & -2L_r C_\alpha \end{bmatrix} \tag{4.21}$$

Matrices 4.19-4.21 describe the three configurations and their ability to generate the global vehicle forces $v(t) = \begin{bmatrix} F_x & F_y & M_z \end{bmatrix}^T$. Observe how the yaw moment M_z can only be applied by the mechanical brakes and steering for configuration 1 and 2. This due to the fact that open differentials are used in the drive line in these configurations. This results in that traction actuators such as the combustion engine, ISG, and E4WD motors cannot be used for gaining M_z.

4.1 Control Law and Feedback Linearization

First step in creating the control system is to design the control law as illustrated in Fig. 2. The purpose for the controller, as mentioned earlier in the paper, is to follow a desired trajectory. The controller is based on feedback linearization, see e.g. [21]. The idea with feedback linearization is to transform the nonlinear system into a linear one, so that linear techniques can be used. In its simplest form it can be seen as a way to cancel the nonlinearities by a nonlinear state feedback. Looking at the system, we notice that the first term on the right hand side of (4.14) is the only one including the nonlinearities of the system. If the nonlinear term, $f(x)$, is cancelled, the multi-input, multi-output (MIMO)-

system becomes linear. Furthermore, by cancelling $f(x)$ the MIMO-system becomes decoupled. Then, using PI-controllers, the control law becomes

$$v = -f(x) + K_p e + K_i \int_0^t e d\tau \tag{4.22}$$

where e is the error between the desired vehicle motion and the vehicles actual motion. The design parameters for the PI-controllers, K and T_i, are chosen as

$$K_i = 5 \begin{bmatrix} m & 0 & 0 \\ 0 & 0.6m & 0 \\ 0 & 0 & 1.5I_z \end{bmatrix} \tag{4.23}$$

$$K_p = 4m\sqrt{K_i/m}. \tag{4.24}$$

Figure 12 shows how the feedback linearization $\alpha(x)$ is summed together with the PI-controller signals before the control allocator. To handle the saturation of actuators the PI-controllers were extended with anti-windup based on back calculation [22]. When the actuators are not saturated the error $e_s = Bu - v$ will be zero and there will therefore be no effect on the sum of integrator gain, see also Fig. 12. The windup was minimized with $\frac{1}{T_t} = 5I_{3x3}$.

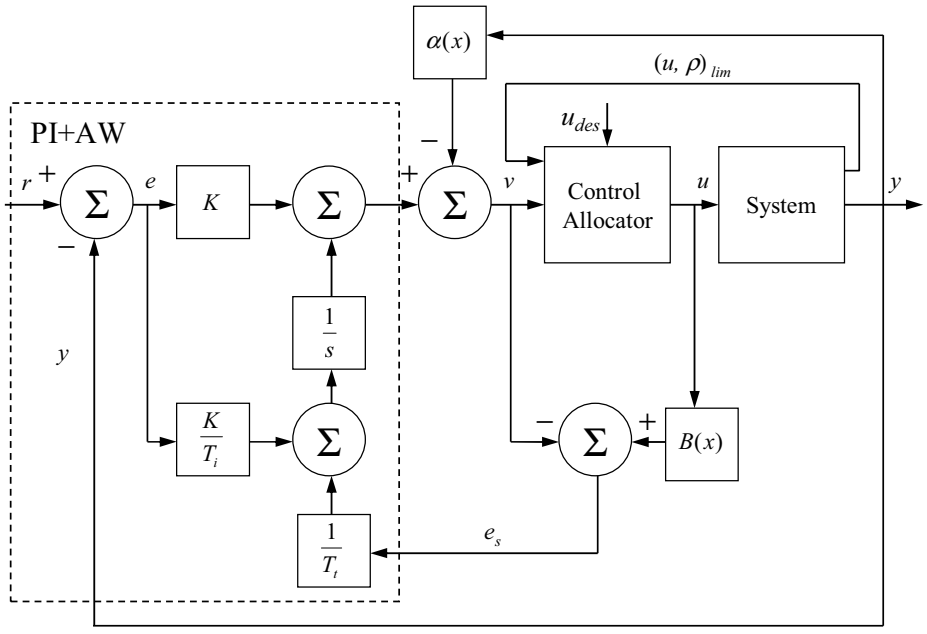

Figure 12: Layout of the control system with the PI-controller,anti-windup, feedback linearization, and control allocation.

4.2 Control Allocation

The second step in the control design is to create the control allocator. The key issue is how to select the control input set u from all possible combinations. In control allocation an optimization based selection is used. According to [4] the

optimal control input u can be seen as two-step optimization problem

$$u = \arg \underbrace{\min}_{u \in \Omega} \|W_u(u - u_{des})\|_p \tag{4.25}$$

$$\Omega = \arg \underbrace{\min}_{\underline{u} \leq u \leq \overline{u}} \|W_v(Bu - v)\|_p \tag{4.26}$$

where W_u and W_v are weighting matrices and u_{des} is the desired control input. The two step optimization problem actually suits very well for HEVs. Eq. 4.26 constrains the possible set $u \in \Omega$ to only be possible u's that will be in nullspace of $N(Bu - v)$ or minimize the error of the desired forces, $Bu - v$, needed for fulfilling the desired motion of the vehicle. This can be seen as the vehicle motion controller. Eq. 4.25 minimizes the error of the desired control input, $u_{des} - u$. The desired control input, u_{des}, which comes from the energy management controller, declares how the electric motor(s) and the mechanical brakes should be used when optimizing the use of onboard energy. This can be seen as a smooth arbitration between energy management and vehicle motion control. Fig. 2 shows how energy management is included in the control allocator and Fig. 12 shows how the control allocator fits in the control system in more detail. Numerically Eqs. 4.25- 4.26 are solved in one step

$$u = \arg \underbrace{\min}_{\underline{u} \leq u \leq \overline{u}} \|W_u(u - u_{des})\|_p + \gamma \|W_v(Bu - v)\|_p. \tag{4.27}$$

The optimization problem is solved as weighted least square, $p = 2$. Setting the weighting parameter γ to a high value gives priority to minimizing the error $Bu - v$ which is here related to the desired motion.

Actuator Limits

The limits which are sent to the control allocator are the limits from the motion related actuators, in other words, the actuators need to send feedback to the control allocator about the actual dynamical limits $[\underline{u}(t), \overline{u}(t)]$ and their limits in rate of change $[\underline{\rho}, \overline{\rho}]$. This specific way of designing the control system allows the control law to be independent of the available actuators, i.e. reusable for different hardware configurations, and also allows the control allocator to handle limits and even the failure of actuators. The rate limits can be rewritten as position constraints using an approximation of the time derivative

$$\dot{u}(t) \approx \frac{u(t) - u(t - t_T)}{t_T} \tag{4.28}$$

where t_T is the sampling time. The position constraints can now be written as

$$\overline{u}(t) = \min\left(\overline{u}(t), u(t - t_T) + t_T \overline{\rho}\right) \tag{4.29}$$

$$\underline{u}(t) = \max\left(\underline{u}(t), u(t - t_T) + t_T \underline{\rho}\right). \tag{4.30}$$

In a ground vehicle the limits of the control input must also consider the force limits each wheel. Each wheel's longitudinal force limit $F_{x,lim,i}$ is a function of the normal force $F_{z,i}$, tyre/road friction μ_i, and the amount of lateral force $F_{y,i}$

applied to the wheel. So by estimating $F_{x,lim,i}$ for each wheel the actuator limits are adjusted for what the tyres actually can handle. The function is here called tyre fusion. The tyre fusion basically checks if the electrical torque limits for the electric motors, $u_{el,lim,i}$, are above the longitudinal force limits and if so adjusts the limits to be equal to what the tyre can handle. If the sum of electrical and mechanical torque limits $u_{el,mech,lim,i}$ are more than the tyre force limit, then the mechanical limits are set as the difference of the tyre force limit and electrical limit. The idea is to always try to give electric motors the possibility to act within the tyre's limits. In equation form this would look something like

$$\underline{u}_{\mathrm{el},i} = \begin{cases} -\overline{F}_{x,i} R_w, & \text{if } \underline{u}_{\mathrm{el},i} \leq -\overline{F}_{x,i} R_w \\ \underline{u}_{\mathrm{el},i}, & \text{else} \end{cases} \tag{4.31}$$

$$\overline{u}_{\mathrm{mech},i} = 0 \tag{4.32}$$

$$\underline{u}_{\mathrm{mech},i} = \begin{cases} 0, & \text{if } \underline{u}_{\mathrm{el},i} \leq -\overline{F}_{x,i} R_w \\ -\overline{F}_{x,i} R_w - \underline{u}_{\mathrm{el},i}, & \text{elseif } (\underline{u}_{\mathrm{el},i} + \underline{u}_{\mathrm{mech},i}) \leq -\overline{F}_{x,i} R_w \\ \underline{u}_{\mathrm{mech},i}, & \text{else} \end{cases} \tag{4.33}$$

where $\underline{u}_{\mathrm{el},i}$ and $\overline{u}_{\mathrm{mech},i}$ are the tyre limits for the electrical and mechanical braking torques. A bit different tyre limits are used for the configurations CV and HEV E4WD configurations. These configurations have open differential(s) in their drivelines where the actuators behind the open differential such as ICE and ISG, and the motor E4WD were limited by the minimum longitudinal force that either of the wheels had on the considered front or rear axles.

5 Simulations

The vehicle system models were implemented as s-functions in Matlab/Simulink. Due to the open differential in the driveline model the system becomes a differential algebraic equation system, a (DAE) system. The equations for the open differential were rewritten to be in ordinary differential equation (ODE) form by using a mass matrix. Solver *ode23t* was used in the simulation, since it can solve problems with a singular mass matrix. The controller was implemented in Simulink using the standard block-sets. The QCAT toolbox [23] has been used in this paper to solve the control allocation problem. The code was modified by the authors to allow for dynamical change in constraints u_{lim}.

The simulated test procedures focus on braking situations where the coordination of mechanical disc brakes and electric motors would be expected. The three vehicle configurations are compared and the only parts changed in the control system were the control effectiveness matrix B and the tyre fusion algorithm which was slightly different for configurations 1 and 2 with an open differential in the driveline. For configurations 1 and 2 the third gear was set as a default. The initial temperature for the disc brakes and electric motors was set to 30 ^{o}C.

The following parameters were used for the control allocator: the time step was

set to $T = 10$ ms, the weighting matrix for the desired global forces was set to $W_v = \text{diag}[\ 1 \quad 1 \quad 1\ ]$ for all three configurations, and the weighting matrix for the desired input signals was set to

$$W_{u,1} = \text{diag}[\ 1 \quad 0.5 \quad 0.5 \quad 1 \quad 1 \quad 1e3 \quad 2e3\ ], \tag{5.1}$$

$$W_{u,2} = \text{diag}[\ 1 \quad 0.1 \quad 0.25 \quad 0.5 \quad 0.5 \quad 1 \quad 1 \quad 1e3 \quad 2e3\ ], \tag{5.2}$$

$$W_{u,3} = \text{diag}[\ 0.1 \quad 0.1 \quad 0.25 \quad 0.25 \quad 0.5 \quad 0.5 \quad 1 \quad 1 \quad 1e3 \quad 2e3\ ] \tag{5.3}$$

for configurations 1, 2, and 3 respectively.

All simulations were performed on the complete vehicle system as modelled in Section 3, i.e. a vehicle model including all modelled nonlinearities and major time constants.

5.1 Test Procedures

The selected driving situations are derived from [24] and modified to trigger the energy management algorithm that can be found in the vehicle system controller within a hybrid electric vehicle. The following test procedures have been selected for simulation:

i. a) Braking on asphalt with the tyre road friction set to 1.0.
   b) Braking on ice with the tyre road friction set to 0.3.
   Both 1a and 1b have the following initial conditions: $v_{init} = 100$ km/h, soft braking with a deceleration of 0.1g until 80 km/h, then hard braking with a deceleration of 0.8g until 40 km/h, and finally soft braking with a deceleration of 0.1g until standstill.

ii. Stability when braking in a circle on ice. This procedure contains the following initial conditions: the initial velocity v_{init} is decided by limit cornering without skidding for a radius of 200 m, tyre road friction is set to 0.3, constant steering, soft braking and deceleration is set to 0.1g to keep the vehicle in re-generative mode and try to maintain vehicle stability.

5.2 Test procedure 1a and 1b - Straight Braking

Figure 5.2 shows the longitudinal reference velocity and the simulated velocity of the vehicle for all three configurations during test procedure 1a. It is interesting to note that when braking on high friction, all configurations have no major problems following the reference velocity during hard braking. Configuration WM, with the most electrical braking power is the fastest to respond and follows the reference velocity very well. In Fig. 5.2 the longitudinal velocity is shown for test procedure 1b with low friction. Still no configuration is outperformed by another configuration.

During test procedure 1a and 1b none of the wheels lock for any of the configurations. The reason for this is that the combined limits are used for the

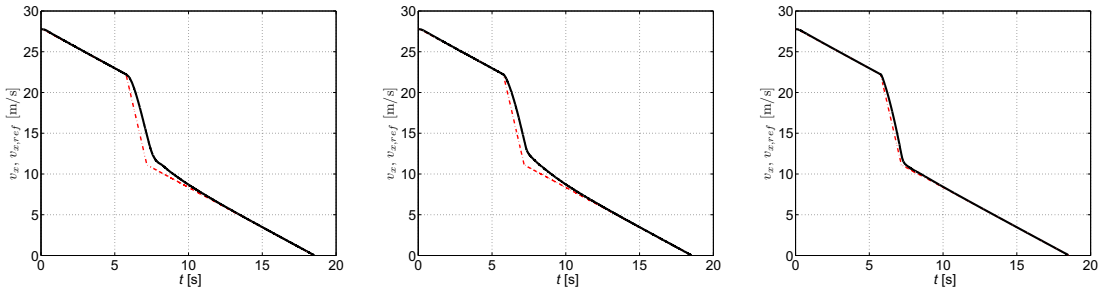

Figure 13: Longitudinal velocity v_x for configurations CV (left), HEV E4WD (centre), and HEV WM (right) during test procedure 1a.

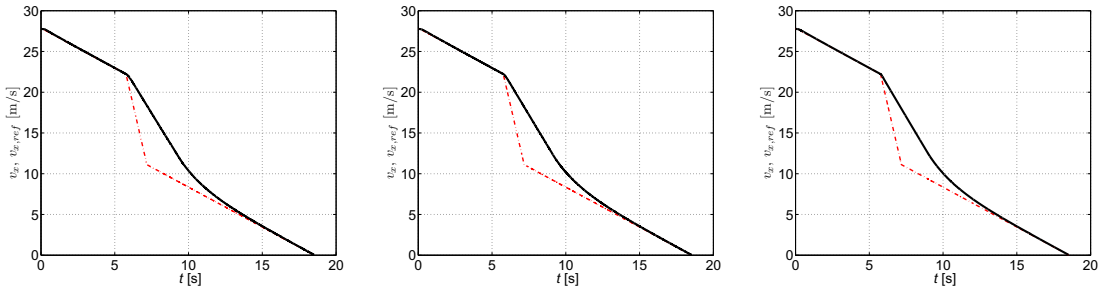

Figure 14: Longitudinal velocity v_x for configuration CV (left), HEV E4WD (centre), and HEV WM (right) during test procedure 1b.

possible input set u for the available actuators. First the actuator limits and their rate of change limits are considered, see Eq. 4.30. Then the limits are compared with how much longitudinal force each tyre can handle, see Eq. 4.33, which gives the combined limits. Figure 15 shows the combined limits and the actual values of u for configuration CV during test procedure 1a. The black solid lines correspond to the actual u, the dashed red and blue lines correspond to the upper and lower combined limits respectively. The vehicle is braking more on the front brakes (actuators 2 and 3) when compared to the rear brakes (actuators 4 and 5). This load distribution is easily allowed by the weighting matrix W_u, see Eq. 5.1, where the front brakes are less penalized. We can also see that actuator 1, the combustion engine, applies positive torque for a short period when the hard braking part has ended. The reason for this is that the controller tries to follow the reference velocity, i.e. the controller applies a positive torque to avoid an undershoot. The only way to apply positive torque for this configuration is to use the combustion engine. Within Figs. 15-5.2 the actuator signals corresponding to the steering are omitted, since they are zero during the complete simulations.

Figs. 5.2 and 5.2 show the input set u and the combined limits for configurations HEV E4WD and HEV WM respectively during test procedure 1a. Here it can be seen how the electrical braking is prioritized before mechanical, the reason is that electrical braking is less penalized in the weight matrix W_u. Another factor is that the tyre fusion algorithm always prioritizes the electrical braking. This is shown in Fig. 5.2 where actuators 7 and 8, the rear mechanical brakes, are limited to null during hard braking. It can also be seen how actuators 3 and 4 are reduced during hard braking due to the major pitching of the vehicle.

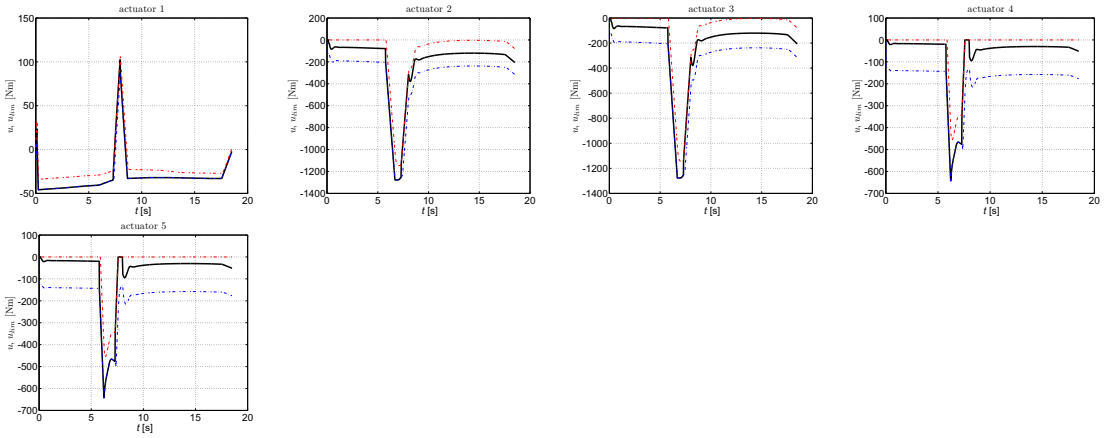

Figure 15: Input set u and their limits for configuration CV during test procedure 1a.

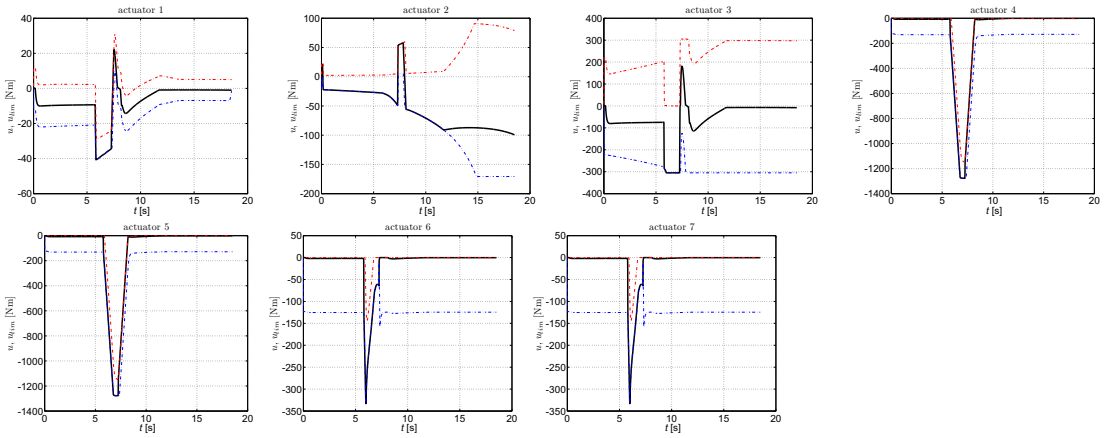

Figure 16: Input set u and their limits for configuration HEV E4WD during test procedure 1a.

The pitching reduces the vertical load on the rear wheels which then directly reduces the available force limits on the rear tyres.

For test procedure 1b with low friction it can be seen how the tyre fusion algorithm significantly reduces the combined limits, see Figs. 5.2-5.2 for configurations CV, HEV E4WD, and HEV WM, respectively. For configuration WM all mechanical brakes are reduced to 0 and the combined limits of the wheel motors are affected by the pitching.

5.3 Test Procedure 2 - Circle Braking on Low Friction

Here, the vehicle is trying to maintain the stability when making a circle on low tyre/road friction. A simple calculation gives the maximum vehicle speed that can be maintained, v_{max}, when making a circle with a radius of $R = 200$ meter

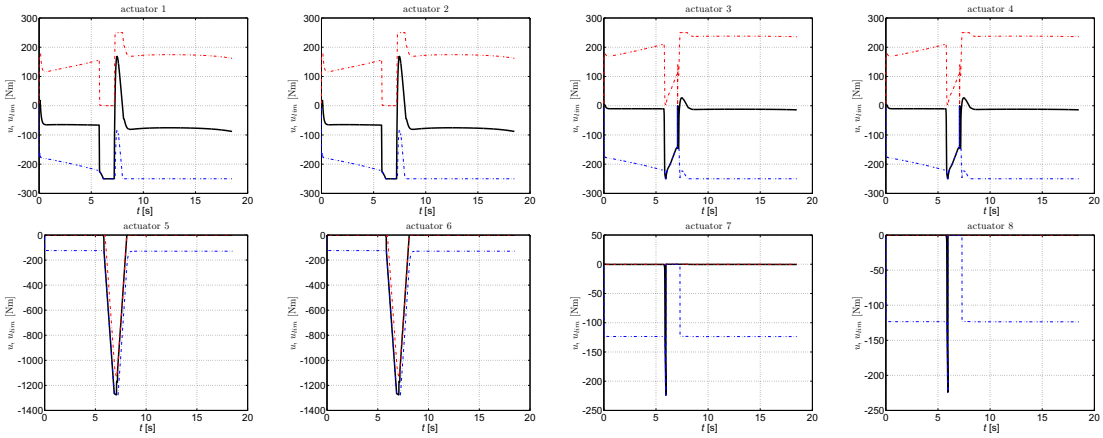

Figure 17: Input set u and their limits for configuration WM during test procedure 1a.

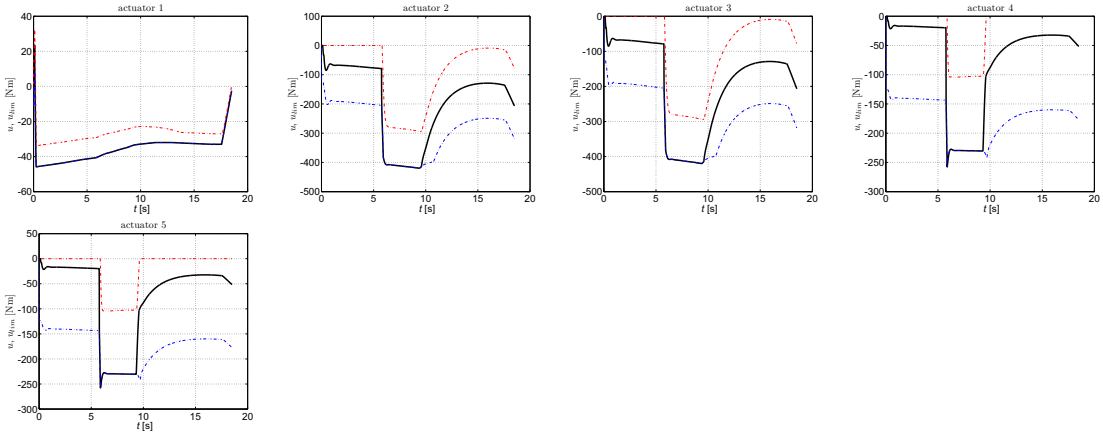

Figure 18: Input set u and their limits for configuration CV during test procedure 1b.

on ice with friction μ =0.3.

$$\delta_f = \frac{L}{R} = \frac{2.674}{200} = 0.0134 \text{ rad} \tag{5.4}$$

$$F_{fric} = F_{centripetal} \Leftrightarrow \mu \cdot m \cdot g = \frac{m \cdot v_{max}^2}{R}$$

$$v_{max} = \sqrt{\mu \cdot g \cdot R} = 24.26 \text{ m/s} \tag{5.5}$$

In the simulations the v_{max} was reduced by 10 percent to assure steady state circle driving, which was verified by simulating a full circle with all three configurations. The vehicle was first driven straight for 0.1 seconds and then the reference yaw velocity was ramped up to $v_x/200$ rad/s in 1 second. Soft braking was then started with 0.1g deceleration was started after the full yaw velocity was achieved with the aim of maintaining the circle during the braking until standstill.

The reference and achieved velocities are shown in Fig. 5.3. It shows how all configurations are able to track the longitudinal and yaw reference velocities

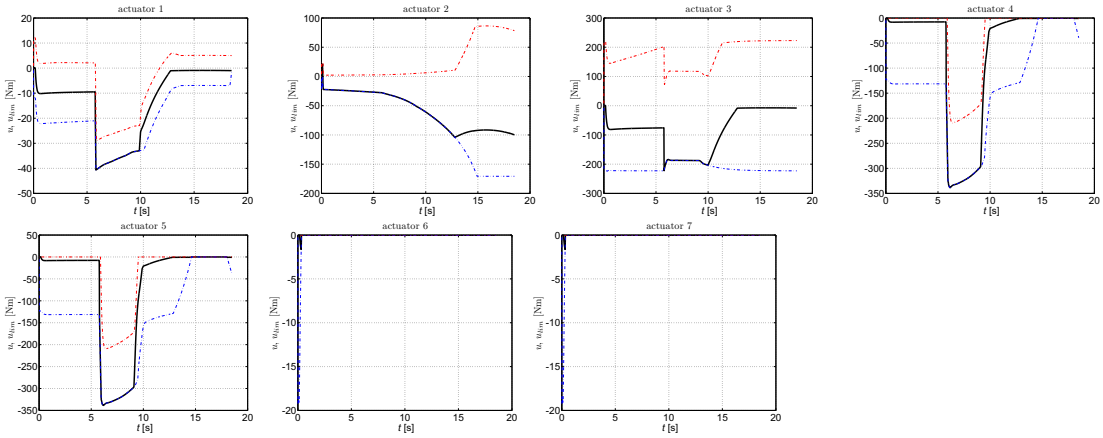

Figure 19: Input set u and their limits for configuration HEV E4WD during test procedure 1b.

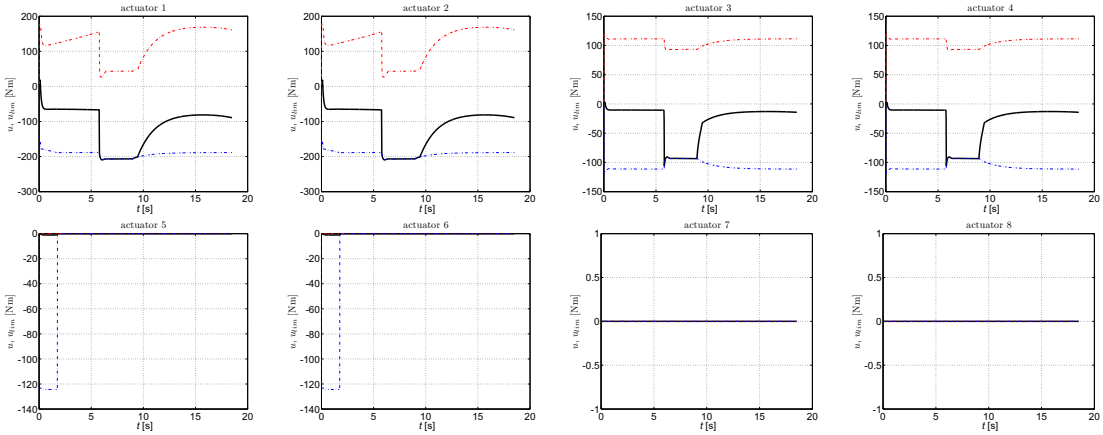

Figure 20: Input set u and their limits for configuration WM during test procedure 1b.

and how the lateral velocity is almost zero. All configurations could hold the circle path until standstill.

Figs. 5.3-5.3 shows the input set u and its combined limits for configurations CV, HEV E4WD, and HEV WM, respectively. The black solid lines correspond to the actual u, the dashed red and blue lines correspond to the upper and lower combined limits, respectively. In configuration CV, Fig. 5.3, the braking is mainly performed by the front mechanical brakes, actuators 2 and 3. It can also be seen that it uses the engine as a brake as well. In configuration HEV E4WD, Fig. 5.3, it can be seen that the braking is performed by the engine and the electric motors. The mechanical brakes are almost not used at all. It is interesting to see that actuator 7, the right rear mechanical brake, is not used at all. This is the result of the optimization. In configuration HEV WM, Fig. 5.3, the front wheel motors, actuators 1 and 2, are braking considerably more than the rear wheel motors, actuators 3 and 4. This is similar to the mechanical braking for configuration CV. Furthermore, the steering action on the front and rear rack steering is automatically performed by the control allocation. All three configurations have similar steering inputs for the test case, which was also

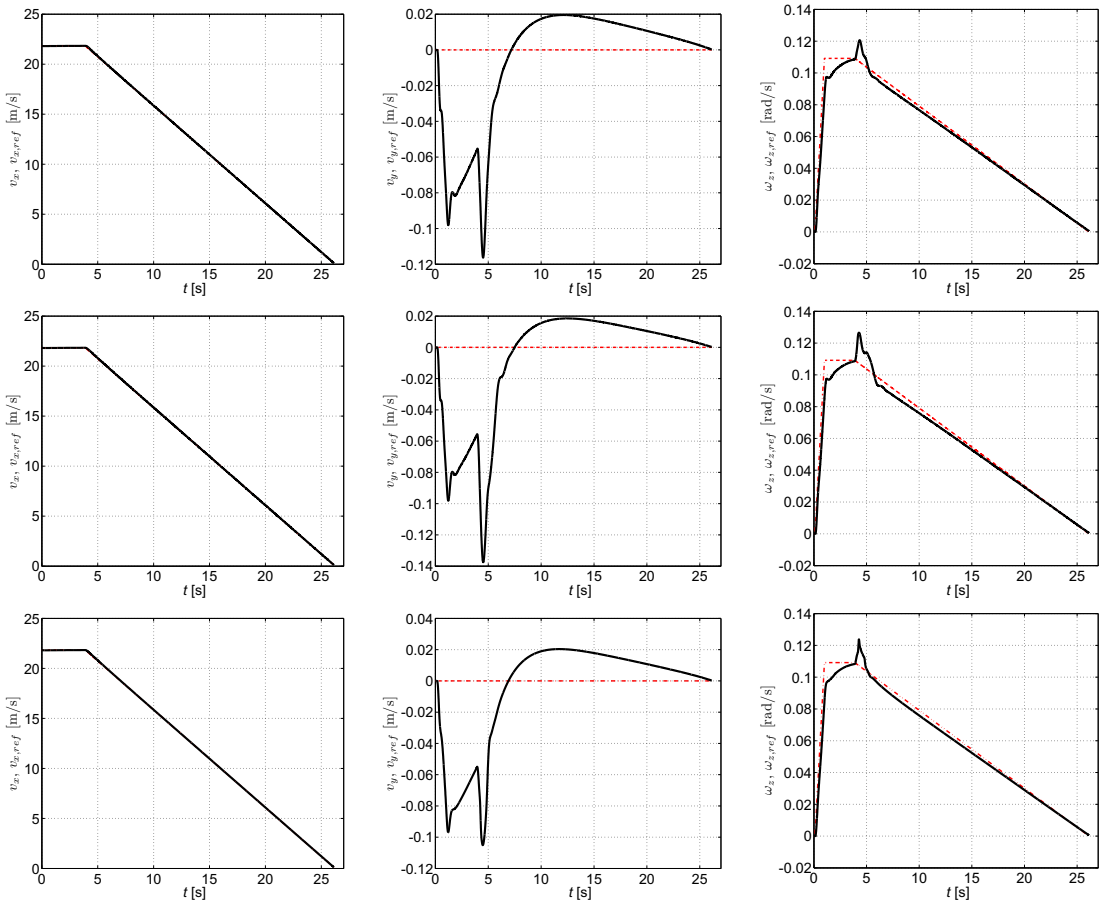

Figure 21: Longitudinal v_x, lateral v_y, and yaw ω_z velocity for configuration CV (top), HEV E4WD (middle), and HEV WM (bottom) respectively during test procedure 2.

expected. The steering angle was also limited by the tyre fusion. This was done by checking how much maximum lateral force could be applied on either tyre on each axle, see also actuators 6 and 7 for configuration CV in Fig. 5.3, actuators 8 and 9 for configuration HEV E4WD in Fig. 5.3, and finally actuators 9 and 10 for configuration HEV WM in Fig. 5.3.

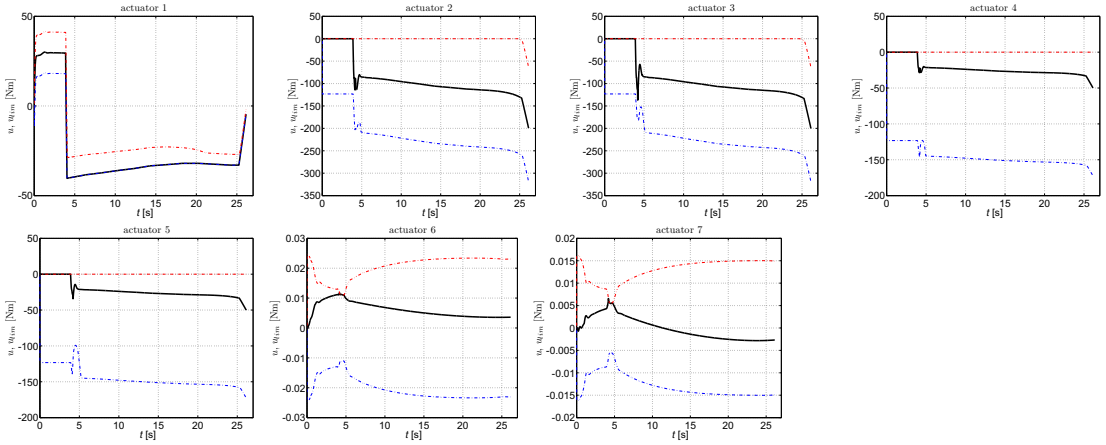

Figure 22: Input set u and its limits for configuration CV during test procedure 2.

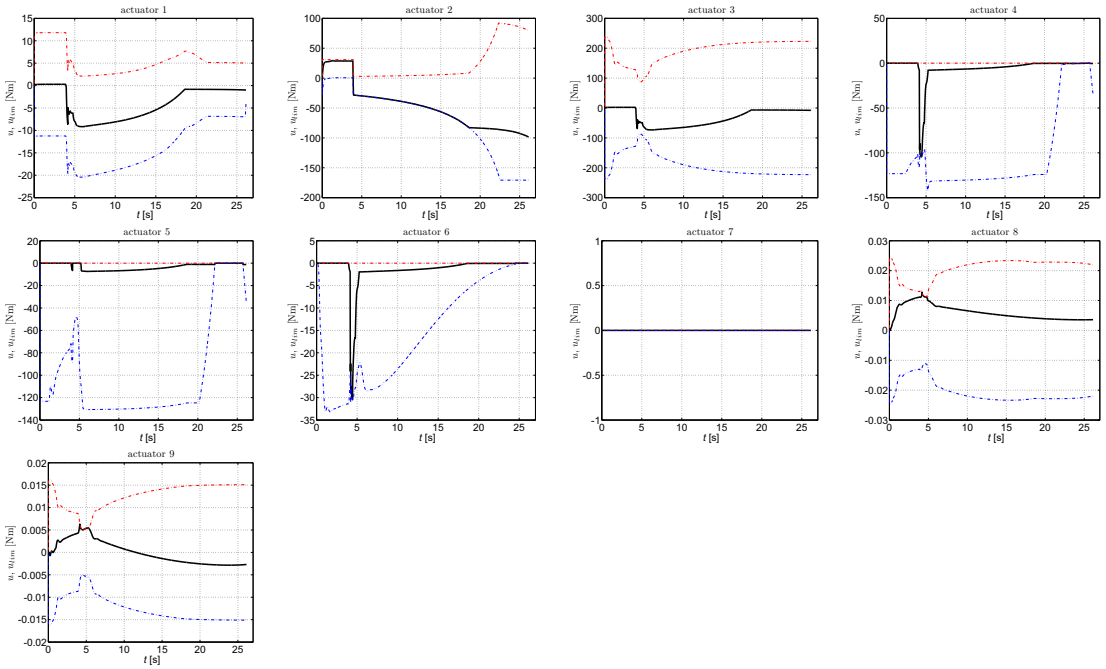

Figure 23: Input set u and its limits for configuration HEV E4WD during test procedure 2.

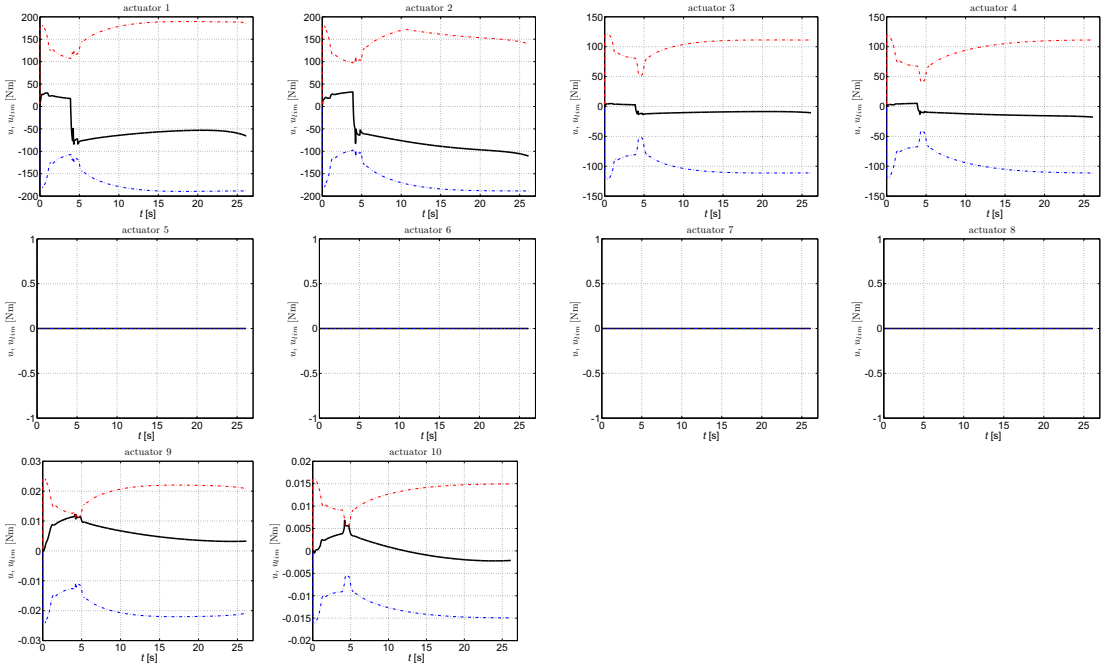

Figure 24: Input set u and its limits for configuration HEV WM during test procedure 2.

6 Conclusions

The vehicle model presented in this paper has been used for the evaluation of a control system architecture. It is quite simple but detailed enough for the intended purpose. The presented model is a so-called two track model and has five degree of freedom: longitudinal-, lateral-, yaw-, roll-, and pitch motion. Additional degrees of freedom have been added by including the driveline and the motion related actuators. A novel suggestion is also given for how the torque limits of an permanent magnet synchronous motor depend both on mechanical speed and temperature.

Furthermore, the separation of control law and control allocation makes the control system reusable for different vehicle configurations. This was shown here where the same controller was used for three different vehicle configurations. This leads to the possibility of developing a wide range of configurations without the need to redesign the control system for each one. The weighted least square control allocation algorithm developed by [4] also works excellently for brake blending in hybrid electric vehicles. Additionally, algorithm is also fast which would easily allow real time implementation in vehicles.

The simulations not only showed that brake blending is automatically performed but also that vehicle stability is automatically included in the global optimization problem formulation of the control allocator. Another interesting observation was that it is important to consider how the brake load distribution on the front and rear axles is made for the electric motors. During electrical braking the load distribution should be more on the front than the rear, as it is usually set for mechanical brakes. The load distribution can be tuned by the weight matrix W_u. Actuator limits and rates together with the suggested tyre fusion algorithm provides sufficient information to make the correct coordination of the available actuators for different braking situations.

References

[1] A. T. van Zanten, "Bosch esp systems: 5 years of experience," *SAE 2000-01-1633*, 2000.

[2] E. K. Liebemann, K. Meder, J. Schuh, and G. Nenninger, "Safety and performance enhancement: The bosch electronic stability control (esp)," *SAE 2004-21-0060*, 2004.

[3] Auto Motor und Sport, "http://www.auto-motor-und-sport.de/," 2006.

[4] O. Härkegård, "Backstepping and control allocation with applications to flight control," Ph.D. dissertation, Department of Electrical Engineering, Linköping University, SE–581 83 Linköping, Sweden, May 2003.

[5] T. Johansen, T. Fossen, and S. P. Berge, "Constrained nonlinear control allocation with singularity avoidance using sequential quadratic programming," *IEEE Transactions on Control Systems Technology, vol. 12, no. 1*, 2004.

[6] T. Johansen, T. Fuglseth, P. Tøndel, and T. I. Fossen, "Optimal constrained control allocation in marine surface vessels with rudders," in *IFAC Conf. Manoeuvring and Control of Marine Craft*, Girona, 2003.

[7] P. Tøndel and T. A. Johansen, "Control allocation for yaw stabilization in automotive vehicles using multiparametric nonlinear programming," in *Proc. of American Control Conf.*, Portland, OR, June 2005.

[8] J. Plumlee, D. Bevly, and A. Hodel, "Control of a ground vehicle using quadratic programming based control allocation techniques," in *Proc. of American Control Conf.*, Boston, MA, July 2004.

[9] J. Plumlee, *Mult-Input Ground Vehicle Control Using Quadratic Programming Based Control Allocation.* Master thesis report, Auburn University, Alabama, 2004.

[10] AUTomotive Open System ARchitecture(AUTOSAR), "http://www.autosar.org/," 2004.

[11] B. Hardung, T. Kölzow, and A. Krüger, "Reuse of software in distributed embedded automotive systems," *Fourth ACM International Conference on Embedded Software (EMSOFT 2004), PISA, Italy*, 2004.

[12] L. Laine, *On Vehicle System Control Architecture for Fuel Cell- and Hybrid Electric Vehicles.* Licentiate thesis, Department of Applied Mechanics, Chalmers University of Technology, Sweden, 2005.

[13] J. Andreasson, L. Laine, and J. Fredriksson, "Evaluation of a generic vehicle motion control architecture," in *The Fédération Internationale des Sociétés d'Ingénieurs des Techniques de l'Automobile (FISITA)*, Barcelona, Spain, May 2004.

[14] J. Fredriksson, J. Andreasson, and L. Laine, "Wheel force distribution for improved handling in a hybrid electric vehicle using nonlinear control," in *Proceedings of 43rd IEEE Conference on Decision and Control*, Bahamas, December 2004.

[15] SAE, "Surface vehicle recommended practice, vehicle dynamics terminology," *SAE 1976-07, J670e*, 1976.

[16] H. B. Pacejka, *Tyre And Vehicle Dynamics 2^{nd} edition.* Butterworth-Heinemann, 2002.

[17] A. Serrarens, *Coordinated control of the Zero Inertia Powertrain.* Technische Universiteit Eindhoven, 2001.

[18] B. Lennartson, *Reglerteknikens grunder.* Studentlitteratur, 2001.

[19] S. Eppler and T. Klenk, "Thermal simulation within the brake system design process," *SAE Transactions, paper 2002-01-2587*, 2002.

[20] J. P. Holman, *Heat Transfer 8^{nd} edition.* McGraw-Hill, Inc., 1997.

[21] H. Khalil, *Nonlinear Systems, 3^{rd} edition.* Prentice Hall Inc., 2002.

[22] K. Åström and T. Hägglund, *PID Controllers: Theory, Design, and Tuning*. Instrument Society of America, 1995.

[23] QCAT, "Quadratic programming control allocation toolbox for matlab," http://www.control.isy.liu.se/ ola/qcat/doc/, 2005.

[24] A. Norelius, *FKB CV BRAKE PERFOMANCE (confidential)*. Volvo Car Corporation, 2005.

Appendices

A Parameters

Table 1: Parameters used for the chassis model including brush tyre.

Parameter	value
Curb weight (full tank, no driver or pass.) m (kg)	1675
Moment of inertia, around CoG I_{xx} (kgm^2)	540
Moment of inertia, around CoG I_{yy} (kgm^2)	2398
Moment of inertia, around CoG I_{zz} (kgm^2)	2617
Wheel base L (m)	2.675
Distance along X-axis from CoG to front axle L_f (m)	$0.4L$
Distance along X-axis from CoG to rear axle L_r (m)	$L - L_f$
Distance along Z-axis from front axle to CoG h (m)	0.227
Track width front wheels b_f (m)	1.517
Track width rear wheels b_r (m)	1.505
Pitch centre height above ground h_p (m)	0.149
Front roll centre height above ground $h_{r,f}$ (m)	$4.49{\cdot}10^{-3}$
Rear roll centre height above ground $h_{r,r}$ (m)	0.110
Front area A_f (m^2)	2.17
Air drag coefficient C_d (-)	0.3
Front roll stiffness $K_{\phi_{x,f}}$ (Nm/rad)	$7.0896{\cdot}10^4$
Front roll damping $D_{\phi_{x,f}}$ (Nms/rad)	$8.0545{\cdot}10^3$
Rear roll stiffness $K_{\phi_{x,r}}$ (Nm/rad)	$6.7732{\cdot}10^4$
Rear roll damping $D_{\phi_{x,r}}$ (Nms/rad)	$8.1541{\cdot}10^3$
Pitch stiffness K_{ϕ_y} (Nm/rad)	$2.2457{\cdot}10^5$
Pitch damping D_{ϕ_y} (Nms/rad)	$2.6562{\cdot}10^4$
Tyre lag to longitudinal force build up L_x (m)	0.18
Tyre lag to lateral force build up L_y (m)	1.89
Half contact length @ Fz0=3000 N a_0 (m)	0.1
Brush stiffness $c_p = 60e3/\left(2 \cdot 0.1^2\right)$ (N/(m^{2}rad))	$3{\cdot}10^6$

Table 2: Parameters used for the three different drive line configurations.

Parameter	value
Frictional losses combustion eng. d_c (Nms)	0.001
Comb. eng. inertia with/without flywheel J_c (kgm^2)	0.244/0.06
Frictional losses ISG d_{isg} (Nms)	0.001
ISG inertia J_{isg} (kgm^2)	0.085
Transmission gear ratio's r_i, (-)	4.7, 3, 2, 1.3, 1
Transmission inertia J_{tr} (kgm^2)	0.04
Transmission losses d_{tr} (Nms)	0.001
Final gear ratio, front r_{fgf} (-)	2.44
Final gear + differential inertia J_{fgf} (kgm^2)	0.033
Differential gear ratio, front r_{diff} (-)	1
Drive shaft stiffness k_{ds} (Nm/rad)	1200
Drive shaft damping d_{ds} (Nms/rad)	400
Final gear ratio, rear r_{fgr} (-)	2.44
Final gear + differential inertia J_{fgr} (kgm^2)	0.033
Frictional losses E4WD d_{e4wd} (Nms)	0.001
E4WD inertia J_{e4wd} (kgm^2)	0.02
Final gear ratio, wheel motor r_{wm} (-)	2.44
Frictional losses wheel motor d_{wm} (Nms)	0.001
Wheel motor inertia J_{wm} (kgm^2)	0.05
Wheel radius R_w (m)	0.3

Table 3: Used parameters for PMSM model.

Parameter	value
PMSM type	ISG / E4WD / wheel motor
Time constant t_m, (s)	0.056 / 0.096 / 0.078
Max/min torque (2 min) $T_{m,lim}$, (Nm)	±178 / ±305 / ±250
Max/min torque (cont.) $T_{mc,lim}$, (Nm)	±67 / ±130 / ±100
Max/min power(2 min) $P_{m,lim}$, (kW)	±11 / ±50 / ±40
Max/min power (cont.) $P_{mc,lim}$, (kW)	±5 / ±32 / ±20
Temperature thresholds T_h T_l, (^{o}C)	200, 100
Motor system mass m, (kg)	11 50 40
Capacity mass m_m, (kg)	1.4 6.3 5
Convection area $A_{m,conv}$ (m^2)	0.02 / 0.06 / 0.05
Radiation area $A_{m,rad}$ (m^2)	0.02 / 0.06 / 0.05
Average sp. heat capacity cp_m (J/(kgK))	430
Conductivity k_{cond} (W/(mK))	57
Conduction length (est.) l (m)	0.03 / 0.25 / 0.1
Forced air convection h_v (W/(m^{2}K)	$7.8v^{0.78}$
Emissivity e (-)	0.6
Stefan-Boltzmann's c. σ (W/(m^{2}K^4))	5.669e-8
Max/min torque rate$\frac{dT_{bi}}{dt}$ (Nm/s)	2000, -2000

Table 4: Parameters for a passenger car hydraulic disc brake model.

Parameter	value	
Time constant t_b	(s)	0.1
Asymptotic pressure p_{asym}	(MPa)	15
Hydraulic piston diam. d_p and area A_p	(m), (m^2)	0.0513, 0.021
Disc outer D_o and inner D_i diameter	(m), (m)	0.282, 0.13
Radius for braking torque r_b	(m)	0.103
Disc thickness td	(m)	0.011
Disc density ρ_d	(kg/m^3)	7849
Specific heat capacity of disc cp_d	(J/(kgK))	465
Conductivity at 100 ^{o}C k_{cond}	(W/(mK))	57
Conduction length l	(m)	0.1
Convection from disc α_{conv}	($W/(m^2K)$	60
Convection area from disc A_{conv}	(m^2)	0.0363
Radiation area from disc A_{rad}	(m^2)	0.0363
Emissivity e	(-)	0.5
Stefan-Boltzmann's constant σ	($W/(m^2K^4)$)	5.669e-8

Table 5: Used parameters for buffer model.

Parameter	value
Buffer for	conf. 2 / conf. 3
Capacity C, (Ah)	6.5 / 6.5
Nominal voltage u_b, (V)	250 / 500
mass of buffer m_b, (kg)	41 / 90
Power density during discharge $P_{den,dis}$, (W/kg)	1500 / 1500
Power density during charge $P_{den,char}$, (W/kg)	1500 / 1500

Paper V

Traction and braking of hybrid electric vehicles using control allocation

in

Tech. Report R012/2007, Department of Signals and Systems, Chalmers University of Technology, Göteborg, Sweden, 2007. A shorter version is also accepted (under revision) to *Int. Journal of Vehicle Design, Special Issue on: Advanced Traction/Braking Vehicle Control*.

Traction and Braking of Hybrid Electric Vehicles using Control Allocation

Leo Laine* and Jonas Fredriksson

Department of Applied Mechanics* and Department of Signals and Systems,
Chalmers University of Technology SE-412 96 Göteborg, Sweden
E-mail: leo.laine@chalmers.se and jonas.fredriksson@chalmers.se
* corresponding author

Abstract

This paper considers how ground vehicles such as hybrid electric vehicles can be controlled when traction, braking and steering are considered. When several different actuators are combined the desired motion can be performed in several ways. Here, a reusable control structure is suggested which includes a reusable control law for longitudinal, lateral, and yaw motion and a control distributor which distributes the desired control signals on the available actuators. By separating the control law and control distribution a wide range of vehicle configurations can use the same control system. The control distribution is designed using a technique called control allocation. The control allocator also handles performance limits which combine the limits of the tyres and the actuators. The same motion controller has been used for three different vehicle configurations. The proposed control system not only works as a traction and braking controller, it also works as a vehicle stability controller. Furthermore, the controller is easy to tune. These findings have been confirmed by simulations.

Keywords: Traction, Hybrid Electric Vehicles, Control Allocation.

1 Introduction

The introduction of Hybrid Electric Vehicles (HEV) into the market on a larger scale opens up the potential for a wide range of vehicle configurations, e.g. conventional vehicles, series hybrid electric vehicles, and parallel hybrid electric vehicle. The development of HEV technology has made it so that vehicles have different possibilities for making tractive and/or braking forces. In order to generate the desired force, the actuators (the combustion engine, electric motor(s), and mechanical brakes) need to be coordinated. For example, tractive force could be generated with the combustion engine and electric motor(s) in combination. The braking force could be achieved with the electric motor(s)in

combination with the mechanical brakes. This paper deals with the efficient coordination of several actuators for vehicle traction, braking, and steering.

To allow for a broad range of vehicle configurations to be produced without major costs related to the control system development it is highly desirable to have standardized interface signals, [1], and reusable controllers, [2]. This is of special importance for hybrid vehicles where, as mentioned earlier, a number of configurations can be considered. To handle this efficiently a hierarchical control architecture is preferable. In [3], a vehicle control system architecture for fuel cell- and hybrid electric vehicles is proposed. The system architecture is generic in the sense that the information flow structure allows for the adding and removing of components. The control architecture is derived from functional decomposition and is configured in a modular fashion, see Fig. 1.

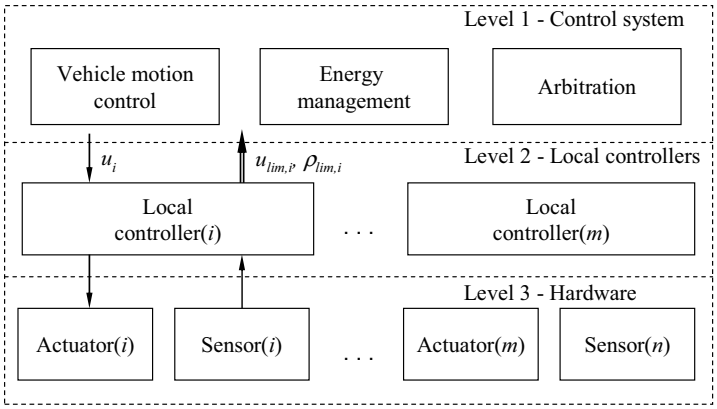

Figure 1: Illustration of functional levels within a vehicle system controller.

The highest functional level includes the overall functionality and decision making to generate the vehicle motion such as the vehicle motion controller and energy management. The vehicle motion controller is a short time horizon controller that tries to keep the desired vehicle course. Energy management is more of a long time horizon controller for how the on board energy sources should be used when considering the vehicle states and the environment. Functional level 2 includes the local controllers for different functions, for example, a local controller for an electric motor. Here in this paper it is shown how the interface signals between level 1 and level 2 should formed in order to design a vehicle controller considering both vehicle motion control and energy management. Fig. 1 illustrates this in that the local controller i is sending the limits u_{lim} and the rate of change limits ρ_{lim} to functional level 1. The third level is what could be called an advanced actuator/sensor level (hardware level). The general idea is that the highest level should remain unchanged no matter how the vehicle is configured.

Figure 2 illustrates how the control system and vehicle system are configured. The control system is comparable to functional level 1 in Fig. 1 and the system refers to levels 2 and 3. Observe how the control system is split into two parts. The reason for this is that the control law only tells the net effort that needs to be produced but not how it can be produced with the available actuator configuration within the system. This is solved by the control distributor or

control allocator. If the mapping is successful then the system generates the net effort $v_{sys} = v$.

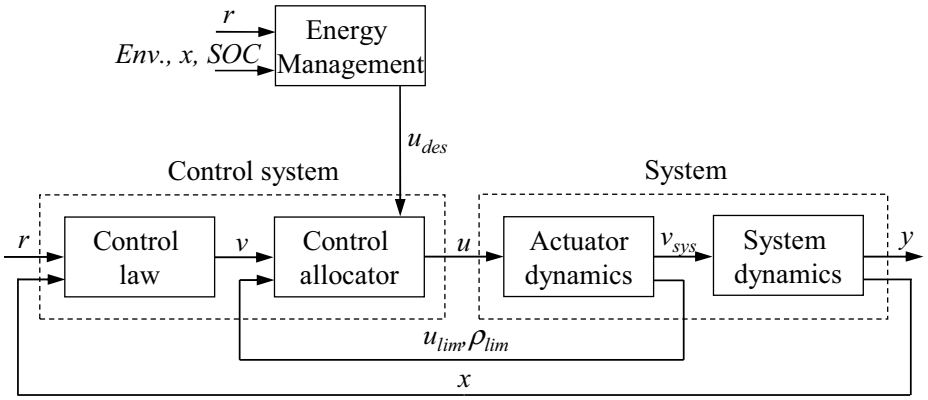

Figure 2: Control system structure when control allocation is used.

Systems which have more motion actuators than motions controlled are called overactuated systems. Overactuated systems are common in application areas such as flight and marine vessels, but also in automotive systems. Flight systems are often configured as overactuated systems which allow several possible input sets for the actuators to achieve the desired motion. One promising way to solve the coordination of overactuated systems in automotive applications is to use control allocation. Control allocation has been successfully used within flight applications, see [4]. It has also been used within marine vessels, see [5] and [6]. For ground vehicles, control allocation has been used for yaw stabilization, see [7], [8] and [9]. In these articles the mechanical brakes and steering were in focus, however no detailed considerations of the actuator limits were shown.

In this paper a reusable control law is set up for the longitudinal, lateral, and yaw-motions of a ground vehicle. Control allocation is used to distribute the task of generating the desired motion on the available actuators. The studied vehicle systems, a conventional car, a parallel hybrid vehicle with two electric motors, and a series hybrid vehicle with wheel motors, are modelled to include the main time constants of a vehicle when generating the desired motion and the actuators include models of the internal states that affect its performance, i.e. their limits and rate of change of limits. For an electric motor these internal states are the angular velocity of the drive shaft and the temperature of the windings.

The outline of the paper is as follows: Section 2 gives an introduction to control allocation, a technique which has been used in the paper. Section 3 outlines the models and vehicle configurations studied in the paper. In Section 4 the control design is presented in detail in addition to how the control allocator was set up with the limits of the actuators. In Section 5 simulations of different traction and braking situations are presented to show how the control system functions. Section 6 concludes the findings.

2 Control Allocation

In linear control theory there exists a wide range of methods which can handle overactuated systems, like LQ- and $\mathcal{H}_\infty$-control. Unfortunately, most of these methods can not handle actuator saturations and/or constraints efficiently. As mentioned earlier control allocation is an option for coordination when one has more input signals going into the system than the number of output states. Control allocation is attractive since it can handle actuator constraints, no reconfiguration is necessary if the effectiveness of the actuators changes over time and the actuator utilization can be treated independently, [4]. Control allocation can be applied to a class of linear and nonlinear systems. If it can be applied, the control design can be divided into two steps. The first step is to design a control law determining the net control effort. The second step is mapping the net control demand onto the individual actuators.

Control allocation is an option for coordination when one has more input signals $u \in R^m$ to the system than the number of output states $y \in R^k, k < m$. An optimization objective is used to select the input set vector u of the available actuators. Limits of the input vector u_{lim} reduce the possible combinations of the input vector u. Using control allocation allows for reconfiguration, so that the same control system can be used for different hardware configurations. It also makes it so that the control system can easily handle actuator failure.

Independent of the specific application studied, a class of nonlinear systems can be described in the affine form

$$\dot{x} = f(x) + g(x)\,u \tag{2.1}$$
$$y = h(x) \tag{2.2}$$

If the studied nonlinear system can be written in this affine form and certain conditions are fulfilled the control system design can be divided into two steps.

The first step is to design a control law that controls the net effort $v \in R^k$ to be produced for the nonlinear system

$$\dot{x} = f(x) + v(t) \tag{2.3}$$
$$y = h(x) \tag{2.4}$$

where $v(t) = g(x)u$ is also called the virtual control input. The second step is to design a control allocator that maps the net effort of virtual control input to true control input u. For linear systems, the mapping can be described by a control effectiveness matrix $B(x)$ with size $k \times m$ and rank k

$$Bu(t) = v(t) \tag{2.5}$$

A key issue is how to select the control input set u from all possible combinations. In control allocation an optimization based selection is used. According to [4]

the optimal control input u can be seen as two-step optimization problem

$$u = \arg \underbrace{\min}_{u \in \Omega} \|W_u(u - u_{des})\|_p \tag{2.6}$$

$$\Omega = \arg \underbrace{\min}_{\underline{u} \leq u \leq \overline{u}} \|W_v(Bu - v)\|_p \tag{2.7}$$

where W_u and W_v are weighting matrices, and u_{des} is the desired control input. Numerically, Eqs. 2.6- 2.7 are solved in one step

$$u = \arg \underbrace{\min}_{\underline{u} \leq u \leq \overline{u}} \|W_u(u - u_{des})\|_p + \gamma \|W_v(Bu - v)\|_p. \tag{2.8}$$

The optimization problem is solved as weighted least square $p = 2$. Setting weighting parameter γ to a high value gives priority to minimizing the error $e = Bu - v$.

The possible limits of the input control are calculated by

$$\overline{u_i} = \min\left(\overline{u}_{i-1}, u_{i-1} + T\overline{\rho}_{i-1}\right) \tag{2.9}$$

$$\underline{u_i} = \max\left(\underline{u}_{i-1}, u_{i-1} + T\underline{\rho}_{i-1}\right) \tag{2.10}$$

where ρ is the limits in the rate of change of the control input signal and T is the fixed time step for the control allocator.

3 System Modelling

Three different vehicle configurations are considered in the paper, a conventional configuration, a parallel HEV with electric four wheel drive and a series HEV with wheel motors. The three studied vehicle configurations are modelled with a focus on including both the necessary dynamics of the system and the most important system specific time constants.

The chassis model is the same for all three vehicles. It is a so-called two track model and has five degree of freedom: longitudinal-, lateral-, yaw-, roll-, and pitch motion. The model aims at being capable of predicting the chassis dynamics on a flat surface. The SAE standard [10] has provided the main guidance for defining the axis orientations. A brush tyre model [11] is used together with dynamic relaxation to describe the tyre dynamics. The chassis used for all three configurations is comparable to a commercial medium sized sedan car. Details about modelling and used chassis parameters can be found in [12].

The driveline includes weak drive shafts, inertias, and losses open differentials for two of the configurations. The mechanical brakes and electric motors are modelled as first order systems with a lumped mass model describing the internal temperature of the actuators. The temperature will directly affect the limits of the actuators. The combustion engine is modelled as a second order system [13].

The limits of the electric motor, combustion engine, and mechanical brakes are illustrated in Eq.4.1.

$$\begin{aligned} \underline{u}_{\mathrm{el},i}(\omega_i, T_i) \leq u_{\mathrm{el},i} \leq \overline{u}_{\mathrm{el},i}(\omega_i, T_i) \\ \underline{u}_{\mathrm{ice}}(\omega) \leq u_{\mathrm{ice},i} \leq \overline{u}_{\mathrm{ice}}(\omega) \\ \underline{u}_{\mathrm{mech},i}(T_i) \leq u_{\mathrm{mech},i} \leq \overline{u}_{\mathrm{mech},i}(T_i) \end{aligned} \tag{3.1}$$

where ω_i and T_i are the angular velocity and temperature of the actuator.

By combining together the modelled components and the chassis, the three different vehicle configurations can be configured. These three vehicle models represent and simulate the system in Fig. 2. A detailed description of the system modelling is found in [12], where all parameters are also specified. The models are implemented as first level s-functions in the Matlab/Simulink environment. A summary of the vehicles is presented below:

i. *Conventional vehicle (CV).* The combustion engine has 133 kW at 6000 rpm as the maximum output power and a maximum torque of 230 Nm. It is connected to the front wheels via an open differential (1 input). Conventional vehicles usually have a pre-determined mechanical brake distribution between the front and rear axles, however when a dynamical limit of e.g. yaw is exceeded then individual braking is allowed. This model is seen as individual mechanical braking (4-input) which gives a total of 5 inputs to control the traction and braking.

ii. *Parallel HEV with electric four wheel drive (HEV E4WD).* Every wheel has individual mechanical braking (4-inputs), the rear axle has an electric motor of 50 kW connected by a differential (1-input). The front wheels are connected to a powertrain which includes an Integrated Starter Generator (ISG) of 11 kW located between the gear box and the combustion engine, same as CV (2-input). This model is seen as a 7-input configuration.

iii. *Series HEV with wheel motors (HEV WM).* Each wheel has individual mechanical braking (4-inputs) and is also equipped with wheel motors of 40 kW (4-inputs). This model is seen as an 8-input configuration. An extra energy source such as a fuel cell is needed to allow a continuous output power of 30 kW. The continuous power is sufficient to overcome the resistance forces at a constant speed of 130 km/h. The total output power is 30 kW plus 135 kW when the buffer mass of 90 kg is selected.

If front and rear axle steering is included the total number inputs on each configuration is increased by two.

4 Control Design

The objective is to control the longitudinal-, lateral-, and yaw-motions of a ground vehicle. For control design purposes the vehicle system is rewritten in

the affine form

$$\dot{x} = f(x) + g(x)\,u \tag{4.1}$$
$$y = h(x) \tag{4.2}$$

This can be accomplished by selecting following states $x = \begin{bmatrix} v_x & v_y & \dot{\phi}_z \end{bmatrix}^T$. The roll and pitch motion are seen as secondary effects for generating the desired motion on a flat surface and are thus neglected.

The lateral slip, α_i, can be separated into two parts, one due to the steering angle and one due the to vehicle states as

$$\alpha_1 = \delta_1 - \frac{x_2 + L_f x_3}{x_1 + \frac{b_f}{2} x_3} \tag{4.3}$$
$$\alpha_2 = \delta_2 - \frac{x_2 + L_f x_3}{x_1 - \frac{b_f}{2} x_3} \tag{4.4}$$
$$\alpha_3 = \delta_3 - \frac{x_2 - L_r x_3}{x_1 + \frac{b_r}{2} x_3} \tag{4.5}$$
$$\alpha_4 = \delta_4 - \frac{x_2 - L_r x_3}{x_1 - \frac{b_r}{2} x_3} \tag{4.6}$$

where L_f and L_r are the distances from the front and rear axles to centre of gravity, resectively. If small angles are assumed the lateral force, $F_{y,i}$, can be calculated as

$$F_{y,i} = C_{\alpha,i}\alpha_i \tag{4.7}$$

where $C_{\alpha,i}$ is the cornering stiffness for tyre i. This separation means that the lateral tyre force can be written as a sum of lateral forces due to steering angle, $F_{y,i}(\delta)$, and vehicle states, $F_{y,i}(x)$.

$$F_{y,i} = F_{y,i}(\delta) + F_{y,i}(x) \tag{4.8}$$

By using Eqs. 4.7-4.8 in combination with Eqs. 4.3-4.6 where the track width in the front and rear is assumed to be equal $b_t = b_f = b_r$ and all four wheels are assumed to be equal, i.e. the cornering stiffness is equal for all four wheels, $C_\alpha = C_{\alpha,i}$, and the radius is also equal, $R_w = R_{w,i}$, the chassis system can be written as

$$M\dot{x} = f(x) + g(x)u \tag{4.9}$$
$$y = h(x) \tag{4.10}$$

where M is the mass matrix

$$M = \begin{bmatrix} m & 0 & 0 \\ 0 & m & 0 \\ 0 & 0 & I_z \end{bmatrix}$$

and

$$f(x) = \begin{bmatrix} mx_2x_3 - D_1x_1 - D_2m\text{sgn}(x_1)x_1^2 \\ -mx_1x_3 - C_\alpha \frac{8x_1(2x_2+(L_f-L_r)x_3)}{4x_1^2-b_t^2x_3^2} \\ -L_fC_\alpha \frac{8x_1(2x_2+L_fx_3)}{4x_1^2-b_tx_3^2} + L_rC_\alpha \frac{8x_1(2x_2-L_rx_3)}{4x_1^2-b_tx_3^2} \end{bmatrix} \tag{4.11}$$

$$g(x)u = \begin{bmatrix} \sum_{i=1}^{4} F_{x,i} \\ C_\alpha \sum_{i=1}^{4} \delta_i \\ L_fC_\alpha \sum_{i=1}^{2} \delta_i - L_rC_\alpha \sum_{i=3}^{4} \delta_i + \frac{B_t}{2} \sum_{i=3}^{4} (-1)^{1+i} F_{x,i} \end{bmatrix} \tag{4.12}$$

$$h(x) = \begin{bmatrix} x_1 & x_2 & x_3 \end{bmatrix}^T \tag{4.13}$$

where D_1 and D_2 are constants related to aerodynamical and rolling resistance. Since the mass matrix is invertible, the system can be written in affine form. Furthermore, the vehicle system model presented is general and independent of the three configurations. The next step is to incorporate the powertrain configurations.

Looking at $g(x)u$ it is seen that it can be written as a constant matrix times the control signal, Bu. The B matrix is often called the *control effectiveness matrix*. For the three configurations the following control input signals exists:

$$u_{c_1} = \begin{bmatrix} \tau_{ice} & \tau_{mb_1} & \tau_{mb_2} & \tau_{mb_3} & \tau_{mb_4} & \delta_f & \delta_r \end{bmatrix}^T \tag{4.14}$$

$$u_{c_2} = \begin{bmatrix} \tau_{ice} & \tau_{isg} & \tau_{ram} & \tau_{mb_1} & \tau_{mb_2} & \tau_{mb_3} & \tau_{mb_4} & \delta_f & \delta_r \end{bmatrix}^T \tag{4.15}$$

$$u_{c_3} = \begin{bmatrix} \tau_{wm_1} & \tau_{wm_2} & \tau_{wm_3} & \tau_{wm_4} & \tau_{mb_1} & \tau_{mb_2} & \tau_{mb_3} & \tau_{mb_4} & \delta_f & \delta_r \end{bmatrix}^T \tag{4.16}$$

where τ_i is the torque from the traction and braking actuators and $\delta_{f,r}$ are the steering angles for the front ($\delta_f = \delta_1 = \delta_2$) and rear axle ($\delta_r = \delta_3 = \delta_4$). By including the steering in the control allocator the different configurations can be objectively examined. Today's cars usually have conventional steering (rack steer) where the driver is solely managing the steering by a mechanical link from the steering wheel to the wheels. The steering angles were set equal for the front and rear axle in order to emulate rack steering. The Ackermann angle is neglected. If conventional steering is used within the simulation this would delete the last two elements in the control signal vector, u_{c_i}, and also the corresponding columns in the control effectiveness matrix.

If the motion related actuators and the driveline are added to the system model, the control effectiveness matrix is unfortunately not constant any longer, in fact it includes dynamics. However, if no inertia effects in the driveline or wheels, no weak drive shafts, no losses, and no time delays or nonlinearities in developing tyre forces are assumed, a constant control effectiveness matrices can be formulated. The assumptions are realistic for the control design phase, i.e. the actuators are assumed to be fast. The control effectiveness matrices for the

three cases become:

$$B_1 = \begin{bmatrix} \frac{r_j r_{fgf}}{R_w} & \frac{1}{R_w} & \frac{1}{R_w} & \frac{1}{R_w} & \frac{1}{R_w} & 0 & 0 \\ 0 & 0 & 0 & 0 & 0 & 2C_\alpha & 2C_\alpha \\ 0 & \frac{b_t}{2R_w} & \frac{-b_t}{2R_w} & \frac{b_t}{2R_w} & \frac{-b_t}{2R_w} & 2L_f C_\alpha & -2L_r C_\alpha \end{bmatrix} \tag{4.17}$$

$$B_2 = \begin{bmatrix} \frac{r_j r_{fgf}}{R_w} & \frac{r_j r_{fgf}}{R_w} & \frac{r_{fgr}}{R_w} & \frac{1}{R_w} & \frac{1}{R_w} & \frac{1}{R_w} & \frac{1}{R_w} & 0 & 0 \\ 0 & 0 & 0 & 0 & 0 & 0 & 0 & 2C_\alpha & 2C_\alpha \\ 0 & 0 & 0 & \frac{b_t}{2R_w} & \frac{-b_t}{2R_w} & \frac{b_t}{2R_w} & \frac{-b_t}{2R_w} & 2L_f C_\alpha & -2L_r C_\alpha \end{bmatrix} \tag{4.18}$$

$$B_3 = \begin{bmatrix} \frac{r_{fg}}{R_w} & \frac{r_{fg}}{R_w} & \frac{r_{fg}}{R_w} & \frac{r_{fg}}{R_w} & \frac{1}{R_w} & \frac{1}{R_w} & \frac{1}{R_w} & \frac{1}{R_w} & 0 & 0 \\ 0 & 0 & 0 & 0 & 0 & 0 & 0 & 0 & 2C_\alpha & 2C_\alpha \\ \frac{r_{fg} b_t}{2R_w} & \frac{-r_{fg} b_t}{2R_w} & \frac{r_{fg} b_t}{2R_w} & \frac{-r_{fg} b_t}{2R_w} & \frac{b_t}{2R_w} & \frac{-b_t}{2R_w} & \frac{b_t}{2R_w} & \frac{-b_t}{2R_w} & 2L_f C_\alpha & -2L_r C_\alpha \end{bmatrix} \tag{4.19}$$

where r_{fgf} is the final gear front, r_{fgr} is the final gear rear, R_w is the wheel radius, b_t is the track width, and r_j is the discrete ratio of the selected gear j. The gear selection is vehicle state based as

$$j = \begin{cases} 1 \text{ if } v_x \leq \frac{45}{3.6} \\ 2 \text{ elseif } \frac{45}{3.6} < v_x \leq \frac{90}{3.6} \\ 3 \text{ elseif } \frac{90}{3.6} < v_x \leq \frac{120}{3.6} \\ 4 \text{ elseif } \frac{120}{3.6} < v_x \leq \frac{160}{3.6} \\ 5 \text{ else.} \end{cases} \tag{4.20}$$

where v_x is the vehicle's longitudinal velocity. The gear selection function is designed to be aggressive driving. A more sophisticated gear selection function which also consdirers the drivers desire to accelerate could easily be implemented and used. To account for the fact that some actuators are unable to perform during a gear shift due to an open clutch the cost effectiveness matrices were modified so that all cells including r_j are set to 0 during gear shifting. This was done for a preset gear shifting time of 0.3 s.

Looking at the vehicle system it can easily be seen that the system is over-actuated, it contains three control objectives and has 7, 9 or 10 input signals depending on the vehicle configuration. This allows us to separate the control law for keeping the desired path of the vehicle from the control allocation of the specific motion actuators. The virtual control input is set equal to the global vehicle forces acting in the centre of gravity of the vehicle, $v = \begin{bmatrix} F_x & F_y & M_z \end{bmatrix}^T$.

The matrices, Eqs. 4.17-4.19, describe the three configurations and their ability to generate the global vehicle forces $v(t) = \begin{bmatrix} F_x & F_y & M_z \end{bmatrix}^T$. Observe how the yaw moment M_z can only be applied by the mechanical brakes and steering for configurations 1 and 2. This due the fact that open differentials are used in the drive line in these configurations. This results in that traction actuators such as the combustion engine, ISG, and E4WD motors cannot be used for gaining M_z.

4.1 Control Law

First step in designing the control system is to design the control law as illustrated in Fig. 2. The purpose of the controller, as mentioned earlier in the paper, is to follow a desired trajectory. The controller is based on feedback linearization, see e.g. [14]. The idea with feedback linearization is to transform the nonlinear system into a linear one, so that linear techniques can be used. In its simplest form it can be seen as a way to cancel the nonlinearities by a nonlinear state feedback. Looking at the system, we notice that the first term on the right hand side of (4.9) is the only one including the nonlinearities of the system. If the nonlinear term, $f(x)$, is cancelled, the multi-input, multi-output (MIMO)-system becomes linear. Furthermore, by cancelling $f(x)$ the MIMO-system becomes decoupled. Then, using a PI-controller, the control law becomes:

$$v = -f(x) + K_p e + K_i \int_0^t e d\tau \tag{4.21}$$

where e is the error between the desired vehicle motion and the vehicles actual motion. The design parameters for the PI-controllers, K_p and K_i, are chosen as

$$K_i = 20 \begin{bmatrix} 0.2m & 0 & 0 \\ 0 & 0.7m & 0 \\ 0 & 0 & 1.5I_z \end{bmatrix} \tag{4.22}$$

$$K_p = \frac{2}{3} m \sqrt{K_i \begin{bmatrix} \frac{16}{m} & 0 & 0 \\ 0 & \frac{1}{m} & 0 \\ 0 & 0 & \frac{1}{I_z} \end{bmatrix}} \tag{4.23}$$

To handle the saturation of actuators the PI-controllers were extended with anti-windup based on back calculation [15]. When the actuators are not saturated the error $e_s = Bu - v$ will be zero and therefore there is no effect on the sum of integrator gain, see also Fig. 3. The windup was minimized with $\frac{1}{T_t} = 20 I_{3x3}$.

Figure 3 also shows how the combined actual limits of the actuators and the tyres are sent back to the control allocator.

4.2 Tyre Fusion

To really be able to know how much each actuator can contribute to the net tractive and braking force one has to also consider the actual limits of the tyre(s) to which the actuator(s) are connected. Firstly, each actuator has its own limits and rate change limits. Secondly, these limits need to be combined with the tyre limits. Each tyre's longitudinal force limit $F_{xlim,i}(F_{z,i}, \mu_i, F_{y,i})$ is a function of the normal force $F_{z,i}$, tyre/road friction μ_i, and the amount of lateral force $F_{y,i}$ applied to the wheel. By estimating $F_{xlim,i}$ for each wheel the actuator limits are adjusted for what the tyres can actually handle. The function is here called *tyre fusion*, see also Fig. 3 for an illustration.

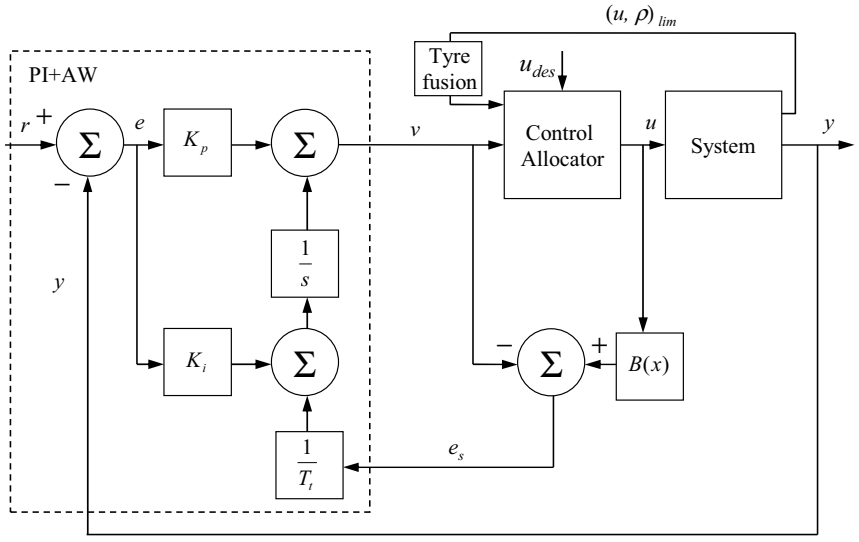

Figure 3: Layout of the control system with PI-controller, anti-windup, control allocation, and tyre fusion.

When several actuators are connected to the same wheel their limits need to be prioritized. During traction the electric motor(s) are given priority over the combustion engine if the combined traction force from the electric motor(s) and the combustion engine are larger than the tyre can handle. By using this priority the tyre fusion function basically checks if the electric motors torque limits, $\overline{u}_{el}$, are above the tyre's capacity, $\overline{F}_{x,i}$, and if so adjusts the limits to be equal to what the tyre can handle. During braking the electric motor(s) are given priority over the combustion engine and the disc brakes. By using this priority the tyre fusion function basically checks if the sum of electrical and disc brake torque limits are more than the tyre force limit. Then the mechanical brake limits are set as the difference of the tyre force and electrical limits. The idea is to always try to give the electric motors the possibility to act within the tyres limits. Some examples are presented below in Figs. 4-6.

The tyre fusion function for the case of an electric motor in combination with mechanical disc brakes can be written as

$$\overline{u}_{\mathrm{el},i} = \begin{cases} \overline{F}_{x,i} R_w, & \text{if } \overline{u}_{\mathrm{el},i} \geq \overline{F}_{x,i} R_w \\ \overline{u}_{el,i}, & \text{else} \end{cases} \tag{4.24}$$

$$\underline{u}_{\mathrm{el},i} = \begin{cases} -\overline{F}_{x,i} R_w, & \text{if } \underline{u}_{\mathrm{el},i} \leq -\overline{F}_{x,i} R_w \\ \underline{u}_{\mathrm{el},i}, & \text{else} \end{cases} \tag{4.25}$$

$$\tag{4.26}$$

$$\overline{u}_{\mathrm{mech},i} = 0 \tag{4.27}$$

$$\underline{u}_{\mathrm{mech},i} = \begin{cases} 0, & \text{if } \underline{u}_{\mathrm{el},i} \leq -\overline{F}_{x,i} R_w \\ -\overline{F}_{x,i} R_w - \underline{u}_{\mathrm{el},i}, & \text{elseif } (\underline{u}_{\mathrm{el},i} + \underline{u}_{\mathrm{mech},i}) \leq -\overline{F}_{x,i} R_w \\ \underline{u}_{\mathrm{mech},i}, & \text{else} \end{cases} \tag{4.28}$$

This corresponds to configuration 3, HEV WM. In Fig. 4 the force limit circles for two independent tyres on an "axle" are illustrated. The left wheel is assumed

to be on higher friction, which leads to a larger circle. The dashed line illustrates the actual lateral force of the wheel. Each wheel has two actuators connected, an electric motor with limits $\underline{\overline{u}}_{\text{el}}$ and a mechanical disc brake with limits $\underline{\overline{u}}_{\text{mech}}$. The left circle in Fig. 4 is larger than the limits $\underline{\overline{u}}_{\text{el}}$ but not larger than the sum of limits $\underline{\overline{u}}_{\text{el}} + \underline{\overline{u}}_{\text{mech}}$ and therefore the mechanical brake limits are additionally restricted. For the right wheel the available electric motor torque is larger than the wheel limits and thus is reduced to correspond to the wheel's limits. In this case the mechanical brake limits are set to zero.

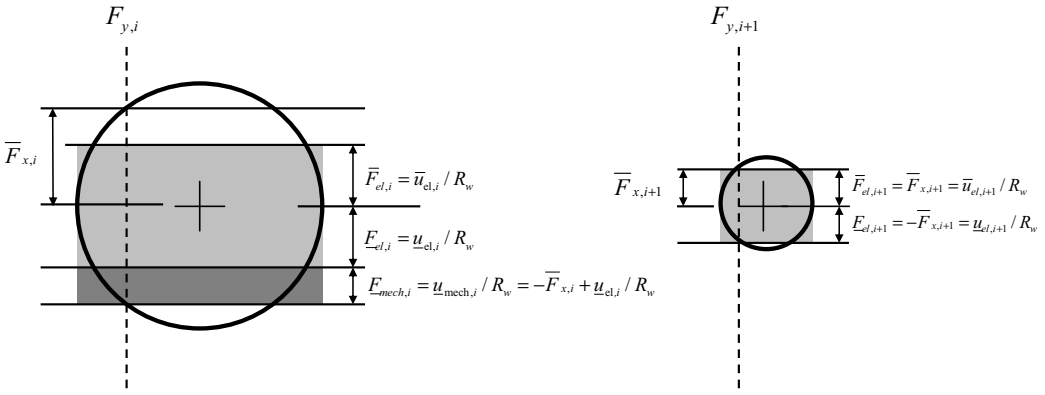

Figure 4: Illustration of how tyre fusion considers the case when two independent wheels with an electric motor and a disc brake are connected. This is comparable to configuration 3 HEV WM. Dashed lines illustrate the actual lateral force F_y.

For a wheel on an axle with an electric motor connected by an open differential and mechanical brakes connected to each wheel, the tyre fusion algorithm becomes:

$$\overline{u}_{\text{el}} = \begin{cases} 2\min(\overline{F}_{x,i}, \overline{F}_{x,i+1}) R_w / r_{fgr}, & \text{if } \overline{u}_{\text{el}} \geq 2\min(\overline{F}_{x,i}, \overline{F}_{x,i+1}) R_w / r_{fgr} \\ \overline{u}_{el}, & \text{else} \end{cases} \tag{4.29}$$

$$\underline{u}_{\text{el}} = \begin{cases} -2\min(\overline{F}_{x,i}, \overline{F}_{x,i+1}) R_w / r_{fgr}, & \text{if } \underline{u}_{\text{el}} \leq -2\min(\overline{F}_{x,i}, \overline{F}_{x,i+1}) R_w / r_{fgr} \\ \underline{u}_{\text{el}}, & \text{else} \end{cases} \tag{4.30}$$

$$\overline{u}_{\text{mech},i} = 0 \tag{4.31}$$

$$\underline{u}_{\text{mech},i} = \begin{cases} 0, & \text{if } \underline{u}_{\text{el}} \leq -2\min(\overline{F}_{x,i}, \overline{F}_{x,i+1}) R_w / r_{fgr} \\ -\overline{F}_{x,i} R_w - \underline{u}_{\text{el}} r_{fgr} / 2 & \text{elseif } (\underline{u}_{\text{el}} r_{fgr} / 2 + \underline{u}_{\text{mech},i}) \leq -\overline{F}_{x,i} R_w \\ \underline{u}_{\text{mech},i}, & \text{else} \end{cases} \tag{4.32}$$

This corresponds to the rear axle of configuration 2, HEV E4WD. Figure 5 illustrates the tyre's force limits. In this configuration the electric motor's limits $\underline{\overline{u}}_{\text{el}}$ are restricted by the right wheels longitudinal force limit, geared by the final gear and the differential. The right wheel can still combine electrical and

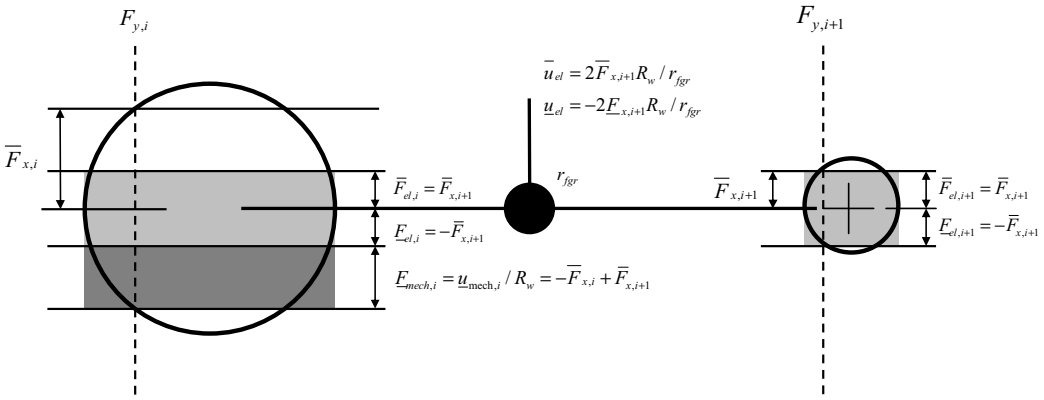

Figure 5: Illustration of how tyre fusion considers the case when an electric motor is connected to two wheels by an open differential and with individual disc brakes. This is comparable to configuration 2 HEV E4WD rear axle. Dashed line illustrates the actual lateral force F_y.

mechanical braking. The mechanical disc brakes are limited by its tyre force limit reduced by the part which is generated by the electrical motor.

The same system can be extended with a combustion engine, which corresponds to the front axle of configuration 2. This case is shown in Fig. 6. In the figure, the electric motor is limited by internal states, meaning that it can not generate $\overline{F}_x$. Instead the combustion engine is used to generate more force. The combustion engine's limits $\underline{\overline{u}}_{\mathrm{ice}}$ are limited by the right wheel. The limits of the combustion engine and the electric motor automatically set constraints on the left wheel according to Fig. 6.

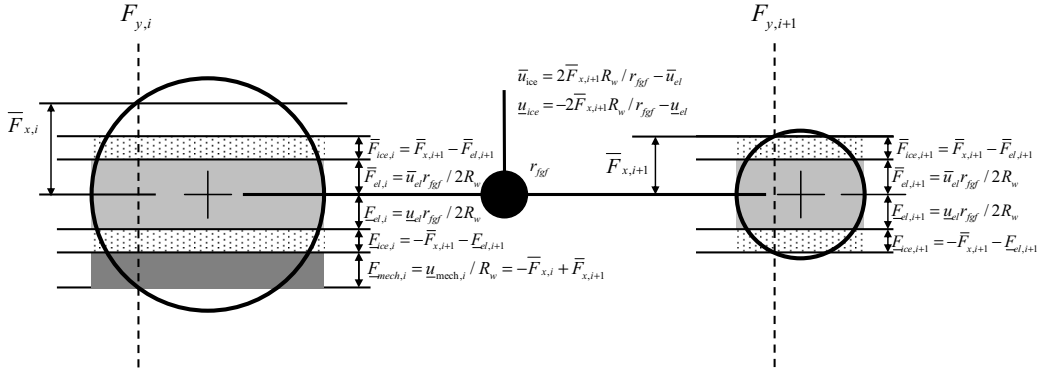

Figure 6: Illustration of tyre fusion for configuration 2 front axle with open differential connected to a combustion engine and an electric motor.

The limits for the steering actuators are also limited by the tyre fusion function

according to the following expression

$$\overline{F}_{y,\text{axle}} = \min\left(\sqrt{\overline{F}_{x,i}^2 - F_{x,i}^2}, \sqrt{\overline{F}_{x,i+1}^2 - F_{x,i+1}^2}\right) \tag{4.33}$$

$$\overline{u}_{\text{steer},i} = \min\left(\overline{u}_{\text{steer},i}, \frac{2\overline{F}_{y,\text{axle}}}{C_{\alpha,r,f}}\right) \tag{4.34}$$

$$\underline{u}_{\text{steer},i} = -\overline{u}_{\text{steer},i} \tag{4.35}$$

where $C_{\alpha,r,f}$ is the cornering stiffness for the front and rear axle respectively.

4.3 Control Distribution

The two step optimization problem actually suits very well for ground vehicles. Equation 2.7 constrains the possible set $u \in \Omega$ to only be possible u's that will be in nullspace of $N(Bu-v)$ or minimize the error of the desired forces $e = Bu-v$ needed for fulfilling the desired motion of the vehicle. Equation 2.7 can be seen as the vehicle motion controller. The limits which are sent to the control allocator are the combined limits from the tyre fusion function. Equation 2.6 minimizes the error of desired control input $e_{des} = u_{des} - u$. In ground vehicles this can be seen as a smooth arbitration between energy management and vehicle motion control. The desired input signals u_{des} from energy management declare how the electric motor and mechanical brakes should be used when optimizing the use of onboard energy. Figure 2 shows how energy management is included in the control allocator and Fig. 3 shows how the control allocator fits in the control system in more detail.

The weighting matrix, W_u, has been designed to facilitate a stable braking and traction performance

$$W_{u,1} = \text{diag}[\ 1 \quad 0.5 \quad 0.5 \quad 1 \quad 1 \quad 1e3 \quad 2e3\ ], \tag{4.36}$$

$$W_{u,2} = \text{diag}[\ 1 \quad 0.1 \quad 0.25 \quad 0.5 \quad 0.5 \quad 1 \quad 1 \quad 1e3 \quad 2e3\ ], \tag{4.37}$$

$$W_{u,3} = \text{diag}[\ 0.1 \quad 0.1 \quad 0.25 \quad 0.25 \quad 0.5 \quad 0.5 \quad 1 \quad 1 \quad 1e3 \quad 2e3\ ] \tag{4.38}$$

for configuration 1, 2, and 3 respectively. The desired input signals u_{des} from energy management are set to zero during the simulations, i.e. energy management desires to use the motion actuators as little as possible. The weighting matrix, W_v, has been designed not to prioritize any of the motions, longitudinal, lateral or yaw motion, $W_v = \text{diag}[\ 1 \quad 1 \quad 1\ ]$.

5 Simulations

The vehicle system models were implemented as s-functions in Matlab/Simulink. Due to the open differential in the driveline model the system becomes a differential algebraic equation system, a (DAE) system. The equations for the open differential were rewritten to be in ordinary differential equation (ODE) form by using a mass matrix. Solver *ode23t* has been used in the simulation, since

it can solve problems with a singular mass matrix. The used weighted least square with constraints solver was coded by [4]. The code was modified by the author to allow vehicle state x dependent control effectiveness matrix $B(x)$ and dynamical change in constraints u_{lim}.

5.1 Test Procedures

The simulations focus on traction and braking situations. The three vehicle configurations are compared and the only part changed in the control system was the control effectiveness matrix B and the tyre fusion algorithm which was slightly different for configurations 1 and 2 with open differential in the driveline. For configuration 1 and 2 the initial gear is set by Eq. 4.20. The initial temperature for disc brakes and electric motors was set to 30 ^{o}C. The following two test procedures were selected for simulation:

A: Acceleration from an initial velocity of 50 km/h to 120 km/h with a desired acceleration of 0.3g. During the acceleration a lane change manoeuvre is made. This is followed by medium braking of 0.5g until standstill with step friction. The friction is lowered from 1.0 to 0.3, occurring at 60 km/h and lasting for about 2 seconds.

B: Soft acceleration of 0.05g during driving a circle with constant radius of 200 m. The initial velocity is set to 50 km/h and friction is set to 0.3.

5.2 Test procedure A -medium acceleration with lane change followed by medium braking on step friction

This test procedure combines steering and traction in the first part of the test. In the second part a step friction occurs during braking. Fig. 5.2 shows how the three different vehicle configurations follow the reference velocity in longitudinal, lateral, and yaw motion. Configuration 1 is outperformed by configuration 2 and 3 especially during acceleration due to lack of power after gear shifting. It can be seen how configuration 1, the conventional vehicle, cannot produce enough power to accomplish the desired acceleration, which is especially noticeable for the third gear. Configurations 2 and 3 have no problem producing the desired acceleration. They use the four wheel drive option to accomplish the acceleration. During the braking all three configurations diverge from the desired velocity when they hit the step friction. The fastest one to pick up the lost braking after the step friction is configuration 3. The oscillations visible in the yaw motion, especially for configuration 1, are due to gear shifting during low friction.

The actuator signals u and their combined limits (from the tyre fusion algorithms) are shown in Figs. 6-11 for configurations 1, 2, and 3 respectively. The black solid line corresponds to actual u, the dashed red and blue lines are upper and lower combined limits respectively. It can be seen that during gear shifting,

the control allocator automatically reduces the desired power of the combustion engine and the ISG, see actuator 1 in Fig. 6 and actuators 1 and 2 in Fig. 10. This is achieved by using a control effectiveness matrix $B(x)$ that has zeros in the cells where the transmission gear ratio r_j is occurring during the gear shift. During the step friction, about 14 to 16 s, it is noticeable that the motion actuators limits are reduced. This is especially clear for configuration 3 and the wheel motors, actuator 1 to 4 in Fig 11.

5.3 Test Procedure B -soft acceleration of 0.05g during driving in a circle with a constant radius of 200 m.

In this test procedure the aim is to try to see how close the three different vehicle configurations come to the maximum velocity that one can drive in a circle with a radius 200 m on a road with a friction of 0.3. The limiting velocity v_{lim} can be calculated as

$$\begin{aligned} F_{fric} = F_{centripetal} \Leftrightarrow \mu \cdot m \cdot g = \frac{m \cdot v_{init}^2}{R} \\ v_{lim} = \sqrt{\mu \cdot g \cdot R} = 24.26 \text{ m/s} \end{aligned} \tag{5.1}$$

Figure 5.3 shows the reference and simulated longitudinal, lateral, and yaw velocities for all three configurations. It can be noted that all three configurations reach about 90 percent of the maximum speed before they start to diverge from the reference yaw velocity. Another interesting observation is that configuration 1 with only a combustion engine connected to the front wheels, starts to use the mechanical brakes when the vehicle is almost reaching the critical velocity.

In Fig. 12 the use of the actuators and their combined limits are shown. Observe how actuator 1, the combustion engine, increases the tractive torque when mechanical brakes, actuators 3 and 5, are beginning to be used as yaw stabilizing actuators at time 15 s. This is basically what today's ESP systems do, however here it is automatically performed by the control allocator. The actuators and their combined limits for configurations 2 and 3 during test procedure B, are shown in Fig. 13 and 14, respectively. In configuration 2 the electric motors, actuator 2 and 3, are mainly used for traction, but they also use the combustion engine, actuator 1. The mechanical brakes are not used at all as yaw stabilizing actuators in comparison to configuration 1. Similar behaviour could be observed for configuration 3.

In Figs. 15-17 the tyre forces $F_{x,i}$, $F_{y,i}$, and the longitudinal limit $\overline{F}_{x,i}$ are shown for all three configurations during test procedure B. One can see that the lateral force $F_{y,i}$ is increasing during the constant acceleration and thus reduces the longitudinal force limit $\overline{F}_{x,i}$. All three configurations handle this very well. The major difference is that configuration 1 has a negative force on the right rear wheel induced by the mechanical brakes.

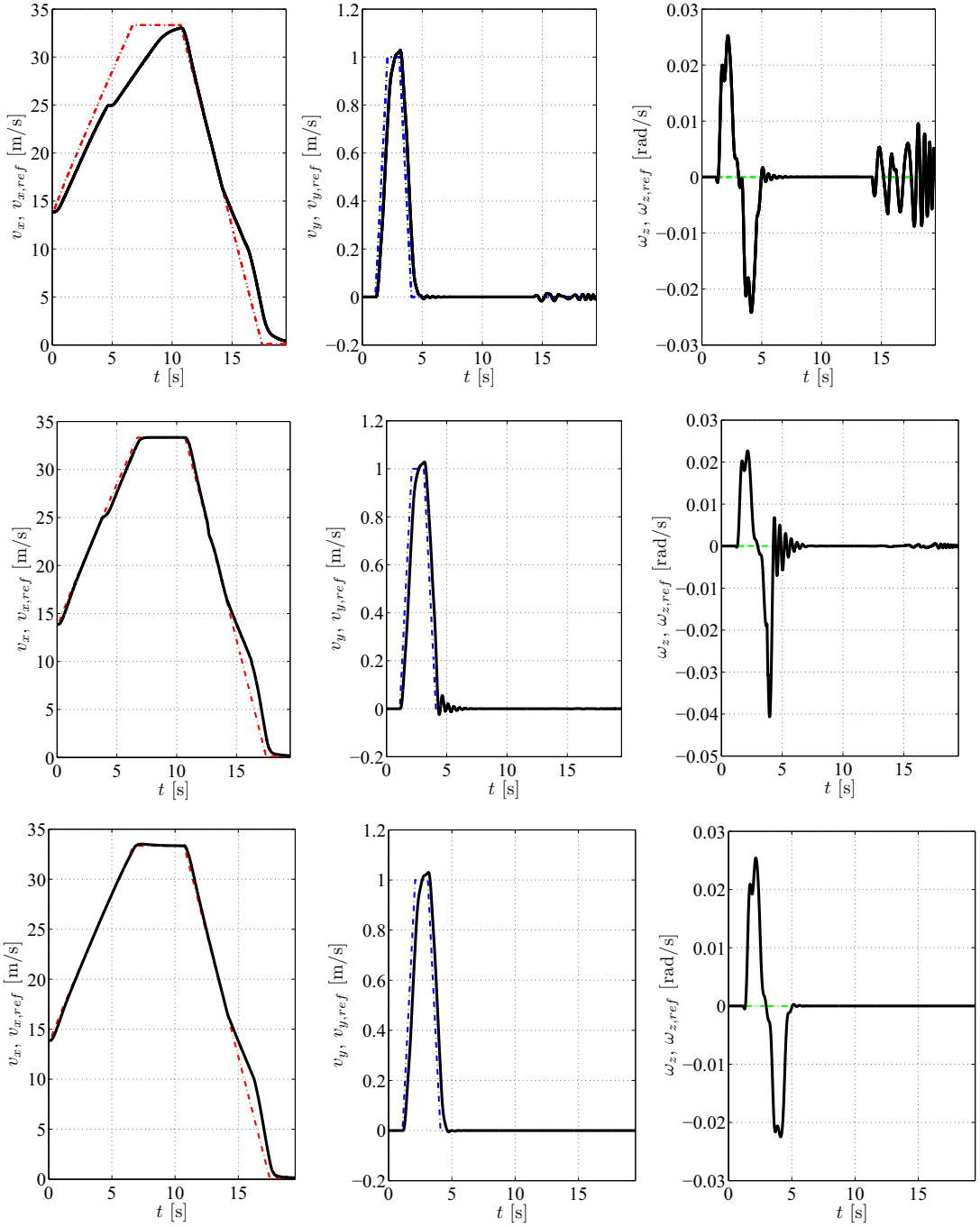

Figure 7: Longitudinal v_x, lateral v_y, and yaw ω_z velocity for configuration 1 (top), 2 (middle), and 3 (bottom) respectively during test procedure A.

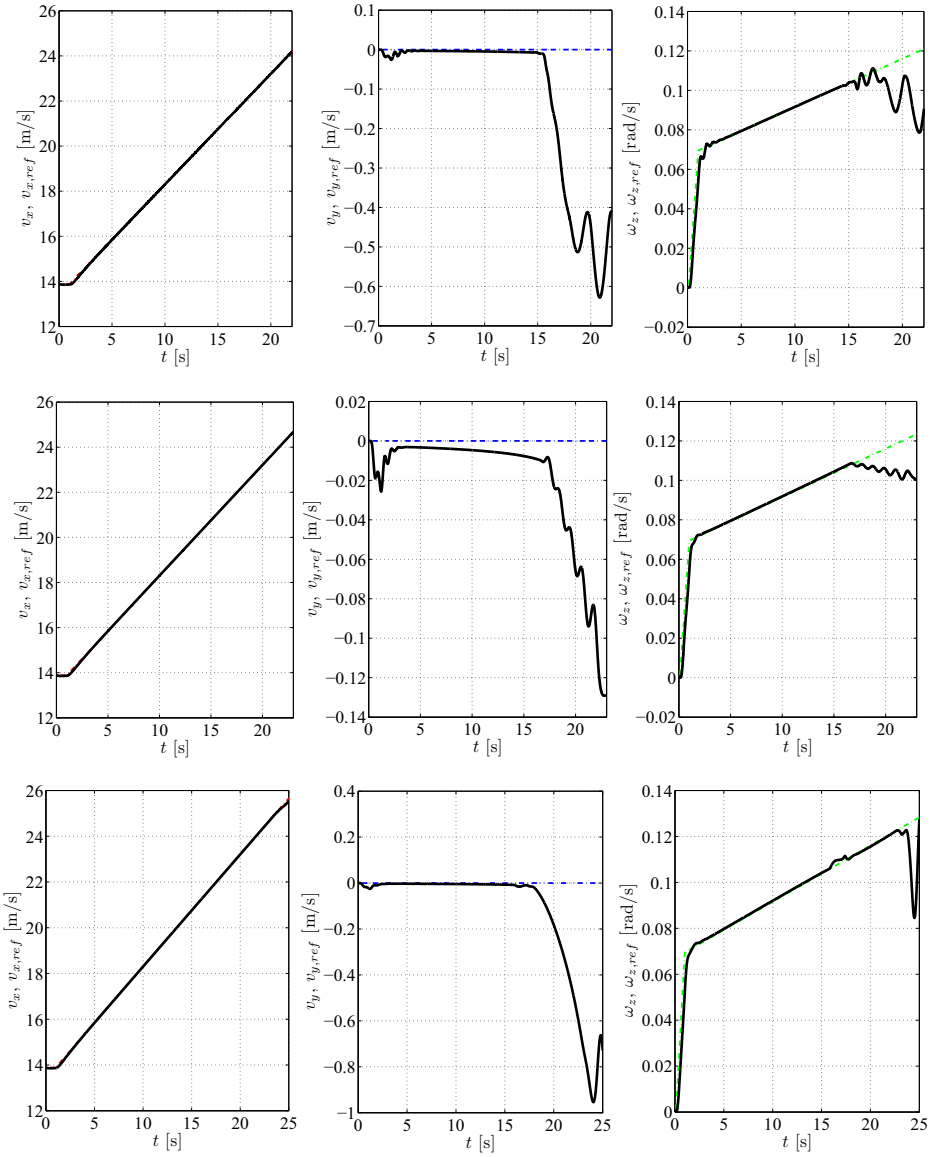

Figure 8: Longitudinal v_x, lateral v_y, and yaw ω_z velocity for configuration 1 (top), 2 (middle), and 3 (bottom) respectively during test procedure B.

6 Conclusions

The separation of control law and control allocation makes the control system reusable for different vehicle configurations, which was shown here for three configurations. This makes it possible to develop a wide range of configurations without the need for redesigning the control system for each one.

The weighted least square control allocation algorithm developed by [4] also works excellently for hybrid electric vehicles when traction and braking are considered. This is also a fast algorithm which would easily allow real time implementation in vehicles.

By using a vehicle state dependent control effectiveness matrix $B(x)$ features such as gear shifting can automatically be considered by the control allocator. This was illustrated by simulations where the torque of the combustion engine and ISG were reduced when gear shifting was occurring.

Actuator limits and rates together with the suggested tyre fusion algorithm give excellent information for making the correct coordination of the available actuators for different braking situations.

The simulations showed that for achieving better vehicle stability during circle driving and constant acceleration the traction force on the rear wheels should be used more than on the front wheels. This can easily be tuned in by the weight matrix W_u. During braking, the opposite force distribution is desired, i.e. more braking force generated on the front wheels than the rear wheels.

The proposed control system not only works as a traction and braking controller, it also works as a vehicle stability controller. The controller is easy to tune, containing only a few parameters, and takes a global optimization approach instead of a local optimization as is the case when developing a traction controller and a vehicle stability controller individually.

Acknowledgments

This work is supported by the Swedish national research program Gröna Bilen / FCHEV. Gröna Bilen is financed by the Swedish automotive industry and the Swedish research foundation Vinnova.

References

[1] AUTomotive Open System ARchitecture(AUTOSAR), "http://www.autosar.org/," 2004.

[2] B. Hardung, T. Kölzow, and A. Krüger, "Reuse of software in distributed embedded automotive systems," *Fourth ACM International Conference on Embedded Software (EMSOFT 2004), PISA, Italy*, 2004.

[3] L. Laine, *On Vehicle System Control Architecture for Fuel Cell- and Hybrid Electric Vehicles.* Licentiate thesis, Department of Applied Mechanics, Chalmers University of Technology, Sweden, 2005.

[4] O. Härkegård, "Backstepping and control allocation with applications to flight control," Ph.D. dissertation, Department of Electrical Engineering, Linköping University, SE–581 83 Linköping, Sweden, May 2003.

[5] T. Johansen, T. Fossen, and S. P. Berge, "Constrained nonlinear control allocation with singularity avoidance using sequential quadratic programming," *IEEE Transactions on Control Systems Technology, vol. 12, no. 1*, 2004.

[6] T. Johansen, T. Fuglseth, P. Tøndel, and T. I. Fossen, "Optimal constrained control allocation in marine surface vessels with rudders," in *IFAC Conf. Manoeuvring and Control of Marine Craft*, Girona, 2003.

[7] P. Tøndel and T. A. Johansen, "Control allocation for yaw stabilization in automotive vehicles using multiparametric nonlinear programming," in *Proc. of American Control Conf.*, Portland, OR, June 2005.

[8] J. Plumlee, D. Bevly, and A. Hodel, "Control of a ground vehicle using quadratic programming based control allocation techniques," in *Proc. of American Control Conf.*, Boston, MA, July 2004.

[9] J. Plumlee, *Mult-Input Ground Vehicle Control Using Quadratic Programming Based Control Allocation.* Master thesis report, Auburn University, Alabama, 2004.

[10] SAE, "Surface vehicle recommended practice, vehicle dynamics terminology," *SAE 1976-07, J670e*, 1976.

[11] H. B. Pacejka, *Tyre And Vehicle Dynamics 2^{nd} edition.* Butterworth-Heinemann, 2002.

[12] L. Laine and J. Fredriksson, "Brake blending for hybrid electric vehicles using control allocation," *Submitted to Int. J. Vehicle Systems Modelling and Testing, Special issue on: Modelling and Testing of Alternative Vehicular Propulsion*, 2006.

[13] A. Serrarens, *Coordinated control of the Zero Inertia Powertrain.* Technische Universiteit Eindhoven, 2001.

[14] H. Khalil, *Nonlinear Systems, 3^{rd} edition.* Prentice Hall Inc., 2002.

[15] K. Åström and T. Hägglund, *PID Controllers: Theory, Design, and Tuning.* Instrument Society of America, 1995.

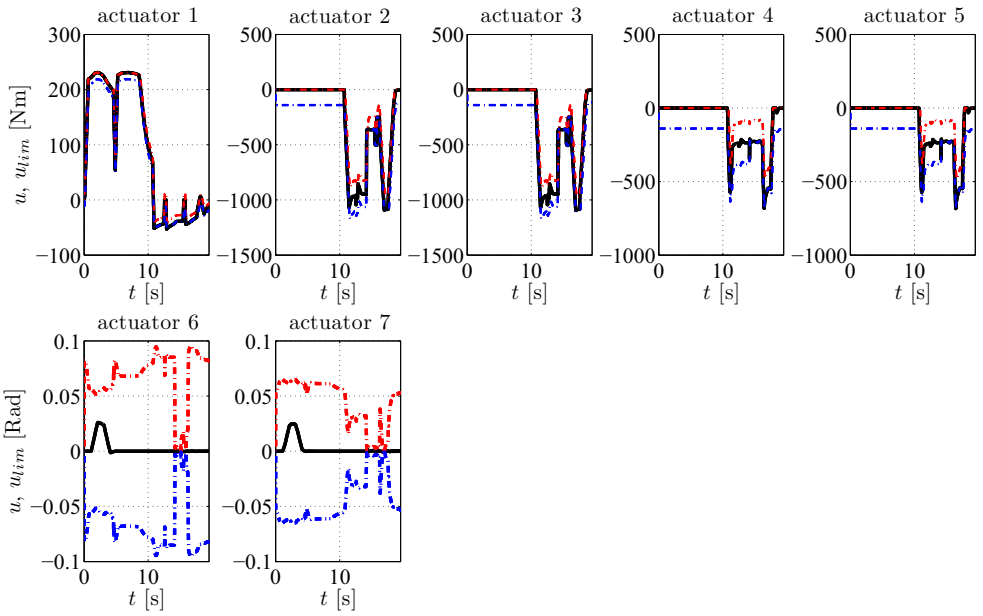

Figure 9: Input set u and their limits for configuration 1 during test procedure A. The black solid line corresponds to the actual u, the dashed red and blue lines are the upper and lower combined limits, respectively.

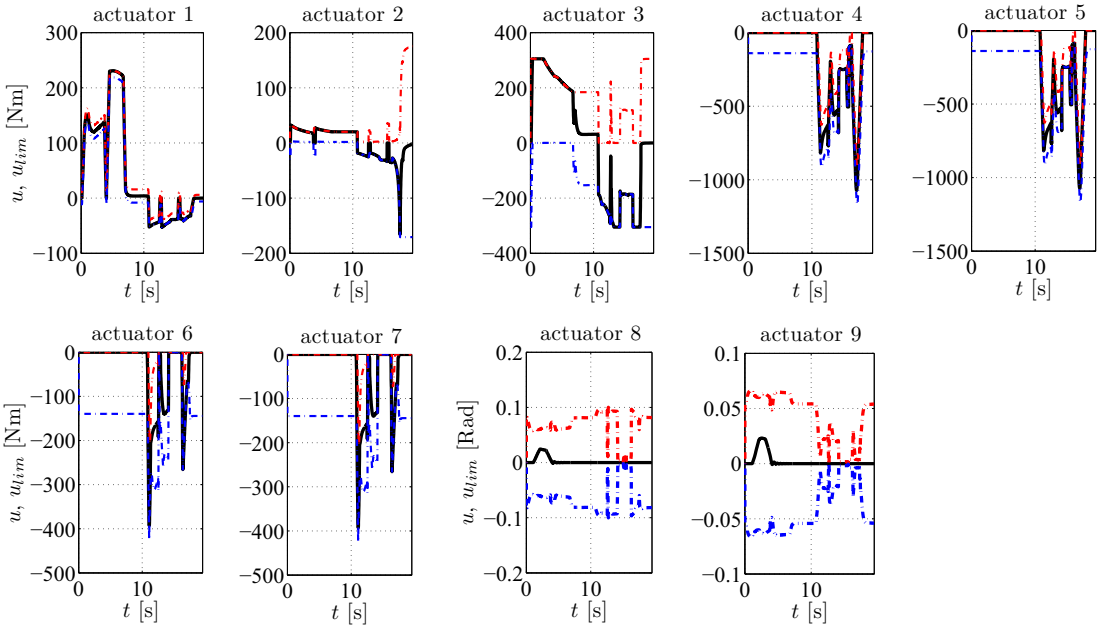

Figure 10: Input set u and their limits for configuration 2 during test procedure A. The black solid line corresponds to the actual u, the dashed red and blue lines are the upper and lower combined limits, respectively.

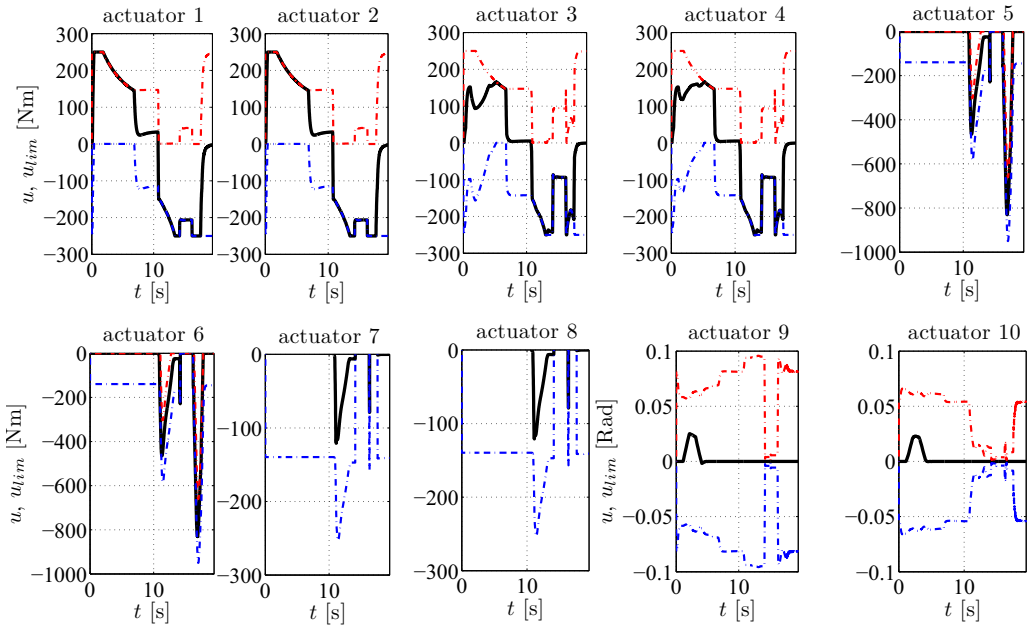

Figure 11: Input set u and their limits for configuration 3 during test procedure A. The black solid line corresponds to the actual u, the dashed red and blue lines are the upper and lower combined limits, respectively.

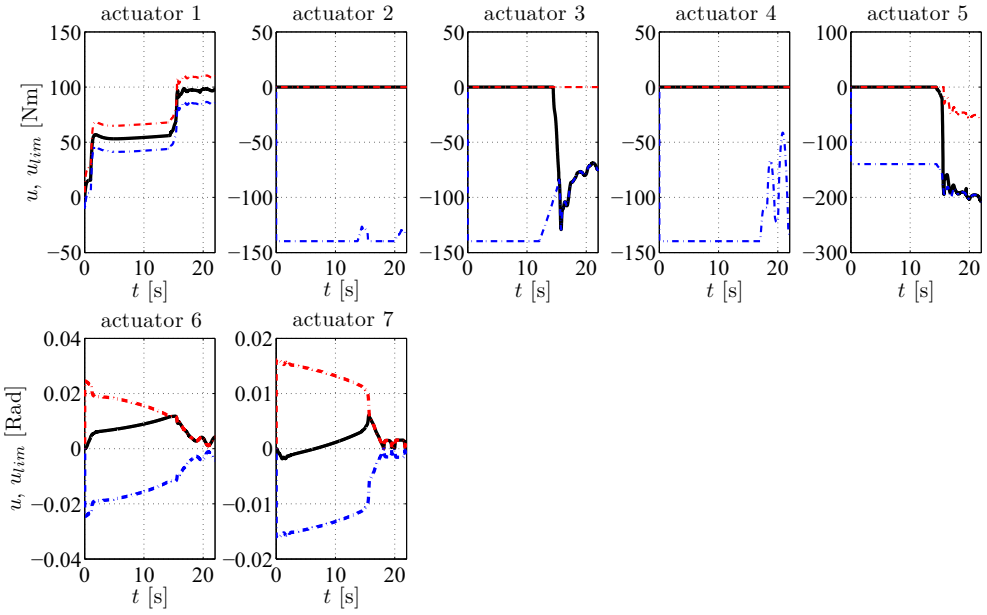

Figure 12: Input set u and their limits for configuration 1 during test procedure B. The black solid line corresponds to the actual u, dashed red line and blue line upper and lower combined limits, respectively.

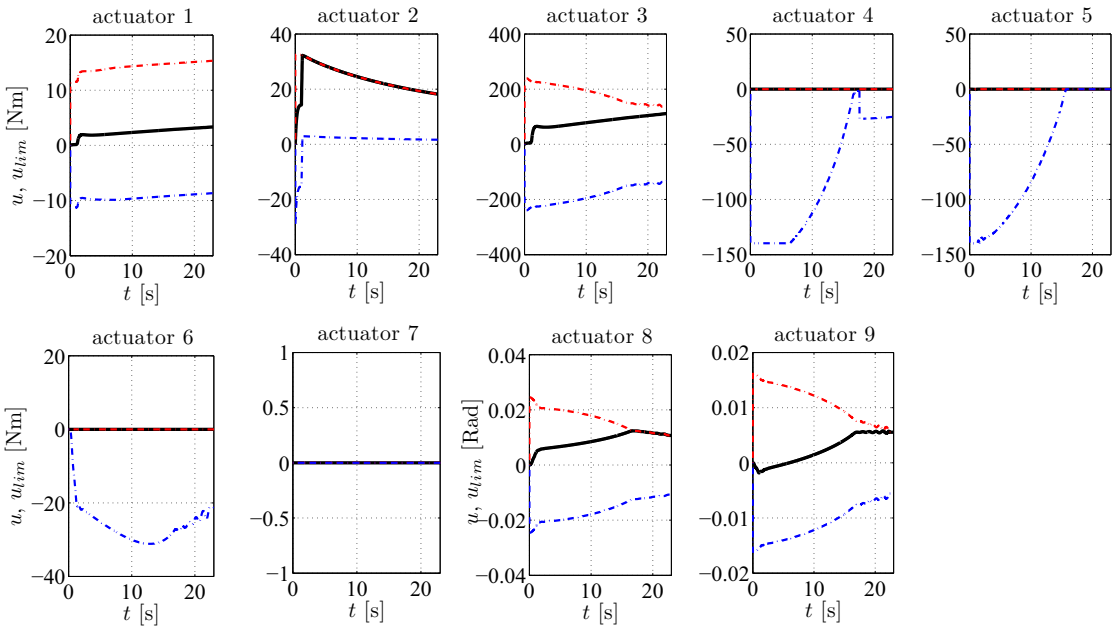

Figure 13: Input set u and their limits for configuration 2 during test procedure B. The black solid line corresponds to the actual u, the dashed red and blue lines are the upper and lower combined limits, respectively.

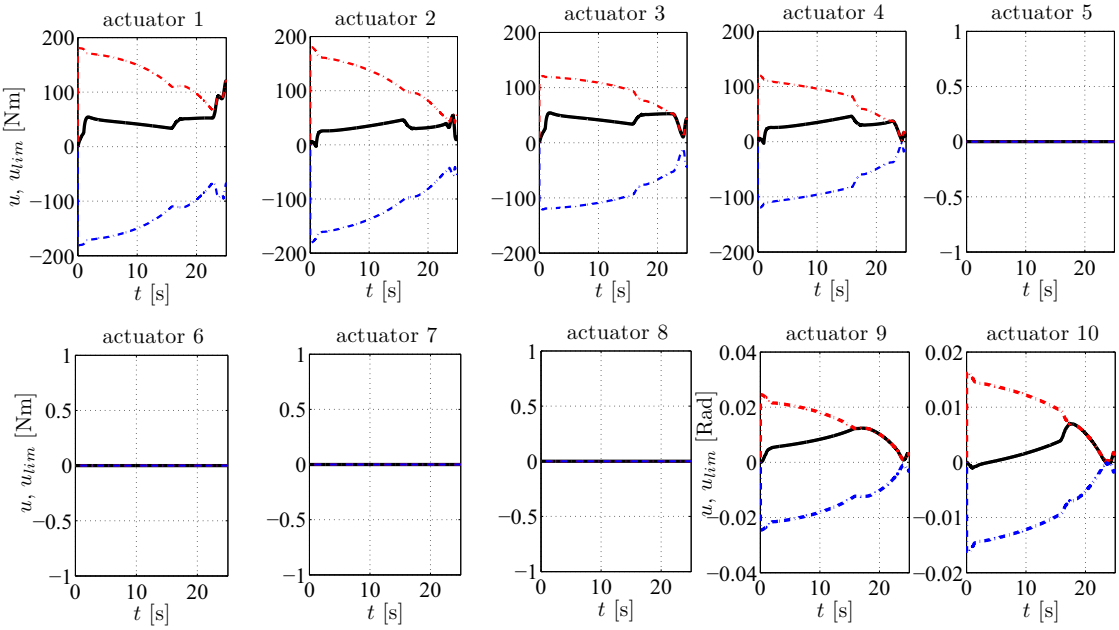

Figure 14: Input set u and their limits for configuration 3 during test procedure B. The black solid line corresponds to the actual u, the dashed red and blue lines are the upper and lower combined limits, respectively.

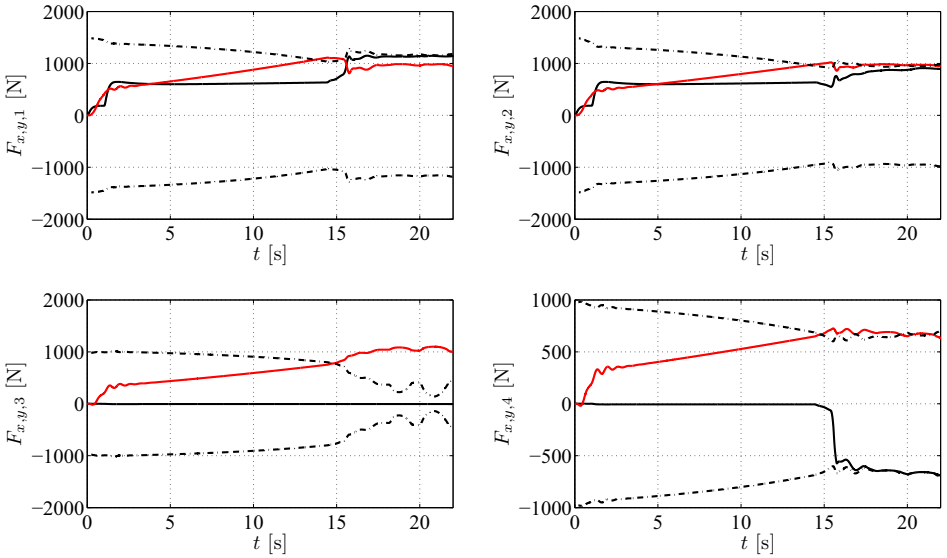

Figure 15: Tyre forces $F_{x,i}$ and $F_{y,i}$ and longitudinal force limits $\overline{F}_{x,i}$ for configuration 1 during test procedure B. Front left tyre (upper left figure), front right (upper right figure), rear left (lower left figure), and rear right (lower right figure). The black solid line corresponds to the actual $F_{x,i}$, the red solid line represents $F_{y,i}$, and the dashed black line $\overline{F}_{x,i}$.

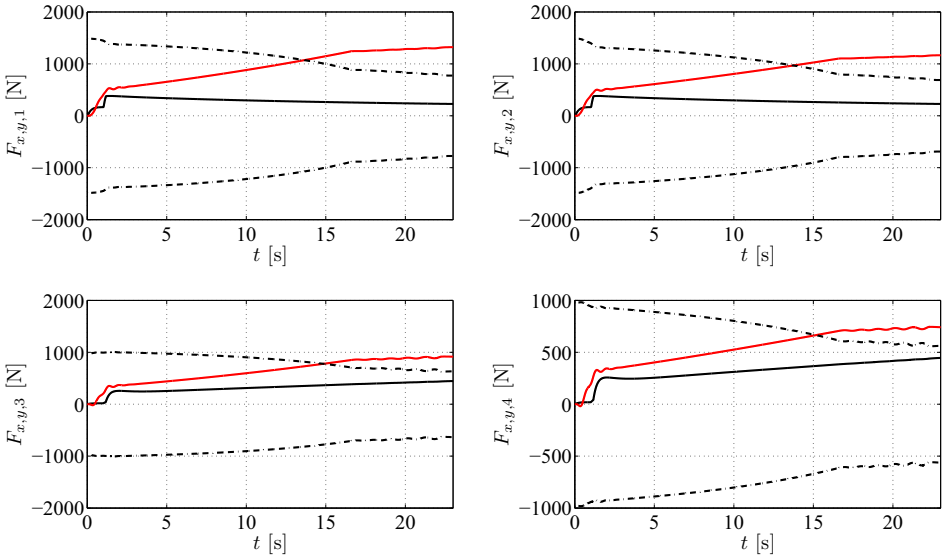

Figure 16: Tyre forces $F_{x,i}$ and $F_{y,i}$ and longitudinal force limits $\overline{F}_{x,i}$ for configuration 2 during test procedure B. Front left tyre (upper left figure), front right (upper right figure), rear left (lower left figure), and rear right (lower right figure). The black solid line corresponds to the actual $F_{x,i}$, the red solid line represents $F_{y,i}$, and the dashed black line $\overline{F}_{x,i}$.

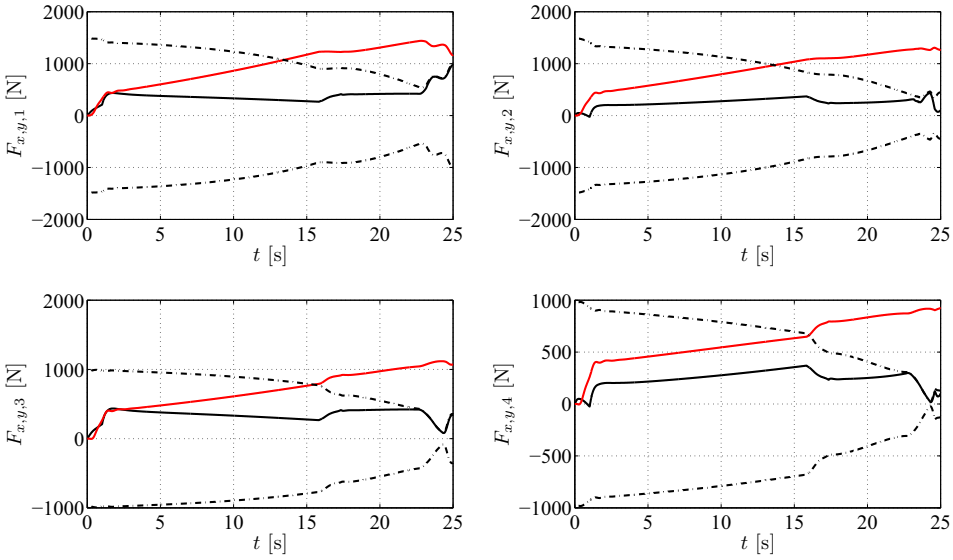

Figure 17: Tyre forces $F_{x,i}$ and $F_{y,i}$ and longitudinal force limits $\overline{F}_{x,i}$ for configuration 3 during test procedure B. Front left tyre (upper left figure), front right (upper right figure), rear left (lower left figure), and rear right (lower right figure). The black solid line corresponds to the actual $F_{x,i}$, the red solid line represents $F_{y,i}$, and the dashed black line $\overline{F}_{x,i}$.

Paper VI

Coordination of vehicle motion and energy management control systems for wheel motor driven vehicles

in

Proceedings of the 2007 IEEE Intelligent Vehicles Symposium (IV'07), Istanbul, Turkey, June 2007.

Coordination of Vehicle Motion and Energy Management Control Systems for Wheel Motor Driven Vehicles

Leo Laine and Jonas Fredriksson

Abstract— **This paper shows how smooth coordination of vehicle motion controller and energy management can be achieved when control allocation is used for over-actuated ground vehicles. The ground vehicle studied here is equipped with four electric wheel motors, four disc brakes, and front and rear steering. This gives a total of ten input signals to control the desired vehicle motion in longitudinal-, lateral-, and yaw-direction. Simulations show that the desired input signals from energy management and steering can be fulfilled, but when needed the actual input signals for the motion actuators are smoothly diverted from the desired input signals due to vehicle stability reasons and/or saturation of the actuators.**

I. INTRODUCTION

If or when the era of the combustion engine within automotive applications ends or becomes less dominating, the propulsion system of the vehicles will most likely be electrified. The first transition away from the combustion engine dependence has already started, with the launch of the Toyota Prius in 1997. The car is equipped with the Toyota Hybrid System (THS) [1] which combines the combustion engine with electric motors. This allows the combustion engine to be downsized. The Prius has been followed by several other commercially available hybrid electric vehicles. The final transition will come when the prices for oil will become too high or when environmental legislations demands for alternative fuels. One possible option to meet the new demands is the fuel cell (fc) which converts hydrogen and oxygen into electricity and water.

When automotive vehicles become more electrified many hydraulical and mechanical functions can be replaced by electrical ones [2]. In this paper a future vehicle configuration is studied which has replaced the combustion engine with four electric motors mounted on each wheel. The motors are propelled by a fuel cell in combination with a battery. The mechanical braking is assumed to be independently controlled, and the steering is assumed to be by-wire, with independent front and rear steering. Clearly, by introducing so many motion actuators the desired global longitudinal-, lateral-, and yaw- motion of the vehicle can be realized in many different ways by using the available motion actuators. This type of systems are called over-actuated systems.

This work is supported by the Swedish national research programme Gröna Bilen/FCHEV. Gröna Bilen is financed by Swedish automotive industry and the Swedish research foundation Vinnova.

L. Laine is with the Department of Applied Mechanics, Div. of Vehicle Safety and Vehicle Dynamics, SAFER, Chalmers University of Technology, SE-417 56 Göteborg, Sweden, leo.laine@chalmers.se

J. Fredriksson is with the Department of Signals and Systems, Div. of Automatic Control, Automation and Mechatronics, Chalmers University of Technology, jonas.fredriksson@chalmers.se

In this paper it is shown how control allocation [3] can be a viable option to ease the control design of over-actuated ground vehicle systems when both the vehicle motion and energy management are considered. The outline of the paper is as follows: Section I-A gives a background of using control allocation within the control system. Section II explains how the ground vehicle is modelled. Section III describes the control design. Section IV and V explains the simulated cases and the results. Finally in Section VI concluding remarks are made.

A. Background

One promising way to manage the coordination of over-actuated systems is to use control allocation. Control allocation deals with the problem of distributing the control demand within an available set of actuators. The control demand $v \in R^k$ is mapped onto the true control input of the actuators $v \mapsto u$, where $u \in R^m$ and $k < m$. The allocation problem lies in that there are several input sets of u that can give the control demand v. The control allocation problem is posed as a constrained optimization problem which provides automatic redistribution of the control effort when one actuator saturates in position or in rate. Control allocation has been used successfully in flight applications [3], marine vessels [4], [5], and for ground vehicles [6], [7], [8]. In [6]-[8] the mechanical brakes and steering were in focus without direct considerations to the actuator limits.

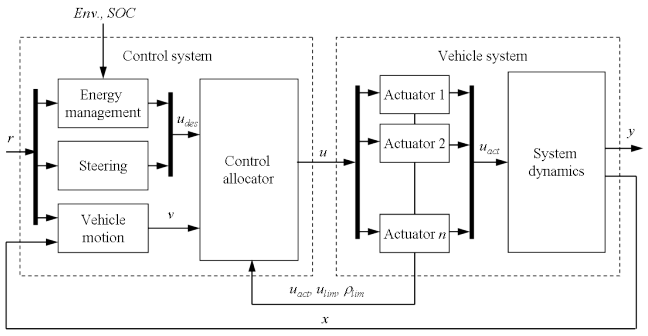

Fig. 1. Suggested control system architecture when control allocation is used for Hybrid Electric Vehicle systems.

In earlier work by the authors, [9] and [10], it was shown how the control system can be made reusable for different vehicle configurations when one separates the control law from the control allocation for achieving the vehicle motion. Wheel force limits in combination with constraints due to vehicle configuration allowed a reusable structure. Here, in

this paper the limits are taken one step further, actuator position and rate of change limits in combination with tyre force limits are considered as constraints for the control allocator. Additionally, it is here shown that the proposed control system also allows separate control laws for energy management and steering in addition to vehicle motion as shown in Fig. 1. The authors have not found any work showing how one smoothly combines energy management and vehicle motion control for a HEV by using constrained control allocation with optimization formulation.

II. SYSTEM MODELLING

The system modelling is separated into three parts:

A. Chassis including tyre dynamics

The chassis model is a so-called two track model and has five degree of freedom: longitudinal-, lateral-, yaw-, roll-, and pitch motion. The model aims at being good enough in representing the chassis dynamics on a flat surface. The SAE standard [11] has provided the main guidance for defining the axis orientations. A brush tyre model [12] is used together with dynamic relaxation to describe the tyre dynamics. The used chassis parameters are comparable to a commercial medium sized sedan car.

B. Power Supply including energy buffer

Here one type of Power Supply system is studied, a series vehicle configuration with a fuel cell and a buffer. The fuel cell can deliver a continuous output power of 30 kW, the power is sufficient to overcome the resistance forces at a constant speed of 130 km/h for a medium sized sedan car. Fig. 2 shows the efficiency curve as a function of output power for the fuel cell model, which also includes parasitic losses. One can see that output power lower than 10 kW yields bad efficiency and should be avoided. Good efficiency is found between 10 and 40 kW. The optimal output power from the fuel cell is about 20 to 30 kW.

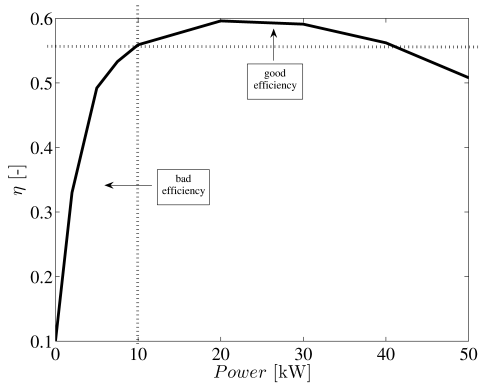

Fig. 2. Efficiency as a function of output power for simulated fuel cell.

A fuel cell stack such as Proton Exchange Membrane (PEM) can deliver short pulses of output power before the compressor reaches desired speed. This can be seen as there are two time constants one 'instantaneous' and one 'steady state' [13]. The experimental results in [13] showed that the instantaneous time constant was in the order of 11 μs and the steady state about 400 ms to reach 63 percent of its final value. However, the time constants will get shorter if the fuel cell is already operating with high output power as a initial condition. Here only a simplified first order model is used for the fuel cell output power with a time constant of 400 ms which then neglects the instantaneous time constant.

An energy buffer is needed to be able to handle peak accelerations and store regenerated brake energy. According to [14] the most efficient buffer is a battery when performance, such as peak acceleration, towing, and price are compared for battery, ultracapacitors, and a combination of battery and ultracapacitors. A battery with a high energy density allows the fuel cell to work at efficient operating points or even to be shut down when low output power is needed.

The peak output power is 175 kW of which 40 kW is from fuel cell and 135 kW is from buffer. The buffer power is achieved by selecting a battery mass of 90 kg with 1500 W/kg charge and discharge power density. The selected power density is based upon that Ni/MH batteries have about 1200 W/kg and Li-ion about 2000 W/kg [15]. However the Li-ion have still not had a break through in automotive applications due to problems in cost, life, abuse tolerance, and low temperature performance [15]. The operating State of Charge (SOC) window was set to $SOC_{min} = 40$ % and $SOC_{max} = 90$ %.

C. Motion actuator dynamics

The series HEV has wheel motors mounted on each wheel with maximum output power of 40 kW, which gives four control inputs. Additionally, each wheel has individually controlled disc brakes, which give additional four control inputs. The actual torque limits delivered for the actuators are modelled by thermal lumped mass models for both electric motors and mechanical brakes. The temperature model tightens the actual limits due to overheating of the electric motor windings and the permanent magnets. For the mechanical brakes the friction is temperature dependent. Additionally the rotational speed is constraining the electric motor. The actuator limits from electric motors $\overline{\underline{u}}_{\mathrm{el},i}$ and mechanical brakes $\overline{\underline{u}}_{\mathrm{mech},i}$ can be expressed as

$$\begin{aligned} \underline{u}_{\mathrm{el},i}(\omega_i, T_i) \leq u_{\mathrm{el},i} \leq \overline{u}_{\mathrm{el},i}(\omega_i, T_i) \\ \underline{u}_{\mathrm{mech},i}(T_i) \leq u_{\mathrm{mech},i} \leq \overline{u}_{\mathrm{mech},i}(T_i) \end{aligned} \tag{1}$$

where ω_i and T_i are the angular velocity and temperature of the actuator. The actuator models give also information of the rate of change limits. Finally, steering is seen as steer by wire by front and rear rack steer which gives two additional control inputs, i.e. the configuration has a total of 10 control inputs.

III. CONTROL DESIGN

Independently of the specific applications studied, a class of nonlinear systems can be described in the affine form

$$\dot{x} = f(x) + g(x)u \tag{2}$$

$$y = h(x) \tag{3}$$

Control allocation can be applied if the control input can be perturbed without affecting the system dynamics. The system can therefore rewritten as

$$\dot{x} = f(x) + v \tag{4}$$
$$y = h(x) \tag{5}$$

where $v = g(x)u$, v is also called the virtual control input.

The control design can be divided into two steps. The first step is to design a control law that controls the net effort v. The second step is to design a control allocator that maps the net effort of virtual control input to true control input, $v(t) \mapsto u(t)$. Unfortunately, the mapping of the net effort to the true control signal is complicated since the $g(x)$-matrix is not invertible. Using a pseudo-inverse to find a solution could be one way of solving this. However, this could lead to an unrealistic solutions since the true control signals are limited by several different constraints, see Eq. 1. Instead a constrained optimization problem is proposed and solved.

The chassis system can be written as

$$M\dot{x} = f(x) + g(x)u \tag{6}$$
$$y = h(x) \tag{7}$$

where M is the mass matrix

$$M = \begin{bmatrix} m & 0 & 0 \\ 0 & m & 0 \\ 0 & 0 & I_z \end{bmatrix}$$

and

$$f(x) = \begin{bmatrix} mx_2x_3 - D_1x_1 - D_2m\mathrm{sgn}(x_1)x_1^2 \\ -mx_1x_3 - C_\alpha \frac{8x_1(2x_2+(L_f-L_r)x_3)}{4x_1^2 - b_t^2x_3^2} \\ -L_fC_\alpha \frac{8x_1(2x_2+L_fx_3)}{4x_1^2-b_tx_3^2} + L_rC_\alpha \frac{8x_1(2x_2-L_rx_3)}{4x_1^2-b_tx_3^2} \end{bmatrix} \tag{8}$$

$$g(x)u = \begin{bmatrix} \sum_{i=1}^4 F_{x,i} \\ C_\alpha \sum_{i=1}^4 \delta_i \\ L_fC_\alpha \sum_{i=1}^2 \delta_i - L_rC_\alpha \sum_{i=3}^4 \delta_i + \frac{B_t}{2} \sum_{i=3}^4 (-1)^{1+i} F_{x,i} \end{bmatrix} \tag{9}$$

$$h(x) = \begin{bmatrix} x_1 & x_2 & x_3 \end{bmatrix}^T \tag{10}$$

where x_1, x_2, and x_3 correspond to longitudinal-, lateral- and yaw- velocity of the vehicle. Here, a linear tyre force model of type $F_{y,i} = C_\alpha \alpha_i$ is assumed and that one can split the lateral tyre forces into steer angle and vehicle state dependence, $F_{y,i} = F_{y,i}(\delta_i) + F_{y,i}(x)$. The lateral tyre forces depending on vehicle states $F_{y,i}(x)$ and depending on steering angles $F_{y,i}(\delta_i)$ can therefore be separated into $f(x)$ and $g(x)u$, respectively. D_1 and D_2 are constants related to aerodynamical and rolling resistance. Since the mass matrix is invertible, the system can be written in affine form. Looking at $g(x)u$ in Eq. 9 it corresponds to longitudinal and lateral global forces and yaw moment of the vehicle and can therefore be considered as the virtual control input v.

A. Control Law for Vehicle Motion

The purpose of the vehicle motion controller is to follow a desired trajectory interpreted from the driver's steering actions. The controller is based on feedback linearization, see e.g. [16]. The idea with feedback linearization is to transform the nonlinear system into a linear one, so that linear techniques can be used. In its simplest form it can be seen as a way to cancel the nonlinearities by a nonlinear state feedback. Looking at the system, it can be noticed that the first term on the right hand side of (6) is the only one including the nonlinearities of the system. If the non-linear term, $f(x)$, is cancelled, the multi-input, multi-output (MIMO)-system becomes linear. Furthermore, by cancelling $f(x)$ the MIMO-system becomes decoupled. Then, using a PI-controller, the control law becomes:

$$v = -f(x) + K_p e + K_i \int_0^t e d\tau \tag{11}$$

where e is the error between the desired vehicle motion and the vehicle's actual motion. The design parameters for the PI-controllers, K_p and K_i, are chosen as

$$K_i = 20 \begin{bmatrix} 0.2m & 0 & 0 \\ 0 & 0.7m & 0 \\ 0 & 0 & 1.5I_z \end{bmatrix} \tag{12}$$

$$K_p = \frac{2}{3} m \sqrt{K_i \begin{bmatrix} \frac{16}{m} & 0 & 0 \\ 0 & \frac{1}{m} & 0 \\ 0 & 0 & \frac{1}{I_z} \end{bmatrix}} \tag{13}$$

To handle saturation of actuators the PI-controllers are extended with anti-windup based on back calculation [17].

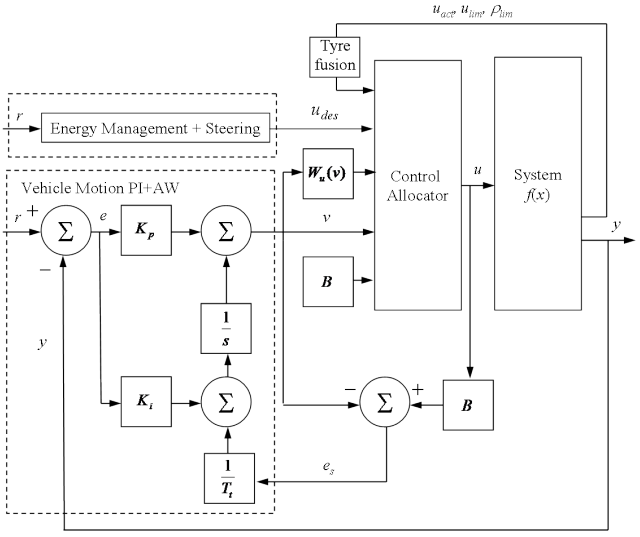

Fig. 3. Control Design illustration with focus on control law for vehicle motion, a PI controller with Anti-Windup strategy that decides the virtual control input $v(t)$ which is then mapped onto the true control input $u(t)$ by the control allocator, where $g(x)u \approx Bu$. The control allocator uses a weight scheduled weighting matrix $W_u(v_1)$.

B. Control Law for Energy Management

The objective of the energy management algorithm is to minimize fuel consumption and assure optimal power availability at any time. The used and implemented energy management strategy is inspired by [18]. It uses a finite state machine which distinguishes between four driving modes:

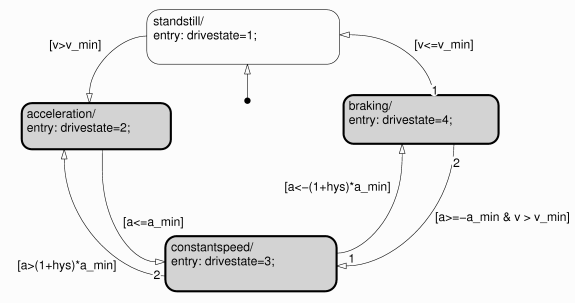

Fig. 4. Driving modes used for Energy Management, inspired by [18].

standstill, acceleration, constant speed, and braking, which are based upon speed and acceleration as illustrated in Fig. 4.

During the four modes different strategies are applied for how the total power demand is divided between the fuel cell and the battery. As shown in Fig. 2 it is important to avoid bad efficiency of the fuel cell as much as possible which is found during low output power less than 10 kW and at maximum output power above 40 kW. Secondly the steady state rise time of output power for a fuel cell is about 400 ms which leads to that highly transient power demands should be delivered by the battery. These two design criteria are considered for the control laws used within the four modes:

1) Standstill:

$$P_{fc} = \begin{cases} P_{fc,opt}, \text{ if } SOC \leq SOC_{min} \\ 0, \text{ else} \end{cases} \tag{14}$$

$$P_{bf} = \begin{cases} -P_{fc}, \text{ if } SOC \leq SOC_{min} \\ 0, \text{ else} \end{cases} \tag{15}$$

2) Acceleration:

$$P_{fc} = \begin{cases} \min\left(\hat{P}_{dem}, 40\right), \text{ if } 10 \text{ kW} \leq P_{dem} \\ 0, \text{ else} \end{cases} \tag{16}$$

$$P_{bf} = \begin{cases} P_{dem} - P_{fc}, \text{ if } 10 \text{ kW} \leq P_{dem} \\ P_{dem}, \text{ else} \end{cases} \tag{17}$$

3) Constant speed:

$$P_{fc} = \begin{cases} P_{fc,opt}, \text{ if } SOC \leq SOC_{min} \ \& \ 10 \text{ kW} \geq P_{dem} \\ \min\left(\hat{P}_{dem}, 40\right), \text{ if } 10 \text{ kW} \leq P_{dem} \\ 0, \text{ else} \end{cases} \tag{18}$$

$$P_{bf} = \begin{cases} P_{dem} - P_{fc}, \text{ if } 10 \text{ kW} \leq P_{dem} \\ P_{dem} - P_{fc}, \text{ if } SOC \leq SOC_{min} \ \& \ 10 \text{ kW} \leq P_{dem} \\ P_{dem}, \text{ else} \end{cases} \tag{19}$$

4) Braking:

$$P_{bf} = \begin{cases} P_{dem}, \text{ if } |P_{dem}| \leq 134 \text{ kW} \ \& \ SOC \leq SOC_{max} \\ P_{bf,max}, \text{ if } |P_{dem}| \geq 134 \text{ kW} \ \& \ SOC \leq SOC_{max} \\ 0, \text{ else} \end{cases} \tag{20}$$

$$P_{mb} = \begin{cases} P_{dem} - P_{bf,max}, \text{ if } |P_{dem}| \geq 134 \text{ kW} \ \& \ SOC \leq SOC_{max} \\ P_{dem}, \text{ if } SOC \geq SOC_{max} \\ 0, \text{ else.} \end{cases} \tag{21}$$

where P_{fc}, P_{bf}, and P_{mb} are fuel cell, buffer, and mechanical brake output power. $P_{fc,opt} = 20$ kW is the optimal output power of fc, see also Fig. 2. P_{dem} is the power demand. $\hat{P}_{dem}$ is the low pass filtered power demand with cutoff frequency of 2 rad/s. The low pass filtering is used for achieving an output within range of the slow response of the fuel cell. The power demand of the vehicle is calculated with the following expression

$$P_{dem} = P_{acc} + P_{loss} + P_{aux}. \tag{22}$$

Where $P_{acc} = mav$ is the acceleration power needed. $P_{loss} = D_1 v + D_2 v^2$ is the rolling and air resistance, and P_{aux} is the auxiliary power needed for other electric loads such as air conditioner, here assumed to be a constant of 0.5 kW.

The desired torque on the specific electrical and mechanical actuators are assumed to be evenly distributed

$$\tau_{wm_i} = \frac{\left(P_{fc} + P_{bf}\right) R_w}{4 v_x r_{fg}} \tag{23}$$

$$\tau_{mb_i} = \frac{P_{mb} R_w}{4 v_x} \tag{24}$$

where i is the wheel number, R_w is the wheel radius, and r_{fg} is the final gear of the electric wheel motor. For low vehicle velocities $v_x < 0.1$ m/s the desired torques are set equal to zero and solely solved by the vehicle motion control law and the control allocator. These desired torques will give the first eight positions of the vector

$$u_{des} = \begin{bmatrix} \tau_{wm_1} & \tau_{wm_2} & \tau_{wm_3} & \tau_{wm_4} & \tau_{mb_1} & \tau_{mb_2} & \tau_{mb_3} & \tau_{mb_4} & \delta_f & \delta_r \end{bmatrix}^T, \tag{25}$$

see also Fig. 3.

C. Control Law for Steering

The reference model within the driver interpreter of the vehicle is assumed to deliver the desired reference signal $r = \begin{bmatrix} v_x & v_y & \omega_z \end{bmatrix}$, vehicle's longitudinal-, lateral-, and yaw-velocity, to the steering function, see also Fig. 1. Here the inverse dynamics of a linear bicycle model is used to derive the desired front and rear steering angle inputs δ_f and δ_r. The linear bicycle model assumes: v_x to be constant, steering angles to be small, and a linear tyre force model $F_y = C_\alpha \alpha$. The model can be then expressed as

$$\dot{x}_{steer} = A x_{steer} + B u_{steer} \tag{26}$$

$$A = -\begin{bmatrix} \frac{C_{\alpha_f} + C_{\alpha_r}}{m v_x} & v_x + \frac{L_f C_{\alpha_f} - L_r C_{\alpha_r}}{m v_x} \\ \frac{L_f C_{\alpha_f} - L_r C_{\alpha_r}}{I_z v_x} & \frac{L_f^2 C_{\alpha_f} + L_r^2 C_{\alpha_r}}{I_z v_x} \end{bmatrix} \tag{27}$$

$$B = \begin{bmatrix} \frac{C_{\alpha_f}}{m} & \frac{C_{\alpha_r}}{m} \\ \frac{L_f C_{\alpha_f}}{I_z} & -\frac{L_r C_{\alpha_r}}{I_z} \end{bmatrix} \tag{28}$$

where $x_{steer} = \begin{bmatrix} v_y & \omega_z \end{bmatrix}$ and $u_{steer} = \begin{bmatrix} \delta_f & \delta_r \end{bmatrix}$. By assuming that the desired accelerations $\hat{\dot{x}}_{steer}$ can be estimated by time discrete differentiation of the reference signal $\hat{\dot{r}} = \frac{r(k+1) - r(k)}{t(k+1) - t(k)}$, the needed input can be solved by

$$u_{steer} = B^{-1}\left(\hat{\dot{x}}_{steer} - A x_{steer}\right) \tag{29}$$

where B^{-1} exists because B has full rank. For low longitudinal velocities v_x the A matrix becomes singular, however for low velocities the steering is more a geometrical problem such as $\delta_f = L_f / R$ and $\delta_r = -L_r / R$, where R is the turning radius. Eq. 29 gives the last two positions of the vector u_{des}, Eq. 25, see also Fig. 3.

D. Control Allocation

The second step in the control design is to create the control allocator. The key issue is how to select the control input set u from all possible combinations. Here, a constrained control allocation with mixed optimization is used to map the virtual control input $v(t)$ onto true control input $u(t)$. The virtual control input is the global longitudinal and lateral forces and the yaw moment of the vehicle $v(t) = \begin{bmatrix} F_x & F_y & M_z \end{bmatrix}^T$, which is controlled by the control law for vehicle motion, see Section III-A. Looking at the model (Eqs. 8-7) the true control signals are the longitudinal wheel forces $F_{x,i}$ and the wheel steering angles δ_i. The wheel forces are controlled by the electric motors via the driveline and the mechanical brakes. Thus the true control input is selected as $u(t) = \begin{bmatrix} \tau_{wm_1} & \tau_{wm_2} & \tau_{wm_3} & \tau_{wm_4} & \tau_{mb_1} & \tau_{mb_2} & \tau_{mb_3} & \tau_{mb_4} & \delta_f & \delta_r \end{bmatrix}^T$, where τ_i is the torque from the traction and braking actuators. i is the wheel number starting at front left, front right, rear left, and rear right. $\delta_f = \delta_1 = \delta_2$ and $\delta_r = \delta_3 = \delta_4$ are the front and rear rack steering angle were the Ackermann angle is neglected. The mapping is realised by using a control effectiveness matrix $B \in R^{k \times m}$ which describes how each actuator can contribute to the global forces and moment by $v(t) \approx Bu(t)$. According to [3] the optimal control input u can be seen as two-step optimization problem, sequential least squares (sls),

$$u = \arg \underbrace{\min}_{u \in \Omega} \|W_u(u - u_{des})\|_p \tag{30}$$

$$\Omega = \arg \underbrace{\min}_{\underline{u} \le u \le \overline{u}} \|W_v(Bu - v)\|_p \tag{31}$$

where W_u and W_v are weighting matrices and u_{des} is the desired control input. The two step optimization problem is well suited for FCVs and HEVs. Eq. 31 constrains the possible set $u \in \Omega$ to only be u's that will be in nullspace of $N(Bu - v)$ or minimize the error of the desired forces, $Bu - v$, needed for fulfilling the desired motion of the vehicle. This can be seen as the vehicle motion controller. Eq. 30 minimizes the error of desired control input, $u_{des} - u$. The desired control input, u_{des}, coming from the energy management controller and the control law for steering, specifies how the electric motor(s) and the mechanical brakes should be used when optimizing onboard energy and desired vehicle steering. This can be seen as a smooth arbitration between energy management and vehicle motion control. Figure 1 shows how energy management is included in the control allocator and Fig. 3 shows how the control allocator fits in the control system in more detail. Numerically Eqs. 30- 31 can also be solved in one step, using weighted least squares (wls),

$$u = \arg \underbrace{\min}_{\underline{u} \le u \le \overline{u}} \|W_u(u - u_{des})\|_p + \gamma \|W_v(Bu - v)\|_p. \tag{32}$$

where $p = 2$. Setting the weighting parameter γ to a high value gives priority to minimize the error in motion $Bu - v$.

1) Actuator limits: The control allocator receives the limits from the motion related actuators, $[\underline{u}(t), \overline{u}(t)]$ and their limits in rate of change $[\underline{\rho}, \overline{\rho}]$. This specific way of designing the control system allows the control law to be independent of the available actuators, i.e. reusable for different hardware configurations, and also allows the control allocator to handle both limits and even actuator failure. The rate limits can be rewritten as position constraints using an approximation of the time derivative. The position constraints can now be written as

$$\overline{u}(t) = \min\left(\overline{u}(t), u(t - t_T) + t_T \overline{\rho}\right) \tag{33}$$

$$\underline{u}(t) = \max\left(\underline{u}(t), u(t - t_T) + t_T \underline{\rho}\right) \tag{34}$$

where t_T is the sampling time of the control allocator.

In a ground vehicle the limits of the control input must also consider the force limits of each wheel. The longitudinal force limit $F_{x,lim,i}$ is a function of the normal force $F_{z,i}$, tyre/road friction μ_i, and the amount of lateral force $F_{y,i}$ applied to the wheel. By estimating $F_{x,lim,i}$ for each wheel the actuator limits are adjusted for what the tyres can handle. The 'tyre fusion' basically checks if the electrical torque limits for the electric motors, $u_{el,lim,i}$, are above the longitudinal force limits and if so, adjusts the limits to be equal to the tyre force capacity. If the sum of electrical and mechanical torque limits $u_{el,mech,lim,i}$ are more than the tyre force limit, then the mechanical limits are set as the difference between the tyre force limit and the electrical limit. The idea is to always try to give the electric motors the possibility to act within the tyre's limits. In equation form this would look something like

$$\underline{u}_{\text{el},i} = \begin{cases} -\overline{F}_{x,i} R_w, & \text{if } \underline{u}_{\text{el},i} \le -\overline{F}_{x,i} R_w \\ \underline{u}_{\text{el},i}, & \text{else} \end{cases} \tag{35}$$

$$\overline{u}_{\text{mech},i} = 0 \tag{36}$$

$$\underline{u}_{\text{mech},i} = \begin{cases} 0, & \text{if } \underline{u}_{\text{el},i} \le -\overline{F}_{x,i} R_w \\ -\overline{F}_{x,i} R_w - \underline{u}_{\text{el},i}, & \text{elseif } (\underline{u}_{\text{el},i} + \underline{u}_{\text{mech},i}) \le -\overline{F}_{x,i} R_w \\ \underline{u}_{\text{mech},i}, & \text{else} \end{cases} \tag{37}$$

where $\underline{u}_{\text{el},i}$ and $\overline{u}_{\text{mech},i}$ are the tyre limits on electrical and mechanical braking torques. The traction torque limits are derived in similar manner. The steering angles are also limited by how much lateral force is still available when actual longitudinal force and its limits are considered.

2) Control Effectiveness matrix B: Here the idea is to linearize $g(x) \approx B$ where B is called the control effectiveness matrix. As mentioned earlier, the virtual control signals are the global forces. Under the assumption that there are no inertia effects in the driveline nor in the wheels, no weak drive shafts, no losses and no time delays or nonlinearities in developing tyre forces, a constant control effectiveness matrix can be formulated. The assumptions are realistic for the control design phase, i.e. the actuators are assumed to be fast. The matrix for the studied configuration becomes

$$B = \begin{bmatrix} \frac{r_{fg}}{R_w} & \frac{r_{fg}}{R_w} & \frac{r_{fg}}{R_w} & \frac{r_{fg}}{R_w} & \frac{1}{R_w} & \frac{1}{R_w} & \frac{1}{R_w} & \frac{1}{R_w} & 0 & 0 \\ 0 & 0 & 0 & 0 & 0 & 0 & 0 & 0 & 2C_\alpha & 2C_\alpha \\ \frac{r_{fg} b_t}{2R_w} & \frac{-r_{fg} b_t}{2R_w} & \frac{r_{fg} b_t}{2R_w} & \frac{-r_{fg} b_t}{2R_w} & \frac{b_t}{2R_w} & \frac{-b_t}{2R_w} & \frac{b_t}{2R_w} & \frac{-b_t}{2R_w} & 2L_f C_\alpha & -2L_r C_\alpha \end{bmatrix} \tag{38}$$

where r_{fg} is the final gear, R_w is the wheel radius, and b_t is the track width. The control effectiveness matrix B describes how the global forces of the vehicle can be generated by the available motion actuators. Observe how many ways the moment M_z, row 3 in B, can be generated which clearly illustrates the over actuation of the vehicle system.

3) Weight Scheduling of $W_u(v)$: Mechanical braking in conventional cars has a certain brake load distribution on the front and rear axles just to ensure vehicle stability during braking. If a vehicle have additional electric motors that will be used during regenerative braking they should also obey similar brake load distribution settings as the mechanical brakes. For example, if a vehicle have large electric motors mounted only on the rear wheels and they are solely used during braking to maximize the regenerative braking it will result in that all of the brake load is taken up on the rear wheels. This will lead to instability and if conditions rapidly change such as friction or in combination when turning. This would almost be an example of the classic 'use the parking brakes to turn' maneuver. For the configuration studied here, the use of electric motors are penalized in the rear more than for the front during braking as is described by

$$W_{u,brake} = \text{diag}[\ 0.1\ 0.1\ 0.3\ 0.3\ 0.5\ 0.5\ 1\ 1\ 1e3\ 2e3\ ]. \quad (39)$$

The opposite load force distribution of the electric motors is found to be desirable during traction to ensure vehicle stability, accordingly

$$W_{u,trac} = \text{diag}[\ 0.3\ 0.3\ 0.1\ 0.1\ 0.5\ 0.5\ 1\ 1\ 1e3\ 2e3\ ]. \quad (40)$$

To handle this efficiently in the control system, the following weight scheduling by linear interpolation of v_1 is suggested

$$W_{u,1,1} = W_{u,2,2} = 0.1, \text{ if } v_1 \leq 0 \quad (41)$$

$$W_{u,3,3} = W_{u,4,4} = 0.1 + \frac{0.3-0.1}{-1g}\frac{v_1}{mg}, \text{ if } v_1 \leq 0 \quad (42)$$

$$W_{u,1,1} = W_{u,2,2} = 0.1 + \frac{0.3-0.1}{1g}\frac{v_1}{mg}, \text{ if } v_1 \geq 0 \quad (43)$$

$$W_{u,3,3} = W_{u,4,4} = 0.1, \text{ if } v_1 \geq 0 \quad (44)$$

where v_1 is the desired longitudinal force, see also Fig. 3.

IV. SIMULATIONS

The selected test procedures are trying to come close to vehicle motion limits, and therefore lead to the fact that arbitration is needed in between the vehicle motion, energy management, and steering laws. The aim is to show that the arbitration is handled smoothly by the control allocator, see Eqs. 30, 31, and 32.

The vehicle system models are implemented as s-functions in Matlab/Simulink. The used control allocator, weighted least squares wls and sequential least squares sls with constraints solvers were coded by [3]. The code was modified by the authors to allow weight scheduling of Wu as a function of the desired virtual signals v and dynamical change in constraints u_{lim}.

A. Test procedures

The following two test procedures were selected for simulation:

TP-A: The purpose is to drive in a circle with a constant radius of 200 m on ice with friction 0.3. The initial velocity was set to 1 m/s. The vehicle is accelerated with 0.1g until 90 percent of the limiting velocity, $v_{lim} = \sqrt{\mu \cdot g \cdot R} = 24.26$ m/s, is reached. Then the velocity is kept constant for 5 s. The final part is braking with -0.1g until reaching 1 m/s as stop velocity. During the whole procedure the aim is to keep the driving circle radius constant.

TP-B: The purpose is to change the deceleration during straight braking on asphalt with friction 1.0. The initial velocity was set to 27.78 m/s. First part is soft braking with -0.1g until 80 km/h is reached then hard braking applied with -0.8g until 11.11 m/s is reached. The final part of the braking is performed again with -0.1g until standstill.

V. RESULTS

A. TP-A results

In Fig. 5 the reference velocities are compared with actual velocities for the sls solution. When 90 percent of the limiting velocity v_{lim} is reached one can see on the yaw rate that the vehicle becomes unstable and stays that way until the braking phase has started and reduced the velocity to about 12 m/s. The desired input signals u_{des} and actual input signals u for the wheel motors and front and rear steering are shown in Fig. 6. The input signals for the disc brakes are not shown because they are not used at all during this test procedure. It can be seen that both the front and rear steering is saturated when 90 percent of the limiting velocity is reached. The limits for the actuators in the plots does not only account for actuator limits but also the tyre force limits. The desired input signals u_{des} are smoothly followed by the wheel motors except for when the steering limits are reached in that time, about 20 s. Motors 1 and 3 then jump up and try to compensate for the loss of steering capability.

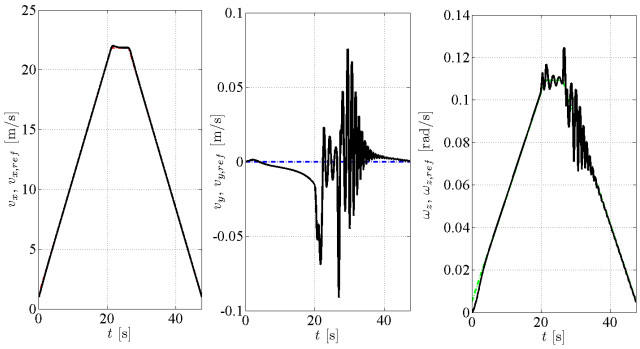

Fig. 5. Reference and actual longitudinal v_x, lateral v_y, and yaw ω_z velocity for sls solution for TP-A.

The constant radius on ice test procedure was used for a sensitivity analysis of the weighting parameter γ found in the wls solver, see Eq. 32 and also for comparing with the sls solver. The comparison was made by studying the least mean squares error, $mse = \frac{1}{n}\sum_{i=1}^{n} e(i)^2$, of the desired path compared with the actual states of the vehicle $e = r - x$, the least mean squares error for the desired motion actuator signals and the actual signals $e = u_{des} - u$. The results are shown in Table I. The wls solver is very robust and quite insensitive when the γ value is varied. When the γ value is varied between $1 \cdot 10^7$ and $1 \cdot 10^{-3}$ only small changes can be observed in results. However when it is lowered to

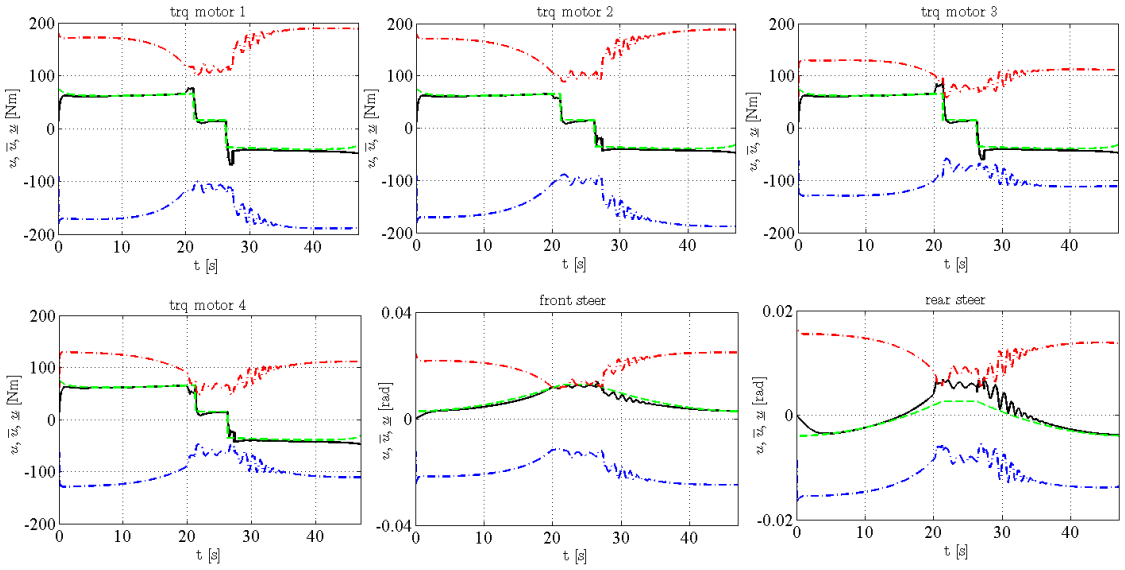

Fig. 6. Input set u and their limits u_{des} during TP-A. The black solid line corresponds to actual u, the dashed green line corresponds to desired u_{des}, and the dotted/dashed red and blue lines are the upper and lower combined limits, respectively.

$\gamma = 1 \cdot 10^{-4}$, both the path and actuator errors jumps. For this test procedure the sls solver outperformed the wls.

TABLE I

SENSITIVITY ANALYSIS OF γ FOR WLS AND COMPARISON WITH SLS FOR TP-A.

solver	γ	mse_{path}	mse_{act}
wls	$1 \cdot 10^{7}$	$7.887 \cdot 10^{-4}$	34.383
wls	$1 \cdot 10^{6}$	$7.882 \cdot 10^{-4}$	34.383
wls	$1 \cdot 10^{5}$	$7.880 \cdot 10^{-4}$	34.383
wls	$1 \cdot 10^{4}$	$7.880 \cdot 10^{-4}$	34.383
wls	$1 \cdot 10^{3}$	$7.881 \cdot 10^{-4}$	34.383
wls	$1 \cdot 10^{2}$	$7.888 \cdot 10^{-4}$	34.383
wls	$1 \cdot 10^{1}$	$7.887 \cdot 10^{-4}$	34.382
wls	$1 \cdot 10^{0}$	$7.871 \cdot 10^{-4}$	34.375
wls	$1 \cdot 10^{-1}$	$7.888 \cdot 10^{-4}$	34.288
wls	$1 \cdot 10^{-2}$	$8.068 \cdot 10^{-4}$	33.214
wls	$1 \cdot 10^{-3}$	$9.447 \cdot 10^{-4}$	26.823
wls	$1 \cdot 10^{-4}$	1.600	189.898
sls	-	$7.868 \cdot 10^{-4}$	21.218

B. TP-B results

The straight braking on asphalt test procedure is simulated both with the wls ($\gamma = 1 \cdot 10^{6}$) and sls solvers. Only small differences can be seen in the results when the least mean squares error is studied for the path and actuator signals. However, this time the wls solver turned out to be slightly better in both path and actuator signal errors.

The reference velocities and actual velocities for TP-B are shown in Fig. 7. One can see the fast response when the braking acceleration is increased from 0.1g to 0.8g. When the braking acceleration is reduced again to 0.1g, at about 7s, the actual longitudinal velocity slightly overshoots.

The desired and actual input signals for wheel motors and disc brakes are shown in Fig. 8. The steering input signals are neglected because no steering is needed in this test procedure. The overshoot in velocity is due to the fact that the rate limits of the mechanical disc brakes takes some time to release the brake pressure. This is however attempted to be compensated for by the wheel motors giving a positive torque at about 8s.

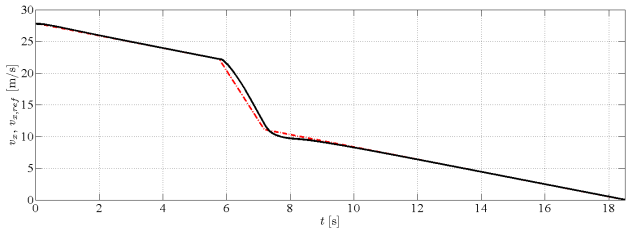

Fig. 7. Reference and actual longitudinal v_x velocity for wls solution for TP-B.

The desired input signals u_{des} from energy management for the wheel motors are smoothly followed whenever this is allowed by the combined limits and providing that the vehicle is following the desired path, see also Fig. 8. However, the desired input signals from energy management for the disc brakes were poorly followed and there are two major reasons for this. Firstly, the combined limits of the actuators and tyre forces did not allow for any other solution. Secondly the weight scheduling $Wu(v)$ requires more load force on front axle than on the rear axle during braking to achieve vehicle stability.

VI. CONCLUSIONS

This paper shows by modelling and simulation that the coordination of control laws for energy management, steering, and vehicle motion can be achieved smoothly by using

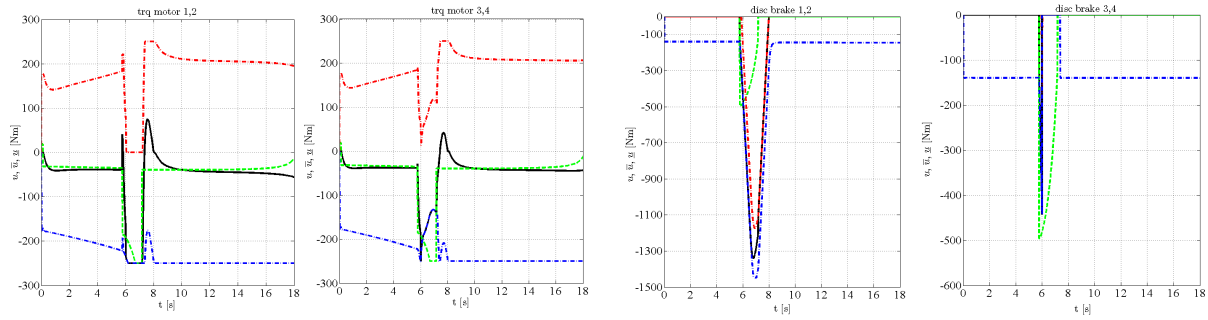

Fig. 8. Input set u for the wheel motors (left plots) and mechanical brakes (right plots) and their limits u_{des} during TP-B. The black solid line corresponds to actual u, the dashed green line corresponds to desired u_{des}, and the dotted/dashed red and blue lines are the upper and lower combined limits, respectively.

control allocation within the control system. Simulations show that whenever possible the desired input u_{des} from energy management and steering is followed. When needed, the actual input u is smoothly diverted to ensure vehicle stability and obey the combined limits of the actuators and tyre forces. The smooth coordination is essential for hybrid electric vehicles where energy management has a long time planning horizon and the vehicle motion controller has a shorter planning horizon.

VII. ACKNOWLEDGMENTS

Bengt Schmidtbauer, Professor Emeritus, is greatly acknowledged for his interest and guidance. The authors would also like to thank the Swedish national research programme Gröna Bilen.

REFERENCES

[1] A. Kimura, T. Abe, and S. Sasaki, "Drive force control of a parallel-series hybrid system," *Society of Automotive Engineers of Japan JSAE Rev. 20,pp. 337−341*, 1999.

[2] A. Emadi, S. Williamson, and A. Khaligh, "Power electronics intensive solutions for advanced electric, hybrid electric, and fuel cell vehicular power systems," *Power Electronics, IEEE Transactions on Vol. 21, Iss. 3, pp. 567−577*, 2006.

[3] O. Härkegård, "Backstepping and control allocation with applications to flight control," Ph.D. dissertation, Department of Electrical Engineering, Linköping University, SE–581 83 Linköping, Sweden, May 2003.

[4] T. Johansen, T. Fossen, and S. P. Berge, "Constrained nonlinear control allocation with singularity avoidance using sequential quadratic programming," *IEEE Transactions on Control Systems Technology, vol. 12, no. 1*, 2004.

[5] T. Johansen, T. Fuglseth, P. Tøndel, and T. I. Fossen, "Optimal constrained control allocation in marine surface vessels with rudders," in *IFAC Conf. Manoeuvring and Control of Marine Craft*, Girona, 2003.

[6] P. Tøndel and T. A. Johansen, "Control allocation for yaw stabilization in automotive vehicles using multiparametric nonlinear programming," in *Proc. of American Control Conf.*, Portland, OR, June 2005.

[7] J. Plumlee, D. Bevly, and A. Hodel, "Control of a ground vehicle using quadratic programming based control allocation techniques," in *Proc. of American Control Conf.*, Boston, MA, July 2004.

[8] J. Plumlee, *Mult-Input Ground Vehicle Control Using Quadratic Programming Based Control Allocation*. Master thesis report, Auburn University, Alabama, 2004.

[9] J. Andreasson, L. Laine, and J. Fredriksson, "Evaluation of a generic vehicle motion control architecture," in *The Fédération Internationale des Sociétés d'Ingénieurs des Techniques de l'Automobile (FISITA)*, Barcelona, Spain, May 2004.

[10] J. Fredriksson, J. Andreasson, and L. Laine, "Wheel force distribution for improved handling in a hybrid electric vehicle using nonlinear control," in *Proceedings of 43rd IEEE Conference on Decision and Control*, Bahamas, December 2004.

[11] SAE, "Surface vehicle recommended practice, vehicle dynamics terminology," *SAE 1976-07, J670e*, 1976.

[12] H. B. Pacejka, *Tyre And Vehicle Dynamics 2nd edition*. Butterworth-Heinemann, 2002.

[13] M. Schenck, J.-S. Lai, and K. Stanton, "Fuel cell and power conditioning system interaction," in *Applied Power Electronics Conference and Exposition, APEC 2005, 20th Annual Conference of IEEE*, March 2005.

[14] J. Marshall and M. Kazerani, "Design of an efficient fuel cell vehicle drivetrain, featuring a novel boost converter," in *Industrial Electronics Society, IECON 2005, 32nd Annual Conference of IEEE*, November 2005.

[15] R. Spotnitz, "Advanced ev and hev batteries," in *Vehicle Power and Propulsion, 2005 IEEE Conference*, Sept. 2005.

[16] H. Khalil, *Nonlinear Systems, 3rd edition*. Prentice Hall Inc., 2002.

[17] K. Åström and T. Hägglund, *PID Controllers: Theory, Design, and Tuning*. Instrument Society of America, 1995.

[18] J. Schiffer, O. Bohlen, R. D. Doncker, D. U. Sauer, and K. Ahn, "Optimized energy management for fuelcell-supercap hybrid electric vehicles," in *Vehicle Power and Propulsion, 2005 IEEE Conference*, Sept. 2005.

Paper VII

Control Allocation based Electronic Stability Control System for a Conventional Road Vehicle

Submitted to

the 10th International IEEE Conference on Intelligent Transportation Systems (ITSC'07), Seattle, WA, October 2007.

Control Allocation based Electronic Stability Control System for a Conventional Road Vehicle

Leo Laine and Johan Andreasson

Abstract— **This paper shows how control allocation with an optimization formulation can be used as an electronic stability control system for a conventional road vehicle. Control allocation is used in systems with more actuators than the degrees of freedom controlled, which are also known as over-actuated systems. Here it is assumed that the steering is solely managed by the driver. The control allocator uses the combustion engine and the four mechanical disc brakes to compensate any understeering or oversteering behaviour. Simulations showed that the suggested control system passed the proposed test procedure for Electronic Stability Control systems, sine with dwell, suggested by the National Highway Traffic Safety Administration (NHTSA).**

I. INTRODUCTION

Electronic Stability Control (ESC) systems have been shown to be extremely efficient in preventing single vehicle loss of control crashes [1]-[2]. ESC helps the driver to keep the vehicle on the road and therefore prevents road run off crashes, of which a significant amount are rollover crashes [1]-[2]. ESC is proposed to become a new Federal Motor Vehicle Safety Standard (FMVSS) in the USA for all light vehicles[1] from September 1, 2011 [1]-[2]. The National Highway Traffic Safety Administration (NHTSA) believes that the level of life saving associated with ESC is only outperformed by seatbelts out of all the equipment and elements included under FMVSS [1]. NHTSA estimates, from US crash data, that ESC will reduce single vehicle car crashes of passenger cars by 34 percent and single vehicle crashes of Sport Utility Vehicles (SUVs) by 59 percent, including a much greater reduction of rollover crashes [1]. NHTSA also estimates that ESC has the potential for preventing single vehicle rollover crashes by 71 and 84 percent of passenger cars and SUVs, respectively [1]. The vast majority of all real life roll over crashes occur when a vehicle runs off the road and strikes a tripping mechanism such as soft soil, a ditch, a curb or a guardrail [1]. The ESC system can indirectly prevent exposure to off-road tripping mechanisms by assisting the driver in keeping the vehicle on the road during loss of control situations [1], see also Fig 1. The new proposed FMVSS for ESC will be gradually introduced to the market. On September 1, 2008 30 percent of newly produced light vehicles must be equipped with ESC. By September 1, 2009 the percentage will increase to 60 percent, and again by September 1, 2010 to 90 percent [1]. About 29 percent of the sold light vehicles in the USA with a model year of 2006 were equipped with ESC [1]. So even without the proposed FMVSS, vehicle manufacturers are already aiming to increase the number of vehicles equipped with ESC [1].

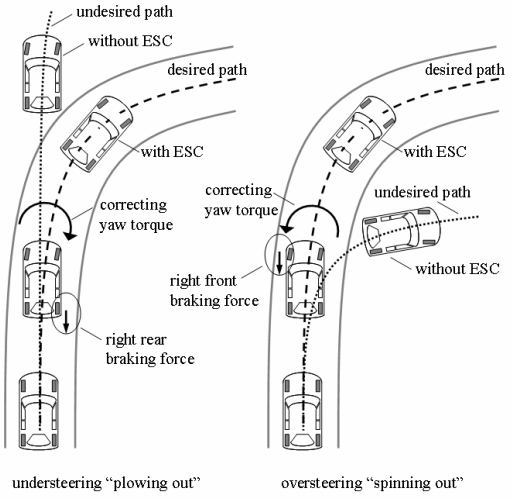

Fig. 1. Illustration of how conventional ESC systems work during understeering and oversteering situations.

This paper is a continuation of a project investigating control design for over-actuated road vehicle systems such as hybrid electric vehicles. An over-actuated system has more motion actuators than the number of motions controlled. Earlier papers in this project have shown how different road vehicle configurations could have the same control law for longitudinal-, lateral-, and yaw-motion by separating the control law for motion from the distribution among the available motion actuators, [3], [4], [5]. The distribution was made by control allocation which provides automatic redistribution when one actuator saturates in position or in rate. The idea with the suggested control system is that it not only solves future vehicle configurations with increased number of motion actuators, but it can also replace the conventional ESC system. The aim of this paper is to show, by simulation, that control allocation can be used as an ESC according to the proposed FMVSS for a conventional road vehicle which is configured with four mechanical brakes and is front wheel driven by a combustion engine. This gives a total of five motion actuators for the control allocator to use

This work is supported by the Swedish national research programme Gröna Bilen/FCHEV. Gröna Bilen is financed by Swedish automotive industry and the Swedish research foundation Vinnova.

L. Laine is with the Department of Applied Mechanics, Div. of Vehicle Safety and Vehicle Dynamics, Chalmers University of Technology, SE-412 96 GÖTEBORG, Sweden, leo.laine@chalmers.se

J. Andreasson is with MODELON AB, Ideon Science Park, SE-22370 LUND, Sweden johan.andreasson@modelon.se

[1]Passenger cars, multipurpose vehicles, trucks, and buses with a gross vehicle weight up to 4536 kg (10000 lbs)

to achieve the desired ground motion.

The outline of the paper is as follows: Section I-A gives a background both on ESC systems and on using control allocation within the control system. Section II explains how the vehicle system was modelled. Section III describes the control design. Section IV and V explain the simulated test procedure, sine with dwell, proposed by FMVSS for ESC and provide the results. Finally, Section VI contains the concluding remarks.

A. Background

The main purpose of ESC is to assist the driver in loss of control situations. ESC is a closed loop algorithm that can use the mechanical brakes individually to apply a correcting yaw torque to keep the vehicle on its desired path. Fig. 1 illustrates two different ESC path correction scenarios. The first is an understeering scenario where the vehicle without ESC is 'plowing out' off the road. If the vehicle is equipped with ESC, a correcting yaw torque is applied by using the right rear brake. This makes the vehicle less understeered and therefore keeps the vehicle on the road and following the desired path. The second is an oversteering scenario in which the vehicle without ESC 'spins out' during the right hand curve. In the vehicle with ESC, a correcting yaw torque is applied by using the front left brake. This reduces oversteering and allows the vehicle to follow the desired path. Vehicles equipped with ESC measure the vehicle's longitudinal velocity and lateral acceleration and compute the radius of the desired paths circle. Since it knows the radius and longitudinal velocity it can therefore calculate the correct yaw rate. This calculated yaw rate is compared with the measured yaw rate from a sensor. When the calculated and measured yaw rates start to diverge the vehicle is determined to be losing control. A vehicle without ESC would start to experience loss of control by understeering or oversteering. The ESC system counteracts this by applying a correcting yaw torque with the mechanical brakes.

Road vehicles, such as those that are equipped with ESC, can be viewed as over-actuated systems. One promising way to manage the coordination of over-actuated systems is through to the use of control allocation. Control allocation addresses the distribution of control demand within an available set of actuators. This is posed as a constrained optimization problem which provides an automatic redistribution of the control effort when one actuator saturates in position or in rate. Control allocation has been used successfully both in flight applications, see [6], and also in marine vessels, see [7] and [8]. Most importantly, however, control allocation has also been used for achieving yaw stabilization, see [9], [10] and [11]. In these articles the mechanical brakes and steering were in focus without direct consideration to the actuator limits. In earlier work by the authors, [3] and [4], it was shown how control systems can be made reusable for different vehicle configurations when the control law is separated from the control allocation for achieving the vehicle motion. Actuator position and rate of change limits in combination with tyre force limits were considered as constraints for the control allocator. In [5] the authors showed by modelling and simulation that the smooth coordination of the control laws for energy management, steering, and vehicle motion can be achieved by using control allocation within the control system for a series hybrid vehicle which was wheel motored and front and rear steered by wire. In this paper we actually take a step back to show that the same control allocation method that has been shown to be successful for highly over-actuated vehicles, could first be used and implemented as an ESC system for conventional vehicles. Then if the number of motion actuators increase in future vehicle configurations, due to hybridization and/or steer by wire, the control system is easily upgraded as shown in earlier papers [3], [4], and [4].

In this paper we have separated the control law for vehicle motion and the control allocation of the actuators within the control system, as shown in Fig.2. The vehicle motion controller calculates the desired path $r = \begin{bmatrix} v_x & v_y & \omega_z \end{bmatrix}^T$ within the driver interpreter and then the path controller tries to keep the desired path by correcting the global forces and yaw torque $v = \begin{bmatrix} F_x & F_y & M_z \end{bmatrix}^T$. The correcting v are then distributed by the control allocator onto the available motion actuators, $v \mapsto u$ where $u = \begin{bmatrix} \tau_{ice} & \tau_{mb1} & \tau_{mb2} & \tau_{mb3} & \tau_{mb4} \end{bmatrix}^T$ and $\text{rank}(v) < \text{rank}(u)$. This conventional front wheel driven vehicle has five motion actuators as illustrated in Fig 2. In this configuration the driver is solely managing the steering input of the vehicle system, which is what most current model year configurations have today.

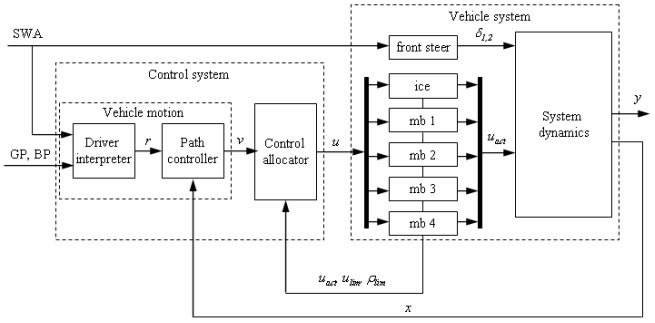

Fig. 2. Illustration of how control allocation is suggested to be used within the control system for a conventional road vehicle. Used abbreviations in illustration: Steering Wheel Angle(SWA), Brake Pedal (BP), Gas Pedal (GP), internal combustion engine (ice), and mechanical brakes (mb).

II. SYSTEM MODELLING

The system modelling is separated into three parts:

A. Chassis including tyre dynamics

Two different chassis models were used in the analysis to make a more objective evaluation of the suggested control allocation based ESC system. One model was developed in [3] and the other one is a commercially available chassis model Vehicle Dynamics Library. The used chassis parameters are comparable to a medium sized sedan car.

- Ch.A Home made chassis model
  This chassis model is a so-called two track model

which has five degree of freedom: longitudinal-, lateral-, yaw-, roll-, and pitch motion. The aim of the model is to be capable of predicting the chassis dynamics on flat surfaces. The SAE standard [12] provided the main guidance for defining the axis orientations. A brush tyre model [13] was used together with dynamic relaxation to describe the tyre dynamics. Details about the modelling and used chassis parameters can be found in [3].

- Ch.B The VehicleDynamics Library
  The planar chassis model is defined with additional degrees of freedom for roll, pitch and vertical motion that also specify the suspension compression giving a total of 12 states for the chassis motion. Thanks to the wheel's lack of vertical dynamics, the fidelity can still be kept low. Additionally, there is one degree of freedom per wheel rotation and one for the steering elasticity. The tyre model is a version of the MagicFormula as specified in [13]. It is a curve fit that considers combined-slip, camber, load dependencies and first-order transient effects. More details are found in [14].

B. Drivetrain

The drivetrain includes the most important time specific constants such as the inertia of the wheels and elastic drive shafts. The combustion engine propels the front wheels by a transmission connected to the drive shafts through an open differential. Losses in drag from the combustion engine and transmission are included. More details and used parameters can be found in [3].

C. Motion actuator dynamics

Each wheel has individually controlled disc brakes. The hydraulic pressure in the brake system was modelled as a first order system. The friction between brake pad and disc, $\mu_{mb,i}(T_i)$, was expressed as being temperature dependent. The temperature was calculated by a thermal lumped mass model. The temperature constrained the actual limits of the brakes as

$$\underline{u}_{\mathrm{mb},i}(T_i) \leq u_{\mathrm{mb},i} \leq \overline{u}_{\mathrm{mb},i}(T_i) \tag{1}$$

which means that when brake fading occurs in the braking system it can be accounted for as an actuator constraint in the control allocator. The limits in rate of change are simply a function of the time constant of the first order system.

The combustion engine's mean torque was modelled by a non-linear second order system, due to the fact that it takes approximately two crank shaft turns to reach the next stationary torque for a four cylinder four stroke engine [15]. The limits in torque are dependent on the angular speed of the engine accordingly

$$\underline{u}_{\mathrm{ice}}(\omega_i) \leq u_{\mathrm{ice}} \leq \overline{u}_{\mathrm{ice}}(\omega_i) \tag{2}$$

The rate limits for the combustion engine can be determined using an equivalent time constant definition for second order systems as described in [16]. A detailed description of the modelling and used parameters of the motion actuators can be found in [3].

III. CONTROL DESIGN

Independently of the specific applications studied, a class of nonlinear systems can be described in the affine form

$$\dot{x} = f(x) + g(x)u \tag{3}$$
$$y = h(x) \tag{4}$$

Control allocation can be applied if the control input can be perturbed without affecting the system dynamics. The system can therefore be rewritten as

$$\dot{x} = f(x) + v \tag{5}$$
$$y = h(x) \tag{6}$$

where $v = g(x)u$, v is also called the virtual control input. The control design is divided into two steps. The first step is to design a control law that controls the net effort v. The second step is to design a control allocator that maps the net effort of virtual control input to true control input, $v(t) \mapsto u(t)$. Unfortunately, the mapping of the net effort to the true control signal is complicated since the $g(x)$-matrix is not invertible. Using a pseudo-inverse to find a solution could be one way of solving this. However, this could lead to unrealistic solutions since the true control signals are limited by several different constraints. Instead a constrained optimization problem is proposed and solved.

The longitudinal tyre forces $F_{x,i}$ which are directly affected by the motion actuators, combustion engine and mechanical brakes are easily split into the desired affine form and are found within $g(x)u$. Due to the fact that steering is excluded from the input that is controlled by the control allocator, see Fig.2, the lateral forces are only seen as part of the nonlinear system $f(x)$. The chassis system can then be written as

$$M\dot{x} = f(x) + g(x)u \tag{7}$$
$$y = h(x) \tag{8}$$

where M is the mass matrix

$$M = \begin{bmatrix} m & 0 & 0 \\ 0 & m & 0 \\ 0 & 0 & I_z \end{bmatrix}$$

and

$$f(x) = \begin{bmatrix} mx_2x_3 - D_1x_1 - D_2m\mathrm{sgn}(x_1)x_1^2 \\ -mx_1x_3 + C_\alpha\left(\sum_{i=1}^{2}\delta_i - \frac{8x_1(2x_2+(L_f-L_r)x_3)}{4x_1^2-b_t^2x_3^2}\right) \\ L_fC_\alpha\left(\sum_{i=1}^{2}\delta_i + \frac{8x_1(2x_2+L_fx_3)}{4x_1^2-b_tx_3^2}\right) + L_rC_\alpha\frac{8x_1(2x_2-L_rx_3)}{4x_1^2-b_tx_3^2} \end{bmatrix} \tag{9}$$

$$g(x)u = \begin{bmatrix} \sum_{i=1}^{4}F_{x,i} \\ 0 \\ \frac{b_t}{2}\sum_{i=3}^{4}(-1)^{1+i}F_{x,i} \end{bmatrix} \tag{10}$$

$$h(x) = \begin{bmatrix} x_1 & x_2 & x_3 \end{bmatrix}^T \tag{11}$$

where b_t is front and rear track width, D_1 and D_2 are constants related to aerodynamical and rolling resistance,

and δ_1, δ_2 are the front left and front right steering angles, respectively. Since the mass matrix M is invertible, the system can be written in the desired affine form. Furthermore, the vehicle system model presented is general and independent of the powertrain configuration. However, in this configuration the steering is excluded from $g(x)u$ due to that the driver is directly controlling it. In earlier works [3]-[4] contain information on how the system could be described in affine form when the steering is assumed to be steer by wire and thus included in the control allocator formulation.

A. Vehicle Motion

The first step in designing the control system is to design the control law for vehicle motion as illustrated in Fig. 2. Here the vehicle motion is separated into two parts, the driver interpreter and path controller. This is necessary because the driver input Steering Wheel Angle (SWA) is basically predefined by the test procedure, sine with dwell, which is used in the proposed FMVSS for ESC [1], [2], [17].

1) Control law for driver interpreter: The purpose of a driver interpreter is to use the driver's input to define the desired path $r = \begin{bmatrix} v_x & v_y & \omega_z \end{bmatrix}^T$, see also Fig. 3. This driver interpreter is made only sufficient enough to be able to handle the proposed test procedure, sine with dwell, of FMVSS for ESC. In the test procedure the vehicle coasts in high gear at an initial speed of 80 km/h when the steering input of Steering Wheel Angle (SWA) starts. No braking is applied by the driver during the entire manoeuvre. This means that the driver interpreter must be designed to handle what should be done when both the Gas Pedal (GP) and Brake Pedal (BP) are equal to zero, i.e. coasting. Here the following control law is suggested for the longitudinal velocity v_x:

$$r_1 = v_x(k+1) = \begin{cases} v_x(k) - 0.1g\Delta t, \text{ if } v_x \geq 0 \\ 0, \text{ else} \end{cases} \tag{12}$$

where $\Delta t = t(k+1) - t(k)$. A linear bicycle model is used to predict desired lateral velocity v_y and yaw rate ω_z. The bicycle model is defined as follows

$$\dot{x} = Ax + Bu \tag{13}$$

$$A = -\begin{bmatrix} \frac{C_{\alpha_f} + C_{\alpha_r}}{mv_x} & v_x + \frac{L_f C_{\alpha_f} - L_r C_{\alpha_r}}{mv_x} \\ \frac{L_f C_{\alpha_f} - L_r C_{\alpha_r}}{I_z v_x} & \frac{L_f^2 C_{\alpha_f} + L_r^2 C_{\alpha_r}}{I_z v_x} \end{bmatrix} \tag{14}$$

$$B = \begin{bmatrix} \frac{C_{\alpha_f}}{m} & \frac{C_{\alpha_r}}{m} \\ \frac{L_f C_{\alpha_f}}{I_z} & -\frac{L_r C_{\alpha_r}}{I_z} \end{bmatrix} \tag{15}$$

where $x = \begin{bmatrix} v_y & \omega_z \end{bmatrix}$ and $u = \begin{bmatrix} \delta_f & \delta_r \end{bmatrix}$. By calculating the state x we can predict a desired yaw rate motion which the driver defines by his steering input δ_f. This works fine as long as the input u is in the linear regime. Therefore the desired yaw rate calculated by the bicycle model also needs to be limited by what is physically possible due to the maximum centripetal force for the specific road/tyre friction. We know the desired lateral acceleration from the bicycle model $a_y(k)$ and the desired vehicle velocity $v_x(k)$. From these we can calculate the radius R of the desired path by setting the global lateral force equal to centripetal force:

$$F_y = F_{centripetal} \Leftrightarrow \min\left(\mu mg, \left|ma_y\right|\right) = \frac{m \cdot v_x^2}{R}$$

$$R = \frac{v_x^2}{\min\left(\mu g, \left|a_y\right|\right)} \text{ [m], if } a_y \neq 0 \tag{16}$$

where the lateral force F_y is limited by frictional force μmg. When $a_y(k) \approx 0$ then R is set to be 'Inf' in Matlab. Now we can define the desired yaw rate as

$$r_3 = \omega_z(k+1) = \begin{cases} \text{sgn}(x_2)\min\left(\left|\frac{v_x(k)}{R(k)}\right|, |x_2|\right), \text{ if } R \neq 0 \\ 0, \text{ else} \end{cases} \tag{17}$$

where x_2 is the desired yaw rate from the bicycle model Eq. 13. The desired lateral velocity v_y is of minor importance due to that it can't directly be affected by the motion actuators used by the control allocator, see Eq. 10 where row 2 is equal to zero.

2) Control law for path controller: The purpose of the vehicle motion controller and its path controller is to follow a desired path. The path controller could be based on feedback linearization, see e.g. [18]. The idea with feedback linearization is to transform the nonlinear system into a linear one, so that linear techniques can be used. In its simplest form it can be seen as a way to cancel the nonlinearities by a nonlinear state feedback. Looking at the system, we notice that the first term on the right hand side of Eq. 7 is the only one including the nonlinearities of the system. If the nonlinear term, $f(x)$, is cancelled, the multi-input, multi-output (MIMO)-system becomes linear. Furthermore, by cancelling $f(x)$ the MIMO-system becomes decoupled. Then, using a PI-controller, the control law becomes:

$$v = -f(x) + K_p e + K_i \int_0^t e d\tau \tag{18}$$

where $e = r - y_2$ is the error between the desired vehicle motion and the vehicles actual motion, see also Fig. 3. However, it has shown to be unnecessary in the current road vehicle application to cancel the nonlinear term $f(x)$, because the term is basically stabilizing the vehicle. In the simulations $f(x)$ is set to be equal to zero in Eq. 18.

The following design parameters for the PI-controllers, K_p and K_i, gives adequate path control even for the worst case of SWA demanded by the test procedure

$$K_i = 5\begin{bmatrix} 1.0m & 0 & 0 \\ 0 & 0 & 0 \\ 0 & 0 & 30I_z \end{bmatrix} \tag{19}$$

$$K_p = 8m\sqrt{\frac{K_i}{m}}. \tag{20}$$

To handle the saturation of actuators the PI-controllers were extended with anti-windup based on back calculation [19]. When the actuators are not saturated the error $e_s = Bu - v$ will be zero and therefore there is no effect on the

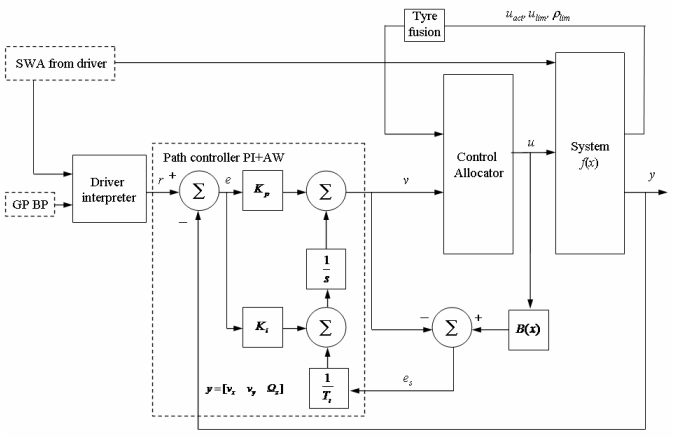

Fig. 3. Illustration of the Control Design with a focus on control law for vehicle motion and its path controller, a PI controller with Anti-Windup strategy. Used abbreviations in the illustration: Gas Pedal(GP), Brake Pedal (BP), and Steering Wheel Angle (SWA).

sum of integrator gain, see also Fig. 3. The windup was minimized with $\frac{1}{T_t} = 20\text{diag}\begin{bmatrix} 1 & 0 & 1 \end{bmatrix}$.

B. Control Allocation

The second step in the control design is to create the control allocator. The key issue is how to select the control input set u from all possible combinations. In control allocation an optimization based selection is used. According to [6] the optimal control input u can be seen as a two-step optimization problem, sequential least square (sls),

$$u = \arg\underbrace{\min_{u\in\Omega}} \|W_u(u-u_{des})\|_p \tag{21}$$

$$\Omega = \arg\underbrace{\min_{\underline{u}\le u\le\overline{u}}} \|W_v(Bu-v)\|_p \tag{22}$$

where W_u and W_v are weighting matrices and u_{des} is the desired control input. In the two step optimization problem Eq. 22 constrains the possible set $u \in \Omega$ to be u's in the nullspace of $N(Bu-v)$ or minimizes the error of the desired global forces, $Bu-v$, needed for fulfilling the desired motion of the vehicle. This can be seen as the vehicle motion controller. Eq. 21 minimizes the error of desired control input, $u_{des}-u$. Here, in this paper we use a zero vector for the desired input $u_{des} = 0_{5\text{x}1}$ which means that the motion actuators are optimized to be used as little as possible.

The used control allocation optimization also suits well for fuel cell vehicles and hybrid electric vehicles. Eq.21 can be seen as smooth arbitration between the vehicle motion controller and energy management. The desired input u_{des} coming from the energy management controller specifies how the electric motor(s) and the mechanical brakes should be used when optimizing the use of onboard energy, see [5].

Numerically Eqs. 21- 22 can also be solved in one step, using weighted least square (wls),

$$u = \arg\underbrace{\min_{\underline{u}\le u\le\overline{u}}} \|W_u(u-u_{des})\|_p + \gamma\|W_v(Bu-v)\|_p. \tag{23}$$

where $p = 2$. Setting the weighting parameter γ to a high value gives priority to minimizing the error in motion $Bu-v$.

1) Actuator limits: The control allocator receives the limits from the motion related actuators, $[\underline{u}(t), \overline{u}(t)]$ and their limits in rate of change $[\underline{\rho}, \overline{\rho}]$. This specific way of designing the control system allows the control law to be independent of the available actuators, i.e. reusable for different hardware configurations, and also allows the control allocator to handle both limits and even actuator failure. The rate limits can be rewritten as position constraints using an approximation of the time derivative. The position constraints can now be written as

$$\overline{u}(t) = \min(\overline{u}(t), u(t-t_T) + t_T\overline{\rho}) \tag{24}$$

$$\underline{u}(t) = \max(\underline{u}(t), u(t-t_T) + t_T\underline{\rho}) \tag{25}$$

where t_T is the sampling time.

In a road vehicle the limits of the control input must also consider the force limits of each wheel. The longitudinal force limit $F_{x,lim,i}$ is a function of the normal force $F_{z,i}$, tyre/road friction μ_i, and the amount of lateral force $F_{y,i}$ applied to the wheel. By estimating $\overline{F}_{x,i}$ for each wheel the actuator limits are adjusted for what the tyres can handle. The 'tyre fusion' basically checks if the torque limits for the mechanical brakes, $\overline{u}_{mb,i}$, are above the longitudinal force limits and if so, adjusts the limits to be equal to the tyre force capacity. In equation form this would look something like

$$\overline{u}_{\text{mb},i} = 0 \tag{26}$$

$$\underline{u}_{\text{mb},i} = \begin{cases} -\overline{F}_{x,i}R_w, & \text{if } \underline{u}_{\text{mb},i} \le -\overline{F}_{x,i}R_w \\ \underline{u}_{\text{mb},i}, & \text{else.} \end{cases} \tag{27}$$

The traction torque limits are derived in similar manner. The steering angles are also limited by how much lateral force is still available when actual longitudinal force and its limits are considered. A more detailed description of how combinations of electric motors, combustion engine, and mechanical brakes are handled by tyre fusion is found in [5].

2) Control Effectiveness matrix B: Here the idea is to linearize $g(x) \approx B$ where B is called the control effectiveness matrix. As mentioned earlier, the virtual control signals are the global forces. Looking at the model (Eqs. 9-8) the control signals are the longitudinal wheel forces $F_{x,i}$. The wheel forces are controlled by the motion actuators via the driveline. The following control input signals exist for the studied configuration:

$$u = \begin{bmatrix} \tau_{ice} & \tau_{mb_1} & \tau_{mb_2} & \tau_{mb_3} & \tau_{mb_4} \end{bmatrix}^T \tag{28}$$

where τ_i is the torque from the traction and braking actuators. i corresponds to the wheel number starting with front left, front right, rear right, and rear left.

Under the assumption that there are no inertia effects in the driveline nor in the wheels, no weak drive shafts, no losses and no time delays or nonlinearities in developing tyre forces, a constant control effectiveness matrix can be formulated. The assumptions are realistic for the control design phase, i.e. the actuators are assumed to be fast. The matrix for the studied configuration becomes

$$B = \begin{bmatrix} \frac{r_i r_{fgf}}{R_w} & \frac{1}{R_w} & \frac{1}{R_w} & \frac{1}{R_w} & \frac{1}{R_w} \\ 0 & 0 & 0 & 0 & 0 \\ 0 & \frac{b_t}{2R_w} & \frac{-b_t}{2R_w} & \frac{b_t}{2R_w} & \frac{-b_t}{2R_w} \end{bmatrix} \tag{29}$$

where r_i is the actual gear in transmission, r_{fg} is the final gear, R_w is the wheel radius, and b_t is the track width. The control effectiveness matrix B describes how the global forces of the vehicle can be generated by the available motion actuators. The longitudinal global force $v_1 = F_x$, row 1 in B, can be generated by all five motion actuators and the lateral force $v_2 = F_y$, row 2 in B, by non. Finally the yaw torque $v_3 = M_z$, row 3 in B, can be generated by the mechanical brakes individually. The combustion engine is mounted on an open differential and thus cannot apply any yaw torque ($F_{x,1} = F_{x,2}$).

3) Weight matrices W_u and W_v: Earlier work stated the importance of prioritizing correctly among the available actuators during braking and acceleration [3]-[5]. For the configuration studied here we need to penalize the use of mechanical brakes in the rear more than the front during braking to have a decent brake load distribution on the front and rear axles. Here the following weighting matrices are used

$$W_u = \text{diag}[\ 1\ 0.5\ 0.5\ 1\ 1\ ] \tag{30}$$

$$W_v = \text{diag}[\ 1\ 1\ 1\ ]. \tag{31}$$

IV. SIMULATIONS

The vehicle system models were implemented as s-functions in Matlab/Simulink. The used control allocator, weighted least square wls and sequential least square sls with constraints solvers were coded by [6]. The code was modified by the author to allow for dynamical change in constraints u_{lim} and ρ_{lim}.

A. Test procedure sine with dwell

Sine with dwell is a proposed test procedure that aims to become a standard in evaluating commercial road vehicles equipped with ESC systems [1], [17]. The test procedure is designed to trigger oversteering in the vehicle on dry asphalt. Even though ESC can prevent both understeering and oversteering behaviours no general test procedure is proposed for understeering. This is due to the fact that vehicles with high centre of gravity are made understeered in order to avoid untripped[2] rollover. Roll stability control systems actually work by introducing understeering when the roll angle of the vehicle becomes critical, which is opposite to the ESC. An understeered test procedure for ESC that could work for all light vehicles is an ongoing research topic for NHTSA [1].

The test procedure is performed as follows. First the $\delta_{\text{SWA},0.3g}$ input that gives 0.3g in lateral acceleration is derived for the studied vehicle by an initial test, slowly increasing steering. The steering is increased with a ramp rate of 13.5 deg/s. The speed is kept constant at 80 km/h. The main test procedure, sine with dwell, is started by letting the vehicle coast in high gear and an initial velocity of 80 km/h when the SWA input is given, see Fig. 4. The first SWA amplitude is set to be $1.5\delta_{\text{SWA},0.3g}$ and increased stepwise by $0.5\delta_{\text{SWA},0.3g}$ until $6.5\delta_{\text{SWA},0.3g}$ or 270 degrees is reached which ever is greatest.

[2]No tripping mechanism is needed for rollover on flat road.

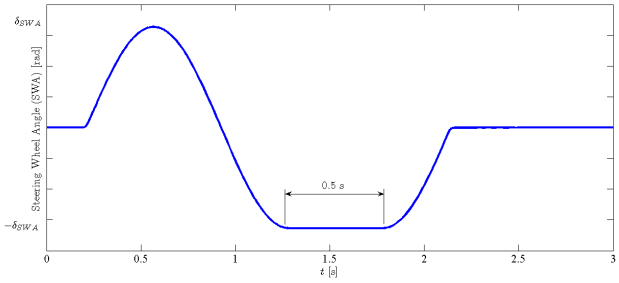

Fig. 4. Steering Wheel Angle (SWA) input as a sine with dwell with frequency 0.7 Hz and amplitude δ_{SWA}. The dwell is 0.5s and occurs after $3/4$ of the period.

The performance of the ESC is measured by criteria its stability and responsiveness criteria. The stability criteria verifies that the yaw rate should have reduced to 35 and 20 percent of its maximum value after 1 s and 1.75 s respectively, after Completion of Steer (CoS) input:

$$\frac{\omega_z(t_{CoS} = 1.0)}{\omega_{z,max}} \leq 0.35 \tag{32}$$

$$\frac{\omega_z(t_{CoS} = 1.75)}{\omega_{z,max}} \leq 0.2. \tag{33}$$

An highly understeered vehicle would more easily meet this stability criteria without having any responsiveness. Therefore a responsiveness criteria is also defined, which basically states that the vehicle should have a minimum lateral displacement during the test. Because this is a test for all light vehicles the test needs to be adjusted so that all vehicles can achieve the criteria. According to NHTSA the least responsive vehicles were not large pickup trucks nor 15-passenger vans, instead it was SUVs equipped with roll stability control [1]. The highest responsiveness criteria that could be used to allow roll stability control implementation was a minimum lateral displacement of 1.83m, half a 12 foot lane width. This minimum lateral displacement should be achieved 1.07 s after SWA input initiation

$$d_y(t = 1.07) \geq 1.83 \tag{34}$$

V. RESULTS

Slowly increasing steer showed that the steering needed for achieving 0.3g in lateral acceleration was $\delta_{\text{SWA},0.3g}$ =25 degrees. Steer gear ratio was set to be 16.6. The steering input sine with dwell was started at simulation time 0.2 s for chassis Ch.A and at 2.0 s for Ch.B. The amplitude was increased from $1.5\delta_{\text{SWA},0.3g}$ in steps of $0.5\delta_{\text{SWA},0.3g}$ up to 270 degrees. The ESC system was turned both off and on to study how far the vehicle could work without ESC. Fig. 5 illustrates the yaw rate, lateral acceleration, and side slip of the vehicle when chassis Ch.A was used, see Sect. II-A. Already at a SWA of 75 degrees one of the stability criteria's

were not met when ESC was turned off, see also Tab. I. When SWA was increased to 87.5 the vehicle without ESC is out of control. This can be clearly seen in Fig. 5 by the almost constant yaw rate and lateral acceleration after 2 s. However, when ESC is enabled much higher SWA amplitudes can be used without violating the stability criteria. In Fig. 6 the yaw rate, lateral acceleration, and side slip are shown for chassis Ch.A with ESC on. The SWA amplitude is varied from 100-270 degrees.

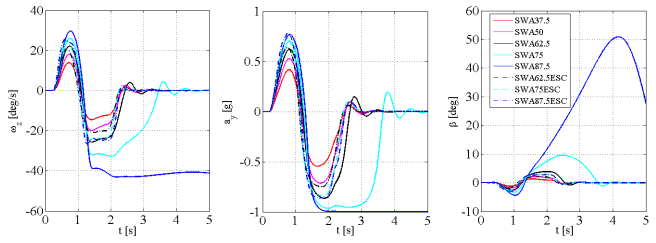

Fig. 5. Results with chassis Ch.A and its yaw rate, lateral acceleration, and sideslip, when ESC is both on and off. SWA max amplitude was varied between 37.5-87.5 degrees.

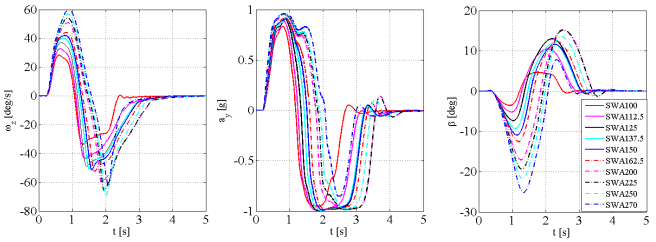

Fig. 6. Results for Chassis Ch.A and its yaw rate, lateral acceleration, and sideslip, when ESC is on. SWA max amplitude was varied between 100-270 degrees.

Now when studying the wheel forces, see Fig. 7, for a SWA amplitude of 162.5 degrees with the ESC on for chassis Ch.A, we can see how positive and negative longitudinal forces are developed. During the first part of the sine manoeuvre, 0.2 to 1.27 s, wheels 1 and 3 have negative longitudinal force. Wheel 2 has positive longitudinal force and wheel 4 has approximately zero longitudinal force. During the dwell part 1.27 to 2.12 s and above, wheel 1 has positive longitudinal force and wheel 3 has basically none. At the same time wheel 2 and 4 develop mostly negative longitudinal forces.

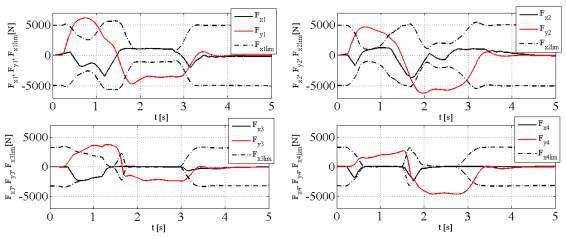

Fig. 7. Results for Chassis Ch.A and its tyre forces when ESC is on. SWA max amplitude was set to 162.5 degrees.

The wheel forces are realised by the control allocator and its use of the available actuators included in the optimization formulation. In Fig. 8 the actual actuator torques and their combined limits are shown. The combined limits means that not only are the actual position limits and their rate of change considered, see Eq. 25, but also what tyre forces can be applied, see Eq. 27. The positive force is realised by using the ice during the whole procedure and by giving positive torque distributed on the front wheels it allows positive longitudinal forces to be developed at the front wheels. This feature can be switched of by just defining the upper limits of the ice to be equal to zero. When not using the combustion engine the vehicle became less responsive but still managed to handle all the SWA amplitudes. Fig. 8 shows also how the mechanical brakes were used during the test procedure. One interesting observation was that the time constants on the mechanical brakes must not be too slow in order to successfully allocate the brakes during the worst SWA 270 degrees. The used time constant for the mechanical brakes was set to 0.06 s.

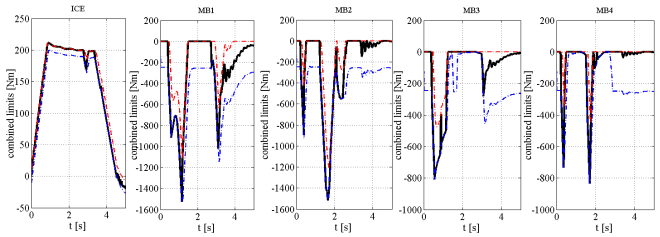

Fig. 8. Results for Chassis Ch.A and how the actuators are used by the ESC. SWA max amplitude was set to 162.5 degrees. The black solid line corresponds to actual u and the dotted/dashed red and blue lines are the upper and lower combined limits, respectively.

In Tab. I the responsiveness and stability criteria's are studied for all simulated cases for Ch.A. The table shows that when the ESC is off the first stability criteria is not fulfilled for SWA 75 degrees. When ESC is on the whole range of SWA amplitudes demanded by the proposed test procedure are handled with ease.

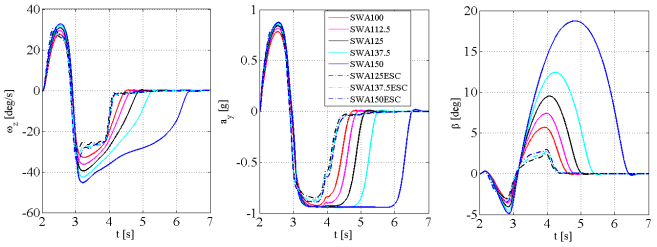

Fig. 9. Results with chassis Ch.B and its yaw rate, lateral acceleration, and sideslip, when ESC is both on and off. SWA max amplitude varied between 100-150 degrees.

The simulation results from chassis Ch.B verifies the results from Ch.A. However, Ch.A gave more conservative results. Fig. 9 and Fig. 10 shows yaw rate, lateral acceleration, and side slip for Ch.B. The Ch.B with ESC off fails one of the stability criteria at SWA 137.5 degrees and both stability criteria's at SWA 150 degrees, which is higher

TABLE I

RESULTS OF RESPONSIVENESS AND STABILITY CRITERIA WITH CHASSIS CH.A AND CH.B.

SWA	$d_y > 1.83$m	$\frac{\omega_z(t_{CoS}=1.0)}{\omega_{z,max}} \leq 0.35$	$\frac{\omega_z(t_{CoS}=1.75)}{\omega_{z,max}} \leq 0.2$	ESC
		Ch.A		
62.5	1.830	0.003	0.002	off
75	2.114	0.464	0.058	off
87.5	2.362	0.987	0.956	off
62.5	1.836	0.003	0.001	on
75	2.108	0.001	0.002	on
87.5	2.319	0.008	0.001	on
100	2.519	0.017	0.004	on
112.5	2.718	0.061	0.017	on
125	2.857	0.066	0.019	on
137.5	2.948	0.060	0.017	on
150	3.007	0.063	0.018	on
162.5	3.075	0.070	0.017	on
200	3.290	0.191	0.022	on
225	3.393	0.171	0.021	on
250	3.461	0.091	0.015	on
270	3.490	0.032	0.009	on
		Ch.B		
100	2.739	0.002	0.000	off
112.5	2.896	0.009	0.000	off
125	3.022	0.009	0.001	off
137.5	3.122	0.418	0.005	off
150	3.201	1.038	0.380	off
125	2.920	0.004	0.007	on
137.5	3.005	0.031	0.009	on
150	3.076	0.033	0.010	on
162.5	3.128	0.034	0.010	on
200	3.176	0.033	0.010	on
225	3.192	0.033	0.010	on
250	3.205	0.038	0.011	on
270	3.490	0.032	0.012	on

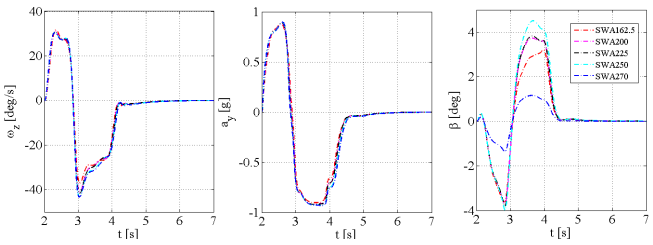

Fig. 10. Results for Chassis Ch.B and its yaw rate, lateral acceleration, and sideslip, when ESC is on. SWA max amplitude varied between 162.5-270 degrees.

than what seen with Ch.A, see Tab. I. Ch.B confirms that the proposed control system pass the criteria's of the test procedure for ESC.

VI. CONCLUSIONS

The control allocation based Electronic Stability Control System passed the proposed test procedure, sine with dwell, for ESCs. It was found to be critical that the time constant of the mechanical brakes should be faster than 0.1 s for successful control allocation when the most extreme steering wheel angle, 270 degrees, is used. When the time constant was reduced to 0.06 s then SWA 270 degrees was easily handled. The test procedure sine with dwell that FMVSS for ESC suggests has a major drawback. For future vehicles which may have software controlled steering, the steering wheel input does not actually mean anything in a physical aspect, i.e. the input can be manipulated by the software. To handle future vehicle configurations the input should be given as desired yaw rate instead or make a cone based manoeuvre that would trigger the same oversteering behaviour as sine with dwell.

VII. ACKNOWLEDGMENTS

The authors would like to thank the Swedish national research programme Gröna Bilen. Authors would also like to thank Matthijs Klomp at Chalmers for excellent discussions and feedback.

REFERENCES

[1] *Federal Motor Vehicle Safety Standards; Electronic Stability Control Systems*. US Department of Transportation, National Highway Traffic Safety Administration, Docket No. NHTSA-2006-25801, RIN:2127-AJ77, 2006.

[2] *Proposed FMVSS No. 126 Electronic Stability Control Systems, Preliminary Regulatory Impact Analysis*. US Department of Transportation, National Highway Traffic Safety Administration, Aug. 2006.

[3] L. Laine and J. Fredriksson, *Brake Blending for Hybrid Electric Vehicles using Control Allocation*. Tech. Report R011/2007, Department of Signals and Systems, Chalmers University of Technology, Göteborg, Sweden, 2007.

[4] ——, "Traction and braking of hybrid electric vehicles using control allocation," *Accepted(under revision) to Int. J. Vehicle Design, Special issue on: Advanced Traction/Braking Vehicle Control*, 2006.

[5] ——, "Coordination of vehicle motion and energy management control systems for wheel motor driven vehicles," in *Accepted to 2007 IEEE Intelligent Vehicles Symposium (IV'07)*, Istanbul, Turkey, June 2007.

[6] O. Härkegård, "Backstepping and control allocation with applications to flight control," Ph.D. dissertation, Department of Electrical Engineering, Linköping University, SE–581 83 Linköping, Sweden, May 2003.

[7] T. Johansen, T. Fossen, and S. P. Berge, "Constrained nonlinear control allocation with singularity avoidance using sequential quadratic programming," *IEEE Transactions on Control Systems Technology, vol. 12, no. 1*, 2004.

[8] T. Johansen, T. Fuglseth, P. Tøndel, and T. I. Fossen, "Optimal constrained control allocation in marine surface vessels with rudders," in *IFAC Conf. Manoeuvring and Control of Marine Craft*, Girona, 2003.

[9] P. Tøndel and T. A. Johansen, "Control allocation for yaw stabilization in automotive vehicles using multiparametric nonlinear programming," in *Proc. of American Control Conf.*, Portland, OR, June 2005.

[10] J. Plumlee, D. Bevly, and A. Hodel, "Control of a ground vehicle using quadratic programming based control allocation techniques," in *Proc. of American Control Conf.*, Boston, MA, July 2004.

[11] J. Plumlee, *Mult-Input Ground Vehicle Control Using Quadratic Programming Based Control Allocation*. Master thesis report, Auburn University, Alabama, 2004.

[12] SAE, "Surface vehicle recommended practice, vehicle dynamics terminology," *SAE 1976-07, J670e*, 1976.

[13] H. B. Pacejka, *Tyre And Vehicle Dynamics 2nd edition*. Butterworth-Heinemann, 2002.

[14] "The VehicleDynamics Library version 1.1 - Users Guide," http:/www.modelon.se.

[15] A. Serrarens, *Coordinated control of the Zero Inertia Powertrain*. Technische Universiteit Eindhoven, 2001.

[16] B. Lennartson, *Reglerteknikens grunder*. Studentlitteratur, 2001.

[17] G. Forkenbrock, D. H. Elsasser, B. C. O'Harra, and R. E. Jones, *Development of Electronic Stability Control (ESC) Performance Criteria*. US Department of Transportation, National Highway Traffic Safety Administration, report no.DOT HS 809 974, Sept. 2006.

[18] H. Khalil, *Nonlinear Systems, 3rd edition*. Prentice Hall Inc., 2002.

[19] K. Åström and T. Hägglund, *PID Controllers: Theory, Design, and Tuning*. Instrument Society of America, 1995.